



Tomato glandular trichomes: insights into productivity and development

Dissertation

zur Erlangung des

Doktorgrades der Naturwissenschaften (Dr. rer. nat.)

der

Naturwissenschaftlichen Fakultät I

Biowissenschaften

der Martin-Luther-Universität Halle-Wittenberg,

vorgelegt

von

Herr Alejandro Brand Durán

Gutachter:

1. Prof. Dr. Alain Tissier
2. Prof. Dr. Jörg Degenhardt
3. Prof. Dr. Anna Matuszyńska

Verteidigungsdatum: 05.11.2024

*It's not an easy task at all
to take life day by day and shape oneself
to give meaning to everything,
and to appear both natural and convincing
(...)
in order to accomplish something in life,
in order to achieve
what was never truly asked of you.*

Translated fragment of a poem by Elkin Restrepo.

Table of contents

Table of contents.....	I
List of main figures	IV
List of supplementary figures.....	VI
List of tables	VII
Frequently used abbreviations.....	VIII
Overview of the present thesis	X
Chapter 1: Elucidating the role of Rubisco and PEPCCK in photosynthetic glandular trichomes of tomato	1
1.1 Introduction.....	1
1.1.1 Glandular trichomes	1
1.1.2 Glandular trichomes of tomato.....	2
1.1.3 Glandular trichomes of wild tomato accessions	3
1.1.4 Biosynthesis of specialized metabolites in GTs of tomato.....	5
1.1.5 Metabolic productivity and photosynthetic GTs.....	6
1.1.6 Rubisco and the recycling of CO ₂	10
1.1.7 PEPCCK and the C ₄ -like metabolism in GTs of tomato.....	11
1.2 Objectives of the Chapter 1.....	13
1.3 Results.....	14
1.3.1 Identification of <i>NtRbcS-T</i> orthologous gene in tomato	14
1.3.2 Functional characterization of <i>SlRbcS-T</i> in GTs of tomato.....	17
1.3.3 Role of Rubisco in type-VI glandular trichomes.	25
1.3.4 Functional characterization of <i>PEPCCK</i> in the glandular trichomes.....	31
1.4 Discussion	37
1.4.1 A trichome-specific <i>Rubisco small subunit (RbcS-T)</i> in photosynthetic glandular trichomes of tomato.....	37
1.4.2 The role of Rubisco in type-VI GTs trichomes.....	41
1.4.3 A CRISPR-TSKO approach to study the basis of high productivity in GTs.....	43
1.4.4 PEPCCK and carbon allocation between cell compartments.....	45
Chapter 2: Heat stress, productivity and trichome fate.....	50
2.1 Introduction	50
2.1.1 The control of trichome development and productivity	50
2.1.2 The role of jasmonic acid in trichome development and productivity.....	51
2.1.3 Environmental and developmental cues in trichome initiation and productivity.	52
2.1.4 Heat stress, JA, trichome development and productivity.....	53
2.2 Objectives Chapter 2	55

2.3 Results.....	56
2.3.1 Evaluation of the effect of heat stress on type-VI trichome development and productivity.....	56
2.3.2 Metabolite profiling of trichomes under heat stress.....	58
2.3.3 The role of jasmonate signaling in heat stress-induced type-IV trichome development.....	63
2.3.4 Comparative transcriptome analysis of WT and JA-deficient tomato plants upon heat stress.....	66
2.3.5 A JA response upon heat stress.....	69
2.3.6 Heat stress alters cholesterol biosynthesis and zeatin regulating enzymes.....	70
2.3.7 Transcription factors.....	71
2.3.8 Changes in JA biosynthesis and signaling upon heat stress.....	71
2.4 Discussion.....	74
2.4.1 Effect of heat stress on type-VI trichome development and productivity.....	74
2.4.2 The role of jasmonate signaling in heat stress-induced type-IV trichome initiation.....	80
3. Summary and Outlook.....	89
4. Materials and methods.....	92
4.1 Sequence analysis.....	92
4.2 Vector construction.....	92
4.3 Transformation in <i>E. coli</i> and <i>A. tumefaciens</i>	93
4.4 Extraction of genomic DNA.....	94
4.5 Virus-induced gene silencing (VIGS) assay.....	94
4.6 <i>Agrobacterium</i> -mediated genetic transformation of tomato.....	95
4.7 Trichome counting.....	95
4.8 Trichome fraction and leaf material harvesting.....	96
4.9 Heat stress experiments.....	96
4.10 JA treatment.....	96
4.11 RNA isolation, cDNA synthesis and quantitative RT-PCR.....	96
4.12 Quantification of VOCs by gas chromatography-mass spectrometry (GC-MS).....	97
4.13 Quantification of acylsugars by liquid chromatography-mass spectrometry (LC-MS).....	97
4.14 JA-related phytohormones quantification.....	98
4.15 Two-phase metabolite extraction from trichomes and leaves.....	99
4.16 Targeted analysis of hydrophilic metabolites of the central carbon metabolism.....	99
4.17 Fluorescence microscopy.....	100
4.18 Quantification of organic acids and Pi.....	100

4.19 RNA sequencing and data analysis	100
4.20 Statistical and bioinformatic analyses	101
5. References	102
6. Appendix	116
6.1 Supplementary figures	116
6.2 Supplementary tables	127
Acknowledgement	137
Curriculum Vitae	139
Eidesstattliche Erklärung	141

List of main figures

Figure 1. Trichome types and their cell structure in the <i>Lycopersicon</i> section of the genus <i>Solanum</i>	3
Figure 2. Leaf morphology and trichome landscape in different tomato accessions.....	4
Figure 3. Scheme of terpenoid and acylsugar (AS) biosynthesis intermediate pathways in glandular trichomes of cultivated tomato.....	7
Figure 4. Examples of SM produced in GTs of tomato.....	8
Figure 5. Putative and simplified model for the supply of carbon, energy and reducing power in photosynthetic glandular trichomes (GTs) of tomato.....	9
Figure 6. Candidate orthologous genes of <i>NtRbcS-T</i> in tomato.....	15
Figure 7. <i>S. lycopersicum RbcS-T (SlRbcS-T)</i> is expressed in glandular cells of type-I and type-IV GTs.....	16
Figure 8. Relative expression of <i>SlRbcS-T</i> in different tissues.....	17
Figure 9. Functional characterization of <i>RbcS-T</i> in cultivated tomato (<i>SlRbcS-T</i>).....	19
Figure 10. Functional characterization of Rubisco small subunit trichome specific (<i>RbcS-T</i>) isoform in wild tomato accession <i>S. habrochaites (ShRbcS-T)</i>	20
Figure 11. Virus-induced gene silencing (VIGS) assay of <i>Rubisco small subunit trichome specific (RbcS-T)</i> and the simultaneous silencing of the <i>RbcS</i> mesophyll isoforms in the wild tomato <i>S. pennellii</i>	22
Figure 12. Acylsugar (AS) quantification of the VIGS assay using liquid chromatography-mass spectrometry (LC-MS).....	24
Figure 13. Quantification of acylsugars (AS) peaks sharing the same molecular mass (m/z of $[M+HCOO]^-$) but different acyl chain composition.....	25
Figure 14. Transcript levels of mesophyll <i>Rubisco small subunits RbcS</i> in leaves (Lvs) vs trichomes (Trc) of <i>S. lycopersicum</i> compared to <i>RbcS-T</i>	26
Figure 15. Selection of candidate promoters for CRISPR-based tissue-specific knockout system (CRISPR-TSKO) in type-VI GTs.....	27
Figure 16. Proof-of-concept of the CRISPR-based tissue-specific knockout system (CRISPR-TSKO).....	29
Figure 17. CRISPR-TSKO targeting the mesophyll isoforms of <i>RbcS</i> in type-VI GTs of cultivated tomato.....	30
Figure 18. Relative expression levels of <i>PEPCK</i> in trichome-free leaves (Lvs) and trichomes (Trc) of <i>S. lycopersicum (Sl)</i> and <i>S. habrochaites (Sh)</i>	31
Figure 19. CRISPR/Cas9 loss-of-function mutants of <i>PEPCK</i> in cultivated tomato.....	32
Figure 20. Functional characterization of <i>PEPCK</i> in type-VI glandular trichomes of cultivated tomato.....	33

Figure 21. Acylsugar (AS) profiling of <i>pepck</i> mutants using liquid chromatography-mass spectrometry LC-MS.....	34
Figure 22. Profiling of metabolites involved in the central carbon and energy metabolism in GT of <i>pepck</i> mutants.	36
Figure 23. Simplified model illustrating the putative role of PEPCK in type-VI GTs of tomato.	47
Figure 24. Molecular factors regulating the capitate type-I/IV and the peltate type-VI GTs initiation in <i>S. lycopersicum</i>	51
Figure 25. Effect of heat stress on type-VI trichomes and terpenoid profiles.....	57
Figure 26. Central carbon and energy metabolite profiling of glandular trichomes under heat stress (HS).	60
Figure 27. Pathway enrichment analysis of the CCM metabolites in trichomes of CN versus HS.	61
Figure 28. Changes in TCA intermediates and semipolar SM in GTs under heat stress (HS).	62
Figure 29. Changes in type-VI trichome density and productivity upon heat stress (HS).	64
Figure 30. The <i>jai1</i> mutant does not exhibit type-IV trichome induction upon heat stress (HS).	65
Figure 31. JA and JA-related hormone levels after long heat stress (HS) exposure.	66
Figure 32. Transcriptome analysis of WT and <i>jai1</i> tomato under heat stress (HS).	68
Figure 33. Changes in JA biosynthesis and signaling upon heat stress.	73
Figure 34. Changes in gene expression of TFs and TPS genes upon heat stress.	75
Figure 35. <i>MYB13</i> is induced by heat stress and jasmonate.....	86

List of supplementary figures

Figure S 1. Transcripts per million (TPM) reads of <i>RbcS</i> subunits in leaves and trichomes of cultivated tomato cv. AVT04124 and <i>S. habrochaites</i> sp. <i>glabratum</i>	116
Figure S 2. <i>pSITPS20:YFP-GUS</i> expression in the glandular cells of type-VI trichomes.....	117
Figure S 3. Hierarchical clustering dendrogram of CCM metabolic profiles of GTs of <i>pepck</i> mutant lines.	118
Figure S 4. Effect of heat stress on type-VI trichomes and terpenoids in Micro-Tom.	119
Figure S 5. Principal component analysis (PCA) of RNASeq data distribution.	120
Figure S 6. Gene ontology (GO) analysis.	121
Figure S 7. Expression data (\log_2FC) of heat stress (HS) vs control (CN) of genes involved in jasmonate signaling and biosynthesis.	122
Figure S 8. Amino acid sequence alignment between <i>A. thaliana MYB13</i> (At1g06180) and <i>S. lycopersicum MYB13</i> (Solyc06g083900).	123
Figure S 9. Gene expression of <i>S. lycopersicum MYB13</i> in different tissues.	124
Figure S 10. Transcription factor binding sites found within the 2kb upstream sequence of <i>MYB13</i>	125
Figure S 11. <i>Agrobacterium</i> -mediated genetic transformation of tomato.	126

List of tables

Table S 1. Acylsugars of from the three <i>Solanum</i> species detected by liquid chromatography-mass spectrometry (LC-MS/MS).....	127
Table S 2. Top 30 polar metabolites sorted by <i>FDR</i> values after one-way ANOVA analysis, from WT and <i>pepck</i> mutant lines.	128
Table S 3. Polar metabolites significantly different between trichomes under control (CN) vs heat stress (HS) treatment.	129
Table S 4. Peak area of hydrophilic metabolites detected in trichome fractions.	130
Table S 5. Differentially expressed genes (DEGs) in heat stress (HS) compared to control (CN) conditions in the WT, <i>jai1</i> or both genotypes.....	132
Table S 6. Primers used in the present dissertation.....	133
Table S 7. Composition of media used for stable genetic transformation of tomato.	136

Frequently used abbreviations

Acetyl-CoA	acetyl-Coenzyme A
AS	acylsugars
ASATs	acylsucrose acyltransferases
CBB	Calvin-Benson-Bassham cycle
CCM	central carbon metabolism
CN	control condition
COI1	<i>CORONATINE INSENSITIVE1</i>
CRISPR/Cas9	Clustered Regularly Interspaced Short Palindromic Repeats (CRISPR)- associated protein 9
CRISPR-TSKO	CRISPR-based tissue-specific knockout system
DEGs	Differential expressed genes
DMAPP	dimethylallyl diphosphate
FA	fatty acid
FPP	farnesyl diphosphate
GA-3P	glyceraldehyde-3-phosphate
GFP	green fluorescent protein
GO	gene ontology
GTs	glandular trichomes
HS	heat stress
IPP	isopentenyl diphosphate
JA	jasmonic acid
<i>jai1</i>	<i>jasmonic acid-insensitive 1</i>
JA-Ile	(+)-7- <i>iso</i> -jasmonoyl isoleucine
JAZ	JASMONATE ZIM-domain protein
KO	knockout
MEP	2-C-methyl-D-erythritol 4-phosphate pathway
MVA	mevalonate pathway
OAA	oxaloacetate
OPDA	<i>cis</i> -12-oxo-phytodienoic acid
PCA	principal component analysis
PEP	phosphoenolpyruvate
<i>PEPCK</i>	<i>phosphoenolpyruvate carboxykinase</i>

PIs	proteinase inhibitors
PYR	pyruvate
qRT-PCR	quantitative reverse-transcription PCR
RbcL	Rubisco large subunit
RbcS	Rubisco small subunit
RbcS-M	Rubisco small subunit-mesophyll isoform
RbcS-T	Rubisco small subunit-trichome specific isoform
RNASeq	RNA sequencing
Rubisco	Ribulose-1,5-bisphosphate carboxylase/oxygenase
SGAs	steroidal glycoalkaloids
sgRNA	single guide RNA
SM	specialized (secondary) metabolites
TFs	transcription factors
TPS	terpene synthase
VIGS	virus-induced gene silencing
VOCs	volatile organic compounds
WT	wild type

Overview of the present thesis

As an essential part of their communication with the surrounding environment, plants produce diverse compounds referred to as specialized metabolites (SM). These substances are often synthesized in large quantities and within distinct anatomical structures, whose architecture is intricately linked to the mode of action of the compounds they harbor or secrete. Glandular trichomes (GTs) are one of these structures, covering the surface of the above-ground part of the plants and acting as micro-factories of SM that frequently play a crucial role in the defense response to biotic and abiotic stresses.

Tomato (*Solanum lycopersicum*) is an excellent example of how different types of GTs co-develop and coexist with their non-glandular counterparts, producing various classes of SM, with photosynthetic capacity and displaying, in specific cases, changes in their relative density through vegetative growth. Moreover, related wild tomato species, which exhibit remarkable differences in GT number and productivity, provide a valuable resource for investigating the genetic factors that control the biosynthesis of these compounds and their complex diversity. Multi-Omics data provide evidence of the distinct mechanisms supporting chemical reactions in GTs; however, there is still much room for investigation into how these glandular appendages achieve high productivity from a gene function perspective. At the same time, little is known about how environmental factors can modulate SM biosynthesis and, more intriguingly, how they can trigger changes in trichome development.

The present thesis comprises two chapters. The first one attempts to address the role of a trichome-specific Rubisco small subunit (RbcS-T), part of the Rubisco complex, and of the Phosphoenolpyruvate carboxykinase (PEPCK) in the photosynthetic GTs of tomato. Both enzymes participate in the primary metabolism, and their expression pattern in the GTs suggests they fulfill a supporting function in the biosynthesis of SM. The second chapter aims to investigate the general effects of heat stress (HS) on a specific type of trichomes. In the course of this study, a connection between jasmonate signaling and the HS-mediated change in trichome fate was found, and possible factors controlling this phenomenon were identified.

Chapter 1: Elucidating the role of Rubisco and PEPCK in photosynthetic glandular trichomes of tomato

1.1 Introduction

1.1.1 Glandular trichomes

Just as the skin constitutes our body's initial shield against external threats, in plants the epidermis and its cuticle serve as the first protective barrier to cope with environmental disturbances. The plant's aerial surface has several strategies, including wax coating, cutin matrix, thorns, spines, and trichomes, which help these sessile organisms to defend themselves from stressors (War et al., 2012; Arya et al., 2021). Trichomes are structures with a hair-like appearance present in the above-ground surface of many plant species. These appendages originate from epidermal cells that differentiate, extend, and specialize, displaying a diverse architecture, cell composition (uni or multicellular), as well as density and function (Werker, 2000; Kang et al., 2010; Tissier, 2012; Han et al., 2022). Despite their heterogeneity, the presence or absence of glandular cells in the trichomes is the main criterion used to classify them into two categories: non-glandular or glandular trichomes (GTs). Non-GTs play mainly a physical protection role in abiotic stresses, for example as modulators of light absorbance, heat balance and leaf water permeability (Bickford, 2016), as well as in the interaction with biotic stresses, for example reducing the access of herbivores to the plant surface or controlling insect feeding due to antinutritional properties (War et al., 2012; Kariyat et al., 2017). Although these hairs lack a secretion system, they can accumulate phenolic compounds on the cell wall that are associated, for instance, with UV protection (Karabourniotis et al., 2020).

On the other hand, GTs are characterized by the presence of metabolically active cells capable of producing, secreting, and/or storing considerable amounts of specialized or previously referred to as secondary metabolites (SM). These SM comprise, among others terpenoids, phenylpropanoids, flavonoids, fatty acid derivatives and acylsugars (Glas et al., 2012; Tissier, 2012). These substances mediate chemical communication between plants and their environment for diverse purposes, including defense against herbivores and pathogens, attraction of pollinators or protection from abiotic stresses (Wagner et al., 2004). Besides their ecological significance, SM produced by GTs are important for many applications. For instance, several plants of the Lamiaceae family (including peppermint, basil, oregano, lavender, and thyme) secrete essential oils that are used as food additives, as aroma and perfume ingredients or in cosmetics (Maleci Bini and Giuliani, 2006; Zhang et al., 2023). Other

compounds are utilized in medicine like the sesquiterpene lactone artemisinin, a SM produced in the GTs of the sweet wormwood *Artemisia annua* and used for the treatment of malaria disease (Olsson et al., 2009); or the cannabinoids secreted by the GTs of *Cannabis sativa*; employed in many pharmaceutical applications and for recreational purposes (Tanney et al., 2021).

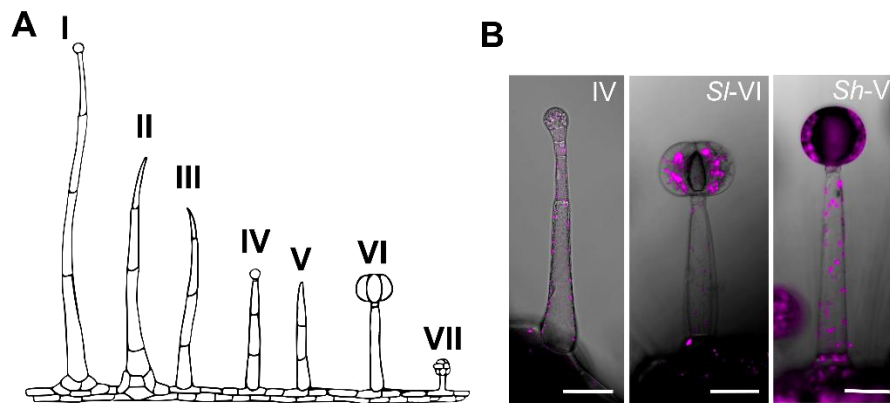
GTs can be found in about 30% of vascular plants, from ferns (Pteridospermatophyta) where they are rarely present, until angiosperms, where they appeared independently multiple times during the evolution and with greater diversity and function (Fahn, 2000; Lange, 2015). Although plant-species dependent, GTs typically consist of different cells including basal, stalk and one to a few secretory cells, with or without an extracellular cavity. This cavity is a space where the metabolites can be stored in high concentrations and prevent self-toxicity to the plants (Tissier et al., 2017). The cellular structure of the GTs is intricately linked to the type of compounds they produce and their mode of action. For example, capitate trichomes lacking a cavity usually produce sticky substances such as acylsugars (AS) that are exudated directly from the glandular cells to the leaf surface creating an adhesive layer that immobilizes predators. On the other hand, peltate or biseriate trichomes possess a storage space where mainly volatile compounds are retained and released upon contact with e.g. insects (Schuurink and Tissier, 2020).

1.1.2 Glandular trichomes of tomato

In *Arabidopsis thaliana*, trichomes are unicellular and non-glandular, making it unsuitable as a model species for studying GTs. While significant amount of knowledge regarding plant cell differentiation is derived from studies on *Arabidopsis* trichomes, some evidence indicates that the mechanisms governing the development of GTs are distinct (Serna and Martin, 2006; Yang and Ye, 2013). Therefore, species like tomato (*Solanum lycopersicum*) or sweet wormwood (*A. annua*) became plant models for studying GTs from a genetic and a metabolic perspective (Chalvin et al., 2020).

In tomato, *Lycopersicon* section of the genus *Solanum*, seven different types of trichomes coexist listed with roman numbers, with type-II, III and V classified as non-GTs, and type-I, IV, VI and VII classified as GTs (**Fig. 1**) (Luckwill, 1943; Glas et al., 2012). Among GTs, two morphologies can be distinguished. The peltate type-VI trichomes possess four secretory cells at the end of the stalk forming a “clover shape”, and they predominantly produce volatile organic compounds (VOCs), including mono- and sesquiterpenes (Schillmiller et al., 2010; Balcke et al., 2017; Zhou and Pichersky, 2020). Surrounded by the glandular cells, there is an intercellular cavity where the VOCs are transported and stored (Bergau et al., 2015; Tissier et

al., 2017). Type-VI are the most abundant type of GTs in *S. lycopersicum*, representing about 80% of them (Balcke et al., 2017). Conversely, the capitate type-I and type-IV trichomes consist of one or multiple basal cells, several stalk cells, and one glandular cell at the end of the stalk (Tissier, 2012) (**Fig. 1**). Both type-I/type-IV trichomes synthesize and secrete AS (Li et al., 2014; Nakashima et al., 2016). The long type-I trichomes can be found in low densities along the vegetative growth of tomato, whereas type-IV trichomes are restricted to the early stages of the plant development (Vendemiatti et al., 2017).



Type	Base	Stalk (cells)	Stalk length (mm)	Gland cells	Sl	Sh	Sp
I	Globular multicellular	6-10	2-3	Single, round	X	X	
II	Globular multicellular	6-10	0.2-1.0	No glands			
III	Flat unicellular	4-8	0.4-1.0	No glands	X	X	
IV	Flat unicellular	Up to 3	0.2-0.4	Single round	X	X	X
V	Flat unicellular	Up to 3	0.2-0.4	No glands	X		
VI	Flat unicellular	2	0.1-0.2	4 glands in Sl and Sp. Single round gland in Sh.	X	X	X
VII	Flat unicellular	Unicellular	0.05	4-8 glands	X	X	

Figure 1. Trichome types and their cell structure in the *Lycopersicon* section of the genus *Solanum*.

(A) Type-I, IV, VI, and VII are glandular trichomes (GTs) while type-II, III, and V are non-GTs. (B) Laser scanning microscopy images of selected GTs. Differences in the type-VI glandular head cells between cultivated *S. lycopersicum* (Sl) and the wild tomato *S. habrochaites* (Sh). Notice the distinct arrangement of the glandular cells, and the differences in the storage cavity. Chlorophyll autofluorescence is displayed in magenta color. Scale bar = 50 µm. Below images, description of trichomes according to Luckwill (1943), revised by Glas et al. (2012) and including the observations made in Vendemiatti et al. (2017). The presence of each trichome type in Sl, Sh and *S. pennellii* (Sp) is indicated by an X mark. Illustration adapted from Kim et al. (2012).

1.1.3 Glandular trichomes of wild tomato accessions

The composition of GTs and the class of metabolites they produce may vary depending on the tomato species. Wild tomato accessions are recognized to produce large amounts and diverse types of SM making them valuable resources for tomato breeders and researchers. For example, in *Solanum habrochaites* accession LA1777, the average productivity of type-VI trichomes is around 97 times higher than in the cultivated tomato, and in certain accessions,

the accumulated sesquiterpene carboxylic acids in those trichomes may reach up to 12% of the fresh weight of the leaves (Frelichowski Jr and Juvik, 2005; Balcke et al., 2017). Some chemotypes of *S. habrochaites* like PI127826 and LA2167, produce plastid-derived sesquiterpenoids such as 7-*epi*-zingiberene which confer a wide spectrum of resistance against diverse classes of arthropods including whiteflies (*Bemisia tabaci*), pinworms (*Tuta absoluta*) and spider mites (*Tetranychus evansi*) (Maluf et al., 2001; Freitas et al., 2002; Maluf et al., 2010; Bleeker et al., 2011). Moreover, accessions like LA1777 possess not only a higher density of type-VI trichomes, but also four glandular head cells at the tip arranged in a compact round shape with a larger intercellular cavity (**Fig. 1B**; **Fig. 2**). In a fully developed type-VI trichome, that cavity can occupy up to 65% of the volume of the glandular head which allows the SM to be stored in presumably higher amounts (Bergau et al., 2015).

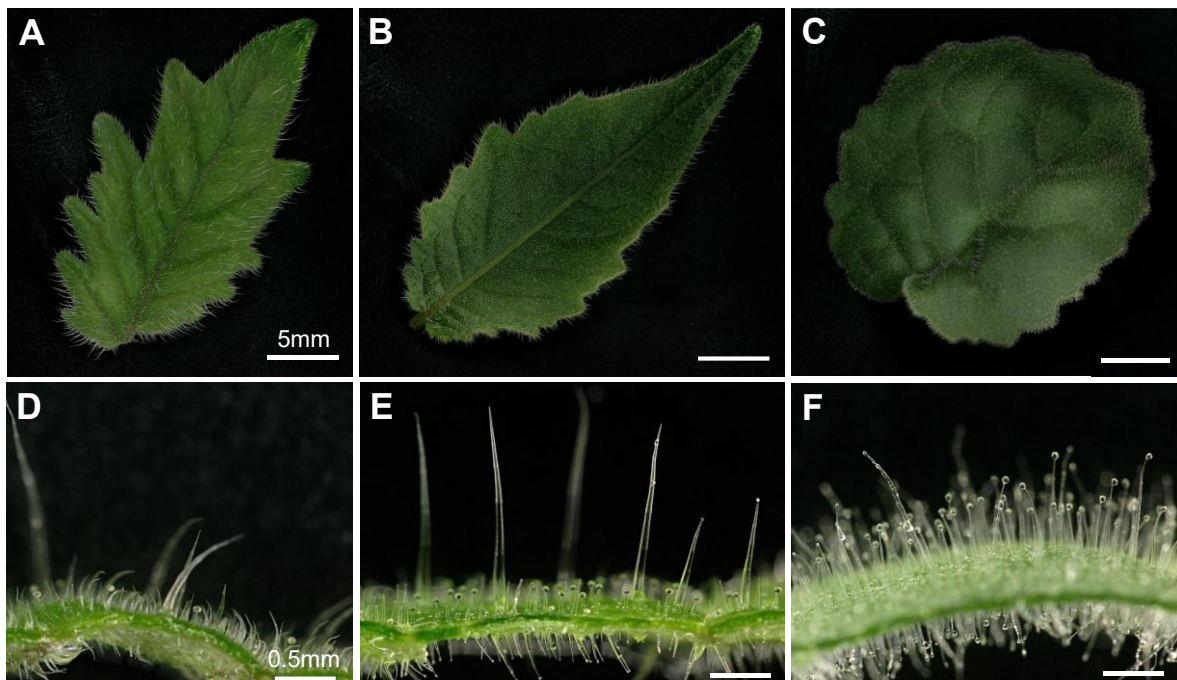


Figure 2. Leaf morphology and trichome landscape in different tomato accessions.

These three tomato accessions were used in the present thesis. **(A)** and **(D)** *Solanum lycopersicum* cv Moneymaker. **(B)** and **(E)** *Solanum habrochaites* sp *glabratum*. **(C)** and **(F)** *Solanum pennellii* LA0716.

An accession of another wild tomato species *Solanum pennellii* LA0716, produces substantial quantities of AS. One reason for this is that, unlike cultivated tomato, *S. pennellii* possesses higher densities of type-IV trichomes throughout vegetative development (**Fig. 2**). In this species, up to 20% of the leaf dry biomass can be attributed to the AS content (Fobes et al., 1985; Schillmiller et al., 2012). Furthermore, *S. pennellii* produces a mixture of AS with different sugar cores (acylglucoses and acylsucroses), with the glucose-core ones being more predominant (Shapiro et al., 1994; Fan et al., 2019). The presence of these viscous compounds on the leaves provides protection against different types of arthropods, for

example aphids, spider mites, whiteflies, moths and thrips (Rodriguez et al., 1993; Maluf et al., 2010; Mirnezhad et al., 2010; Vosman et al., 2019).

1.1.4 Biosynthesis of specialized metabolites in GTs of tomato

SM are defined as species-specific compounds that support plant adaptation and survival in the changing ecological environment (Huang and Dudareva, 2023). Topping the list of SM with more than 80.000 compounds and with the most structural diversity, terpenoids (or isoprenoids) are assemblies of five carbon (C) C₅ isoprene units built from isopentenyl diphosphate (IPP) and its isomer dimethylallyl diphosphate (DMAPP) (Dudareva et al., 2004; Cheng et al., 2007; Huang and Dudareva, 2023). In plants, the biosynthesis of these C₅ isoprene units occurs through two pathways, that take place in distinct cell compartments and utilizing different precursors (**Fig. 3**) (Dudareva et al., 2013; Kortbeek et al., 2016). The 2-C-methyl-D-erythritol 4-phosphate (MEP) pathway takes place in the plastids and uses pyruvate and glyceraldehyde-3-phosphate (GA-3P) to produce IPP and DMAPP, that are converted first in geranyl diphosphate (GDP), and later in geranylgeranyl diphosphate (GGPP), precursors of monoterpenes (C₁₀) and diterpenes (C₂₀) (Cheng et al., 2007). The mevalonate (MVA) pathway primarily operates in the cytosol with certain steps occurring in the peroxisomes. It utilizes acetyl-Coenzyme A (acetyl-CoA) as a precursor, which, through several enzymatic reactions, results in the formation of IPP, that is subsequently condensed in C₁₅ farnesyl diphosphate (FPP), precursor of sesquiterpenes (C₁₅) and triterpenes (C₃₀). Despite occurring in separate cell compartments, cross-talk between the MEP and MVA pathway has been observed, in particular from the plastids to the cytosol (Dudareva et al., 2005) (**Fig. 3**).

Tomato GTs are not an exception and produce specifically mono- and sesquiterpenes among the blend of SM, exhibiting some particularities. For example, in cultivated tomato the C₁₀ precursor neryl-diphosphate (NPP) is used instead of GDP as a precursor for monoterpenes (Schilmiller et al., 2009). The terpene synthase (TPS) TPS20 in the plastids uses NPP to build different monoterpenes, mostly β -phellandrene (Schilmiller et al., 2010; Zhou and Pichersky, 2020) (**Fig. 4B**). In the cytosol, FPP is employed by TPS12 as a substrate to synthesize the sesquiterpenes β -caryophyllene and α -humulene (Schilmiller et al., 2010; Zhou and Pichersky, 2020) (**Fig. 4C**). Another example, is some accessions of *S. habrochaites* that produce sesquiterpene precursors in the plastids, such as Z,Z-farnesyl diphosphate (zFPP) from which plastid-derived sesquiterpenes like α -santalene or 7-epizingiberene are synthesized (Sallaud et al., 2009; Bleeker et al., 2012).

Another class of metabolites produced in tomato GTs are acylsugars (AS). AS consist of sugar cores, frequently sucrose or glucose, that are decorated with short to medium-length fatty acyl

chains, both straight or branched at different positions (Schillmiller et al., 2012; Ning et al., 2015) (**Fig. 3, Fig. 4A**). In *Solanum* species, the acyl groups can be from C₂ to C₁₂ (Ghosh et al., 2014). The common short-branched acyl chains 2-methylpropanoic acid (isoC4), 3-methylbutanoic acid (iC5), and 2-methylbutanoic acid (anteisoC5) originate from the metabolism of the branched-chain amino acids valine, leucine and isoleucine respectively (Walters and Steffens, 1990). It is believed that medium-chain fatty acids (C ≥ 10) are derived from fatty acids, that by the action of the acyl-CoA synthetase (ACS) are converted into acyl-CoAs (Fan et al., 2020). Acyl-CoAs are then attached to the sugar moiety by the action of the acylsucrose acyltransferases (ASATs) in a consecutive fashion (Fan et al., 2016) (**Fig. 3**). In *S. pennellii*, the observed glucose core in the AS is generated by the action of an invertase-like enzyme that cleaves the glycosidic bond of the acylsucroses (SpASFF1), creating new variations of AS (Leong et al., 2019). The standard nomenclature of AS, using S4:24 (2,5,5,12) as an example, is as follows: S, the initial letter indicates the type of sugar core (“S” for sucrose, “G” for glucose); 4, the first number indicates the number of acyl chains; and 24 after the colon indicates the sum of the carbons in all acyl chains. The numbers inside the parentheses indicate the number of carbons in each acyl chain (**Fig. 4A**).

1.1.5 Metabolic productivity and photosynthetic GTs

In most cases, the SM found in the GTs are synthesized *in situ*, and therefore these plant micro-organs have been granted with the designation of cell factories (Huchelmann et al., 2017; Tissier, 2018). The remarkable productivity occurring in GTs implies a consistent provision of precursors and cofactors in a sufficient and regulated manner. Starters of the MVA and MEP pathways, respectively Acetyl-CoA, and pyruvate and GA-3P, are carbon (C) building blocks derived from the primary metabolism (**Fig. 3**). Despite their significance, there is limited understanding of how the central and energy metabolism is organized to guarantee the supply of precursors to the SM pathways in these cell factories (Balcke et al., 2017; Schuurink and Tissier, 2020). In certain plant species such as *A. annua*, tobacco (*Nicotiana tabacum*) or tomato, GTs contain photosynthetically active chloroplast. This could suggest that in these plant species, GTs are C-self-sufficient and that the energy (ATP) and reducing power (NADPH) required, is provided by photosynthesis in these organelles. However, evidence so far indicates that photosynthetic GTs rather act as C-sink organs, relying on sugars provided from the leaf (Balcke et al., 2017), as occurs in non-photosynthetic GTs, for example, in peppermint GTs (*Mentha x piperita*) (Johnson et al., 2017).

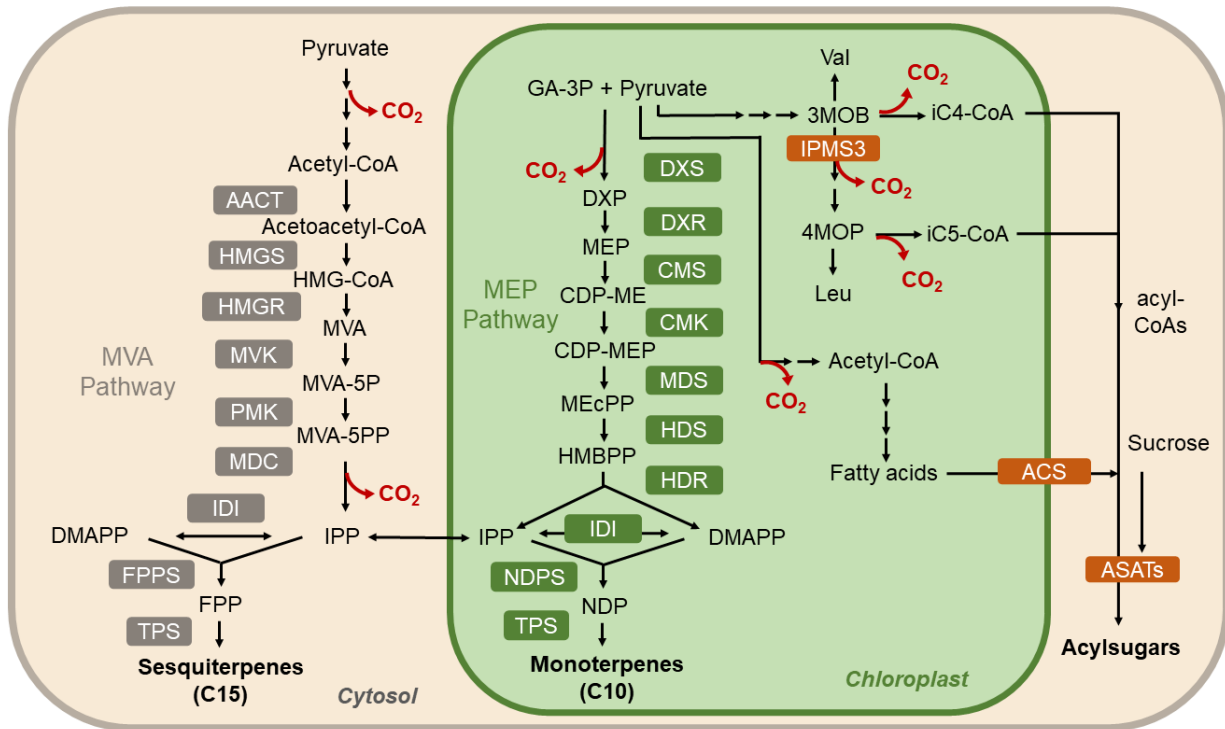


Figure 3. Scheme of terpenoid and acylsugar (AS) biosynthesis intermediate pathways in glandular trichomes of cultivated tomato.

Monoterpenes (C_{10}) are synthesized in the plastids through the methyl-erythritol phosphate (MEP) pathway while the sesquiterpenes (C_{15}) are produced in the cytosol through the mevalonate (MVA) pathway with some steps occurring in the ER and peroxisomes (not indicated). AS are synthesized from acyl-CoAs derived from the branched-chain amino acids and fatty acid biosynthesis. **Abbreviations:** DXP, deoxy-xylulose phosphate; MEP, methyl-D-erythritol-phosphate; CDP-ME, diphosphocytidyl-methylerythritol; CDP-MEP, CDP-ME 2-phosphate; MEcPP, methyl-D-erythritol-cyclo-diphosphate; HMBPP, hydroxy-3-methylbut-2-enyl-diphosphate; NDP, neryl diphosphate; HMG-CoA, 3-hydroxy-3-methylglutaryl-coenzyme A; MVA, mevalonate; MVA-5P, mevalonate-5-phosphate; MVA-5PP, mevalonate-5-pyrophosphate; IPP, isopentenyl diphosphate; DMAPP, dimethylallyl diphosphate; FPP, farnesyl diphosphate; 3MOB, 3-methyl-2-oxobutanoate; 4MOP, 4-methyl-2-oxopentanoate; iC4-CoA, 2-methylpropanoic-coenzyme A; iC5-CoA, 2-methylbutanoic-coenzyme A. **Key enzymes** are depicted in round-edged squares: DXS, deoxy-xylulose phosphate synthase; DXR, deoxy-xylulose phosphate reductoisomerase; CMS, diphosphocytidyl-methyl-D-erythritol synthase; CMK, cytidine 5'-diphospho)-2-C-methyl-D-erythritol kinase; MDS, methyl-D-erythritol cyclodiphosphate synthase; HDS, hydroxy-3-methylbut-2-enyl diphosphate synthase; HDR, hydroxy-3-methylbut 2-en-1-yl diphosphate reductase, NDPS, neryl diphosphate synthetase; TPS, terpene synthase; AACT, acetyl-CoA C-acetyltransferase; HMGS, hydroxymethylglutaryl-CoA synthase; HMGR, hydroxymethylglutaryl-CoA reductase; MVK, mevalonate kinase; PMK, phosphomevalonate kinase; MDC, diphosphomevalonate decarboxylase; IDI, isopentenyl-diphosphate deltaisomerase; FPPS, farnesyl pyrophosphate synthase; IPMS3, isopropylmalate synthase 3; ACS, acyl-CoA synthetase; ASATs, acylsugar acyltransferases. Scheme modified from Zhan et al. (2023).

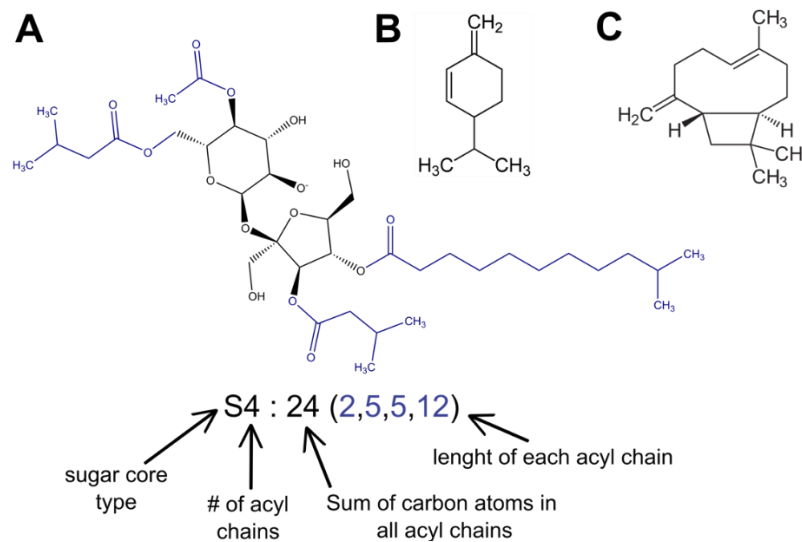


Figure 4. Examples of SM produced in GTs of tomato.

(A) Illustration and nomenclature of acylsugars (AS). S4:24(2,5,5,12) is one of the AS synthesized in type-I/IV trichomes in *S. lycopersicum*. The sucrose core is indicated in black, and the four acyl chains are depicted in blue. (B) β -phellandrene, the most abundant monoterpene produced in type-VI trichomes. (C) β -caryophyllene, a sesquiterpene produced in type-VI trichomes.

Integrating “omics” datasets, including transcriptomics, proteomics, and metabolomics, in addition to ^{13}C -labelling, Balcke et al. (2017) revealed particular features of the central carbon metabolism (CCM) in GTs of tomato that could drive their high metabolic productivity. Based on their data, Balcke and co-authors concluded that despite being photosynthetic, GTs depend on imported sucrose from the leaves as the main C source. Several findings supported this theory including the enrichment of sucrose degrading enzymes in the trichomes, reduced levels of invertase inhibitors, and the 32 times lower CO_2 fixation found in GTs compared to leaves determined by ^{13}C - CO_2 pulse labelling experiments (Balcke et al., 2017). Additional evidence from transcriptomic studies in tobacco reveal upregulation of particular sucrose degrading enzymes such as sucrose synthase isoforms in the GTs (Nautiyal et al., 2020); while proteomic analysis of partially-photosynthetic GTs of cannabis indicate that raffinose, a trisaccharide, serves as the main photo-assimilate fueling the SM reactions (Conneely et al., 2021). Therefore, the C-input dependence in GTs prompts the question about the utility of the photosynthetic plastids in the glandular cells of the trichomes (Schuurink and Tissier, 2020).

Besides carbon supply, GTs require ATP and NADPH to fuel the SM biosynthetic reactions. Balcke and coauthors proposed a first model encompassing the energy distribution in photosynthetic GTs (Fig. 5A). Integration of the data suggested an uncoupling between light photosynthesis and carbon fixation processes in GTs of tomato. The expression of genes encoding photosystems I and II, although lower in the trichomes compared to leaves, differed

by less than 2-fold. Thus, it was proposed that light-dependent reactions still contribute actively to the supply of ATP and NADPH needed, especially for the MEP pathway. In contrast, genes involved in the Calvin-Benson-Bassham (CBB) cycle exhibited a more than 8-fold decrease in expression levels in GTs when compared to those in leaves. Nevertheless, Rubisco remained among the most highly expressed genes in GTs, leading to the hypothesis that Rubisco, outside of the CBB cycle, instead of fixing atmospheric CO₂, would recycle the CO₂ generated as a by-product from the metabolic reactions in what has been termed Rubisco bypass (Balcke et al., 2017; Schuurink and Tissier, 2020).

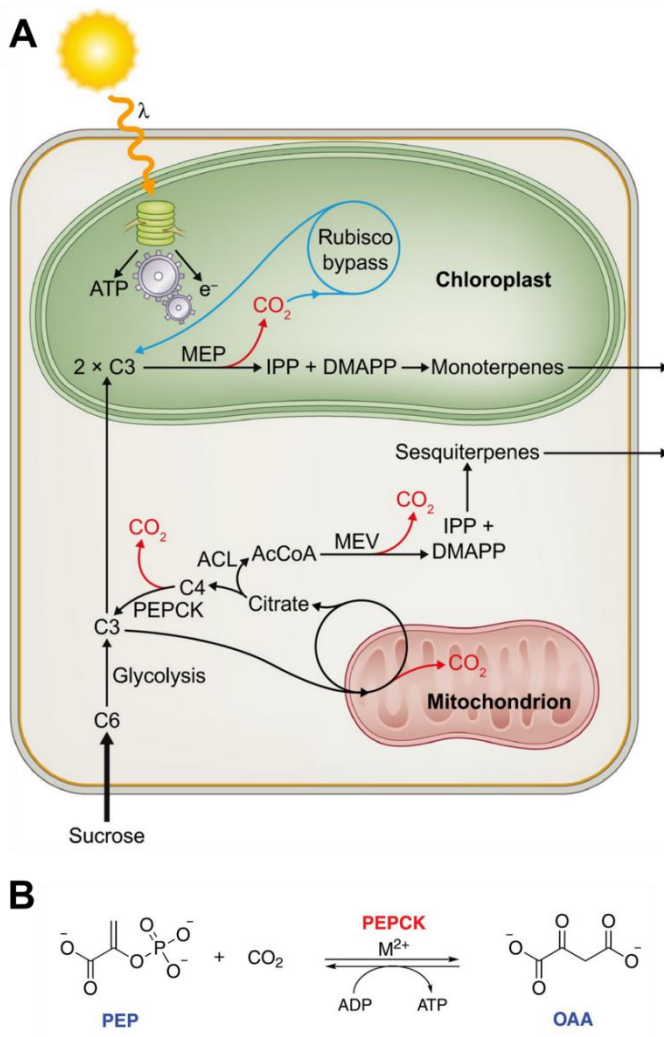


Figure 5. Putative and simplified model for the supply of carbon, energy and reducing power in photosynthetic glandular trichomes (GTs) of tomato.

(A) Chemical energy (ATP) and reducing power (NADPH) produced in the plastids is used to fuel the metabolic reactions, especially required in the MEP pathway. Since atmospheric carbon fixation is reduced in GTs, the carbon source is the sucrose imported from the leaf tissue. This C₆ molecule is converted to C₃ via glycolysis. The C₃ building blocks can enter the TCA cycle in the mitochondrion to produce citrate and subsequently acetyl-CoA, the precursor of the cytosolic MVA pathway. Breakdown of sugars in the plastids produce C₃ molecules that feed the MEP pathway to produce plastid derived monoterpenes. Because CO₂ is released as a byproduct from many reactions, Rubisco without the Calvin cycle, is able to refix it, in a so called Rubisco bypass and in turn, maximizing the carbon efficiency. **Abbreviations:** PEPCK, phosphoenolpyruvate carboxykinase; ACL, ATP-citrate lyase. Figure taken from Schuurink and Tissier, 2020.

(B) Schematic representation of *PEPCK* enzyme bidirectional reaction. PEP: phosphoenolpyruvate; OAA: oxaloacetate. Taken from Amaral et al. (2019).

Intriguingly, a specific isoform of *Rubisco small subunit* was identified in GTs of tobacco, whose expression is localized principally in the glandular cells of the trichomes (Laterre et al., 2017; Pottier et al., 2020). This particular isoform named NtRbcS-T (T stands for trichome) is able to change the kinetic properties of the Rubisco holoenzyme. It increases the catalytic rate and

the K_m , thereby conferring superior activity in acidic conditions (pH values < 8), consistent with the presence of a CO₂-rich environment in the GTs (Laterre et al., 2017). Overall, the evidence about Rubisco without or with a less active CBB cycle and the expression of a particular *NtRbcS-T* isoform in GTs, might hint at a distinct function of Rubisco holoenzyme in these cell factories.

1.1.6 Rubisco and the recycling of CO₂

Ribulose-1,5-bisphosphate carboxylase/oxygenase, commonly referred to as Rubisco catalyzes the key step of carbon fixation by carboxylation of ribulose-1,5-bisphosphate (RuBP) into two molecules of 3-phosphoglycerate (3PGA). In vascular plants, Rubisco is a complex formed by eight large subunits (RbcL), all encoded by a single gene located in the chloroplast, and eight small subunits (RbcS), frequently encoded by different genes in the nucleus, and abbreviated as L8S8 (Andersson and Backlund, 2008; Bracher et al., 2017). Although the catalytic site of Rubisco is located at the interface of two RbcL subunits (55 kDa), the RbcS (15kDa) are required for maximum Rubisco activity and can modify the kinetic properties of the L8S8 complex (Spreitzer, 2003; Ishikawa et al., 2011; Martin-Avila et al., 2020; Matsumura et al., 2020). The RbcL is widely conserved among different taxonomic groups and was recently categorized as one of the slowest evolving enzymes of the CBB cycle (Bouvier et al., 2023). In contrast, RbcS are more diverse in sequence, and copy number, usually present in multigene families across the plant species, although within the species, they share a high amino acid identity (Pottier et al., 2018; Cavanagh et al., 2023).

The discovery of *NtRbcS-T* in GTs of tobacco uncovered a yet uncharacterized phylogenetic cluster of RbcS-T isoforms that are different from the conventional RbcS isoforms found in mesophyll cells (RbcS-M), where most of the photosynthesis takes place (Laterre et al., 2017). Protein homologs to *NtRbcS-T* are spread across the plant kingdom, including the ancient bryophytes and pteridophytes. Based on their expression pattern, RbcS-T isoforms in plants are associated to non-photosynthetic tissues (Morita et al., 2014; Pottier et al., 2018). Recent studies on Rubisco kinetics using *Escherichia coli* (*E.coli*) demonstrated that when *NtRbcS-T* isoform is exclusively combined with RbcL, the Rubisco complex displayed the highest turnover and the lowest affinity to CO₂ in comparison to the other RbcS existing in tobacco (Lin et al., 2020). These two attributes given by *NtRbcS-T* resemble the properties of Rubisco typically associated with C₄ metabolism (Sage, 2002; Laterre et al., 2017), where high CO₂ concentration surrounds the complex in the bundle sheath cells, and low discrimination of CO₂/O₂ does not represent a disadvantage. However, phylogenetic analyses indicated that the presence of RbcS T-type was not associated to C₄ plants (Pottier et al., 2018).

The hypothesis of a CO₂ refixation by T-type RbcS-containing Rubisco could be associated with an adaptive process to the specific microenvironment of the glandular cells, making the biosynthesis of SM more carbon-efficient by reducing C loss. The ability of Rubisco to re-assimilate CO₂ was reported earlier in rapeseed (*Brassica napus*). In this species, Rubisco operates without the CBB cycle, and it can recover up to 40% of the CO₂ generated as a byproduct during the conversion of sugars to fatty acids, thereby increasing the efficiency of oil accumulation in the seeds (Schwender et al., 2004). This phenomenon has also been documented in soybean (Allen et al., 2009) and Arabidopsis (Lonien and Schwender, 2009) but no T-type RbcS are present in the genome of these species (Pottier et al., 2018), separating the CO₂ recycling capability with the possession of this particular T-type subunit. In general, CO₂ refixation can take place in different plant organs, often in non-foliar tissues with low stomata density, where the input of CO₂ from the atmosphere is very low and the C losses during respiration are minimized (Simkin et al., 2020). In conclusion, the recycling of CO₂ facilitated by Rubisco could represent a way to maximize the productivity in the GTs, and the expression of the *RbcS-T* would not necessarily be tied to this process, but rather to a better performance in a high CO₂ microenvironment.

1.1.7 PEPCK and the C₄-like metabolism in GTs of tomato.

The enrichment of specific isoforms involved in the CCM occurring in the GTs of tomato disclosed by Balcke et al. (2017) suggest that the finding of *NbRbcS-T* in tobacco is not an isolated case, and that more enzymes may contribute to the specialized metabolism in these micro-organs. From the “omics” dataset, several genes encoding proteins typically associated with C₄-like photosynthesis were differentially expressed in the GTs of C₃ tomato, including phosphoenolpyruvate carboxylase (PEPC), a plastidic NADP-malic enzyme (NADP-ME) isoform, and the cytosolic phosphoenolpyruvate carboxykinase (PEPCK). In the first step of C₄ photosynthesis, PEPC fixes CO₂ in the mesophyll cells forming oxaloacetic acid (OAA), a C₄ organic acid that is shuttled to the bundle sheath cells (BSC) in the form of malate or aspartate (Schlüter and Weber, 2020). As for NADP-ME and PEPCK, they constitute two different enzymes in charge of the decarboxylation step of the C₄ acid in the BSC, releasing CO₂ near Rubisco (Furbank, 2011).

Apart from their role in C₄ photosynthesis, NADP-ME and PEPCK are involved in different metabolic pathways regardless of the photosynthetic mechanism of the plants. For example, plastidic NADP-ME isoforms are involved in the response to drought and salt stresses (Doubnerová Hýsková et al., 2014; Kandoi and Tripathy, 2023). PEPCK plays a pivotal role in gluconeogenesis following seed germination, where lipid reserves are converted into sugars

that are required for seedling establishment (Eastmond et al., 2015). PEPCK facilitates the reversible conversion of OAA to phosphoenolpyruvate (PEP) and CO₂ through decarboxylation and phosphorylation, utilizing a nucleotide or pyrophosphate (PPi) to transfer a phosphoryl group (**Fig. 5B**) (Leegood and Walker, 2003; Amaral et al., 2019). PEPCK does also requires two metal ions for activity in vivo (generally Mn²⁺ and Mg²⁺) (Chen et al., 2002).

Although PEPCK functions as a decarboxylating enzyme in the afore mentioned processes, when high ATP/ADP ratios are present, PEPCK displays a $K_m(\text{CO}_2)$ comparable to Rubisco from C₃, C₄ and CAM photosynthesis (Chen et al., 2002). Since high physiological ATP/ADP ratios are expected to occur in GTs, it was hypothesized that PEPCK along with PEPC could operate as CO₂ fixing enzymes, producing C₄ acids in the cytosol. These C₄ compounds could be transported to the plastids and subsequently be converted into pyruvate (C₃), serving as a precursor for the MEP pathway, while the CO₂ released could be directly recycled by Rubisco (Balcke et al., 2017). In cannabis, high protein levels of PEPC were detected in the GTs, and it was proposed that this enzyme could play a role in the CO₂ refixation process, optimizing the C-economy in the trichome head cells (Conneely et al., 2021). This piece of evidence, in addition to the *RbcS-T* with C₄-like photosynthetic characteristics, suggest that GTs could harbor a C₄-like metabolism (Balcke et al., 2017).

1.2 Objectives of the Chapter 1

GTs are cell factories capable of producing large quantities of SM. Such productivity appears to be tightly supported by special features of the CCM taking place in these micro-organs. CCM is adapted to supply the required amount of energy and precursor molecules, at the expense of the sugars imported from the green tissues that constitute the main carbon source. Since gas exchange, and therefore atmospheric CO₂ fixation seems to be limited in the GTs (Balcke et al., 2017), the C economy appears to be extensively regulated by different enzymes and mechanisms, here exemplified through two hypotheses: First, the recycling of the CO₂ by Rubisco in a CBB-outside fashion, supported by a specific small subunit *RbcS-T*, that putatively confers better C fixation efficiency in this CO₂-rich environment; and second the activity of C₄-photosynthesis related enzymes such as PEPC, NADP-ME, and PEPCK that might contribute to the carboxylation-decarboxylation dynamics in the GTs.

With this context, the objectives of the first part of the present thesis are:

1. Characterize the orthologous gene of *Rubisco small subunit T-isoform (NtRbcS-T)* in tomato and elucidate the role of Rubisco in the GTs.
2. Determinate the contribution of *phosphoenolpyruvate carboxy-kinase (PEPCK)* in the productivity of the glandular trichomes of tomato.

1.3 Results

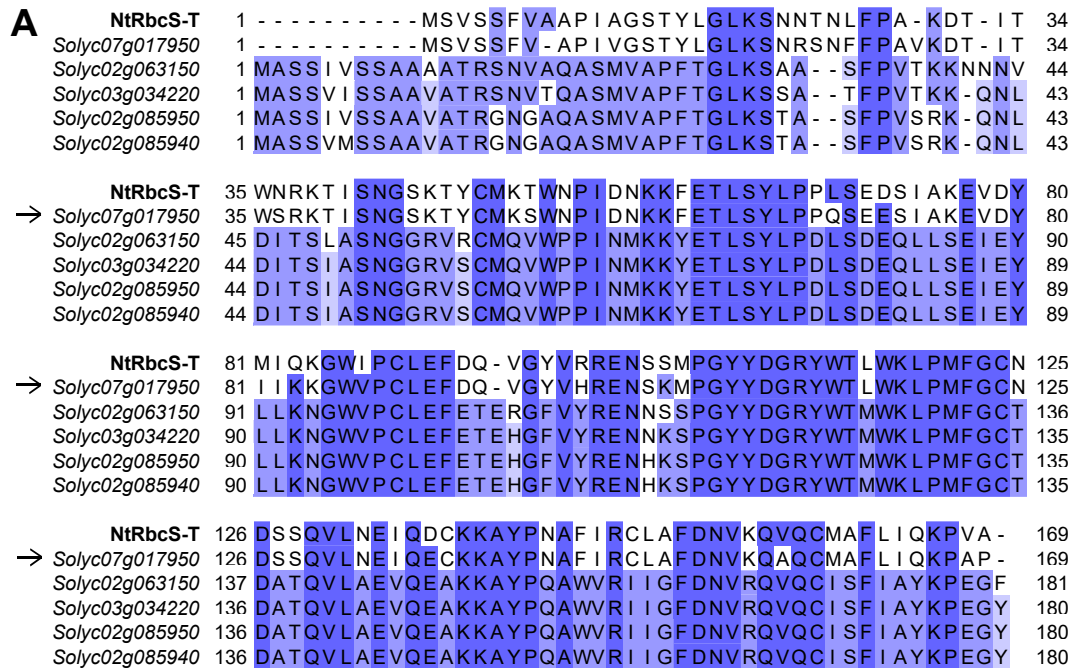
1.3.1 Identification of *NtRbcS-T* orthologous gene in tomato

With the aim to identify a candidate orthologous gene of the *N. tabacum RbcS-T* in tomato, the protein sequence (GenBank accession: DV157962; XP_016450162.1) was used as query to perform local alignments (BLASTP) against the *S. lycopersicum* protein sequences available in the NCBI database. Within the sequences producing significant alignments, five were annotated as Rubisco small subunits (RbcS). These RbcS were retained for global alignments (**Fig. 6A**). From all RbcS, the first hit XP_004243079.1, with gene ID Solyc07g017950 (SolGenomics) shared the highest percentage of identity and similarity with *NtRbcS-T* compared to the other RbcS isoforms in tomato (**Fig. 6B**), and from now on referred to as *S. lycopersicum RbcS-T* (*SIRbcS-T*). References to RbcS in tomato can be found in the literature dating back many years (Sugita and Gruissem, 1987), as well as their transcript regulation by different binding elements located in their promoter sequences (Meier et al., 1995). In general, these isoforms denominated “mesophyll isoforms” (Laterre et al., 2017) have overlapping expression patterns in the leaves, where RbcS-3B is predominant and some differences can be observed during the temporal-space development of the fruits (Meier et al., 1995). Clear differences in the amino acid composition of *SIRbcS-T* contrast with the highly conserved sequences of the mesophyll isoforms (**Fig. 6A**).

To find out whether this candidate gene is expressed in GTs, RNA from isolated trichomes and from trichome-free leaves was extracted and the expression levels of *SIRbcS-T* were measured by qRT-PCR, including samples of the cultivated and the wild tomato *S. habrochaites*. The results showed that *SIRbcS-T* is expressed three and 11 times more in the trichomes compared to leaves in the cultivated and in the wild tomato, respectively (**Fig. 7A**). Due to the higher GT density in *S. habrochaites* compared to the cultivated varieties (**Fig. 2**), the transcripts detected in the leaves could potentially be attributed to traces of trichomes in the samples.

To confirm the previous analysis, 2 kb upstream of the start codon of *S. habrochaites RbcS-T* was amplified by PCR and cloned in front of the green fluorescent protein (*GFP*) and transformed both into the wild *S. habrochaites sp. glabratum* (VI030462) and the cultivated tomato cv. Moneymaker. The transformed *RbcS-T* reporter lines displayed *GFP* fluorescence in GTs, but, surprisingly, exclusively in the gland cells of type-I and type-IV trichomes (**Fig. 7B**). These types of trichomes share the same capitate structure but type-I contain more stalk cells than type-IV which make them longer. The same expression pattern was observed in the reporter lines of the transformed wild accession (**Fig. 7B**). These results explain the almost 200 times higher transcript levels of *RbcS-T* in the trichome samples of the wild accession

compared to the cultivated tomato, since the former possess higher number and constitutively develops type-IV GTs. This type of GTs resembles the capitate GTs of *N. tabacum* not only because of a similar anatomical structure but also because of the type of SM they produce, such as acylsugars (AS) (Uzelac et al., 2021).

**B**

Gene ID	Name	Protein (aa)	Identity	Similarity
Solyc07g017950	<i>RbcS-T</i>	169	89,35%	93,5%
Solyc02g063150	<i>RbcS-1</i>	181	51,22%	61,3%
Solyc03g034220	<i>RbcS-2A</i>	180	53,90%	64,9%
Solyc02g085950	<i>RbcS-3B-1</i>	180	53,90%	65,9%
Solyc02g085940	<i>RbcS-3B-2</i>	180	53,90%	65,9%

Figure 6. Candidate orthologous genes of *NtRbcS-T* in tomato.

(A) Global alignment using amino acid sequence between the Rubisco small subunit trichome-specific from *Nicotiana tabacum* (*NtRbcS-T*) and the different RbcS isoforms present in the genome of *S. lycopersicum*, obtained from NCBI. The gene IDs were acquired from the Sol Genomics Network (solgenomics.net). Intensity of the color depicts the percentage of identity within the sequences. The candidate ortholog of *NtRbcS-T* in tomato is indicated by the arrow, identified with the gene ID Solyc07g017950. **(B)** Percentages of identity and similarity of the different RbcS members of tomato compared with *NtRbcS-T*. Multiple sequence alignment performed with the Clustal Omega v1.2.4. <https://www.ebi.ac.uk/Tools/msa/clustalo/>

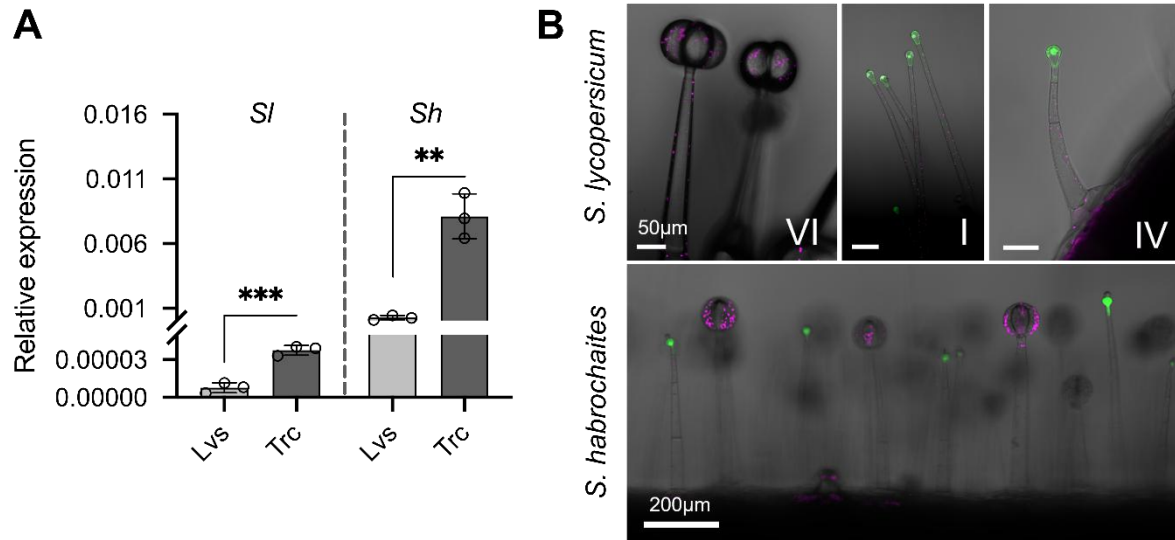


Figure 7. *S. lycopersicum RbcS-T* (*SIRbcS-T*) is expressed in glandular cells of type-I and type-IV GTs.

(A) Relative expression levels of *SIRbcS-T* in leaves (Lvs) and trichomes (Trc) of *S. lycopersicum* (Sl) and *S. habrochaites* (Sh). **(B)** Laser scanning microscope (LSM) images of GTs of *ShRbcS-T* promoter-*GFP* reporter lines. GFP signal is depicted in green color and chlorophyll fluorescence in magenta color. Error bars indicate standard deviation. ** $P < 0.01$, *** $P < 0.001$; using Student's *t*-test.

The first report on *SIRbcS-T* in tomato was made by Morita et al. (2016). The authors used the information of one rice *RbcS* isoform (*OsRbcS1*) that is expressed in non-photosynthetic tissues, to find out orthologous genes in other plant species. In tomato the *SIRbcS-T* is the ortholog of *OsRbcS1* and according to the aforementioned study, *SIRbcS-T* is expressed in floral organs including stamen and pistil, as well as in early stages of the fruit development (Morita et al., 2016). With this information, tissue from the floral organs and from different stages of the fruit were collected and the expression levels were compared. The results showed that the transcript levels of *SIRbcS-T* are more abundant in the pistils and in the immature green fruits (**Fig. 8A-B**) consistent with previous reports. Furthermore, the reporter lines revealed specific expression of *SIRbcS-T* in the exocarp of the green fruits, particularly within the cell layer close to the ongoing cuticle formation (**Fig. 8C**). Unexpectedly, GFP signal was also observed in the stalk cells of the trichomes (typically type-VI GTs) that were covering the surface of the exocarp of the fruit. Additionally, a fluorescent signal was also detected in the seeds of fruits of the same developmental stages (**Fig. 8C**).

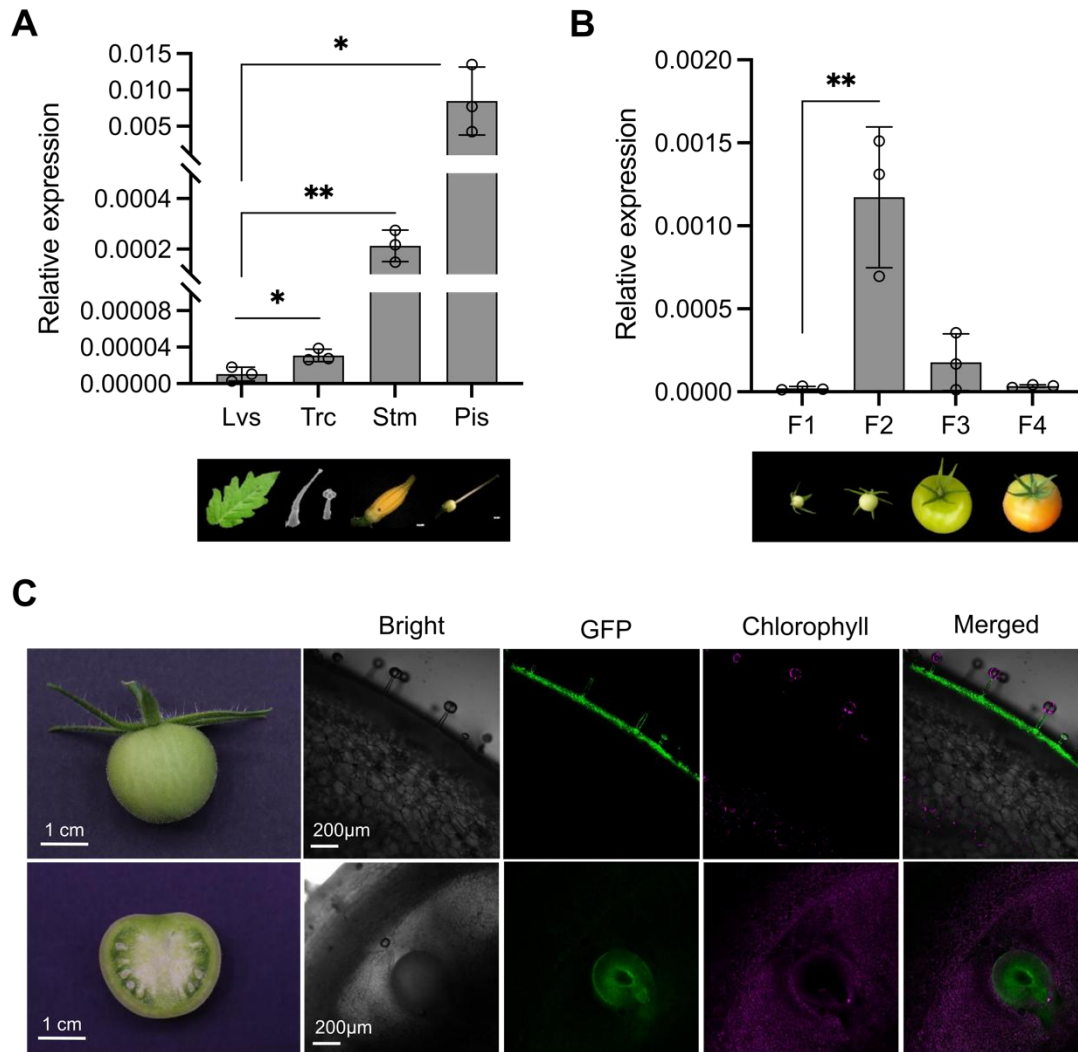


Figure 8. Relative expression of *SIRbcS-T* in different tissues.

(A), such as Leaves (Lvs), trichomes (Trc), stamens (Stm) and pistils (Pis); and different fruit developmental stages (B). F1 \approx 1 cm immature green fruit, 10-day post anthesis (DPA), F2 \approx 2 cm immature green fruit 20-DPA, F3 mature green exocarp, F4 breaker exocarp. (C) Laser scanning microscope (LSM) images of immature green fruit exocarp section (upper panel) and developing seeds (lower panel) of a *SIRbcS-T* GFP reporter line. GFP signal is depicted in green color and chlorophyll fluorescence in magenta color. * $P < 0.05$, ** $P < 0.01$; using Student's *t*-test.

1.3.2 Functional characterization of *SIRbcS-T* in GTs of tomato

The specific expression of *SIRbcS-T* in capitate type-I/IV trichomes prompted us to generate loss-of-function mutants using Clustered Regularly Interspaced Short Palindromic Repeats (CRISPR)- associated protein 9 (CRISPR-Cas9) approach. Three single guide RNAs (sgRNAs) targeting different sites of *SIRbcS-T* sequence were selected and cloned inside an expression vector, including the Cas9 protein and the selection marker for kanamycin resistance (Fig 9A). Construction of the expression vector was performed using the Golden

Gate method (Engler et al., 2008; Weber et al., 2011) and the genetic transformation of tomato cv MoneyMaker was conducted according to the protocol by Van Eck et al. (2019). Two independent transgenic lines were selected, and the point mutations were characterized by sequencing (**Fig. 9A**). Frameshifts caused by insertions/deletions lead to premature stop codons in the coding sequence. The *SIRbcS-T* knock-out (*slrbcS-T KO*) lines were propagated, and the T-DNA was segregated from the plants to obtain T-DNA free homozygous lines. After self-pollination, plants from the T2 progeny were used for metabolite profiling. Although the expression of *SIRbcS-T* was not detected in type-VI GTs, VOCs, including mono and sesquiterpenes produced by this type of trichomes were first evaluated using gas chromatography-mass spectrometry (GC-MS). As expected, VOCs did not show differences between the control and the *slrbcS-T* lines (**Fig. 9B**). Next, changes in the productivity of type-I/IV trichomes were analyzed by quantifying AS, the main products of these type of GTs. In cultivated tomato, the presence of type-IV trichomes has been described as a juvenile trait, since they are only observed at the early stages of plant development (Vendemiatti et al., 2017). AS were extracted from the leaf surface and examined by liquid chromatography-mass spectrometry (LC-MS) using the second set of leaves of 3-week-old plants. After integrating the peak areas of the main AS, although low abundant, the levels did not differ from the control plants (**Fig. 9C**).

To identify a potential phenotype associated with the function of *SIRbcS-T* in type-I/IV trichomes, the *slrbcS-T* mutants were submitted to heat stress (HS). As reported by Säbel et al. (2023), HS can induce type-IV trichome development in non-juvenile leaves, and boost AS productivity in cultivated tomato. The HS experiments were conducted following the experimental set up according to Säbel et al. (2023). In short, WT and *slrbcS-T* mutant lines were germinated in control conditions. After one week, half of the seedlings were transferred to HS, consisting of 37°C during the light phase of the day and 23°C at night, for a period of two weeks. AS were estimated following the same method as the previous experiment. As a result of the HS, the AS increased, but the extent of the increment was comparable between the WT and the *slrbcS-T* mutants, with no significant differences (**Fig. 9C**). RNA from CN and HS samples was extracted, and relative expression of *SIRbcS-T* was measured by qRT-PCR. The results could show that *SIRbcS-T* expression levels increased in HS (**Fig 9D**). However, this increase could be explained most probably by the higher type-IV trichome density. Besides the screening of the typical compounds produced by the GTs, no other differences were observed in the *slrbcS-T* KO lines, for example in the flowers or seed development, where this Rubisco small subunit is also expressed (**Fig. 8**).

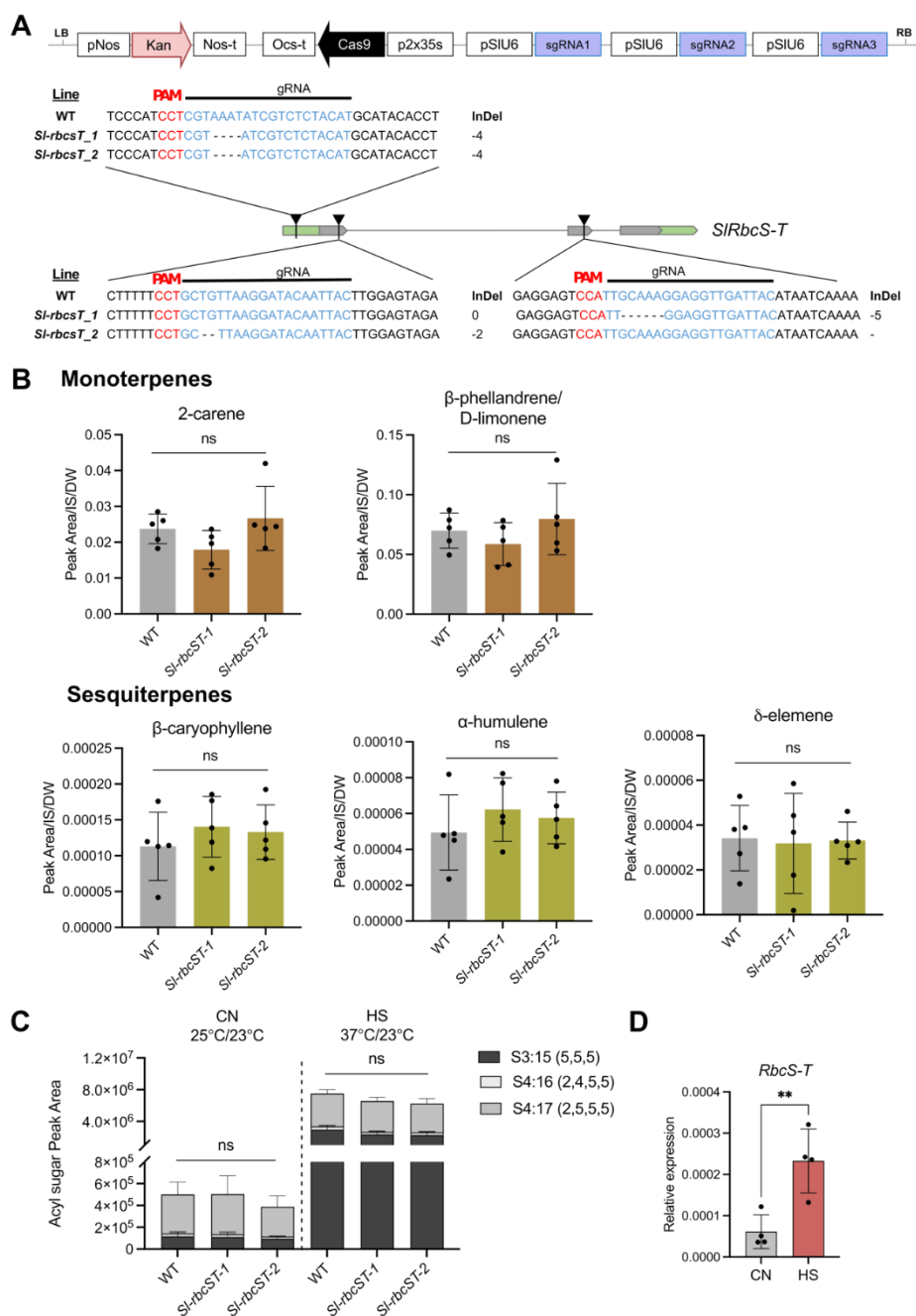


Figure 9. Functional characterization of *RbcS-T* in cultivated tomato (*SIRbcS-T*).

(A) Schematic representation of the T-DNA used to generate mutations in the *SIRbcS-T* gene and the point mutations generated in the different lines. Exons are represented in gray and UTRs in green colors. Location of the expected CRISPR/Cas9 cleavage sites are depicted by the black arrow heads. (B) Quantification of mono and sesquiterpenes using gas chromatography-mass spectrometry (GC-MS) of the *SIRbcS-T* mutant lines ($n = 5$). (C) Acyl sugar quantification of the *slRbcS-T* mutant lines using liquid chromatography-mass spectrometry (LC-MS) ($n = 4$). Plants were grown for two weeks in control (CN) or in heat stress (HS) conditions (37°C during the day). (D) Relative expression of *SIRbcS-T* in CN and HS plants ($n = 4$). Error bars indicate standard deviation. Ns indicate no statistical significance after one-way ANOVA with Tukey's test ($P < 0.05$). ** $P < 0.01$, using Student's *t*-test.

Wild tomato species such as *Solanum habrochaites* develop type-IV trichomes constitutively all over the plant and the AS productivity is much higher compared to the one in the cultivated tomato (McDowell et al., 2011; Balcke et al., 2017). With the aim of testing whether the RbcS-T isoform plays a role in the trichome metabolism of this wild species, CRISPR/Cas9 KO of *S. habrochaites sp. glabratum* (VI030462) (Devi, 2022), were generated following the described approach used for cultivated tomato. Contrary to other *S. habrochaites* accessions, VI030462 can self-fertilized, which is an advantage for seed production. For gene targeting, two sgRNAs used for the cultivated tomato to target *SIRbcS-T* were modified according to the sequence of the gene in *S. habrochaites* (Fig. 10A). Regenerated transgenic plants were propagated in greenhouse conditions and the T-DNA was segregated away. Two homozygous and one bi-allelic lines were examined for AS productivity (Fig. 10A-B). AS were extracted from leaf surface and quantified by LC-MS. AS present in this wild accession were identified and characterized in a previous work (Devi, 2022). Peak areas from the different AS present in the extracts were integrated and compared to the WT. Although slight differences were observed in some AS, they were not statistically different (Fig. 10C).

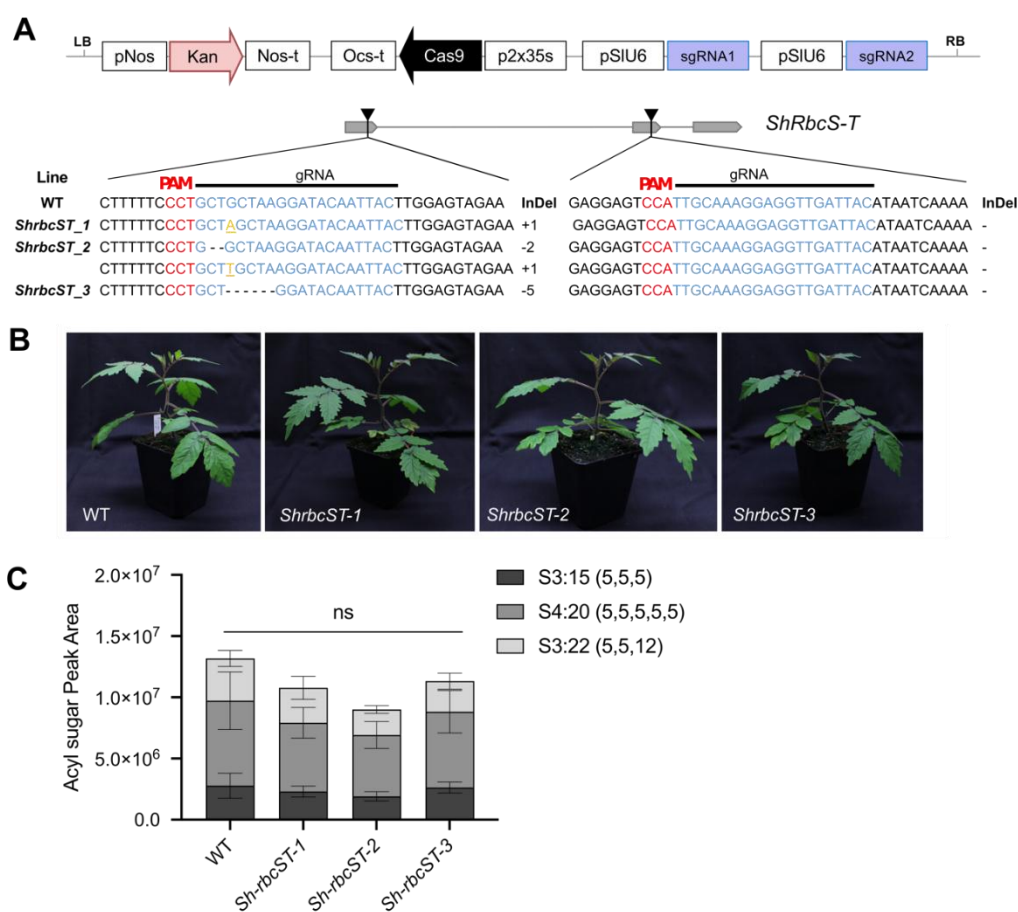


Figure 10. Functional characterization of Rubisco small subunit trichome specific (*RbcS-T*) isoform in wild tomato accession *S. habrochaites* (*ShRbcS-T*).

(A) Schematic representation of the T-DNA used to generate mutations in the *ShRbcS-T* gene and the point mutations generated in the different lines. Exons are represented in gray color. The location of the

expected CRISPR/Cas9 cleavage sites is depicted by the black arrowheads. **(B)** Four weeks old *ShRbcS-T^{KO}* lines grown in phytocabinet in control conditions. **(C)** AS quantification of the *ShRbcS-T* mutant lines using liquid chromatography- mass spectrometry (LC-MS) ($n = 4$). Error bars indicate standard deviation. Ns indicate no statistical significance within individual AS, after one-way ANOVA using the Tukey's test ($P < 0.05$).

In parallel with the ongoing thesis research, an orthologous gene of *SIRbcS-T* was identified in the wild tomato species *Solanum pennellii* with the name *SpRBCS1* (Sopen07g006810) (Ji et al., 2023). *S. pennellii* is recognized for its high type-IV trichome density, producing a blend of AS at elevated quantities representing up to 20% of the leaf dry biomass (Fobes et al., 1985; Schillmiller et al., 2012). *SpRBCS1* was identified as one of the highest differentially expressed genes between high versus low-AS-producing lines from an F2 population, derived from the cross between *S. pennellii* and *S. lycopersicum*. Functional validation using virus-induced gene silencing (VIGS) concluded that the downregulation of *SpRBCS1* resulted in a 23% average reduction of AS levels (Ji et al., 2023). With the aim of validating and building upon the findings reported in the above-mentioned study, VIGS experiment in this wild tomato accession was performed using tobacco rattle virus (TRV)-based silencing vectors (Liu et al., 2002). For this, four different vectors were designed. One vector harboring a specific fragment targeting the *SpRBCS1* mRNA (here simplified as *RbcS-T*) and another vector harboring a highly conserved sequence targeting simultaneously the mesophyll *RbcS* (*RbcS-M*) mRNA isoforms in *S. pennellii*. The idea behind the second vector was to determine the specificity of the VIGS targeting similar isoforms and compare the effects of the silencing of the *RbcS-T* versus the possible effects of the non-trichome specific isoforms for AS productivity. The next two vectors comprised combinations of each Rbc fragment (T or M) with a sequence of *Magnesium Chelatase Subunit H* (*ChlH*), a gene used as a visual marker to spot where the gene silencing occurs (Szymański et al., 2020). A total of six *pTRV1/pTRV2* plasmid combinations were used to inoculate *S. pennellii* LA0716, the same accession used in Ji et al. (2023). After five weeks, plants infected with the co-silencing vectors containing the *ChlH* marker displayed a widespread chlorotic phenotype, providing evidence of the efficiency of the VIGS during the experiment (**Fig. 11A**). Furthermore, while the *RbcS-T* VIGS plants did not show phenotypic differences compared to the *pTRV2* empty vector (*pTRV2-EV*), the *RbcS-M* VIGS plants exhibited light green spots, suggesting that the silencing of the mesophyll isoforms reduced the pigment content (**Fig. 11A**). A similar phenotype can be observed in other plant species when simultaneous mutagenesis of several *RbcS* genes is performed (Donovan et al., 2020).

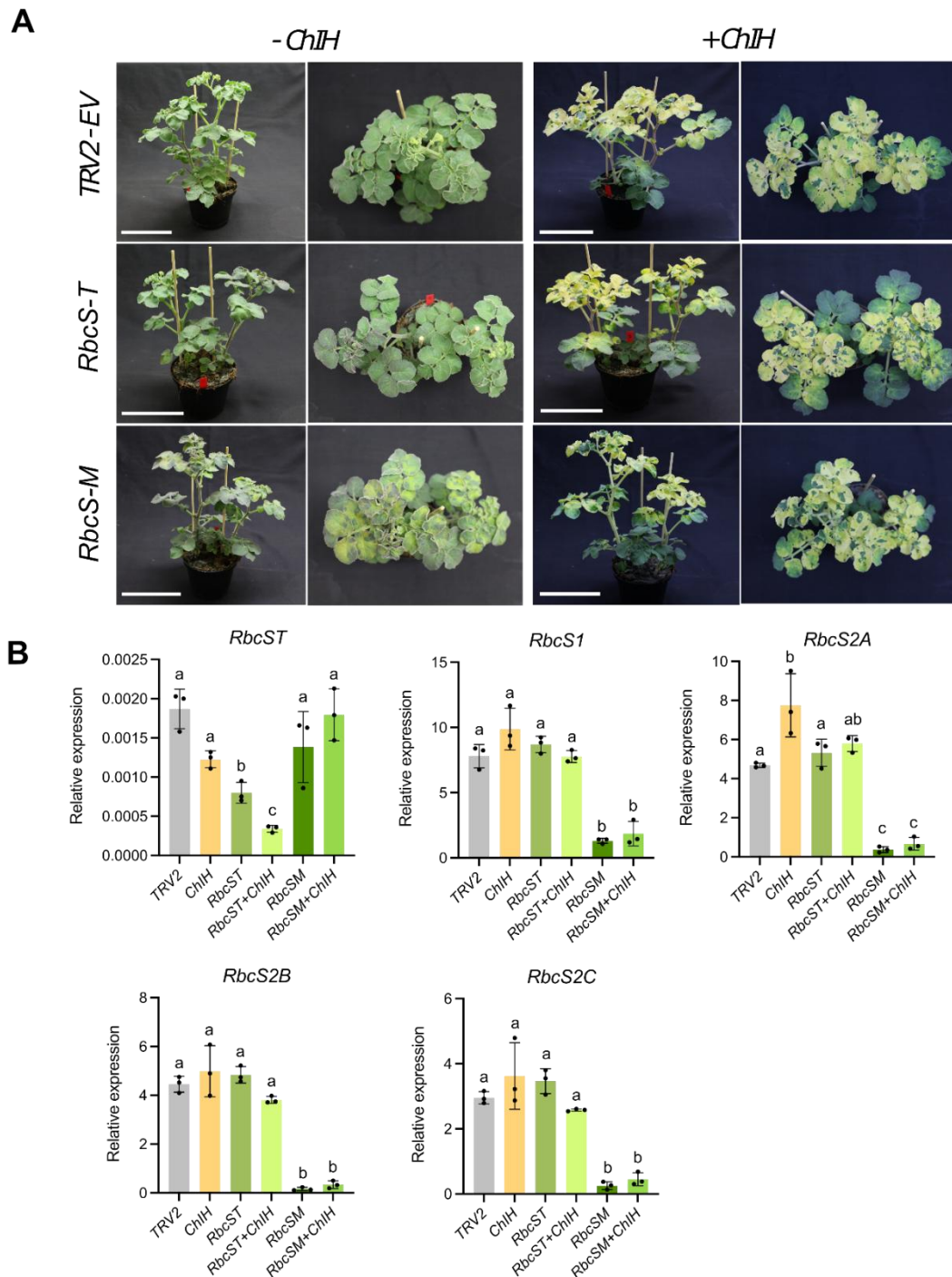


Figure 11. Virus-induced gene silencing (VIGS) assay of *Rubisco small subunit trichome specific (RbcS-T)* and the simultaneous silencing of the *RbcS* mesophyll isoforms in the wild tomato *S. pennellii*.

(A) Images of *S. pennellii* plants after five weeks of inoculation with the VIGS displaying the silencing effect of the single gene vectors and the co-silencing with the visual marker *ChIH* (*Magnesium Chelatase Subunit H*). Scale bars = 8cm. **(B)** Relative expression using qRT-PCR of the *RbcS-T* and the *RbcS-M* isoforms (*RbcS1*, *RbcS2A*, *RbcS2B*, *RbcS2C*) in the silenced plants ($n = 3$). TRV2 denotes the empty vector (pTRV2-EV). Error bars indicate standard deviation. Different letters indicate statistical significance after one-way ANOVA with Tukey's test ($P < 0.05$).

Expression analysis revealed that compared to the *pTRV2-EV* plants, *RbcS-T* transcripts were reduced by 67% using the single fragment vector version, and by 81% in the co-silencing vector containing the *ChlH* fragment (**Fig. 11B**). Moreover, the expression of the different mesophyll isoforms *RbcS-M* (*RbcS1*, *RbcS2*, *RbcS2B*, *RbcS2C*) remained unchanged in the *RbcS-T* VIGS plants, indicating the specificity of the fragment to downregulate this isoform (**Fig. 11B**). Regarding the *RbcS-M* VIGS plants, the level of expression of the individual *RbcS-M* isoforms were reduced from 86 to 96% compared to *pTRV2-EV* plants. The reduced silencing effect observed for *RbcS-T* compared to the *RbcS-M* isoforms in the respective infected plants could be explained by the general heterogeneous silencing effect of VIGS and the potential variation in trichome densities, considering that this isoform is expressed exclusively in the gland cells of type-I/IV trichomes. Additionally, silencing *RbcS-M* resulted in less pigment accumulation in the leaves, facilitating the selection of the silenced tissues for further analyses.

Leaf samples of similar size were sampled from the top branches of the plants for metabolite surface extraction, and the AS were estimated using LC-MS. First, the AS profiles of *pTRV2-EV* and *ChlH* controls were compared to establish whether there was an effect in the productivity due to the chlorosis effect of the visual marker. The results indicated that most of the AS exhibited alterations in the relative abundance (**Fig. 12A**). For example, AS 435/G3:12, 519/G3:18 and 681/S3:18 were significantly reduced while AS 547/G3:20 and 709/S3:20, significantly increased in the *ChlH* samples (**Fig. 12A**). Since the silencing of *ChlH* affected the AS in different ways, the samples from co-silencing were not used for the analysis, and only the samples with single fragments were considered. When comparing the different AS, no differences were observed between the *pTRV2-EV* and *RbcS-T* samples (**Fig. 12B**). Instead, significant differences in specific AS were observed only in the *RbcS-M* samples, where all the mesophyll isoforms were targeted. These particular AS exhibited the same trend (decrease/increase) observed in the *ChlH* samples, suggesting that a potential decrease in carbon fixation and chlorophyll biosynthesis had a significant effect on specific AS.

Besides the prolific amount of AS produced by *S. pennelli* compared to cultivated tomato, these sugar esters are structurally diverse. Most AS in this wild species consist of glucose molecules (acylglucoses) esterified with three acyl chains of different length and composition (Shapiro et al., 1994; Leong et al., 2019). Each class of AS, for which the peak area was calculated, comprises a group of AS sharing the same molecular mass (m/z of $[M+HCOO]^-$) but differing in acyl group composition (**Table S1**). Based on the results of the VIGS experiment, it was noticed that AS showing reductions are particularly enriched in iC_4 acyl chains, whereas those exhibiting increases are enriched in iC_5 acyl chains. A clear example is the AS 435/G3:12 that significantly decreased in both *ChlH* and *RbcS-M* VIGS samples, and whose sugar core

structure is solely esterified by iC4 acyl chains: G3:12(4,4,4) (**Fig. 12A-B**). The rest of the analyzed AS have a mixed acyl chain composition, incorporating both iC4 and iC5 chains, as well as long acyl chains. Two AS 709/S3:20 and 547/G3:20 showed, on average, an increase in the *ChIH* and *RbcS-M* VIGS samples. In the case of 709/S3:20, peak areas from the two classes of AS (S3:20(5,5,10) and S3:20(4,4,11)) were separately integrated based on retention time and the main MS/MS mass fragments observed. The results revealed an increase in AS containing iC5 acyl chains, while those containing iC4 acyl chains were depleted compared to the *pTRV2-EV* and *RbcS-T* silencing samples (**Fig. 13**). In the case of the second AS example, 547/G3:20, although it was not possible to discern an AS exclusively with iC5 acyl chains, the predicted area of S3:20(5,5,10)/(4,6,10) resulted in higher peak areas compared to S3:20(4,4,11), whose peak areas were diminished in the *ChIH* and *RbcS-M* samples (**Fig. 13**). These results imply that the increase in certain AS is likely due to the contribution of the iC5-esterified AS rather than a general boost of AS from a particular molecular mass.

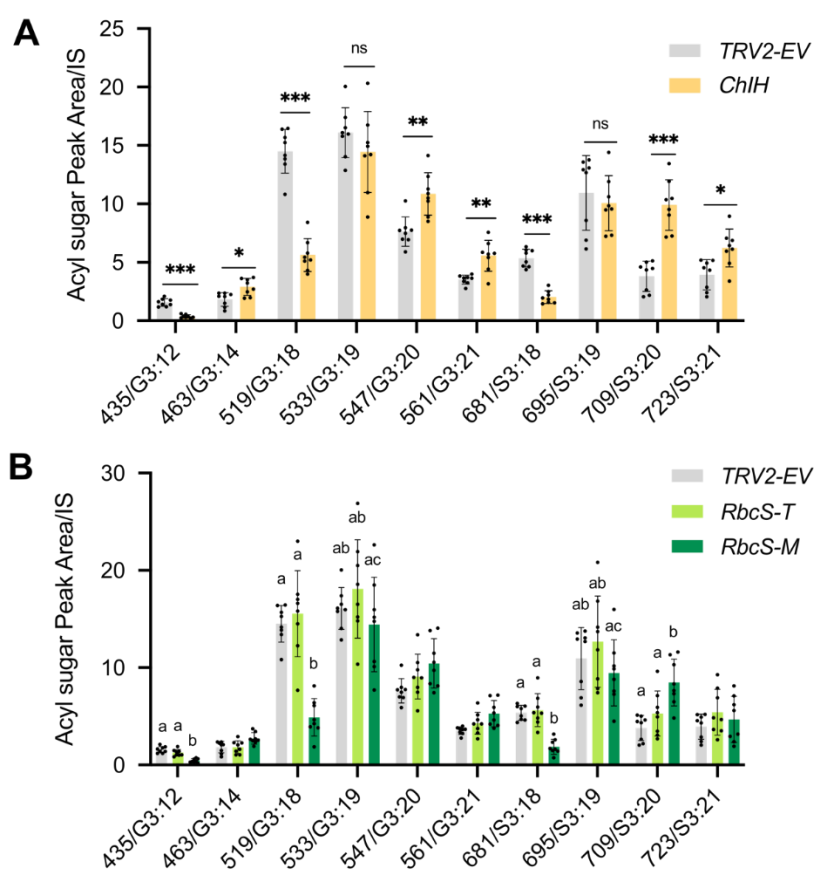


Figure 12. Acylsugar (AS) quantification of the VIGS assay using liquid chromatography-mass spectrometry (LC-MS)

(A) Comparison of different AS in the empty vector (*pTRV2-EV*) and the empty vector version containing the co-silencing visual marker *ChIH* (*Magnesium Chelatase Subunit H*). **(B)** Comparison of different AS after gene silencing of *RbcS-T* and *RbcS-M*. Peak areas of the AS with the same mass (m/z of $[M+HCOO]^-$) were combined and integrated and normalized to the internal standard (IS). Nomenclature

of the AS comprises the first three numbers of the molecular mass (m/z of $[M+HCOO]^-$) followed by first part of the AS standard nomenclature indicating sugar composition (sucrose or glucose), the number of aliphatic acyl groups and the sum of the aliphatic carbons after the colon. Error bars indicate standard deviation ($n = 8$, biological replicates). Pair comparisons were conducted using Student's t -test, $*P < 0.05$; $**P < 0.01$; $***P < 0.001$. Different letters within the three-sample group ($pTRV2$ -EV, $RbcS$ -T, $RbcS$ -M) indicate statistical significance after one-way ANOVA with Tukey's test ($P < 0.05$).

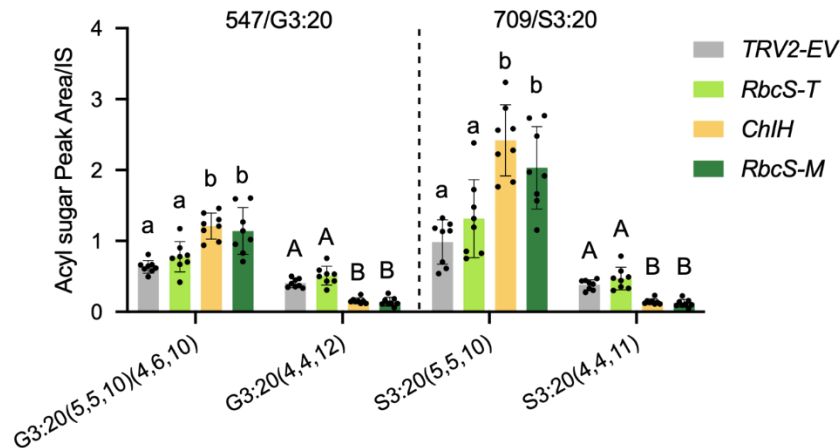


Figure 13. Quantification of acylsugars (AS) peaks sharing the same molecular mass (m/z of $[M+HCOO]^-$) but different acyl chain composition.

Quantification based on retention time and the main MS/MS mass fragments. Peak areas of AS were re-integrated and normalized to the internal standard (IS). AS nomenclature comprises an initial letter that indicates the sugar core (G:glucose or S:sucrose) and the number of acyl chains, then the sum of carbons in all acyl chains after the colon, followed by the number of carbons in each acyl chain in parenthesis. Error bars indicate standard deviation. Different letters indicate statistical significance after one-way ANOVA with Tukey's test ($P < 0.05$).

1.3.3 Role of Rubisco in type-VI glandular trichomes.

Results from different experiments pointed out that, although specific, $RbcS$ -T is expressed at very low levels and exclusively in type-I/IV GTs (Fig. 7-8). Trichome fractions isolated from cultivated tomato are highly enriched with type-VI trichomes, since they are the most abundant type of GTs present throughout vegetative growth (Bergau et al., 2016). Expression analysis on isolated trichomes reveals that, despite a significant reduction in the transcript levels of the $RbcS$ -M in the trichomes compared to leaves, all the mesophyll isoforms were present and expressed at very high levels (Fig. 14).

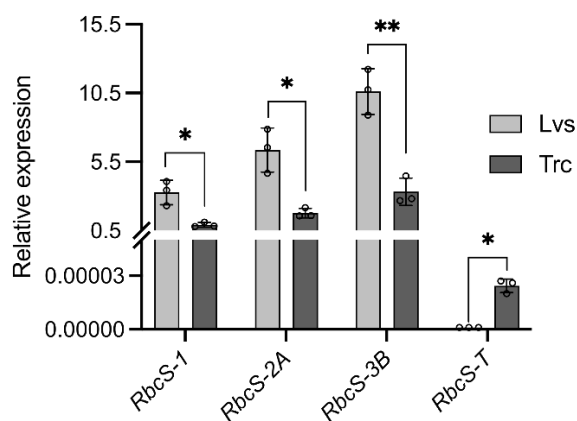


Figure 14. Transcript levels of mesophyll *Rubisco* small subunits *RbcS* in leaves (Lvs) vs trichomes (Trc) of *S. lycopersicum* compared to *RbcS-T*.

Error bars indicate standard deviation, $n = 3$. * $P < 0.05$, ** $P < 0.01$, using Student's t-test.

Creating loss-of-function mutants of Rubisco to study its function in specific tissues or micro-organs, such as GTs, represents a challenge due to the indispensable role this enzyme plays in carbon fixation. To elucidate the contribution of Rubisco holoenzyme in photosynthetic type-VI GTs, a CRISPR-based tissue-specific knockout system (CRISPR-TSKO) (Decaestecker et al., 2019) was implemented to mutate simultaneously all the mesophyll isoforms specifically in the glandular cells of the trichomes without generating pleiotropic growth defects on the plants. The successful application of this technique hinges on the use of a trichome-specific promoter, essential for driving the expression of the Cas9 protein. To select a suitable candidate promoter, transcript levels of different type-VI preferentially-expressed genes were assessed, including different terpene synthases such as *TPS9*, *TPS12* and *TPS20* (Kortbeek et al., 2016; Zhou and Pichersky, 2020), the *Early light-inducible protein 1 (ELIP1)* (Balcke et al., 2017) and the *Metallocarboxypeptidase inhibitor (MCPI)* (Schillmiller et al., 2010; Wang et al., 2022). The qRT-PCR experiments revealed that *MCPI* was expressed about 15 times more than the other tested genes in the GTs (**Fig. 15A**). Reporter lines of *ELIP1* promoter sequence and protein reporter lines of *MCPI* promoter sequence generated via stable genetic transformation displayed fluorescence in the glandular cells of type-IV trichomes (**Fig. 15B**). Based on the elevated transcript levels of *MCPI* and the references from literature regarding the use of this promoter to metabolically engineer type-VI trichomes (Wang et al., 2022), the *MCPI* promoter was selected for the CRISPR-TSKO approach in the trichomes.

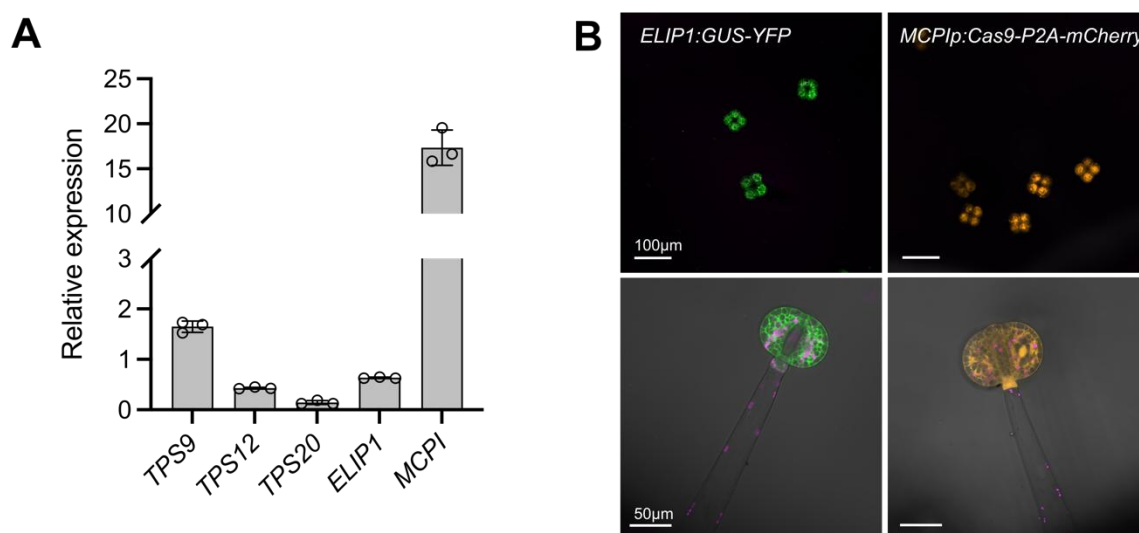


Figure 15. Selection of candidate promoters for CRISPR-based tissue-specific knockout system (CRISPR-TSKO) in type-VI GTs.

(A) Relative transcript levels of candidate genes expressed in glandular cells of type-VI GTs ($n = 3$). *TPS*, Terpene synthase; *ELIP1*, Early light-inducible protein 1; *MCPI*, Metalloprotease inhibitor. **(B)** Laser scanning microscope (LSM) images of transgenic reporter lines showing specific expression of fluorescence markers under the control of the *ELIP1* and *MCPI* promoters in glandular cells of type-VI trichomes.

As proof-of-concept, a construct targeting the coding sequence of the terpene synthase 20 (*TPS20*) was designed using two sgRNAs. *TPS20* catalyzes the formation of the major monoterpenes produced in type-VI trichomes of cultivated tomato. Additionally, the Cas9 coding sequence was fused to *mCherry* marker gene using the P2A ribosomal skipping peptide to track visually the expression of Cas9 (**Fig. 16A**). Subsequently, this construct was transformed into tomato *S. lycopersicum*. After selection and PCR screening, only one positive transgenic line was obtained. Genomic DNA from the leaf tissue of T1 plants was extracted, and a 576-base pair target region, encompassing the cleavage sites of the two gRNAs, was amplified using PCR. The amplification products from the CRISPR line (*TPS20-CR*) and the WT were subjected to sequencing to determine the spectrum and frequency of the targeted mutations. The decomposition analysis based on the capillary sequencing revealed a diverse type of indels, mostly deletions, although the most common indel was the insertion of one nucleotide (**Fig. 16C**). The analysis of VOC from *TPS20-CR* line revealed a drastic reduction of β -phellandrene and 2-carene, both monoterpene products of *TPS20*, while the sesquiterpenes remain unchanged. Simultaneously, the GC-MS chromatogram exhibited the accumulation of a new peak, predicted as Nerol, representing the immediate precursor of the aforementioned monoterpenes (**Fig. 16D**) (Zhou and Pichersky, 2020).

Next, a binary vector was assembled, incorporating the *MCPI* promoter driving Cas9 protein and three sgRNAs targeting each *RbcS-M* isoform (*RbcS1*, *RbcS2A*, *RbcS3B-1* and *RbcS3B-2*), and subsequently transformed into tomato cv MoneyMaker (**Fig. 17A**). Different transgenic lines were obtained and screened for the T-DNA insertion. Some of the regenerated plants showed patchy and lighter green coloration, suggesting that in these lines the *MCPI* promoter leads to some expression in the leaf (**Fig. 17B**). Since the objective was to assess the impact of knocking out Rubisco in the GTs, lines with different phenotypes compared to WT were excluded from further analyses. Three T-DNA positive lines were selected, and seeds of the T1 generation were sown in a phytochamber, under control conditions. After four weeks of growth, VOC profiling was performed using GC-MS (**Fig. 17C**). The results showed a reduction trend in monoterpenes, in some cases significantly different, in at least two out of the three independent lines evaluated (**Fig. 17C**). For example, monoterpenes β -phellandrene/D-limonene, peak with the highest signal intensity, showed between 22 and 34% reduction in average in *MCPI:Cas9* lines 6 and 12 compared to the WT. In contrast, no changes in the sesquiterpenes were observed, except for the *MCPI:Cas9* line 4, which produced higher β -caryophyllene and α -humulene levels than to the other lines (**Fig. 17C**).

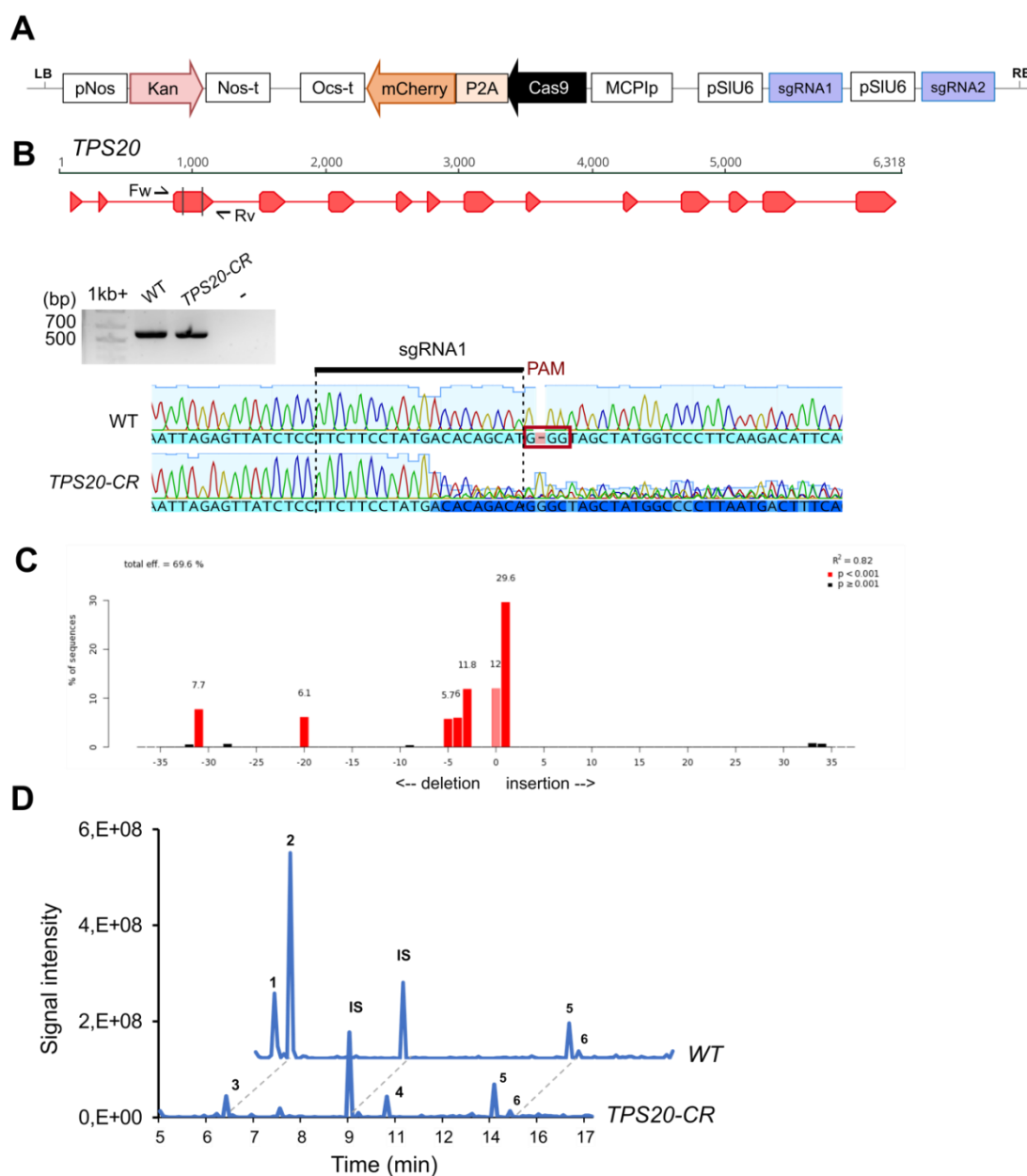


Figure 16. Proof-of-concept of the CRISPR-based tissue-specific knockout system (CRISPR-TSKO).

(A) Schematic representation of the T-DNA used, expressing Cas9 under the control of the *MCPI* promote. **(B)** Two guide RNAs (gRNA) were selected, targeting the third exon of *TPS20* (vertical lines). Forward (Fw) and reverse (Rv) primers location, indicated by black arrow, were used to amplify the 576-base pair PCR product depicted on 1% agarose-gel electrophoresis. Electropherogram alignment of the sequences obtained from WT and the *TPS20* CRISPR line (*TPS20*-CR) displaying the decomposition sequence after the target site the first gRNA. **(C)** Decomposition plot displaying spectrum and frequency of indels around the cleavage site of Cas9, using the TIDE webtool, tide.nki.nl. (Brinkman et al., 2014). **(D)** Comparison of the GC-MS chromatogram of VOCs produced over the leaf surface of WT and *TPS20*-CR line. Peak numbers indicate: 1, 2-carene; 2, β -phellandrene + D-limonene; 3, D-limonene; 4, Nerol; 5, β -caryophyllene; 6, α -humulene; IS, Internal standard: menthol.

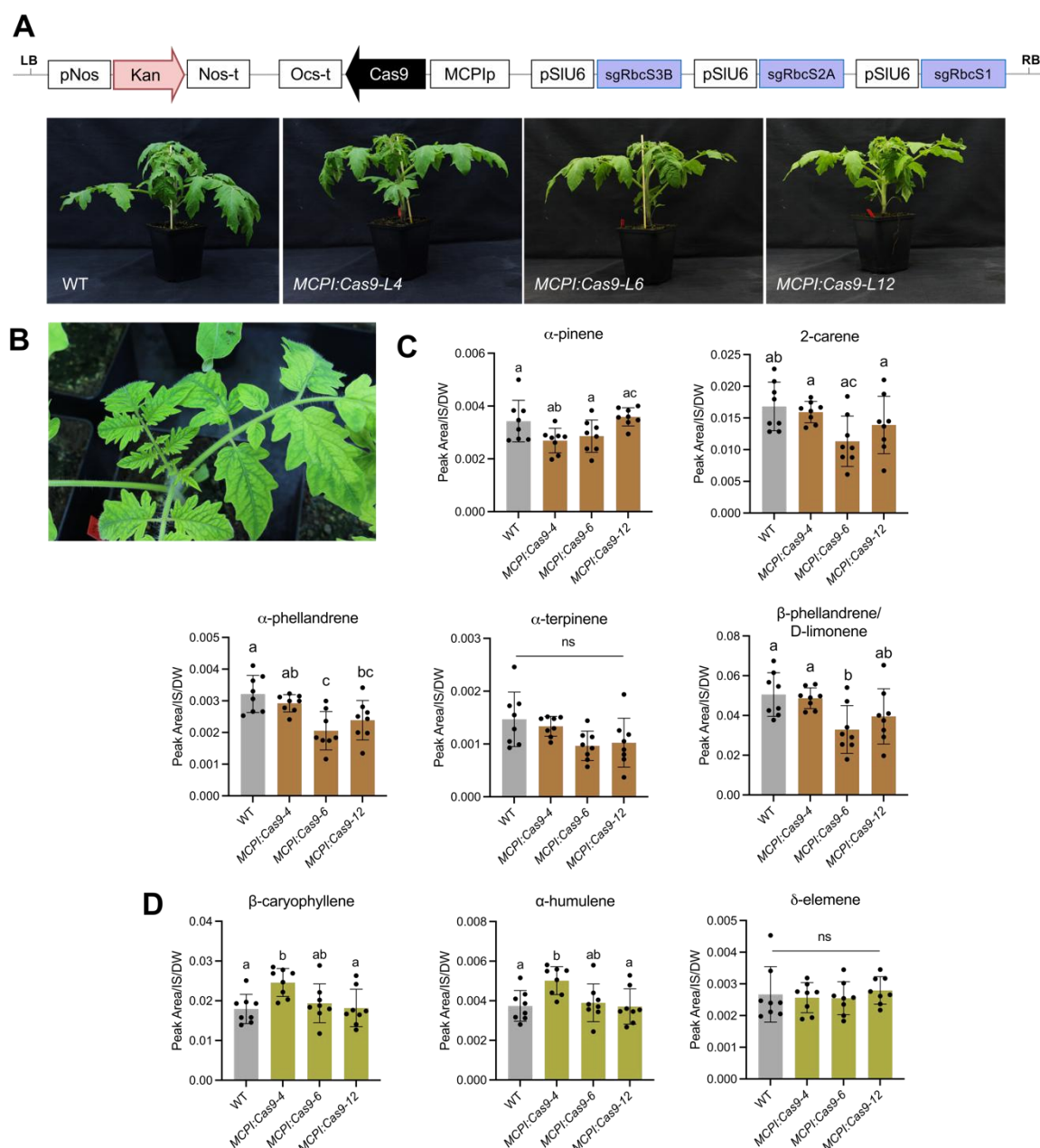


Figure 17. CRISPR-TSKO targeting the mesophyll isoforms of *RbcS* in type-VI GTs of cultivated tomato.

(A) A schematic representation of the T-DNA employed to generate simultaneous knockouts of *RbcS-M* isoforms in type-VI GTs. Each isoform is targeted by individual sgRNAs, except for sgRbcS3B, which targets both *RbcS3B* genes. The phenotype of the T1 transgenic lines is depicted below, after four weeks of growth in phytochamber under control conditions. (B) Image of a transgenic line displaying potential off-target effects on *RbcS* in the mesophyll cells of the leaves. Quantification of monoterpenes (C) and sesquiterpenes (D) using gas chromatography-mass spectrometry GC-MS ($n = 8$ biological replicates). Chromatogram peak areas were normalized to the internal standar (IS) and the leaf dry weight (DW). Error bars indicate standard deviation. Different letters indicate statistical significance after one-way ANOVA with Tukey's test ($P < 0.05$). ns: not significant.

1.3.4 Functional characterization of *PEPCK* in the glandular trichomes.

Higher transcript and protein levels of *Phosphoenolpyruvate carboxykinase (PEPCK)* in trichomes compared to leaves of tomato were reported in the “omics” dataset of (Balcke et al., 2017). Despite being typically associated with decarboxylation processes in the bundle sheath cells of C_4 -plants (Schlüter and Weber, 2020), PEPCK can operate bidirectionally (Chen et al., 2002; Amaral et al., 2019). It was hypothesized that PEPCK could be involved in anaplerotic routes that would facilitate the production of Acetyl-CoA in the cytosol for the MVA pathway, or by decarboxylation reactions, enabling the interconversion between C_4 to C_3 acids, securing the reincorporation of, for example, C_3 molecules into the plastidic MEP pathway (Balcke et al., 2017).

Unlike *Arabidopsis*, tomato has two PEPCK homologues. The first one Solyc04g076880 (AY007226) reported by Bahrami et al. (2001), and the second one Solyc12g088160 mentioned in Huang et al. (2015). The isoforms share 86% of identity, but Solyc12g088160 displays very low expression levels compared to Solyc04g076880, and because Solyc04g076880 downregulation led to reduced PEPCK enzyme activity, it was proposed that Solyc12g088160 is not functional (Huang et al., 2015). In agreement with these findings, *PEPCK* transcript and the protein levels reported in the trichomes by Balcke et al. (2017), correspond to the isoform Solyc04g076880, and therefore subsequent experiments were performed on this gene.

To investigate the role of PEPCK in GTs of tomato, transcript levels were measured by qRT-PCR in the trichomes, and they were compared with the mRNA levels in leaves. In the cultivated tomato, *PEPCK* is expressed almost four times more in the trichomes compared to the trichome-free leaves, while in the wild *S. habrochaites*, the transcript levels reached almost 14 times in relation to the leaves (**Fig. 18**).

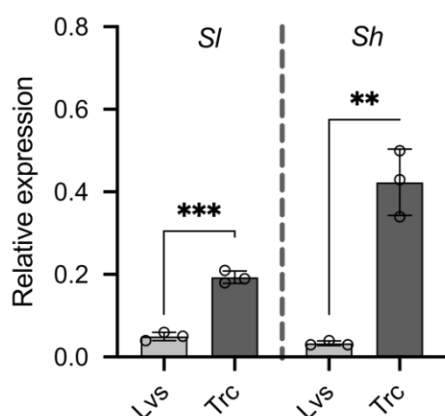


Figure 18. Relative expression levels of *PEPCK* in trichome-free leaves (Lvs) and trichomes (Trc) of *S. lycopersicum (Sl)* and *S. habrochaites (Sh)*.

Error bars indicate standard deviation ($n = 3$). ** $P < 0.01$, *** $P < 0.001$; using Student's t-test.

To study the contribution of *PEPCK* in GTs of tomato, loss-of-function mutants were generated using CRISPR/Cas9 approach as described earlier. In this case, two sgRNAs were selected to target the second and the third exons of *PEPCK* and the synthetic construct was transformed into the cultivated tomato cv Moneymaker (**Fig 19A**). Several transgenic lines were obtained, and the point mutations of three independent lines were characterized by sequencing, all of them leading to premature stop codon (**Fig. 19A**). Subsequently, the T-DNA insertion was segregated out from the plants.

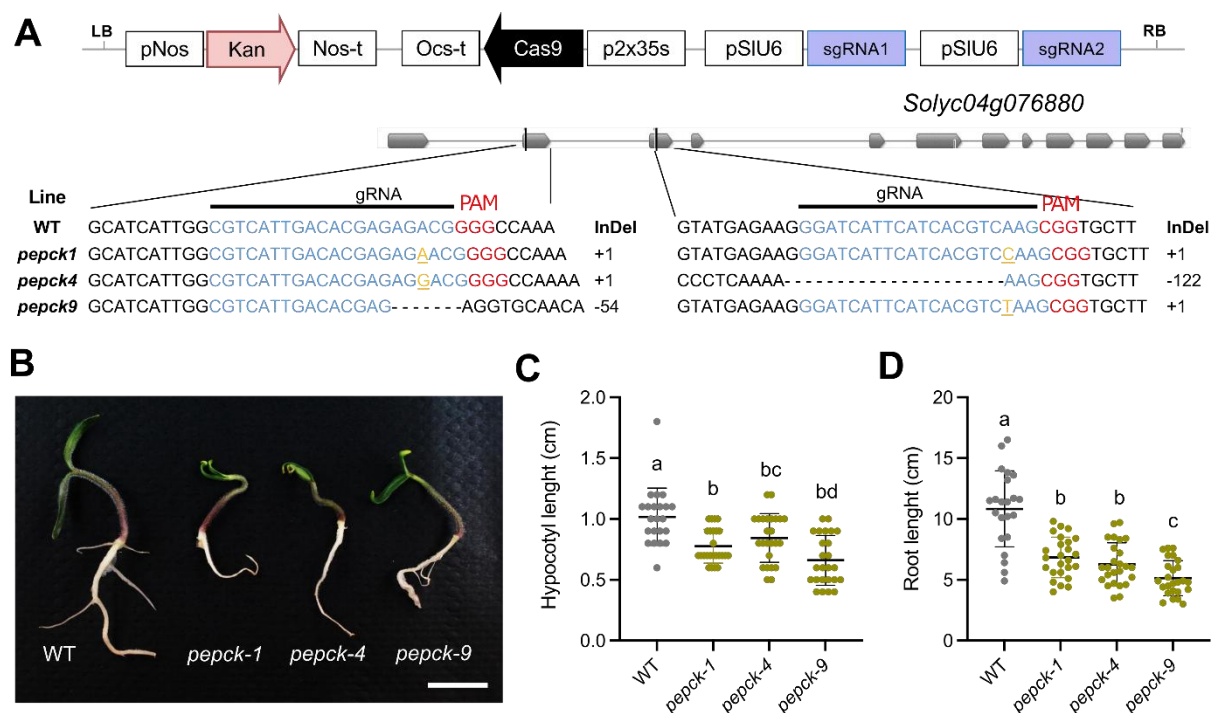


Figure 19. CRISPR/Cas9 loss-of-function mutants of *PEPCK* in cultivated tomato.

(A) Schematic representation of the T-DNA used to generate mutations in *PEPCK* and the point mutations generated in the different lines. Exons are represented in gray. **(B)** Seedling phenotype of *pepck* mutant lines, eight days post germination on Whatman filter paper. Scale bar = 2 cm. Hypocotyl length **(C)** and main root length **(D)** of *pepck* lines compared to WT ($n = 22, 25, 25$ and 25 individual seedlings for WT, *pepck-1*, *pepck-4* and *pepck-9*, respectively). Different letters indicate statistical significance after one-way ANOVA with Tukey's test ($P < 0.05$).

Earlier studies using RNA interference (RNAi) to downregulate *PEPCK* in tomato have reported the essential role of this enzyme in root growth and establishment of the seedlings (Eastmond et al., 2015; Huang et al., 2015). In line with it, homozygous *pepck* mutant lines displayed a diminished hypocotyl elongation and arrestment of the main and lateral root growth during the early stages after seed germination (**Fig. 19B-D**). This observation suggested that the mutant lines carried a nonfunctional PEPCK protein. When the seedlings were placed on soil, the mutant lines exhibit normal vegetative growth, with no morpho-anatomical changes and only a delay in growth compared to the WT.

Next, a screening of the VOCs produced by the *pepck* KO lines were performed and compared to the WT. For that, homozygous *pepck* KO plants were germinated and grown on soil in phytochamber under control conditions (**Fig. 20A**). Leaflets from the same leaf and of similar developmental stage were used for sampling of VOCs. Metabolites were isolated using surface extraction method and detected via GC-MS. The results showed a significant decrease in monoterpenes, e.g. 26 to 40% on average of 2-carene and 32 to 45% on average of β -phellandrene/D-limonene (**Fig. 20B**) while no significant differences were found in sesquiterpenes, except for the line *pepck-9* that produced higher levels of the very low abundant δ -elemene (**Fig. 20C**).

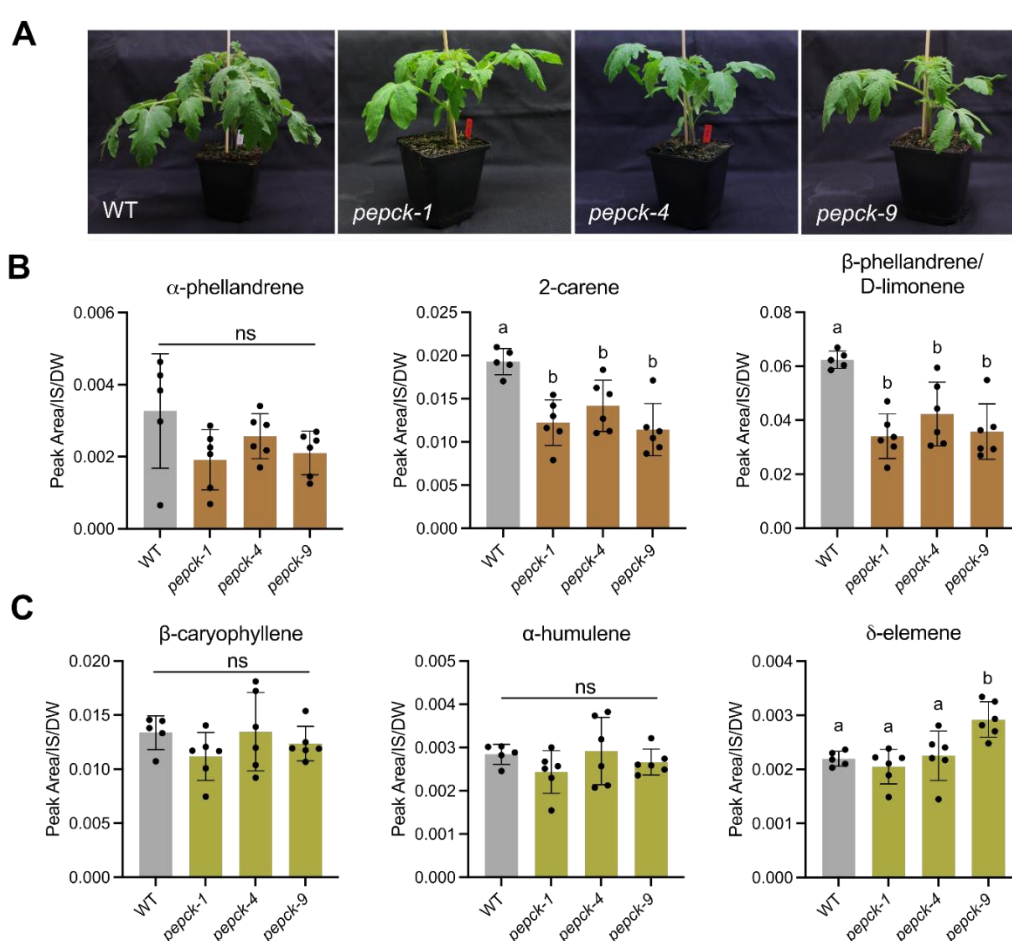


Figure 20. Functional characterization of PEPCK in type-VI glandular trichomes of cultivated tomato.

(A) Four weeks old *pepck* mutant lines grown on soil and used for VOC measurements. Quantification of mono **(B)** and sesquiterpenes **(C)** using gas chromatography-mass spectrometry (GC-MS) of *pepck* mutant lines ($n = 5$ for WT and $n = 6$ for *pepck* lines 1, 4 and 9, biological replicates). Error bars indicate standard deviation. Different letters indicate statistical significance after one-way ANOVA with Tukey's test ($P < 0.05$). ns: not significant.

Since wild *S. habrochaites* develop type-IV trichomes throughout vegetative growth, and *PEPCK* transcript levels were higher in the isolate trichome samples compared to the cultivated tomato trichomes (**Fig. 18**), the productivity of AS was analyzed in the *pepck* mutants. For that, cotyledons from WT and the three *pepck* mutant lines were harvested and AS were isolated by the two-phase extraction method. The organic phase was retained, and AS were subsequently detected by LC-MS. Peak integration of the five most abundant AS in the cultivated tomato indicated no differences between the WT and the *pepck* lines (**Fig. 21A**). The mutants were also challenged to elevated temperature, with the aim to induce type-IV trichomes on non-juvenile tissues and explore the function of *PEPCK* on AS biosynthesis. Following the described experimental set up, the plants were submitted to long days at 37°C for three weeks and leaflets from the third leaf were sampled. AS were then isolated using leaf surface extraction with 80% methanol. After screening the AS via LC-MS, minimal differences were observed in the mutants compared to the WT, resulting in no statistical differences (**Fig. 21B**). Thus, these results suggested that *PEPCK* could play a role mostly in the biosynthesis of VOCs in type-VI GTs.

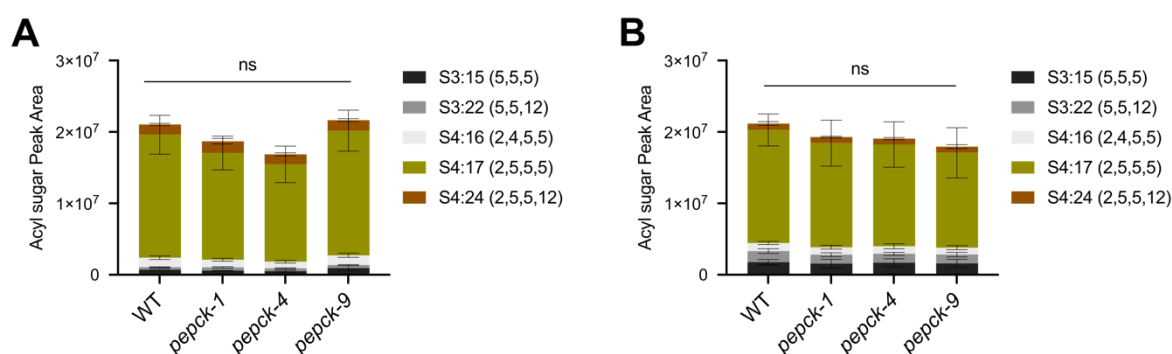


Figure 21. Acylsugar (AS) profiling of *pepck* mutants using liquid chromatography-mass spectrometry LC-MS.

Chromatogram peak areas of individual AS were integrated with PeakView®. **(A)** AS profiling of cotyledons from seedlings germinated under control conditions ($n = 4$ biological replicates). **(B)** AS present in leaflets of the third leaf, from plants submitted to heat stress for three weeks ($n = 4$ biological replicates). Error bars represent standard deviation. Ns: no statistical difference after one-way ANOVA ($P < 0.05$, using Tukey's test).

To gain further insights about the function of *PEPCK* in GTs of tomato, targeted metabolomics analysis of the central carbon (CCM) and energy metabolites was conducted. Briefly, WT and *pepck* mutants were grown in the phytochamber under control conditions. Pure trichomes were isolated from leaves and stems from 6-7 weeks old plants and stored in -80°C. A two-phase extraction method was employed to separate the different metabolites into aqueous and organic fractions. The hydrophilic compounds, commonly comprising the CCM metabolites were measured by LC-MS/MS using negative mode electrospray ionization (ESI) on a

QTrap6500 (AB-Sciex). Peak areas of 105 detected MS¹ mass/retention time features were integrated using MultiQuant® software, and subsequently analyzed using the MetaboAnalyst web-based platform. The principal component analysis (PCA) of the analyzed features indicated a wide range of variation among the genotypes (PC1; 41,4%) and only a mild separation between the WT and the *pepck* lines, observed in the second component (PC2; 20.8%) (**Fig. 22A**). The clustering of the metabolic profiles from the different samples grouped the mutants *pepck-1* and *pepck-9*, being more similar and harboring more differences compared to the WT and the *pepck-4* line that shared more similarities among them (**Fig. 22B**). By examining metabolites commonly altered across the three mutant lines, the levels of 1-deoxy-D-xylulose 5-phosphate (DXP) and glyceraldehyde 3-phosphate (GA-3P) were consistently lower than the levels detected in the WT (**Fig. 22C**). Mutant lines *pepck-1* and *pepck-9* exhibited reduced levels of certain intermediates of the CBB cycle such as ribulose 1,5-bisphosphate (RIB1,5 BP) and sedoheptulose 7-phosphate (S7P), as well as decreased levels of NADPH and specific amino acids including threonine (THR), glutamic acid (GLA) and arginine (ARG) (**Fig. 22B, Fig. 22C**). Out of these metabolites, DXP represents the first enzymatic product of the MEP pathway, catalyzed by DXS in the plastids by combining pyruvate and GA-3P (Wright et al., 2014).

Regarding the direct substrates and products of PEPCK, oxaloacetate is very unstable in solution, and is usually reduced to malate (MAL), making it difficult to estimate the abundance. When analyzing malate, it remained unchanged across all genotypes. In the case of PEP, it exhibited mild, but significantly lower levels in *pepck-9* and a decreasing trend in *pepck-1* (**Fig. 22C**). One of the putative roles of PEPCK is the supply of PEP to the shikimate pathway for the biosynthesis of aromatic amino acids (Walker et al., 1999; Brown et al., 2010). Unexpectedly, in *pepck-1* and *pepck-9*, the levels of the intermediate shikimic acid were notably elevated compared to those in the WT. Despite this rise, the aromatic amino acids tyrosine, tryptophan or phenylalanine were not altered.

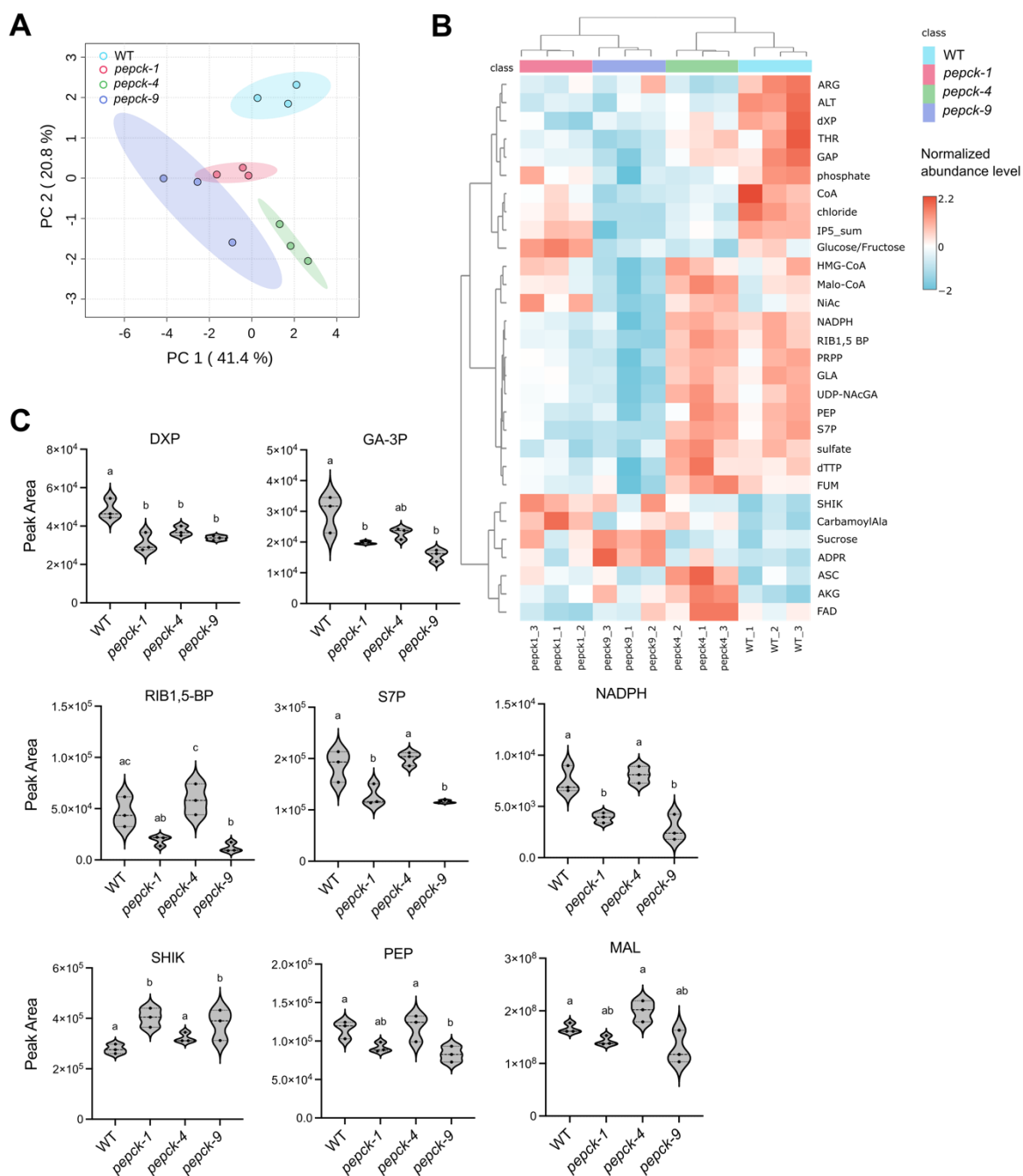


Figure 22. Profiling of metabolites involved in the central carbon and energy metabolism in GT of *pepck* mutants.

(A) Principal component analysis of the polar metabolites detected in the trichome fractions ($n = 3$ biological replicates). **(B)** Hierarchical clustering heatmap of the top 30 polar metabolites according to ANOVA (p value 0,05). Metabolite names corresponding to the abbreviations are listed in Table S2. **(C)** Peak areas of selected metabolites. Different letters indicate significant differences after one-way ANOVA ($P < 0.05$, using Tukey's test). DXP, 1-deoxy-D-xylulose 5-phosphate; GA-3P, glyceraldehyde 3-phosphate; RIB1,5-BP, ribulose 1,5-bisphosphate; S7P sedoheptulose 7-phosphate; SHIK, shikimic acid; PEP, phosphoenolpyruvate; MAL, malate.

1.4 Discussion

1.4.1 A trichome-specific *Rubisco small subunit (RbcS-T)* in photosynthetic glandular trichomes of tomato.

The observed SM productivity in GTs suggests a continuous supply of precursors that are withdrawn from the primary metabolic pathways. These precursors, namely pyruvate, GA-3P and acetyl-CoA, essentially serve as carbon building blocks utilized by the MEP and MVA intermediate pathways to produce the isoprene units, or by alternative pathways to synthesize AS. Despite their relevance, little is known about the factors controlling the interface between the primary and specialized metabolism in the GTs. One of the reviewed mechanisms employed by these micro fabrics to allocate resources into the SM involves gene duplication (Brand and Tissier, 2022). For example, DXS, an enzyme that controls the flux through the MEP pathway, is generally encoded by several genes. While type-I isoforms of DXS (*DXS1*) typically perform housekeeping functions including synthesis of carotenoids, chlorophylls, phytohormones and in developmental processes (Cordoba et al., 2011; García-Alcázar et al., 2017; You et al., 2020), type-II isoforms of DXS (*DXS2*) are preferentially expressed in secretory structures, including GTs of tomato (Besser et al., 2009), *Artemisia* (Zhang et al., 2018), tobacco (Nautiyal et al., 2020) and spearmint (*Mentha spicata*) (Jin et al., 2014) supporting their specialized metabolic reactions.

A specific isoform of *Rubisco small subunit (RbcS)* was identified in GTs of tobacco (*NtRbcS-T*), that belongs to an uncharacterized phylogenetic cluster of *RbcS*, distinct from the cluster that contains the conventional mesophyll isoforms. Laterre et al. (2017) could show that when *NtRbcS-T* was used to complement the *Chlamydomonas reinhardtii rbcS* mutant, Rubisco complex acquired new attributes such as higher catalytic rate and K_m , in addition to a superior performance under acidic conditions, compared to the mesophyll *RbcS* isoforms (Laterre et al., 2017; Pottier et al., 2020). Although functional characterization of this gene was not performed in *N. tabacum*, the enzymatic activity of *NtRbcS-T* hinted at a tailored adaptation to the glandular cells of the trichomes. The present work was able to identify the orthologous gene of *NtRbcS-T* in cultivated tomato, designated as *SIRbcS-T*. Moreover, it was revealed that *SIRbcS-T* is expressed only the glandular cells of the capitate trichomes type-I/IV of tomato, in addition to specific tissues of the flower organs and developing fruits, as suggested in previous reports (Morita et al., 2014, 2016) (**Fig. 8**). With the aim to characterize this isoform in GTs of tomato, loss-of-function mutants were generated in cultivated tomato and in one accession of the wild *S. habrochaites*. Contrary to expectations, there were no significant differences observed between the *rbcS-T* mutants and the WT when quantifying the acylsugars (AS) (**Fig. 9-10**). Despite this, a recent work by Ji et al. (2023), claimed that the

silencing of the ortholog *SIRbcS-T* in *S. pennellii* (*Sopen07g006810*) resulted in 23% reduction in the total AS content. In their analysis of the acyl chain composition of *RbcS-T* silencing plants, they revealed a 20% decrease in short acyl chains iC5/aiC5 (2-methylbutanoic acid and 3-methylbutanoic acid). In contrast the iC4 and the long straight-chain fatty acids (*n*-C10, *n*-C12) exhibited an increasing trend, with some differences being significant (Ji et al., 2023). Furthermore, Ji and coauthors were able to demonstrate CO₂ re-fixation activity by comparing the fractionation of carbon isotopes ($\delta^{13}\text{C}$) in both secreted AS and non-AS containing tissues, for example trichome-free stems. The hypothesis was that if recycled CO₂ is used for the biosynthesis of AS, these sugar esters will contain carbon that has undergone several rounds of fixation. Consequently, the AS will contain less ¹³C, due to the preferential enrichment of ¹²C isotopes during carboxylation reaction catalyzed by Rubisco. The results indeed showed that AS contained less ¹³C than other tissues (around 10-15%), and that when *RbcS-T* is downregulated, the $\delta^{13}\text{C}$ was even lower than in the control samples (around 30% less) (Ji et al., 2023).

The attempt to replicate the silencing experiment from Ji and coauthors using the same wild tomato accession did not lead to similar results (**Fig. 12**). Many factors can affect the outcome of a VIGS experiment, starting with the extent of the downregulation achieved, the high variation due to heterogeneous silencing, and the fact that even minimal levels of expression can be enough to produce a functional protein (Unver and Budak, 2009). Additionally, temperature conditions suitable for VIGS experiment, could not be optimal to uncover the function of the enzyme. This is particularly relevant in order to study the RbcS, because the expression of different isoforms and the kinetics of Rubisco can be modified in response to temperature, light and CO₂ (Dedonder et al., 1993; Cheng et al., 1998; Cavanagh et al., 2023).

In the present thesis, significant changes in certain AS were only observed when RbcS-M isoforms were simultaneously downregulated, which reflected about 9% reduction in the total average peak area of the quantified AS. Although Ji and coauthors reported no phenotypical changes in the *RbcS-T* VIGS plants, the expression levels of the mesophyll isoforms were not quantified. Therefore, potential off-targeting effects of the VIGS cannot be excluded from their experiment. Regarding the effect observed in the *RbcS-M* VIGS plants, it is difficult to determine whether it is due to the silencing of Rubisco in the glandular cells of the trichomes or if it is the result of an impact on carbon fixation in the leaves that alters the productivity of the trichomes. Interestingly, the downregulation of the *Magnesium Chelatase Subunit H* (*ChlH*), an enzyme involved in chlorophyll biosynthesis, and the silencing of *RbcS-M* isoforms led to similar AS changes. Specifically, those that increased were enriched in iC5 acyl chains, and those that decreased were enriched in iC4 acyl chains (**Fig. 12-13**). The precursors of iC4, 3-methyl-2-oxobutanoate, and iC5, 4-methyl-2-oxopropanoate, are derived from the branched-

chain amino acid biosynthesis pathway of valine and leucine, respectively (Walters and Steffens, 1990; Maeda, 2019). This finding contrasts with the results of Ji et al. (2023), where the silencing of the *SpRbcS-T* led to a decrease in both iC5 and aiC5, while the iC4 did not significantly change. Although both valine and leucine are synthesized in the plastids, it is intriguing that the potential impact on carbon fixation due to downregulation of Rubisco produces an effect on certain amino acids. The results presented here suggest that interfering with photosynthesis could impact the amino acid biosynthesis preferentially used to build the acyl groups in AS. It could be hypothesized that after the downregulation of the different RbcS-M isoforms, there is an increased flux towards leucine versus valine, or that more leucine is imported from the leaves into the trichomes. However, the mechanism by which this occurs in the leaf and the trichomes remains to be determined.

In *S. pennellii*, RbcS-T (*Sopen07g006810*, *SpRbcS-T*) was identified among the highest differentially expressed genes (Log₂FC 1,85) between high and low-AS producing F₂ plants from a cross between *S. lycopersicum* and *S. pennellii* (Ji et al., 2023). Despite the superior type-IV trichome density in this wild accession (**Fig. 2F**), *SpRbcS-T* expression levels are relatively low (**Fig. 11B**). Transcriptome data from *N. tabacum* trichome fractions indicate that the expression of *NtRbcS-T* is three to six times lower compared, for example, to that of the mesophyll isoforms (Nautiyal et al., 2020). In the same line, in *S. habrochaites*, where type-IV trichomes are constitutively developed, *RbcS-T* transcripts are 20 to 100 times lower compared to the rest of the *RbcS-M* isoforms (**Fig. S1**). The presence of mesophyll *RbcS* isoforms in the GTs could suggest that *RbcS-T* can be regulated differently. For example, in Arabidopsis, the expression pattern of the four different *RbcS* genes varies with temperature, determining the type of small subunit that forms the Rubisco complex. In cold conditions, the pool of Rubisco complex contains ~65% of the *RbcS-A* subunit, while in warm conditions, this ratio shifts to favor the *RbcS-B* subunit, and by doing this, Rubisco changes its performance according to the temperature, maintaining its carboxylation capacity (Cavanagh et al., 2023). As will be discussed in the second chapter of the present thesis, heat can have a great impact on the productivity of the GTs, especially on the AS produced by the capitate trichomes. Although the response of the different RbcS isoforms to elevated temperatures within the GTs was not assessed, the lack of the *RbcS-T* did not affect the AS productivity in the mutants upon heat treatment. This result, coupled with the significantly higher expression levels of *RbcS-M* compared to *RbcS-T*, calls into question the specific role of *RbcS-T* in the recycling of CO₂ in the glandular cells of the trichomes.

The T-type class of *RbcS* are phylogenetically distant from the M-type of *RbcS* and widely distributed across different plant phyla, mostly found in single copy compared to the multicopy M-type (Pottier et al., 2018). *RbcS-T* is the predominant isoform in different species of

bryophytes and pteridophytes, providing evidence of its ancient origin, even before the emergence of GTs in vascular plants. It is hypothesized that *RbcS-T* was lost several times independently during the evolution of the seed plants (Pottier et al., 2018). Besides *NtRbcS-T*, other T-type *RbcS* have been characterized, for example in rice (Morita et al., 2014), where *OsRbcS1* is expressed in non-photosynthetic tissues including leaf sheath, culm, anther, and root central cylinder. After overexpressing *OsRbcS1*, Rubisco exhibited higher catalytic turnover and increased K_m (reduced affinity for CO_2), which are features of Rubisco typically present in C_4 plants where CO_2 concentration surrounding this enzyme is higher (Morita et al., 2014), although its presence is not directly linked to the C_4 metabolism (Pottier et al., 2018).

Overall, the evidence suggests that the presence of T-type *RbcS* can be associated to non-photosynthetic tissues, and photosynthetic trichomes as well, where there is low or no atmospheric gas exchange, resulting in elevated CO_2 levels. In these C-sink tissues, Rubisco containing *RbcS-T* isoforms display adaptation to acidic conditions, allowing for the reassimilation of CO_2 from respiration or from the biosynthesis of SM, thereby maximizing carbon efficiency. In tomato, besides type-I/IV trichomes, *SIRbcS-T* is expressed in other C-sink organs, such as fruit exocarp and flowers (**Fig. 8**). The expression pattern of *SIRbcS-T* during the early stages of fruit development matches with the formation of the cuticle in the outer layer of the pericarp which protects the fruit from desiccation. The cuticle comprises cutin, long chain alkanes, fatty acids, triterpenoids, and flavonoids that are produced in the epidermis and secreted to the extracellular matrix (Mintz-Oron et al., 2008). Since the epidermis of tomato fruits lacks stomata, and therefore, no atmospheric gas exchange occurs, the function of Rubisco is most likely to re-assimilate CO_2 that is released from respiration or from the biosynthesis of the cuticular metabolites (Simkin et al., 2020).

However, the data presented in this thesis indicates that the recycling activity demonstrated in GTs of *S. pennellii* (Ji et al., 2023) is not associated with T-type *RbcS*. As discussed in the introduction of this chapter, the recycled CO_2 occurring in Brassicaceae species during the accumulation of fatty acids in the seeds, is performed by Rubisco containing M-type of *RbcS* (Schwender et al., 2004). At the same time, a high carbon environment does not seem to determine the exclusive activity of T-type *RbcS*, since mesophylls are also expressed in GTs and at much higher transcript levels. This observation prompts the question of whether the mesophyll isoforms of *RbcS* evolved to be equally adapted to rich CO_2 microenvironments, taking over the function of the T-type isoforms. It is possible that *SIRbcS-T* contributes more to other C-sink organs in tomato. Another possibility is that this isoform is regulated differently in wild varieties with higher AS productivity, and therefore elucidating its function will require further research.

1.4.2 The role of Rubisco in type-VI GTs trichomes

The peltate type-VI GTs in tomato produce VOCs from MEP and MVA intermediate pathways that generate CO₂ as a byproduct (**Fig. 3**), thus creating a C-rich microenvironment surrounding Rubisco. Furthermore, this type of trichomes possess an outer envelope (consisting of cell wall and cuticle) thicker than that of the epidermal cells, reducing the possibilities of gas exchange (Balcke et al., 2017). The co-expression and prevalence of the different mesophyll *RbcS* in the GTs suggest potential redundancy in their putative carbon refixation role. Both transcript and protein levels of all mesophyll isoforms have been detected in type-VI GTs (**Fig. 14**, Balcke et al. (2017)), since the head cells of this type of trichomes are enriched in the isolated trichome fractions obtained with the described method. An independent proteomics analysis, specifically on the gland cells, detected the presence of Rbc large chain (RbcL) and the RbcS-3A (Takemori et al., 2019), which aligns with the observation that *RbcS-3A* isoform exhibits the highest transcript levels. At the same time, investigating the contribution of Rubisco to the productivity in the glandular cells represents an additional challenge, since loss-of-function mutants cannot be generated without affecting the housekeeping functions of the *RbcS* in photosynthetic tissues.

To tackle this question, a CRISPR-TSKO approach was employed in which the promoter of the *MCPI* gene was used to drive the expression of Cas9 in type-IV trichomes, along with three independent gRNAs targeting all the *RbcS-M* isoforms simultaneously. After screening the volatile productivity, a slight reduction in monoterpenes was observed in at least two of the three transgenic lines analyzed, with more noticeable effects on certain monoterpenes than on others (**Fig. 17**). As one could anticipate, the downregulation of Rubisco in these lines affected the plastid-derived monoterpenoids, while the cytosol-derived sesquiterpenoids remained unchanged. This implies that the potential decrease in CO₂ re-assimilation directly impacts the SM produced near Rubisco in this cell compartment. Release of CO₂ occurs in multiple steps during the biosynthesis of short branched and straight-chain fatty acids, as well as in the initial step in the MEP pathway. In the latter, DXS, catalyze the conversion of pyruvate and GA-3P into 2-C-methyl-D-erythritol 4-phosphate (MEP), generating CO₂ as a byproduct (**Fig. 3**). This CO₂ could be recycled into triose phosphates to replenish the MEP pathway itself, or to serve as a precursor of the downstream branch-chain amino acids biosynthesis.

Multi-omics data obtained from the glandular cells suggested that light photosynthesis is uncoupled with the CBB cycle since the genes involved in the later one are underrepresented in the GTs (Balcke et al., 2017). It was then hypothesized that Rubisco operates without CBB, in the so-called Rubisco bypass (Schuurink and Tissier, 2020). In a similar metabolic context, Rubisco improves carbon efficiency during the accumulation of oils in developing seeds of *B. napus* (Schwender et al., 2004). Although GTs and seeds are two different C-sink tissues,

carbon recycling seems to have a greater impact on the accumulation of the fatty acid reserves in the *Brassica* seeds than in the accumulation of VOCs in the GTs. For tomato GTs, the main carbon source is the sucrose that most likely diffuses from the photosynthetic tissues (Balcke et al., 2017), in a source-sink fashion, although the activity of sugar transporters cannot be ignored. Under this analysis, sugars constitute the carbon limiting factor, suggesting Rubisco only has a minor role as a supporting enzyme.

Very recently, it was shown that Rubisco supplies pyruvate for the MEP pathway, fatty acid, and branched-chain amino acid biosynthesis (Evans et al., 2024). The production of pyruvate by Rubisco in the chloroplast is a side reaction that occurs through the β -elimination of a phosphate ion from the *aci*-carbanion intermediate (Andrews and Kane, 1991). This activity of Rubisco is enhanced in low oxygen conditions (Evans et al., 2024), evidence that aligns with the proposed CO₂ rich environment within the GTs (Laterre et al., 2017). Since pyruvate is required for valine, leucine, and fatty acid biosynthesis (**Fig. 3**), removing pyruvate produced by Rubisco in the plastids could affect the productivity of AS in type-IV trichomes. The uncovered role of Rubisco suggests that this enzyme is not necessarily involved in carbon recycling but rather in supplying precursors for the SM biosynthesis. The results illustrated here, which show reduced levels of monoterpenes in the *RbcS-M* CRISPR-TSKO lines, provide the first step in studying the function of Rubisco in the GTs. Further analysis and investigation are required to determine the extent of the downregulation of Rubisco in the trichomes of the different lines and correlate this information with their productivity. This will require protein quantification of RbcS and RbcL protein levels from isolated GTs. Additionally, labelling experiments could help to understand how the lack of Rubisco impacts the biosynthesis of SM in the plastids of type-VI GTs, and whether it also affects the productivity of non-volatile compounds, also produced in the glandular cells, such as flavonoids.

The fact that GTs, regardless of whether they are photosynthetic or not, rely on the sugars produced in other tissues, triggers questions about the advantages of containing photosynthetic plastids in the glandular cells. In non-photosynthetic GTs of peppermint (*Mentha X piperita*) genome-scale modeling studies proposed that the ATP invested to power the monoterpene production is regenerated via oxidative phosphorylation occurring in the mitochondria, and ethanolic fermentation (Johnson et al., 2017). These processes along with the redox balance control under the two ferredoxin and ferredoxin-NADP⁺ reductase isoforms, exert control over SM biosynthetic fluxes (Johnson et al., 2017). In tomato GTs, transcriptomics data indicates that the level of expression of genes involved in mitochondrial electron transport and ATP synthesis are comparable to that found in the leaves. Additionally, genes involved in light photosynthesis reactions represent one of the largest functional categories grouping the highly expressed genes from GTs, and their expression levels differ by less than 2-fold

compared to the leaves. Hence, the photosynthetic plastids could act as active batteries supplying chemical energy and reducing power based on the prominent expression levels of the photosystems I and II (Balcke et al., 2017). A recent report using computational modeling and subsequent experimental design examined the impact of photosynthetic energy supply to the terpenoid production on type-VI GTs. The modeling approach revealed that high energy availability resulting from increased light intensity triggers a shift in carbon partitioning in glandular cells. Specifically, the fraction of precursors (GA-3P, pyruvate, and acetyl-CoA) consumed by catabolic pathways is reduced, and instead, they are redirected towards anabolic reactions, such as SM biosynthesis (Saadat et al., 2023). The model also predicted a switch in carbon flux from the MVA to the MEP pathway, which was later confirmed experimentally, where the major monoterpenes displayed a 2-to-5-fold increase under high light conditions. Interestingly, the modeling approach also considered the contribution of carbon refixation after increasing light intensities. The results predicted that the overall CO₂ refixation activity increases the rate of terpenoid production by almost 20%, which is considerably lower than the impact produced by the energy-dependent shift of carbon partitioning, estimated to result in a 200% increment in terpenoid biosynthesis (Saadat et al., 2023). Overall, this evidence emphasizes the key role of light photosynthesis in the chloroplast of GTs, serving as a modulator of the energy and resource allocation in the SM biosynthesis.

In conclusion, Rubisco may operate in the photosynthetic GTs of tomato as a supporting enzyme in the production of plastid-derived terpenoids. This potentially occurs through one or two mechanisms. First through the re-assimilation of CO₂ released as a by-product of the SM reactions, or second by the supply of precursors such as pyruvate through β -elimination. The evidence presented here suggests that in the case of CO₂ refixation, this function is not exclusive of Rubisco containing a RbcS-T isoforms, and instead, a function that Rubisco conventionally performs in non-photosynthetic tissues. The prevalence of the RbcS-M isoforms challenges the role of RbcS-T in GTs. It opens new questions about the regulation and function of this specific isoform, not only in the glandular cells, but also in other tissues where it is also expressed.

1.4.3 A CRISPR-TSKO approach to study the basis of high productivity in GTs

Multi-omics analysis of tomato GTs revealed that many genes involved in the CCM occur in multiple isoforms, some of which are enriched in the glandular cells compared to leaves, possibly exerting control over the high metabolic fluxes (Balcke et al., 2017). Investigating the function of gene families in GTs requires the development of multiple knockouts, specifically in the glandular cells, without impairing their essential role during plant development. Although

tissue-specific gene silencing could be used for this purpose, the gene downregulation is frequently incomplete, affecting the interpretation of the results (Decaestecker et al., 2019). With the improvement of the gene targeting methods, for example, engineering an intronized Cas9 endonuclease (Grützner et al., 2021), the CRISPR-TSKO system was tested to downregulate the *RbcS-M* isoforms in GTs of tomato.

The selection of the *MCPI* promoter was based on gene expression levels in the glandular cells of the trichomes (**Fig. 15**) and previous reports (Schillmiller et al., 2010; Wang et al., 2022). As a proof of concept, the CRISPR-TSKO approach was tested by targeting a trichome-specific terpene synthase *TPS20*. Although only one positive transgenic line was obtained, the downregulation of this enzyme was evidenced by the absence of monoterpene products (**Fig. 16-D**). The decomposition of the Sanger sequencing PCR product comprising the target sites could detect multiple point mutations, displaying the common indel spectrum of Cas9-mediated cleavage (**Fig. 16-C**), where the highest frequency is associated with 1-bp insertion (Allen et al., 2019). Given that DNA extraction was conducted from entire leaves, and the glandular cells represent a minor fraction, the results imply that targeting of *TPS20* sequence is occurring in other cells besides GTs. This analysis could explain why some of the *RbcS-M* CRISPR-TSKO lines exhibited chlorosis on both leaves and stems as a sign of targeting in *RbcS-M* isoforms not just in trichomes but also in leaves (**Fig. 17-B**). In conclusion, the *MCPI* promoter, although highly expressed, is not suitable for CRISPR-TSKO approaches in type VI trichomes.

Pioneering report emphasizes that the selection of the right promoter is one of the critical aspects for the success of a CRISPR-TSKO experiment (Decaestecker et al., 2019). Trichome-specific genes have been identified in tomato and in other GTs-containing species (Kortbeek et al., 2016). The promoter sequences of certain *TPS* genes, for instance, in type-VI trichomes, are promising candidates when it comes to specificity. However, the expression pattern of these genes could vary even within the same type of trichomes. For example, examination of *pSITPS20:YFP-GUS* promoter reporter lines pointed out that *TPS20* is expressed at higher levels in type-VI trichomes on the petiole or stems, in contrast to those located on the leaf surface. This information aligns with the reported four times more 2-carene and β -phellandrene content in type-VI trichomes from stem compared to leaves (Schillmiller et al., 2010). Moreover, *YFP* signal is hardly detected at early stages of type-VI trichome development, regardless of the organ location (**Fig. S2**).

Decaestecker and coauthors showed that elevated Cas9 levels traced by *mCherry* fluorescence are correlated with the observed targeting efficiency. Likewise, late induction of Cas9 can mask the expected phenotype due to pre-existing mRNAs in the specific targeted cells (Decaestecker et al., 2019). Therefore, choosing the appropriate promoter will require a fair balance between specificity and expression, and will certainly depend on the expression

pattern and the number of genes targeted simultaneously. Besides the fine-tuning of certain components of the technique, CRISPR-TSKO is a powerful tool that can be used to study the basis of the high productivity in the GTs.

1.4.4 PEPCK and carbon allocation between cell compartments

Several insights suggest the existence of a C₄-like metabolism in the GTs. Some include a Rubisco with C₄-like enzymatic features, a potentially rich CO₂ micro-environment and expression of C₄-associated de/carboxylating enzymes. Among the C₄-associated proteins, *Phosphoenolpyruvate carboxykinase (PEPCK)* displays transcript enrichment in the glandular cells of the trichomes of both cultivated and wild tomato accessions (**Fig. 18**). It has been well documented that PEPCK has a major role in gluconeogenesis during seedling development, facilitating the degradation of the fatty acids reserves into sugars, up until the plant becomes photosynthetically active. The absence of PEPCK in *Arabidopsis* seeds leads to 70% less accumulation of soluble sugars after germination due to impaired mobilization of stored reserves (Eastmond et al., 2015). Consequently, *pepck* mutants are moderately affected in seedling growth and establishment. One reason for this mild effect is due to an alternative gluconeogenic pathway, that converts protein reserves into sugars through the biosynthesis of pyruvate (Eastmond et al., 2015). *PEPCK* displays a conserved function in tomato, participating in early events following seed germination (**Fig. 19**). Although PEPCK activity has been associated to GTs and resin ducts (Chen et al., 2002; Balcke et al., 2017), its specific role in these carbon-sink tissues remains unknown.

In the present thesis, the examination of VOCs produced by *pepck* knockouts unveiled diminished levels of monoterpenes (**Fig. 20**). The higher transcript levels detected in the trichome fractions of the wild accession *S. habrochaites* suggested that PEPCK could also participate in the biosynthesis of AS in type-IV trichomes. Although there is no evidence for that in this wild accession, the AS quantification in cultivated tomato *pepck* mutants hinted that this is not the case. From these findings, it is intriguing that despite *PEPCK* being expressed in the cytosol, its inactivation affects the production of plastid-derived terpenoids.

Metabolomics of the central and energy metabolism on the GTs of *pepck* mutants showed moderate changes in GA-3P and DXP, a precursor and an intermediate on the MEP pathway, respectively. This finding could be correlated with the observed decrease in 2-carene and β -phellandrene/D-limonene monoterpenes. While all *pepck* lines exhibited a similar reduction trend in VOCs, the metabolic profiles of two mutant lines showed pronounced and similar differences compared to the WT, for example in the lower accumulation of ribulose 1,5 biphosphate (RIB 1,5-BP) and sedoheptulose 7-phosphate (S7P). These metabolites are

involved in the CBB cycle and in the oxidative pentose phosphate pathway (OPP). A reduction in these metabolites could affect carbon refixation by Rubisco or the generation of reducing power, as it was observed by the reduced levels of NADPH (**Fig. 22**).

PEPCK facilitates the interconversion between C₄ and C₃ compounds. The minor differences in phosphoenolpyruvate (PEP) (C₃) in *pepck* KO lines could suggest that, similarly to its role in the seedlings, PEPCK may be operating as decarboxylating enzyme in the GTs (**Fig. 23**). In these micro-organs, the generation of oxaloacetate (OAA) (C₄) in the cytosol is secured by the action of ATP-citrate-lyases that cleave the exported citrate from the mitochondria to produce acetyl-CoA and OAA (Fatland et al., 2002; Balcke et al., 2017). The demand of acetyl-CoA for the MVA pathway and fatty acid elongation suggest a continuous production of OAA that can be reincorporated to the mitochondria via subsequent conversion to malate and pyruvate, by the cytosolic malate dehydrogenase and malic enzyme, respectively. Alternatively, OAA can be converted to PEP via PEPCK, and later into pyruvate to replenish the cycle, or be transported into the plastids. A PEP/phosphate translocator (SIPPT1, Solyc03g112870) was found equally expressed in GTs as in leaves of tomato (Balcke et al., 2017), which makes it tempting to speculate that PPT facilitates the import of PEP from the cytosol into the chloroplast. The Arabidopsis *cue1* mutant, which harbors a mutation in the *AtPPT1* gene, is unable to transport PEP into the chloroplast, affecting the supply of this precursor to the shikimate pathway and aromatic amino acid biosynthesis (Streatfield et al., 1999; Voll et al., 2003). Recently, it was shown that in *cue1* mutant, the levels of pyruvate are unchanged, indicating that PEP is not the source of pyruvate in the plastids, and instead, reduced levels of DXP and GA-3P were observed (Evans et al., 2024). Additionally, it was proposed that since *PPT1* is expressed preferentially in vascular tissue and roots, this translocator is in charge of supplying PEP into the plastids in sink tissues (Evans et al., 2024). However, multi-omics data suggested that in the GTs, PEP could be produced independently in the plastids, e.g., via glycolysis (Balcke et al., 2017), and therefore, the potential transport of cytosolic PEP could represent just a supporting input of carbon in response to the high fluxes of SM in the chloroplast. On the other hand, a potential carboxylation activity cannot be ruled out, since K_m values for CO₂ of PEPCK are comparable to those of Rubisco from C₃ and CAM plants, and the direction of the reaction can change according to ATP:ADP ratio as well as the concentration of OAA, PEP and CO₂ present in the cell (Leegood and Walker, 2003).

In plastids, PEP could be converted to pyruvate to fuel the MEP pathway. Two plastidic pyruvate kinases enriched in the GTs of both cultivated and wild tomato reported in Balcke et al. (2017), could perform this function. In the scenario of reduced transport of PEP into the plastids, its connection with the lowered CBB intermediates (GA-3P, S7P and RIB 1,5-BP) observed in the GTs of *pepck* mutants requires further investigation. One possible explanation

is that the decreased carbon input into the chloroplast results in less CO₂ that can be reassimilated into the system by Rubisco/CBB cycle. Enzymes participating in glycolysis, including enolase, can convert PEP into 2-phosphoglycerate, and subsequently by the action of phosphoglycerate mutase into 3-phosphoglycerate (3PGA) that can fuel the CBB cycle or the supply of GA-3P, by sequential phosphorylation and reduction reactions (**Fig. 23**). Nevertheless, more research is required to elaborate on these hypotheses. PEP in the chloroplast also serves as a precursor of the shikimate pathway (Flügge et al., 2011), yet the levels of aromatic amino acids were not altered. This supports the hypothesis of the existence of multiple sources of PEP in the chloroplast.

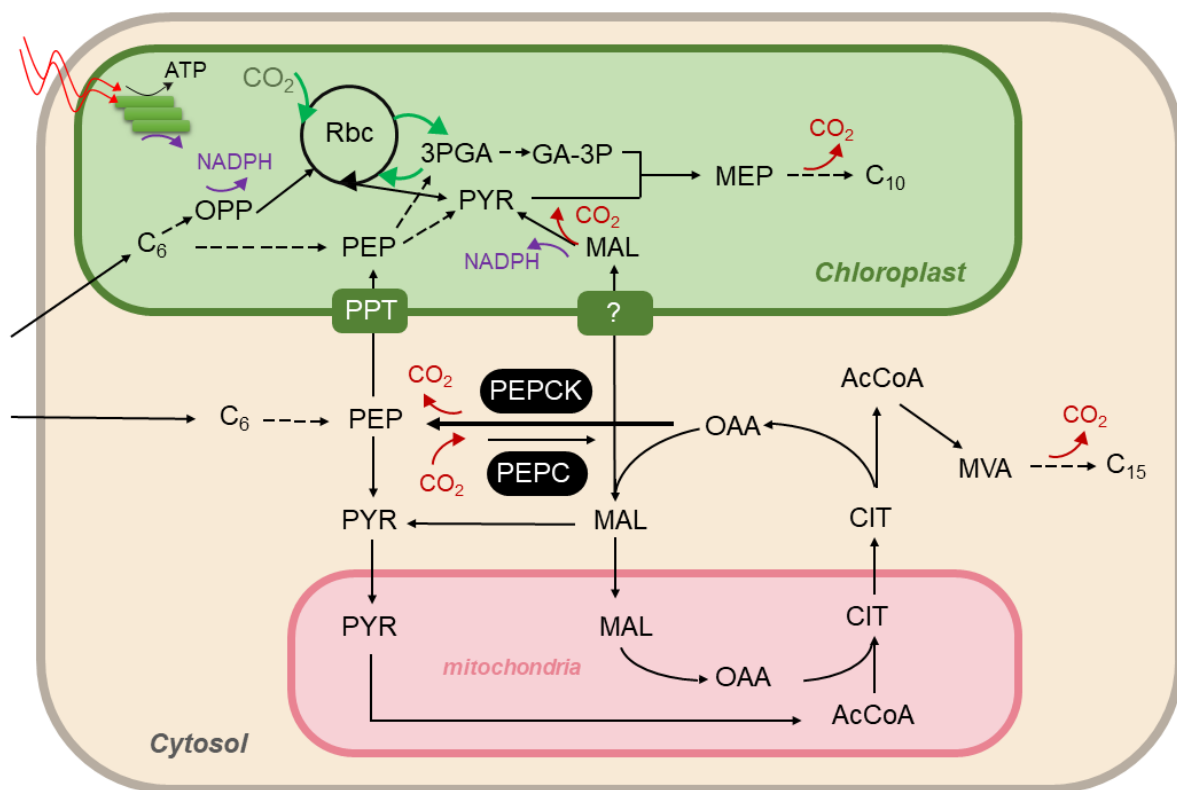


Figure 23. Simplified model illustrating the putative role of PEPCK in type-VI GTs of tomato.

PEPCK plays a role in the interconversion of C₄ (OAA) to C₃ (PEP) carbon precursors that potentially are transported to the plastids to feed the MEP pathway. Reduced import of carbon precursors could affect the redox balance by reducing the generation of NADPH in the chloroplast. **Abbreviations:** Rbc, Rubisco; OPP, oxidative pentose phosphate pathway; PEP, phosphoenolpyruvate; PYR, pyruvate; GA-3P, glyceraldehyde-3-phosphate; MAL, malate; PPT; PEP/phosphate translocator; PEPCK, phosphoenolpyruvate carboxykinase; PEPC, phosphoenolpyruvate carboxylase; OAA, oxaloacetate; CIT, citrate; AcCoA, acetyl-CoA.

The downregulation of *PEPCK* leads to alterations in the primary metabolic pathways. For example, in ripening tomato fruits, where *PEPCK* is also expressed (Bahrami et al., 2001), the silencing of this protein, albeit moderately, decreases the levels of aspartate, citric acid, fructose, and glucose, while increasing malate concentration (Osorio et al., 2013; Huang et al., 2015). In contrast, in *Arabidopsis* adult plants, *PEPCK* T-DNA insertion lines display a slight decrease in alanine, which is derived from PEP, alongside an increase in aspartate, which derives from OAA (Brown et al., 2010) aligning with the eventual accumulation of OAA. The metabolic profiling of CCM of isolated GTs from *pepck* mutants did not show significant changes related to the aforementioned metabolites. Instead, the differences were rather mild, and in general, comparable to the changes reported in *Arabidopsis* or tomato fruits (Brown et al., 2010; Osorio et al., 2013). Despite this, *pepck-1* and *pepck-9* lines exhibited significant decrease in NADPH levels, consistent with the results reported in *PEPCK* RNAi tomato fruits at the breaker stage (Osorio et al., 2013). NADPH is a reducing cofactor needed for both MEP and MVA pathways to generate C₅ isoprene units (Banerjee and Sharkey, 2014). Lowered NADPH levels can alter the NADPH/NADP⁺ redox balance triggering oxidative stress and altering the energy metabolism (Smith et al., 2021).

An additional source of NADPH within the chloroplast, apart from the photosynthetic electron transport chain, may arise from the activity of the plastidic NADP-dependent malic enzyme, which is also expressed in GTs (Balcke et al., 2017). This enzyme catalyzes the conversion of malate to pyruvate, thereby producing NADPH and CO₂ (**Fig. 23**). Alternatively, NADPH can be generated via the OPP pathway (Li and Sharkey, 2013). In the scenario where OAA/malate diminishes due to a missing carboxylation activity in the cytosol, fewer C₄ dicarboxylic substrates will potentially be transported to the plastids and be used by the malic enzyme, leading to less NADPH available (**Fig. 23**). Under this premise, it is worth highlighting the possible contribution of malate transport from the cytosol to the chloroplast, not only for carbon supply but also for alternative sources of reducing power. One strategy to address this question is by studying the function of candidate C₄ transporters in the plastid membrane, that were identified in the omics data and whose function remains unknown (Balcke et al., 2017). Additionally, it is worth mentioning, that carboxylation of PEP in the cytosol can also be performed by phosphoenolpyruvate carboxylase (PEPC), that is expressed in GT as well (Balcke et al., 2017), and therefore, potentially play a role in the OAA/malate pool in the glandular cells (**Fig. 23**).

In summary, PEPCK facilitates the conversion of C₄ (OAA) to C₃ (PEP) carbon precursors in the cytosol that potentially are transported to the plastids to feed the MEP pathway. The lack of PEPCK in the GTs produce moderate changes in the CCM and energy metabolism such as reduced GA-3P and DXP, which are also observed in PEP translocator mutant *cue1* of Arabidopsis (Evans et al., 2024). At the same time, lowered import of PEP could alter the redox balance throughout reduced NADPH levels. These preliminary findings require further confirmation by absolute quantification of the metabolites. ¹³C labeling and analysis of potential triose-phosphate and C₄ acid transporters could provide additional evidence about the carbon fluxes from the cytosol to the chloroplast. The little changes documented here by the inactivation of PEPCK, highlight the complexity and the multiple metabolite pathways co-regulated to sustain the carbon economy in the GTs.

Chapter 2: Heat stress, productivity and trichome fate.

2.1 Introduction

2.1.1 The control of trichome development and productivity

The co-development of different types of trichomes (glandular and non-glandular) and the variety of SM they produce, make tomato a suitable model to investigate several questions such as: how is the distribution and density of different trichome types controlled on the leaf surface, or how is the productivity in the glandular cells regulated? In *S. lycopersicum*, several genes play a role in the initiation of different types of trichomes simultaneously (Chalvin et al., 2020). For example, *Woolly* (*Wo*, Solyc02g080260), a transcription factor (TF) member of the HD-ZIP IV subfamily, controls trichome development by repressing the expression of the cell cycle regulators like the *B-type cyclin 2* (*SICycB2*, Solyc10g083140) (Yang et al., 2011; Gao et al., 2017) (**Fig. 24**). Loss-of-function mutants of *Woolly* display a drastic reduction in long trichomes (type-I, II, III) and 50% reduction of type-VI GTs (Hua et al., 2021). This gene was originally reported in a gain-of-function natural variant (*Wo*^{P63R}), with both increased number of type-I GTs and type-V non-glandular trichomes (Yang et al., 2011; Yang et al., 2011; Wu et al., 2023). The phenotype of *Wo*^{P63R} is different in the brassinosteroid deficient background Micro-Tom, exhibiting more type-III/type-V and increased type-IV trichomes in the cotyledon stage (Vendemiatti et al., 2017). A recent study showed how *Woolly* controls the trichome fate between digitate and peltate trichomes via a concentration-base regulatory circuit. However, more research is needed to elucidate the mechanism that governs *Woolly* dosage during plant development (Wu et al., 2023). A pair of C2H2 zinc-finger proteins named HAIR (H, Solyc10g078970) and SPARSE HAIR (SH, Solyc10g078990), redundantly regulate the initiation and elongation of the long stalk type-I GTs and type-III non-GTs (Chang et al., 2018; Li et al., 2021). At the same time, there are TFs that control exclusively certain types of trichomes; for instance, the bHLH TF *SIMYC1* (Solyc08g005050) positively regulates type-VI GTs as well as the biosynthesis of mono- and sesquiterpenes produced in their glandular cells (Xu et al., 2018). Similarly, *SIMIXTA-like* (Solyc02g088190), a TF member of the R2R3-MYB subfamily regulate the differentiation of epidermal cells and type-I trichome initiation, and at the same time it can reprogram the primary metabolism affecting the secondary metabolism in the fruits (Ying et al., 2020). Another example of specificity is the scarecrow-like 3 (*SISCL3*, Solyc12g099900) TF, that controls the size of the glandular head cells of type-VI trichomes, and at the same time, regulates the expression of key genes in the MEP and MVA pathways, boosting the productivity of isoprenoids (Yang et al., 2021) (**Fig. 24**).

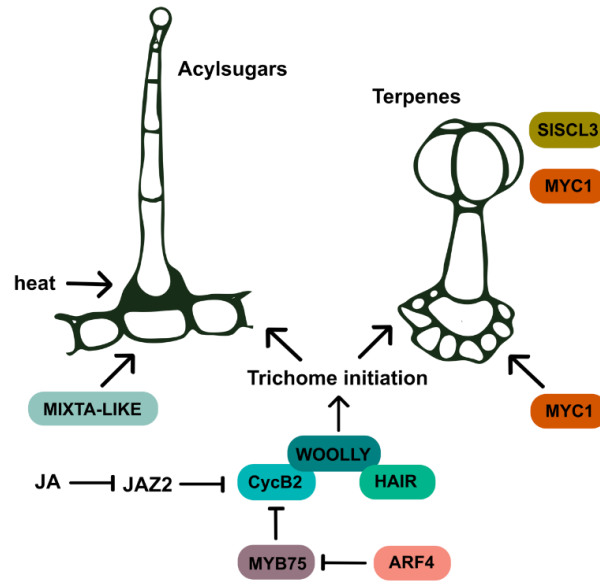


Figure 24. Molecular factors regulating the capitate type-I/IV and the peltate type-VI GTs initiation in *S. lycopersicum*.

The B-type cyclin 2 (CycB2) and the C2H2 zinc-finger protein HAIR interact with the HD-ZIP IV transcription factor Woolly, putatively forming a complex that regulates trichome initiation of digitate and peltate GTs in tomato (Chalvin et al., 2020; Wu et al., 2023). The helix-loop-helix transcription factor MYC1 regulates type-VI trichome development and terpenoid productivity (Xu et al., 2018). The R2R3-MYB subfamily TF MIXTA-like regulate the capitate type-I trichomes (Ying et al., 2020). The JASMONATE ZIM-domain 2 (JAZ2) acts by repressing Woolly/CycB2 (Yu et al., 2018). JA induces the degradation of JAZ2, thereby inducing trichome formation. Other factors described in literature include: MYB75 (Gong et al., 2021); auxin response factor 4 (ARF4) (Yuan et al., 2021); scarecrow-like transcription factor 3 (SISCL3) (Yang et al., 2021). Figure adapted from Chalvin et al. (2020) and Schuurink and Tissier (2020).

2.1.2 The role of jasmonic acid in trichome development and productivity

Trichome initiation and productivity can also be significantly influenced by specific phytohormones or the crosstalk between them (Li et al., 2021). The role of jasmonic acid (JA) and its conjugates in trichome development has been extensively reported in various plant species including *Arabidopsis*, tomato, *artemisia* and cotton (Boughton et al., 2005; Yoshida et al., 2009; Hu et al., 2016; Yan et al., 2017). In general, JA participates in several processes including plant growth and development, as well as in the response to herbivory and environmental factors (Ahmad et al., 2016; Howe et al., 2018). The synthesis of the major bioactive form of JA, the conjugate (+)-7-*iso*-jasmonoyl isoleucine (JA-Ile) starts with the release of fatty acids from the chloroplast membranes, and continues with several enzymatic reactions that take place in different cell compartments, including plastids, peroxisomes, and the cytosol (Schaller and Stintzi, 2009; Wasternack and Hause, 2013). Upon elicitation, JA-Ile is recognized by the F-box protein CORONATINE INSENSITIVE1 (COI1), which is a

component of the SCF^{COI1} receptor complex. This complex targets the JA signaling repressors named JASMONATE ZIM-domain (JAZ) proteins for the 26S proteasome degradation (Chini et al., 2007; Thines et al., 2007; Fonseca et al., 2009). By degrading the JAZs, transcription factors such as MYC2 (and other members of the basic helix-loop-helix family) are released and induce the expression of JA responsive-genes (Fernández-Calvo et al., 2011; Wasternack and Hause, 2013).

As in *Arabidopsis*, the external application of JA or methyl JA (MeJA) prompts the formation of glandular and non-glandular trichomes on the tomato leaf surface and extends the length of their stalk cells (Boughton et al., 2005; Yoshida et al., 2009; Escobar-Bravo et al., 2017; Chen et al., 2018; Hua et al., 2021). When the *JAZ2* repressor is overexpressed, it substantially decreases *Woolly* and *CycB2* transcript levels, accompanied by a lower trichome density in tomato stems (Yu et al., 2018). JA signaling can also promote terpene biosynthesis by inducing degradation of the *JAZ2*, facilitating the interaction of *Woolly* and *SIMYC1*, and together, they activate the expression of several terpene synthase genes (Hua et al., 2021). In *Arabidopsis*, MeJA triggers *MYC2* expression and in turn, sesquiterpene emission by directly binding to the promoter sequence of TPS genes (Hong et al., 2012). In tomato, the JA-insensitive mutant (*jai1*) that lacks the COI1 receptor exhibits a 65 to 75% reduction in type-VI trichome density and a lower monoterpene content than expected based solely on the decreased trichome number (Li et al., 2004). In agreement with this evidence, it has been reported that upon MeJA application, type-VI trichome density almost doubles while the amount of monoterpenes rises more than three-fold (Escobar-Bravo et al., 2017). Overall, these results highlight the role of JA/COI1 signaling in both trichome initiation and productivity.

2.1.3 Environmental and developmental cues in trichome initiation and productivity.

Trichomes can act as a physical barrier and chemical defense against diverse external factors and, as such, constitute an important aspect of how plants interact with their surroundings. Despite the evidence gathered about the role of TFs and phytohormones in trichome initiation, little is known about how environmental or developmental cues influence trichome initiation or modulate their productivity. For example, after herbivore attack, some plants respond by generating new leaves with an increased number of trichomes (Agrawal et al., 2002; Traw and Dawson, 2002; Dalin and Björkman, 2003). In *Arabidopsis*, it is known that wound-induced formation of trichomes in upcoming young leaves requires JA-mediated activation of TFs (Yoshida et al., 2009). Furthermore, trichome density has been associated with tolerance to water-stress deficiency. In *Arabidopsis lyrata*, natural populations with high trichome

abundance are more tolerant to drought compared to glabrous plants (hairless plants) (Sletvold and Ågren, 2012). In line with this report, water stress can trigger increments in trichome densities in tomato (Galdon-Armero et al., 2018) and in *Quercus serrata* (Hernandez and Park, 2022), in both cases of non-GT, coupled with a reduction in stomata, as a possible strategy to face drought conditions.

Moreover, the type and density of trichomes undergo changes throughout the progression of vegetative development. In *Arabidopsis* for example, juvenile leaves exclusively develop trichomes in their adaxial surface, whereas mature leaves exhibit trichomes on both adaxial and abaxial surfaces. The emergence of abaxial trichomes is regulated by aging rather than by leaf growth or expansion, and therefore this trait is used as a marker for juvenile-to-adult phase transition (Telfer et al., 1997; Xu et al., 2019). This age dependent mechanism is controlled by the conserved miR156/*SPL* and miR172/*AP2-like* modules (Wu et al., 2009). During early stages of development, the *AP2-like* TFs repress abaxial trichome initiation by binding the 3' non-coding region of *GLABRA1* (*GL1*). The decrease in the microRNA miR156 during vegetative growth leads to increased levels of *SQUAMOSA PROMOTER BINDING PROTEIN-LIKE* (*SPL*) genes, that activate another miR172, which in turn represses the *APETALA2-LIKE* (*AP2-like*) TFs, releasing *GL1* (Xu et al., 2019).

In contrast to *Arabidopsis*, tomato displays a higher complexity of trichome development during time and space. Among the six different types of trichomes present in cultivated tomato (Glas et al., 2012; Vendemiatti et al., 2017), type-IV GTs receive special attention due to the AS they produce and their anti-pest properties. Observations from Vendemiatti et al. (2017) indicate that in *S. lycopersicum*, type-IV trichomes occur only during the juvenile stages of plant development, starting from cotyledons where they are predominant, followed by the first set of true leaves where their presence begin to decline, until they become rare or entirely absent in adult stages of the plant. Furthermore, the overexpression of the miR156 promotes the juvenile status and, as a consequence, leads to significantly more type-IV trichomes than in the WT (Vendemiatti et al., 2017). Interestingly, while type-IV trichome numbers drop down, the non-GTs type-V, which lack the glandular cell at the tip, increase progressively during vegetative growth. On the other hand, wild tomato species such as *S. pennellii* or *S. habrochaites* exhibit type-IV trichomes along the entire vegetative growth (**Fig. 2**), and therefore it is believed that this trait was negatively selected during the domestication process of cultivated tomato.

2.1.4 Heat stress, JA, trichome development and productivity

A recent study, to which I contributed, using *S. lycopersicum* could show that long exposure to heat stress (HS), induces a shift from non-glandular type-V to glandular type-IV trichomes in

adult stages of the plant (Säbel et al., 2023). Moreover, it was shown that besides influencing type-IV trichome fate, HS boosts the AS biosynthesis to a greater extent than what would be expected solely based on the increase in type-IV trichomes. Therefore, elevated temperature showed a dual role in altering the trichome composition and productivity in cultivated tomato.

How temperature modulates both trichome initiation and/or biosynthesis of SM in GTs has not been investigated. In a different context, in a study whose objective was to test cell ablation in *Arabidopsis* as a proof-of-concept, the researchers used temperature as a switch to control the degradation of the cytotoxic bacterial RNase barnase. As a side effect of the temperature change, it could be observed that WT plants grown under low temperature, in this case 14°C, displayed less trichome density compared to the plants grown at 28°C (Faden et al., 2019). Although this was not a HS experiment, it uncovered how temperature changes can modulate trichome initiation, in this case of the non-GTs of *Arabidopsis*.

Considering the role of JA in trichome development, this raises the question of whether the effect of temperature on trichomes in tomato and *Arabidopsis*, could be mediated by this phytohormone. Jasmonates are recognized as stress phytohormones, participating in the plant's defense response to both biotic and abiotic stresses (Howe et al., 2018; Waadt et al., 2022) but little is known about the connection between JA-mediated trichome regulation and the plant's adaptive response to elevated temperatures.

2.2 Objectives Chapter 2

In tomato, TFs and hormones, especially JA, have a great influence on trichome initiation, either acting over certain trichome types or altering the global trichome composition. At the same time, they can modify the biosynthesis of SM inside the GTs. Although both GTs and non-GTs are part of the defense and communication mechanisms of plants to cope with external factors, it remains largely unknown how environmental cues can impact trichome initiation and productivity.

In Arabidopsis, trichome density can be affected by different growth temperatures (Faden et al., 2019). In tomato, elevated temperature triggers a shift in trichome fate, from non-glandular type-V to glandular type-IV, along with an exponential increment in AS secretion (Säbel et al., 2023). With this background, the question arises whether the effect of HS over type-IV trichome fate and productivity may also be extended to other GTs in tomato or if it is specific to this type of capitate trichomes. Type-VI trichomes are the most abundant type of GTs present in *S. lycopersicum*, which, instead of AS, produce mainly volatiles that are stored in a dedicated extracellular cavity (Bergau et al., 2015).

Different studies in Arabidopsis and tomato indicate that HS triggers JA responses in plants. Since JA is intricately linked to trichome development in tomato, especially to type-VI trichomes and to the biosynthesis of terpenoids they produce, it is tempting to speculate whether the effect of HS over type-IV trichomes, could be mediated by JA.

The objectives of Chapter 2 of the present thesis are:

1. Evaluate the effect of heat stress in type-VI trichome density and productivity.
2. Examine the effect of JA signaling in the interaction of HS and trichome development to find possible regulators responsible for the type-IV phenotype.

2.3 Results

2.3.1 Evaluation of the effect of heat stress on type-VI trichome development and productivity.

With the goal to determine whether HS has an effect on type-VI trichome development and/or in their productivity, experiments at elevated temperatures were conducted, following the protocol established by Säbel et al. (2023). In short, tomato plants cv MoneyMaker were germinated in control conditions CN (25°C/23°C day/night, respectively). After cotyledons fully expanded, half of the plants were transferred to HS conditions (37°C/23°C day/night respectively) for three more weeks. After that period, the number of type-VI trichomes was counted over the adaxial side of leaflets from leaf four and five. The data indicated no significant differences in type-VI trichome numbers comparing the two temperature conditions (**Fig. 25A**). However, distinct alterations in the VOC profiles were detected (**Fig. 25B-C**). In response to heat, the abundance of most of the monoterpenes increased, whereas the levels of sesquiterpenes showed a significant reduction (**Fig. 25D-E**). For instance, average levels of monoterpenes augmented by 43% (β -phellandrene/D-limonene) to 50% (2-carene), while the levels of sesquiterpenes decreased from 28% (δ -elemene) to 77% (β -caryophyllene). Similar results were obtained when exposing the model tomato accession Micro-Tom to HS, where the density of type-VI trichomes did not change between conditions. Still, an increase in monoterpenes and a reduction of sesquiterpenes were registered in heat (**Fig S4**). Here, it is worth mentioning that in the model tomato Micro-Tom, type-VI GTs do not produce high quantities of monoterpenes as in big cultivated tomato (Yang et al., 2021). Therefore, it was intriguing to observe an increase in the accumulation of these compounds after HS application.

It was hypothesized that shifts in the accumulation of these two classes of VOCs (**Fig. 25B-C**) could be supported by changes in the transcriptional activity of genes required for their biosynthesis. Hence, RNA was extracted from leaves of plants grown in CN and HS conditions, and the transcript levels of selected genes were analyzed by qRT-PCR. The expression levels of two sesquiterpene synthases, *Terpene Synthase 9* (*TPS9*) and *TPS12*, whose main reported products are germacrene (isomers A,C,D) and β -caryophyllene/ α -humulene respectively (Zhou and Pichersky, 2020), were significantly reduced in heat (**Fig. 25F**).

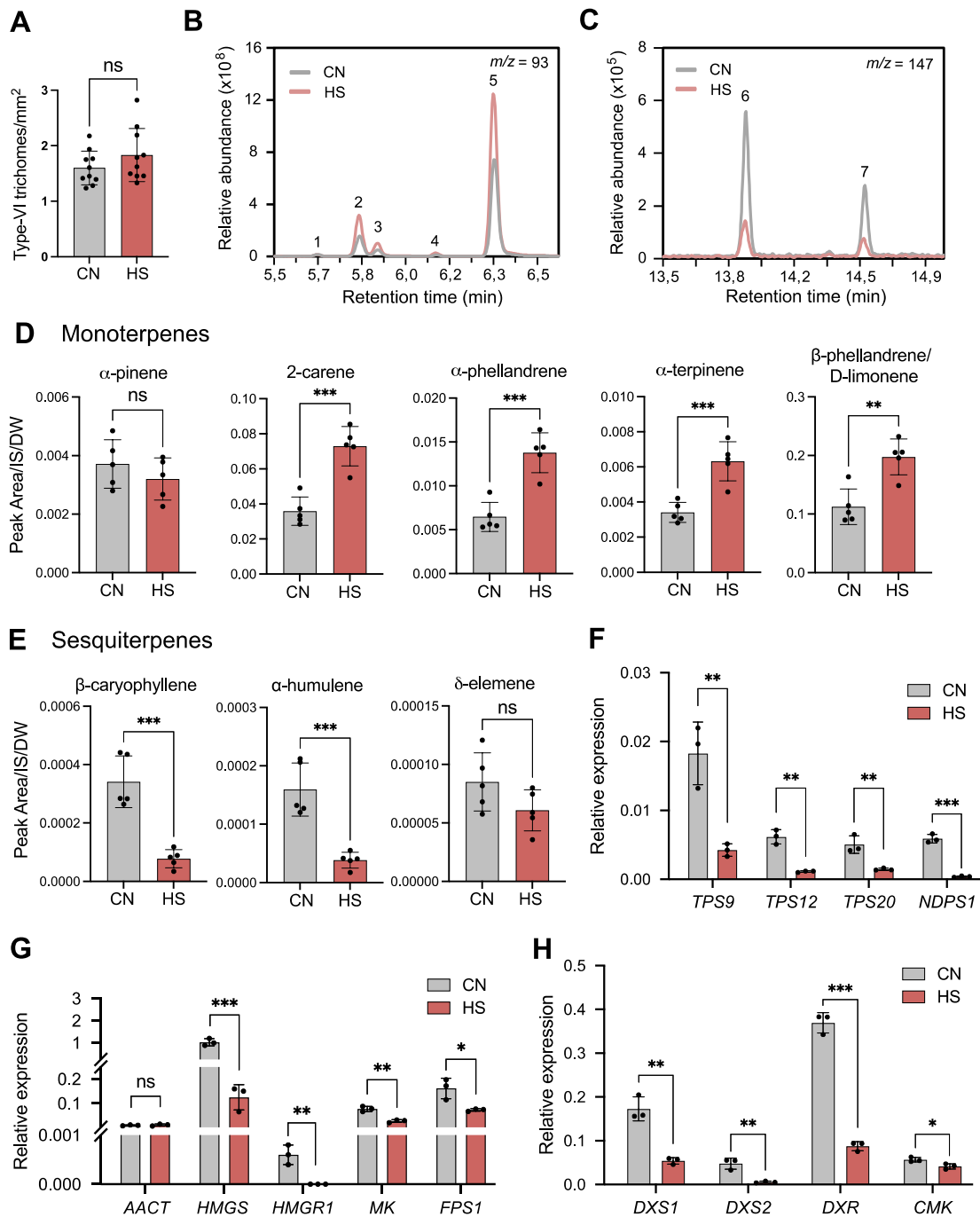


Figure 25. Effect of heat stress on type-VI trichomes and terpenoid profiles.

(A) Type-VI trichome number in tomato plants after three weeks of growth in CN and HS conditions ($n = 10$ biological replicates). Representative chromatograms displaying monoterpene (B) and sesquiterpene peaks (C) in CN and HS. Key: 1: α -pinene, 2: 2-carene, 3: α -phellandrene, 4: α -terpinene, 5: β -phellandrene+D-limonene, 6: β -caryophyllene, 7: α -humulene. Quantification of monoterpenes (D) and sesquiterpenes (E) using gas chromatography-mass spectrometry (GC-MS) ($n = 5$ biological replicates). Chromatogram peak areas were normalized to internal standard (IS) and to leaf dry weight (DW). Relative expression levels of terpene synthases (F) and selected genes involved in the MVA (G) and the MEP (H) pathways ($n = 3$ biological replicates). TPS, terpene synthase; NDPS1, Neryl-diphosphate synthase 1; AACT, Acetyl-CoA C-acetyltransferase; HMGS, hydroxymethylglutaryl-CoA synthase; HMGR1, 3-hydroxy-3-methylglutaryl-coenzyme A reductase 1; MK, mevalonate kinase;

FPS1, farnesyl diphosphate synthase; *DXS*, deoxy-xylulose phosphate synthase; *DXR*, deoxy-xylulose phosphate reductoisomerase; *CMK*, 4-(cytidine 5'-diphospho)-2-C-methyl-D-erythritol kinase. Error bars indicate standard deviation. * $P < 0.05$, ** $P < 0.01$, *** $P < 0.001$; using Student's *t*-test.

At the same time, genes participating in the MVA pathway were investigated, such as *hydroxymethylglutaryl-CoA synthase (HMGS)*, *3-hydroxy-3-methylglutaryl-coenzyme A reductase 1 (HMGR1)*, *mevalonate kinase (MK)* and *farnesyl diphosphate synthase (FPS1)* displaying reduced expression at elevated temperatures (**Fig 3**, **Fig. 25G**). Contrary to expectations, the transcript levels of *TPS20*, responsible for synthesizing the major monoterpenes in type-VI GTs including 2-carene, α -terpinene, α -phellandrene and β -phellandrene (Zhou and Pichersky, 2020), as well as of *Neryl-diphosphate synthase 1 (NDPS1)*, that catalyzes their immediate precursor (Schillmiller et al., 2009), were also downregulated. Similarly, important genes controlling the flux through the MEP pathway, such as *deoxy-xylulose phosphate synthase (DXS1)*, *DXS2*, *deoxy-xylulose phosphate reductoisomerase (DXR)* and *4-(cytidine 5'-diphospho)-2-C-methyl-D-erythritol kinase (CMK)* exhibited a significant reduction in the transcript levels after long-term heat exposure (**Fig. 3**, **Fig. 19H**).

2.3.2 Metabolite profiling of trichomes under heat stress

To gain further insights into the changes in trichome productivity, metabolomics profiling of polar and semipolar metabolites was carried out using LC-MS/MS. Briefly, tomato plants cv Moneymaker were germinated in CN for one week, and then half of the plants were transferred to HS conditions. After five weeks of growth in Phyto cabinets, HS plants displayed a typical thermo-morphogenic response, including elongation of the stem and petioles, upward bending of leaves (leaf hyponasty) and reduction in the size of the leaves (**Fig. 26A**) (Quint et al., 2016; Delker et al., 2022). Trichomes were brushed off from leaf lamina and petioles of WT plants growing in these two temperature conditions. Trichome-free leaves were included for comparison purposes. Different metabolites were obtained using the two-phase extraction method and separated in the aqueous and organic phases. First, hydrophilic compounds comprising metabolites involved in the central carbon and energy metabolism were separated and detected using a negative mode electrospray ionization (ESI) on a QTrap6500. Peak areas of 113 detected MS¹ mass/retention time features already identified were compared within the different samples. Data normalization and scaling were performed using the MetaboAnalyst software. Principal component analysis (PCA) displayed larger separation between leaves and trichome samples (PC1; 65,7%), while separation of the samples in the two temperature conditions, albeit to a lesser extent, was only obtained between the trichome samples (PC2;

13,5%) (**Fig. 26B**). This suggests that when plants are subjected to prolonged periods of HS, major metabolic changes persist in the GTs compared to what occurs in the leaves. Therefore, the subsequent analyses were performed considering only the trichome samples. The top 50 features/compounds with contrasting differences ordered according to the p value from a t -test, are illustrated on a heatmap in **Fig. 26C**. In more detail, a total of 30 compounds showed significant differences ($FDR = 0,05$) (**Fig. 27A, Table S3**), that were subsequently used for pathway enrichment analysis. Significantly enriched pathways included 1. pentose phosphate pathway, (comprising GA-3P, fructose 1,6 biphosphate (FBP), xylulose 5-phosphate and erythrose 4-phosphate (E4P)) 2. pentose and glucuronate interconversion, 3. starch and sucrose metabolism (including sucrose, UDP-glucose, glucose 1-phosphate, glucose 6-phosphate, and ADP-glucose) and 4. CBB cycle (including PEP, GA-3P, FBP, ribulose 5-phosphate + D-xylulose 5-phosphate (RIBU5P+XU5P), sedoheptulose 1,7-bisphosphate (S1,7BP), and E4P) (**Fig. 27B**). Three intermediates of the MEP pathway showed increased levels in trichomes under HS compared to CN, such as methyl-D-erythritol phosphate (MEP), 4-CDP-2-C-methyl-D-erythritol 2-phosphate (CDP-MEP) and 2C-methyl-D-erythritol 2,4-cyclodiphosphate (MEcPP). On the other hand, intermediates of the tricarboxylic acid (TCA) cycle including malonyl-CoA, malate, citrate, and fumarate, exhibited reduced levels in the HS trichome samples (**Fig. 27C, Table S3**). Despite this, the levels of acetyl-CoA remained unchanged between the samples.

Next, to confirm the results from the targeted metabolomics, absolute quantification of some of the organic acids was performed using the available authentic standards. The metabolites were extracted, derivatized, and subsequently measured by GC-MS/MS. The results showed a reduced amount of TCA intermediates in the HS trichome samples, e.g., 52%, 59%, 47% and 42% less citrate, succinate, fumarate, and malate respectively and only phosphate exhibited increased levels in HS (**Fig. 28A**).

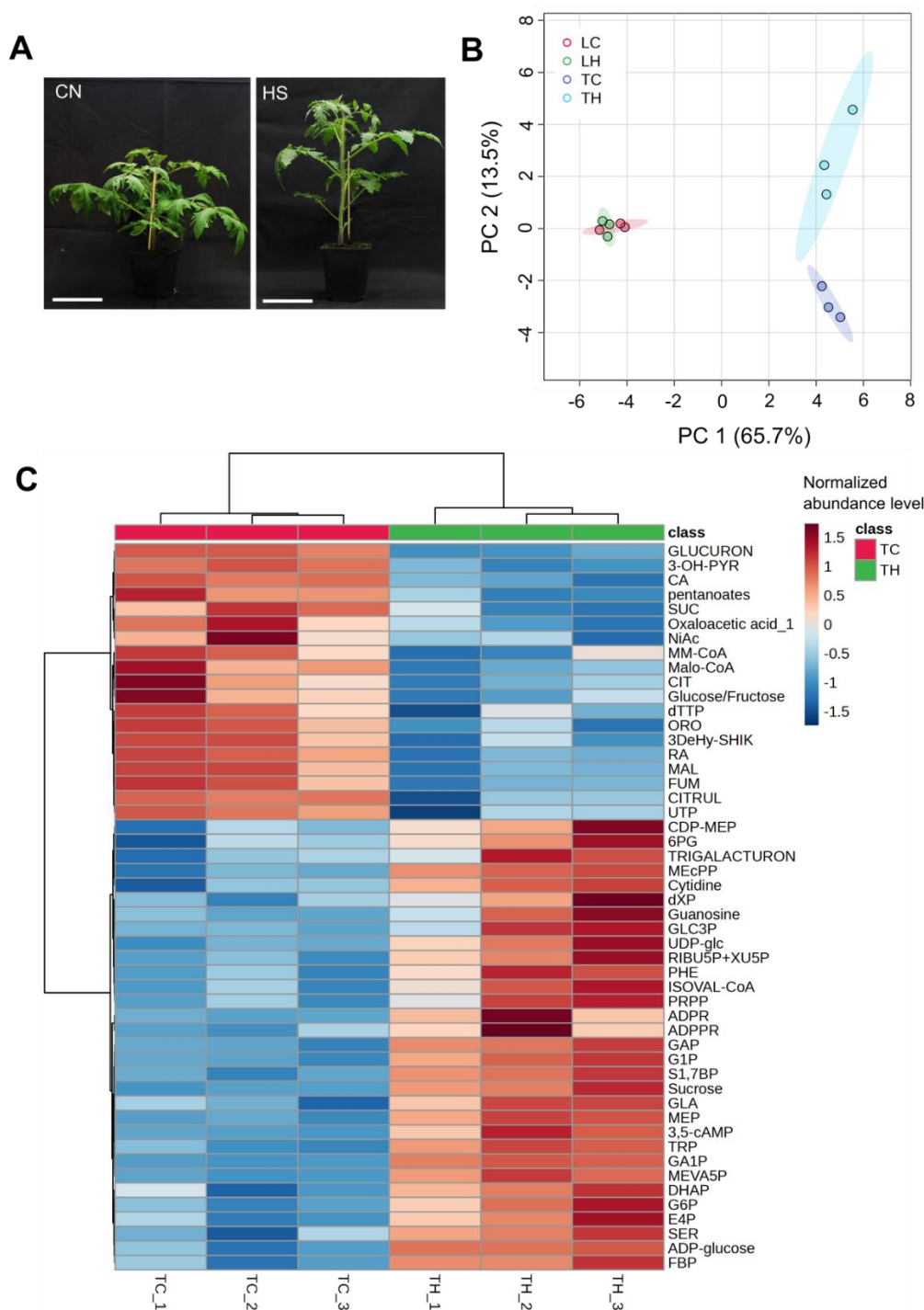


Figure 26. Central carbon and energy metabolite profiling of glandular trichomes under heat stress (HS).

(A) Five-week-old tomato plants displaying thermo-morphogenic phenotype after applying HS for five weeks, compared with plants grown in control (CN) conditions. Scale bar = 11 cm. **(B)** Principal component analysis of polar metabolites separated with the NRG method from leaves and trichomes collected from CN and HS conditions ($n = 3$ biological replicates). **(C)** Hierarchical clustering heatmap of the top 50 different metabolites detected in the trichomes of CN and HS according to the p -value from applied Student's t -test. **Key:** LC, leaves control; LH, leaves heat stress; TC, trichomes control; TH, trichomes heat stress. Metabolite names corresponding to the abbreviations are provided in Table S3.

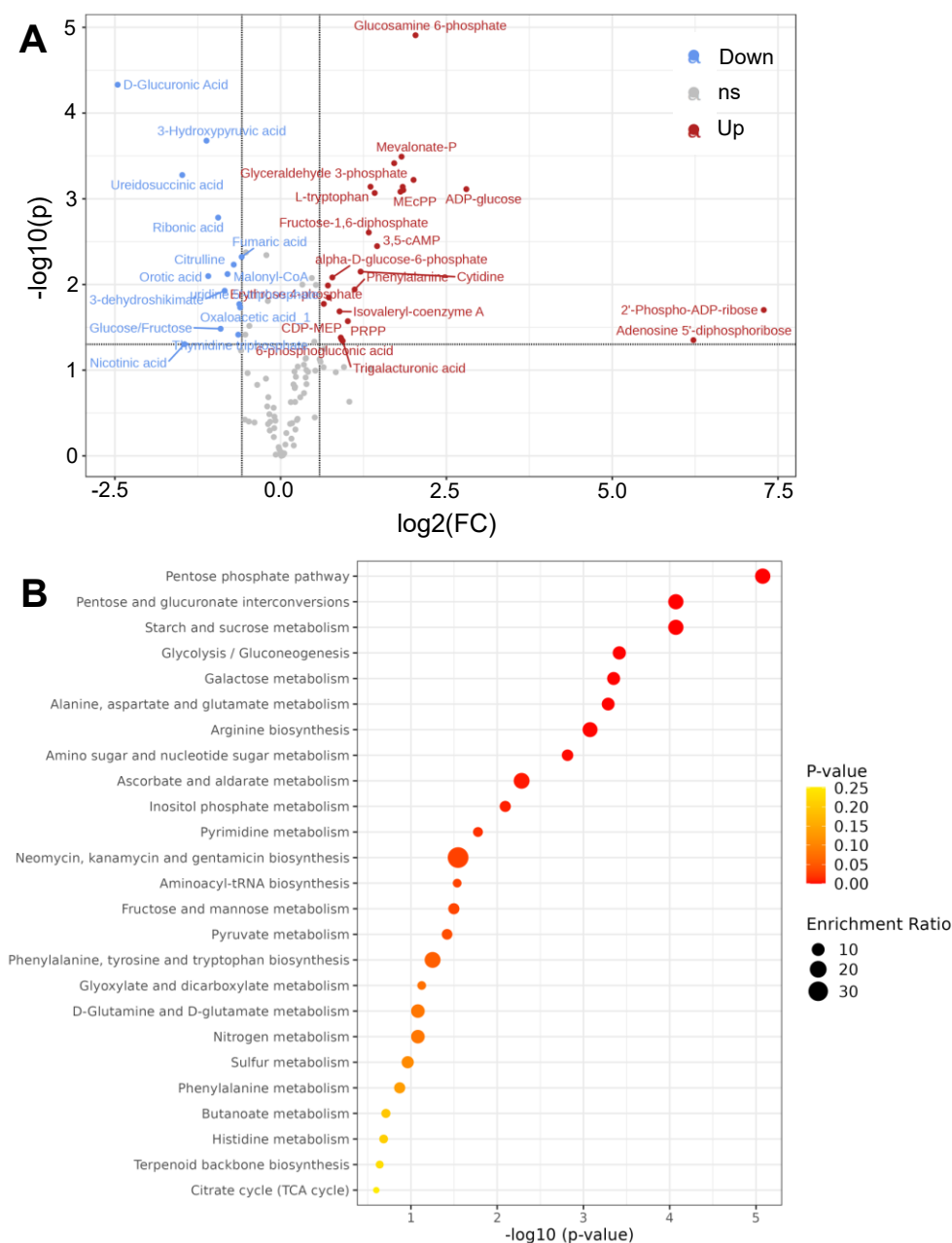


Figure 27. Pathway enrichment analysis of the CCM metabolites in trichomes of CN versus HS.

(A) Volcano plot displaying significantly different polar metabolites between CN and HS trichome samples, $P < 0,05$ using t -test. The X-axis indicates $\text{Log}_2(\text{fold change})$, and the y-axis indicates the $-\log_{10}(p\text{-value})$ where the gray dotted line corresponds to $0,05$. Metabolites in red have a $\log_2(\text{FC}) > 1,5$, and metabolites in blue have a $\log_2(\text{FC}) < -1,5$. Gray dots are metabolites that are non-significant (ns). (B) Pathway enrichment analysis using the significantly different metabolites ($FDR: < 0.05$). Data analysis and graphics were produced using MetaboAnalyst software. <https://www.metaboanalyst.ca/>

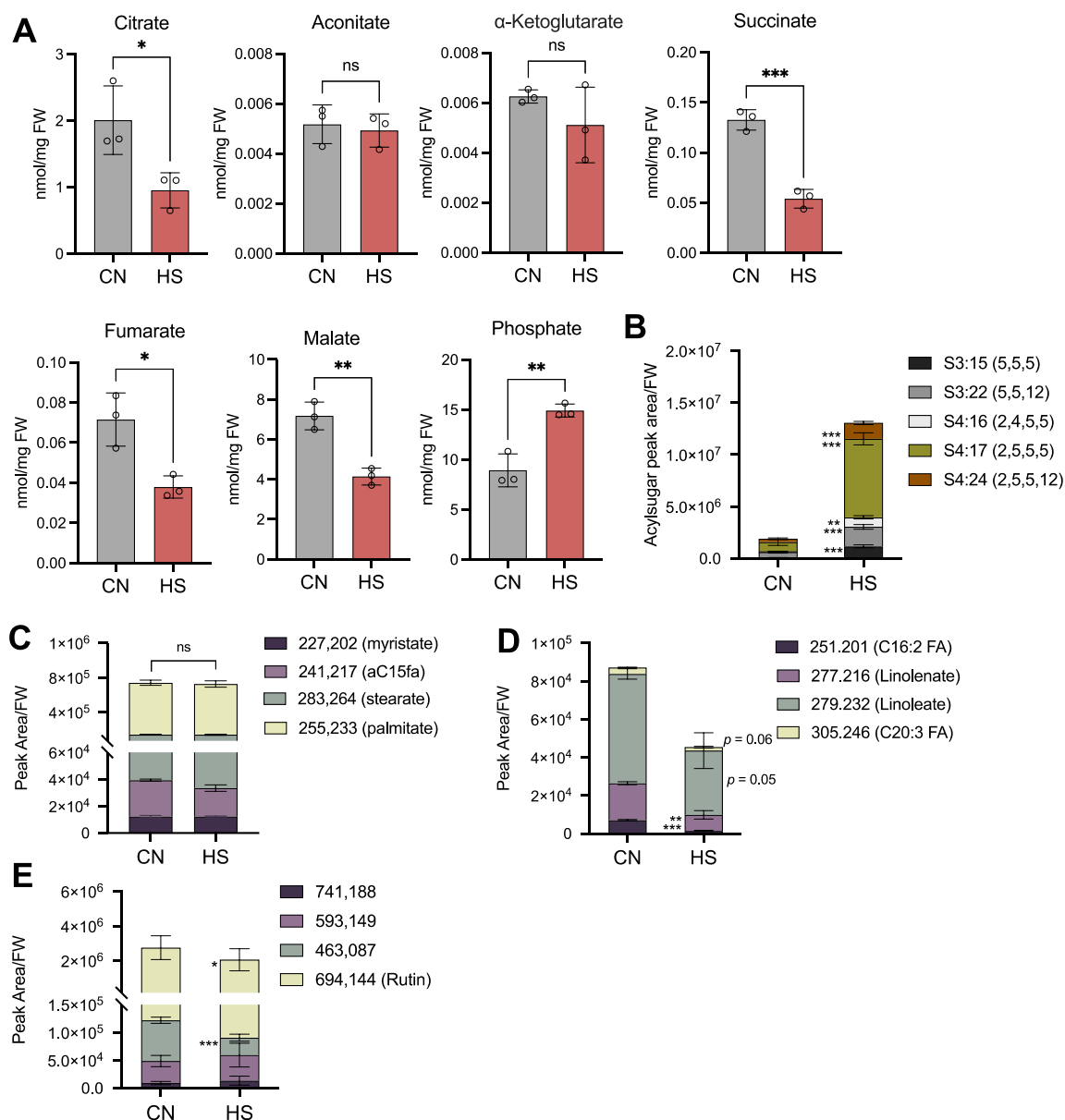


Figure 28. Changes in TCA intermediates and semipolar SM in GTs under heat stress (HS).

(A) Absolute quantification of the organic acids and Pi using gas chromatography-mass spectrometry (GC-MS/MS) ($n = 3$ biological replicates). Metabolite concentrations were calculated using the internal standard and divided by the fresh weight. Assessment of representative acylsugars (AS) **(B)**, saturated fatty acids **(C)** polyunsaturated fatty acids **(D)** and flavonols **(E)** using ultra-performance liquid chromatography-mass spectrometry (UPLC-MS). Chromatogram peak areas were normalized by the trichome fresh weight (FW) ($n = 3$ biological replicates). The name of the AS is indicated with the standard nomenclature. Numbers in C, D and E, specify the m/z of [M-H] and in parenthesis the common name if defined. Error bars indicate standard deviation. * $P < 0.05$, ** $P < 0.01$, *** $P < 0.001$; using Student's t -test.

To complement the metabolite profiling, semipolar metabolites were estimated via untargeted metabolomics using LC-MS/MS. In this case, prevalent SM found in GTs of tomato, reported in Balcke et al. (2017) were screened, and the peak areas of MS¹ mass/retention time of

individual compounds were registered. First, and as expected acylsugars (AS) produced by trichomes exposed to HS increased from 3 to 18-fold, depending on the individual AS (**Fig. 28B**). This increase is partly due to the higher type-IV trichome density but also due to a boost in the AS biosynthesis (Säbel et al., 2023). Although trichome fractions isolated from tomato are enriched in type-VI glandular head cells, broken type-IV trichomes can also be obtained, which explains the high abundance of AS in the samples. Saturated and polyunsaturated fatty acids (FAs) enriched in the trichomes were estimated in both samples. While the saturated FAs remained unchanged, significant differences were obtained for certain unsaturated FAs, resulting in an overall estimated reduction of 50% (**Fig. 28C-D**). Conjugated flavonols, mainly rutin, dominate the metabolite content in GTs of cultivated accessions (Balcke et al., 2017). Although significant, only a moderate decrease in some of the flavonol-derived metabolites was noticed, including rutin, in the HS trichome samples compared to CN (**Fig. 28E**).

In summary, the results showed that HS application did not increase type-VI trichome density as occur with type-IV trichomes, but instead triggered changes in the VOCs metabolic profiles. On the one hand, most of the monoterpenes were induced, while the sesquiterpenes were depleted. Overall, the transcript levels of genes involved in the biosynthesis of the isoprenoids were downregulated at elevated temperatures. These results raise many questions on how, despite the reduced transcript levels of the MEP pathway and the TPS genes, the plants still accumulated moderately higher amounts of plastid-derived monoterpenes. The metabolic profile of trichomes under high temperature differed from that of trichomes under control temperature conditions. This difference was not observed in the leaves. Metabolites belonging to pentose phosphate, CBB and sugar degradation pathways are overrepresented in the trichomes under HS. Moreover, the decreased amount of TCA intermediates was confirmed by absolute quantification. Finally, besides the remarkable increase in AS, polyunsaturated FAs were selectively affected by HS, whereas no major changes were registered in terms of flavonol derivatives.

2.3.3 The role of jasmonate signaling in heat stress-induced type-IV trichome development.

The influence of JA on trichome development across different plant species, alongside recent studies exploring its role in HS responses, motivates us to explore whether JA plays a part in the HS-induced shift of trichome fate. The following experiments included in **2.3.3**, were conducted jointly with Robert Säbel (PhD candidate), and the results from these experiments are included in our recent preprint (Säbel et al., 2023). To answer that question, the *jasmonic acid-insensitive 1 (jai1)* mutant, defective in JA signaling, was submitted to HS regimes. The

jai1 possesses a 6.2 kb deletion in the ortholog of the Arabidopsis *CO11* receptor, which leads to a loss-of-function of the *CO11* gene in tomato (Li et al., 2004). In contrast to Arabidopsis, the *jai1* mutant displays a female sterile phenotype (Li et al., 2004), and therefore, seeds from heterozygous *jai1* plants were screened for zygosity. Seeds of the *jai1* heterozygous parental line cv Castlemart were sown in CN conditions. When the first true leaves were visible, foliar tissue was used for genotyping using conventional PCR. Once genotyped, plants of each genotype (+/+, +/*jai1*, *jai1/jai1*) were either retained in CN or submitted to HS for 20 more days. At the end of this period, trichome density and SM were assessed. First, the results showed that type-VI trichome density did not change significantly after applying HS compared to CN, within each genotype (Fig. 29A). The *jai1* mutant displays a reduced density of type-VI trichomes as reflected in the trichome counting, but the differences are not as pronounced as the ones observed in the *jai1* mutant line within the Micro-Tom background, reported in Li et al. (2004).

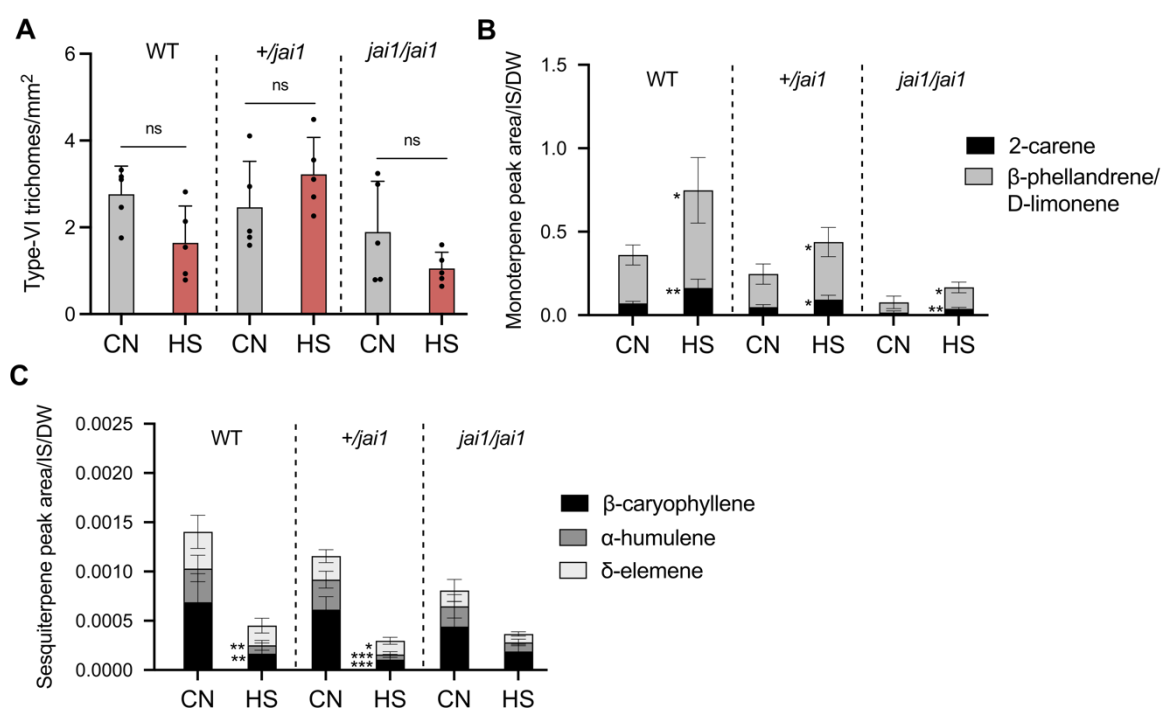


Figure 29. Changes in type-VI trichome density and productivity upon heat stress (HS).

(A) Counting of type-VI trichomes on the abaxial side of leaves of the wild type (WT), heterozygous (+/*jai1*) and homozygous (*jai1/jai1*) plants after 20 days of growth under control (CN) and HS conditions ($n = 5$ biological replicates). Only significant differences are depicted with different letters. Quantification of the most abundant monoterpenes (B) and sesquiterpenes (C) using gas chromatography-mass spectrometry GC-MS ($n = 5$ biological replicates). Error bars display standard deviation. Pairwise comparisons were performed using Student's *t*-test * $P < 0.05$, ** $P < 0.01$, *** $P < 0.001$.

Next, and in agreement with the previous results using the cv Moneymaker, the elevated temperature led to an increment in the monoterpenes and a reduction in the sesquiterpenes. The extent on the rise in monoterpenes was lower in *+jai1* and *jai1/jai1* compared to the WT (*+/+*), while the levels of sesquiterpenes after HS were comparable in all genotypes (**Fig. 29B-C**). On the other hand, type-IV trichomes were induced in heat. Both WT and *+jai1* displayed the increment in type-IV GTs trichomes while type-V decreased, supporting the shift in trichome fate reported before (Säbel et al., 2023) (**Fig. 30A-B**). However, the homozygous *jai1* plants did not show changes in trichome composition, from type-V to type-IV trichomes (**Fig. 30A-B**). Supporting this finding, an increase in AS was only observed in the WT and in *+jai1* but not in the homozygous *jai1* (**Fig. 30C**).

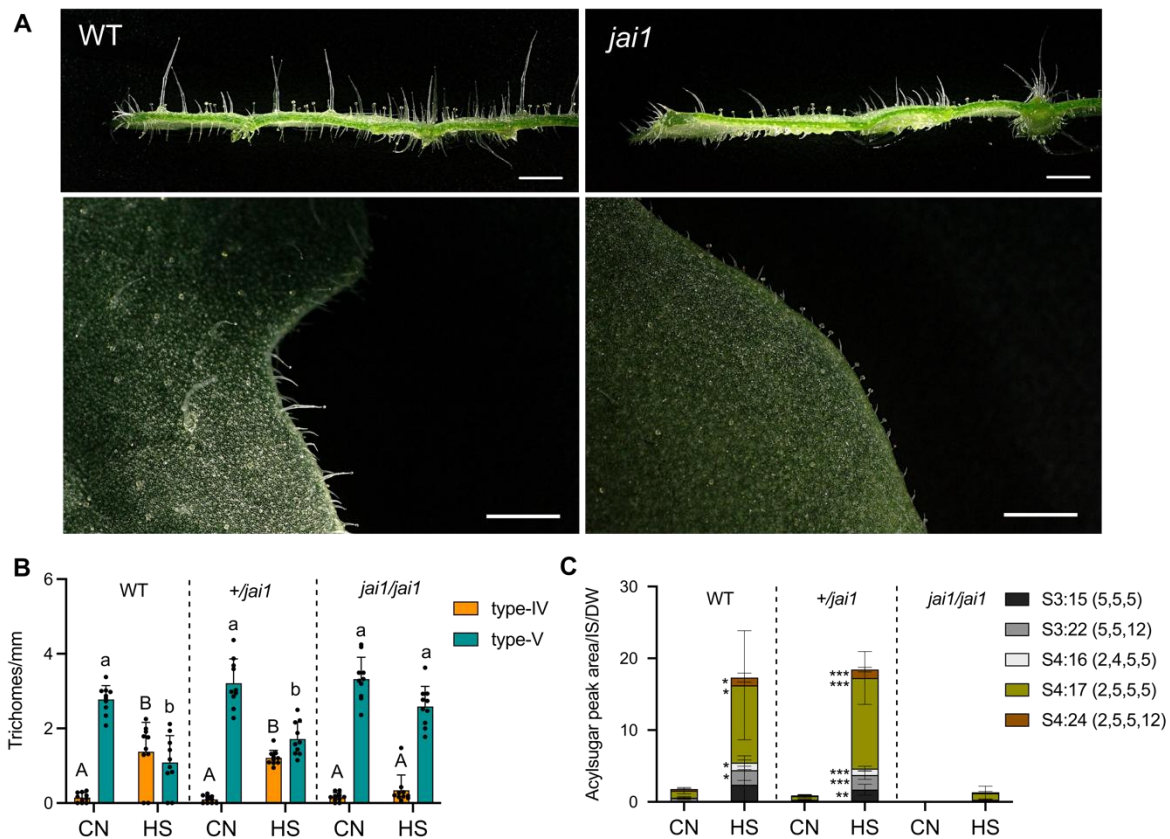


Figure 30. The *jai1* mutant does not exhibit type-IV trichome induction upon heat stress (HS).

(A) Transversal slices (up) and leaf margins (down) of WT and homozygous *jai1* plants grown in HS. (B) Counting of type-IV/V trichomes over leaf margins of the wild type (WT), heterozygous (*+jai1*), and homozygous (*jai1/jai1*) plants after 20 days of growth under control (CN) and HS conditions ($n = 10$ biological replicates). (C) AS quantification using liquid chromatography-mass spectrometry LC-MS. Chromatogram peak areas were normalized to the internal standard (IS) and to leaf dry weight (DW). Error bars display standard deviation. Different letters indicate significant differences after one-way ANOVA ($P < 0.05$, using Tukey's test). Pairwise comparisons in C were performed using Student's t -test, $*P < 0.05$, $**P < 0.01$, $***P < 0.001$.

Presuming that heat could trigger changes in JA and JA-related hormone levels, leaf tissue from the same plant set was collected and used to quantify the phytohormones. The measurements demonstrate no significant differences in JA, JA-Ile, and in the precursor *cis*-12-oxo-phytodienoic acid (OPDA) levels (**Fig. 31**). In summary, tomato *jai1* mutant, deficient in JA signaling, do not exhibit alterations in type-VI trichomes, but they are impaired in the development of type-IV trichomes upon HS, although no alterations in the JA levels were observed between the two temperature conditions.

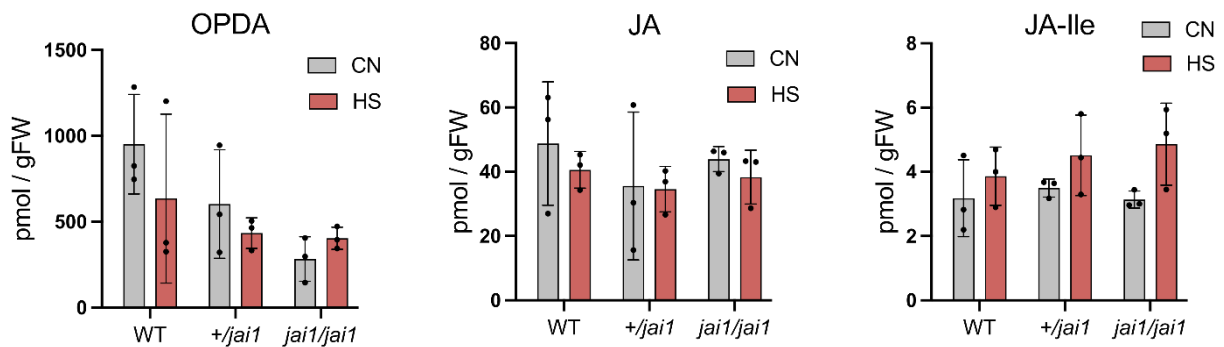


Figure 31. JA and JA-related hormone levels after long heat stress (HS) exposure.

Phytohormone levels in leaf samples of plants growing during 20 days in control (CN) and heat stress (HS) conditions ($n = 3$ biological replicates). OPDA, *cis*-12-oxo-phytodienoic acid; JA, jasmonic acid; JA-Ile, (+)-7-*iso*-jasmonoyl isoleucine. Error bars indicate standard deviation.

2.3.4 Comparative transcriptome analysis of WT and JA-deficient tomato plants upon heat stress.

Experiments performed by Säbel et al. (2023) concluded that the induction of type-IV trichomes and AS increases gradually with the exposure to heat; and that extended periods of HS resulted in higher trichome densities and AS quantities on the tomato leaf surface. Moreover, since the HS-induced shift from type-V to type-IV trichomes occurs upon trichome initiation, the application of heat during the early stages of leaf development exerts a significant impact on the trichome fate, because it is during this stage where the majority of trichomes emerge from the epidermis, and whose density decreases as the leaf grows and expands. The lack of type-IV trichomes in *jai1* mutant submitted to 37°C during the day, uncovers the role of JA/*COI1* signaling in the HS-induced shift of trichome fate. Thus, the contrasting phenotype observed in *jai1* can be used to investigate molecular factors controlling trichome fate upon HS. Here, a transcriptome analysis was conducted with the following experimental design: segregating *jai1* heterozygous seeds were sown on soil and grown for two weeks in CN conditions. After genotyping, only WT and *jai1* homozygous plants were retained, and half of the plants of each

genotype were transferred to HS. The young emerging terminal leaflet of the third leaf was collected after one, two, three, five and eight days of growth in HS as well as the respective samples at CN of each time point, of both genotypes and in triplicates (**Fig. 32A**). RNA was extracted from a total of 60 leaf samples and subsequently sent for RNA sequencing (RNASeq).

The PCA depicted a clear sample separation between CN and HS growth conditions (**Fig. S5**). The largest variation in the samples (PCA1, 43%) roughly aligns with the time point of collection, which correlates to the vegetative growth of the leaf, followed by the two temperature conditions (PCA2, 19%). No separation was observed of the *jai1* from the WT samples within the same temperature (**Fig. S5**). To have an overview of the global changes in the transcriptome of the samples, genes of *jai1* and WT were compared within the same time points and under the two temperature conditions. Differentially expressed genes (DEGs) were filtered by applying a Log_2FC of $-1.5 < \log_2\text{FC} < 1.5$ and a P value < 0.05 . Overall, the number of DEGs between the two genotypes across the five time points was generally higher in the HS samples compared to the CN, especially on days two and five after heat application (**Fig. 32B**).

To examine which biological processes experienced an impact due to the timing of HS, but also whether the response in the *jai1* was different, gene ontology (GO) enrichment analysis was performed using all the samples and conditions. Enriched GO terms related to the category biological process are illustrated in **Fig. S6**. First, as expected, “response to temperature stimulus” was one of the overrepresented processes, and a conserved pattern was observed within the biological replicates in both genotypes. Processes such as carotenoid and pigment biosynthesis and metabolism were downregulated in HS regardless of the genotype. On the other hand, processes such as “regulation of peptidase activity” and “negative regulation of proteolysis” were upregulated much earlier in WT compared to the *jai1* samples, starting from the third day after HS application. Finally, genes linked to the GO term “regulation of defense response” were induced in the WT from the second day of HS application reaching comparable levels to the samples under CN after eight days of growth, while in the *jai1*, the genes that fall into this category remained downregulated in both conditions (**Fig. S6**).

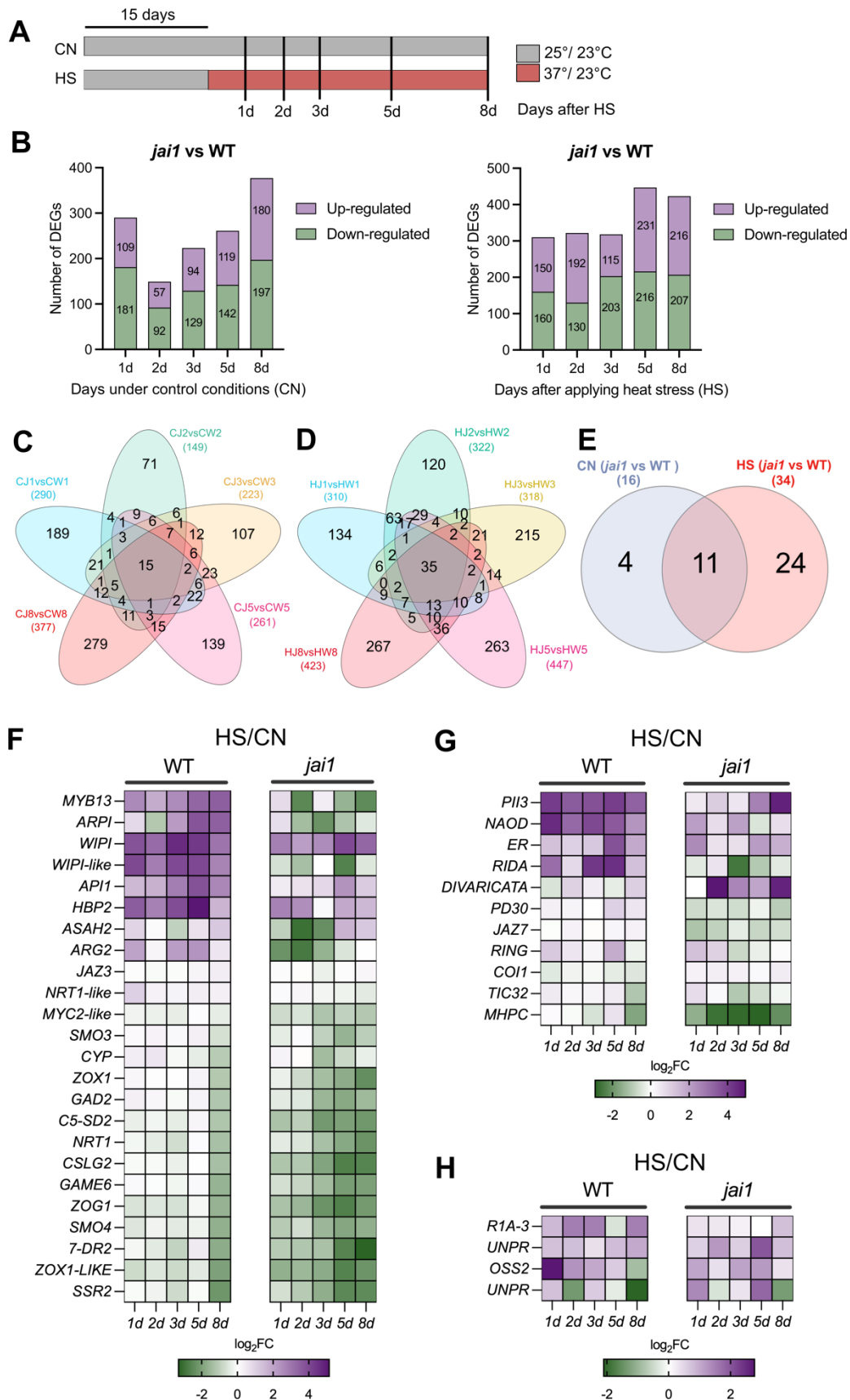


Figure 32. Transcriptome analysis of WT and *jai1* tomato under heat stress (HS).

(A) Scheme of the plant growth conditions, and the time points selected to harvest leaf samples used for the RNASeq analysis. (B) Histograms depicting the number of differentially expressed genes (DEGs)

($-1.5 < \log_2FC < 1.5$; $P < 0.05$) between *jai1* and WT in control (CN) and HS treatments. Venn diagrams depicting the DEGs between the two genotypes across all five time points in CN (**C**) and HS (**D**). (**E**) Venn diagram of the shared DEGs at all time points between *jai1* and WT in CN and HS of the comparisons depicted in C and D. (**F-H**) Heat maps displaying the \log_2FC of HS versus CN of the 39 DEGs shortlisted in the Venn diagram in (**E**) within individual genotypes. Shown are DEGs from HS only (**F**), common to both treatments (**G**), and from CN only (**H**). Corresponding gene names are included in Table S5.

Next, to refine the selection of potential candidate genes, the RNASeq data set was analyzed, looking for genes differentially expressed between the WT and *jai1* in HS, but not in CN conditions. Common DEGs in all-time points within the same temperature condition were retained, and these two subsets of DEGs were compared. The results are illustrated in Venn diagrams (**Fig. 32C-D**). After these comparisons, 24 genes were differentially expressed only in HS, four genes only in CN, and 11 in both conditions and with significant differences in each case (**Fig. 32E, Table S5**). To get an overview of changes in gene expression due to elevated temperature, the 39 shortlisted genes were employed to calculate the \log_2FC between HS versus CN within each genotype and the results were illustrated using heat maps (**Fig. 32F-H**).

2.3.5 A JA response upon heat stress.

Among the DEGs, typical JA response genes were found, including proteinase inhibitors (PIs) and JAZ proteins (Wasternack and Hause, 2013). Some PIs such as *ARPI* (Potato type II proteinase inhibitor family, Solyc11g021060) and *WIPI-LIKE* (Wound-induced proteinase inhibitor 1-like, Solyc09g084490) displayed upregulation in the WT upon HS, while in the *jai1*, they showed instead downregulation throughout the days. On the other hand, genes such as *WIPI* (Wound-induced proteinase inhibitor 1, Solyc09g083440) and *API1* (Aspartic protease inhibitor 1, Solyc03g098780) were commonly induced in the WT and in a lesser extent in the *jai1* in response to elevated temperature (**Fig. 32F-H**). The *Trypsin and protease inhibitor 13* (*PII3*) (Solyc11g022590) showed a progressive increase in the *jai1*, reaching \log_2FC values on day eight, comparable to the WT values after the first day of HS. Some JAZ repressors detected in the RNASeq data exhibited similar expression patterns in the WT and *jai1*. For example, *JAZ4* (Solyc12g049400) was significantly upregulated in the WT (e.g. \log_2FC 1,4 and 2,5; at days two and five respectively) and in the *jai1* (e.g. \log_2FC 2,7 at day three) (**Fig. S7**). Similarly, *JAZ13* (Solyc01g103600) presented higher and significant transcript levels in all time points in the WT and almost all in the *jai1*, with an average \log_2FC of 1,3 in both genotypes. On the other hand, *JAZ7* (Solyc11g011030), although differentially expressed in both genotypes regardless of the temperature, was the only JAZ showing a downregulation trend

in the *jai1* since the first day of heat application, with an average \log_2FC of -0,75 across all the time points (**Fig. S7**).

Regarding JA biosynthesis, some of the genes exhibited similar expression patterns in both WT and *jai1* upon HS (**Fig. S7**). For example, *OPDA reductase 2 (OPR2)* (Solyc01g103390) showed higher transcript levels (average \log_2FC 1,1 in both genotypes) and significant in most of the time points sampled after HS application, while *OPR1* (Solyc10g086220) showed lowered levels (average \log_2FC -0,6 in both genotypes). Genes such as *allene oxide synthase 1 (AOS1)* (Solyc04g079730) and the *lipoxygenase F (loxF)* (Solyc01g006560), exhibited elevated expression throughout the days, although the differences were not statistically significant. An exception to this trend occurred on day eight after HS, when *AOS1* displayed negative regulation in both genotypes.

2.3.6 Heat stress alters cholesterol biosynthesis and zeatin regulating enzymes.

Several genes involved in cholesterol biosynthesis pathway such as *SSR2* (Solyc02g069490), *SMO3* (Solyc01g091320), *SMO4* (Solyc06g005750), *C5-SD2* (Solyc02g086180) and *7-DR2* (Solyc06g074090) and in the steroidal glycoalkaloid (SGA) biosynthesis, including *GAD2 (GAME11)*, (Solyc07g043420), *GAME6* (Solyc07g0434609) and *ZOX1* (also annotated as *GAME17*, Solyc07g043480) were progressively downregulated during the days of HS application (**Fig. 32F, Table S5**). When comparing the \log_2FC of HS versus CN in WT and *jai1*, it can be noticed that elevated temperature exerts a stronger effect on these genes in the *jai1* mutant. These two pathways are intricately linked because cholesterol serves as a precursor for the biosynthesis of the SGAs (Sonawane et al., 2016; Swinnen et al., 2022).

Furthermore, several zeatin O-glycosyltransferases were differentially regulated when comparing WT and *jai1* genotypes in HS, including *ZOX1* and *ZOX1-LIKE* (Solyc05g053120) annotated as *zeatin o-xylosyltransferases*, and *ZOG1* (Solyc11g066670) annotated as *zeatin o-glucosyltransferase*. Like the expression patterns observed in cholesterol and SGAs pathways, the 37°C treatment resulted in a gradual downregulation of the zeatin O-glycosyltransferases, with a more pronounced and earlier effect in the *jai1*, especially *ZOG1* and *ZOX1-LIKE* (**Fig. 32F**). These enzymes participate in the conjugation of zeatin with sugar donors such as uridine diphosphate glucose/xylose (Spíchal, 2012) leading to a reversible inactivation of cytokinins. Therefore, glycosylation of zeatin constitutes one of the controlling mechanisms to balance the phytohormone levels (Mok and Mok, 2001).

2.3.7 Transcription factors.

One of the main goals of the comparative transcriptomics approach was to identify transcription factors (TFs) that potentially control the expression of genes involved in the HS-induced shift of trichome fate mediated by JA signaling. The comparisons shortlisted three TFs. Two TFs were differentially expressed when comparing the *jai1* and WT under HS: *MYB13* (Solyc06g083900) and *MYC2-LIKE* (Solyc01g096370), and only one TF was regulated in both genotypes regardless of the temperature: the MYB TF *DIVARICATA* (Solyc05g052610). By comparing the expression of these TFs in HS versus CN within the genotypes, *MYC2-LIKE* showed a negative regulation trend in both genotypes across the days, with lower \log_2FC values in the *jai1*, especially at days three and eight (-1,3 and -1,2; respectively) compared to the WT (-0,4 and -0,4; respectively). The TF *DIVARICATA* was induced in the *jai1* upon HS from day two, with an average \log_2FC 3,4 between days two and eight. Conversely, *MYB13* was the only TF displaying contrasting expression patterns in WT and *jai1* under HS. In WT, *MYB13* was upregulated in all the sampled days (average \log_2FC 2,8), whereas in the *jai1* the expression was suppressed following heat application, with average \log_2FC -1,1.

2.3.8 Changes in JA biosynthesis and signaling upon heat stress.

Genes related to JA signaling and response displayed changes in expression in the HS treated samples compared to CN, suggesting that JA could play a role in the response to heat. However, the levels of JA and related hormone intermediates in the plants grown at 37°C for three weeks did not differ from those present in plants grown at 25°C (**Fig. 31**). In Arabidopsis the expression of *12-oxophytodienoate reductase 3* (*OPR3*), *MYC2* and the JAZ proteins are induced shortly after heat stress exposition (Agrawal et al., 2002; Tian et al., 2020). Since phytohormone levels were measured after long-term exposure to heat, it triggered the question of whether the JA mediated response could occur at early time points after heat application. Therefore, a HS time series experiment was performed focusing on the heat response within the first six hours. Briefly, WT tomato plants cv Moneymaker were germinated and grown under CN conditions (25°C/23°C, day/night). Two-week-old plants were transferred to 37°C, three hours after light exposition. In Arabidopsis, jasmonates exhibit a circadian accumulation, possibly controlled by light/dark diurnal cycles (Goodspeed et al., 2012). Leaf samples were collected at equal times during the day at CN conditions to rule out changes in JA levels due to diurnal cycles. Samples were then collected at 0, 15, 30 min, 1, 2, 4 and 6 hours after heat application (**Fig. 33A**).

First, the levels of ODPA, JA, and JA-Ile were estimated by LC-MS. The results showed a progressive increase in the phytohormones shortly after 30 mins of HS. In the case of JA and JA-Ile, the levels rose throughout the analyzed 6-hour period, whereas OPDA peaked after two hours post HS (**Fig. 33B**). No changes in the phytohormone levels were observed at CN. Next, RNA was extracted from the same sample set, and the relative expression of JA related genes were measured using qRT-PCR. The RNASeq dataset revealed upregulation of the *Heat shock protein 70 (HSP70)* in the heat-treated samples, and then *HSP70* was used to track the temperature response in the time-series experiment. The results showed a rapid induction of *HSP70*, reaching its peak of expression at 30 mins (**Fig. 33C**). The *COI1* receptor presented a slight increment within 30 mins, whereas *MYC2* TF displayed differential expression only after four hours (**Fig. 33C**). Some of the JAZ repressors displayed an early response such as *JAZ2* that peaked at 30 mins, or *JAZ10* displaying a trend but not significant at the same time point. On the other hand, *JAZ4* gradually increased, mimicking the trend observed for JA and JA-Ile (**Fig. 33B-C**).

In summary, HS experiments using the JA deficient mutant *jai1* revealed that JA/COI1 signaling is required to induce type-IV trichomes in later stages of tomato vegetative development. An RNASeq approach was conducted using WT and *jai1* plants to find molecular factors controlling this HS-induced phenotype. The analysis of the DEGs between the genotypes on these conditions did not reveal major differences but provided insights about the processes that differentially occur in *jai1* mutants. More importantly, the RNASeq data suggested a possible JA response to heat, that was later corroborated by analyzing the phytohormone and gene expression levels of the early time points of the application of HS.

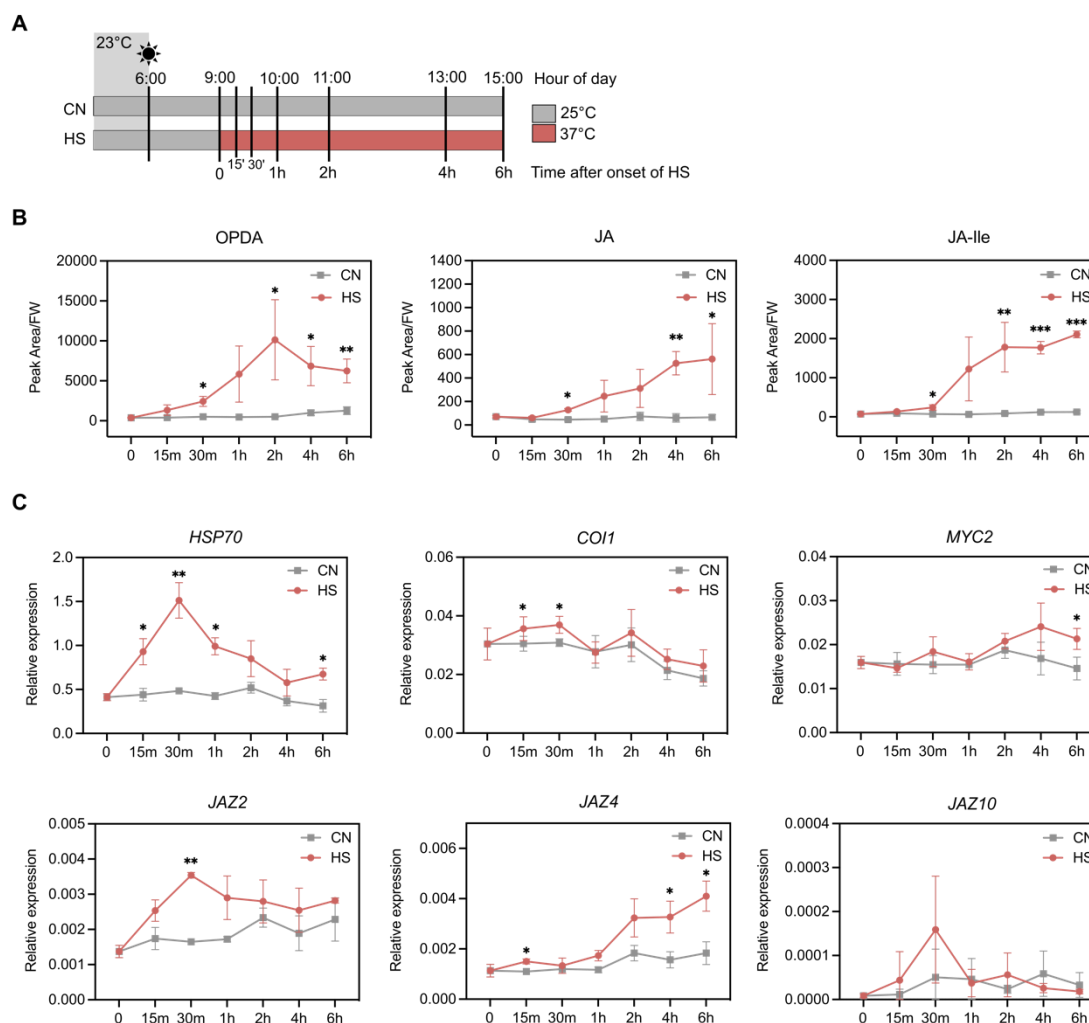


Figure 33. Changes in JA biosynthesis and signaling upon heat stress.

(A) Scheme depicting the time points of sample collection of the HS time series experiment. **(B)** Phytohormone levels after short HS application. Chromatogram peak areas were normalized to the leaf fresh weight (FW) ($n = 3$ biological replicates). OPDA, *cis*-12-oxo-phytodienoic acid; JA, jasmonic acid; JA-Ile, (+)-7-*iso*-jasmonoyl isoleucine. **(C)** Relative expression of JA signaling genes after short HS exposure. *Heat shock protein 70 (HSP70)* was used to monitor the heat treatment. Error bars display standard deviation. Pairwise comparisons between HS and CN were performed using Student's *t*-test $*P < 0.05$, $**P < 0.01$, $***P < 0.001$.

2.4 Discussion

2.4.1 Effect of heat stress on type-VI trichome development and productivity

2.4.1.1 Type-VI trichome density is not affected after prolonged heat stress.

Trichomes are part of the first line of defense for plants against biotic and abiotic stresses (Li et al., 2021). Environmental cues, including changes in temperature, can significantly influence the development and the productivity of trichomes. This has been shown in *Arabidopsis*, where the density of non-GT could be affected by the growing temperature conditions, and in cultivated tomato, where high temperatures could modulate the trichome fate between non-glandular type-V to glandular type-IV trichomes (Faden et al., 2019; Säbel et al., 2023). The impact of HS on trichomes of tomato raised the question of whether the elevated temperature could affect other types of GTs, and in this case, the first part of this chapter was dedicated to exploring the effects on type-VI GTs. Following the HS experimental set-up described in Säbel et al. (2023), it was shown here that WT plants grown under long-day HS conditions for three weeks did not exhibit changes in type-VI trichome density. Mining the transcriptome data generated after days of HS, some of the TFs reported in the literature involved in trichome development were analyzed by looking at the changes in HS compared to CN in each genotype. However, no clear trend was observed (**Fig 34A**). For example, *MYC1*, an important regulator of type-VI GTs density and terpene biosynthesis (Xu et al., 2018), exhibited a slight negative regulation tendency in HS versus CN. A recently described *MYB75* TF was the only one showing a higher tendency for downregulation. This gene acts as a repressor of type-VI trichome initiation, positively regulating the *S/CycB2* expression and at the same time, *MYB75* can repress the expression of TPS genes including the *sesquiterpene synthase 12 (TPS12)* (Gao et al., 2017; Gong et al., 2021). Upon heat, a downregulation of *MYB75* would promote type-VI trichome initiation and an increase in *TPS12* transcript levels, but this was not the case, suggesting that there are other factors downstream controlling both aspects. Genes like *Woolly* required for type-IV trichome initiation in juvenile stages of plant development (Vendemiatti et al., 2017), displayed only slight induction after 24 hours, and after five days, with no significant differences (**Fig 34A**).

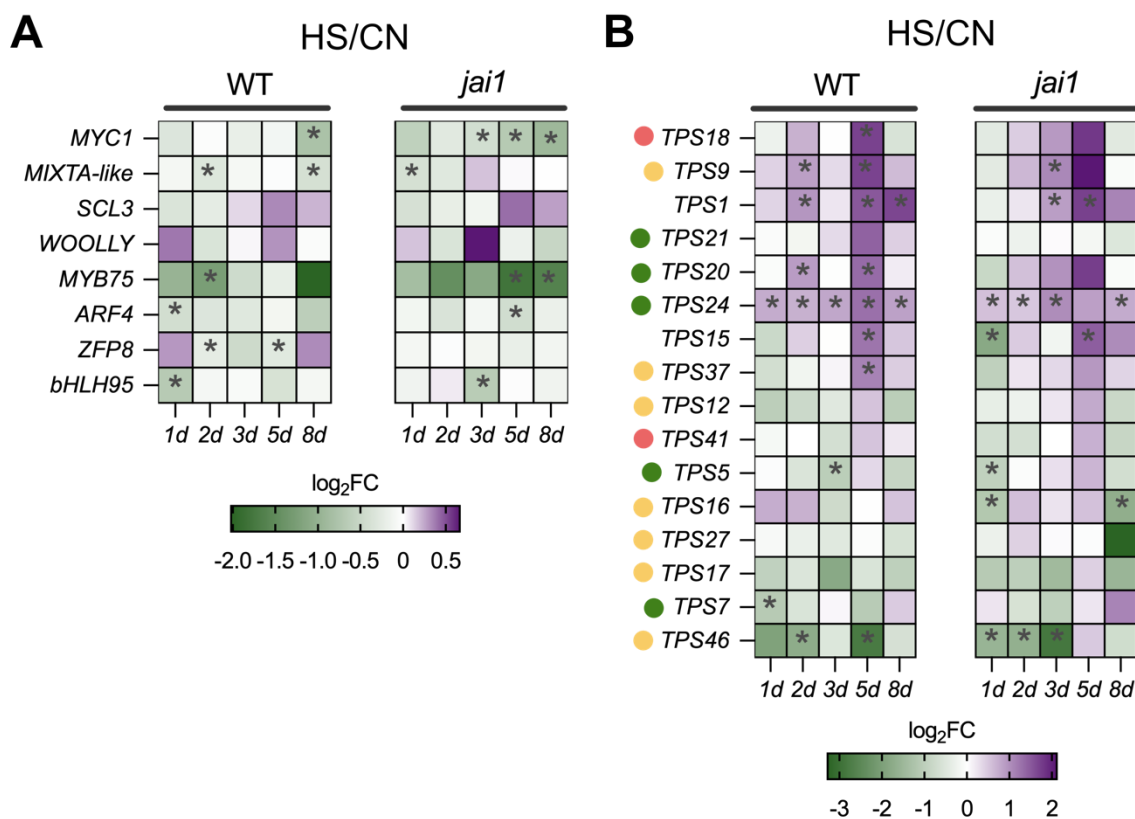


Figure 34. Changes in gene expression of TFs and TPS genes upon heat stress.

Expression data (\log_2FC) of selected transcription factors (TFs) involved in trichome initiation (**A**) and detected terpene synthases (TPS) (**B**) in the transcriptome data, of both WT and *jai1* in heat stress (HS) versus control (CN) during the different days after onset of HS and plotted as heatmaps. Dots next to the TPS genes indicate the subcellular localization as follows: plastid (green), yellow (cytosol) and red (mitochondria). TPS1 and TPS15 are classified as pseudogenes. Cell compartment according to Zhou and Pichersky (2020). References of the TFs included in the heatmap: *MYC1* (Xu et al., 2018), *MIXTA-like* (Ying et al., 2020), *SCL3* (Yang et al., 2021), *Woolly* (Yang et al., 2011), *MYB75* (Gong et al., 2021), *ARF4* (Yuan et al., 2021), *ZFP8* (Zheng et al., 2022) *bHLH95* (Chen et al., 2020). * $P < 0,05$ using Student's *t*-test.

2.4.1.2 Changes in volatiles after prolonged heat stress conditions

Despite not altering type-VI trichome density, heat treatment led to changes in the VOCs profiles, specifically increasing the production of monoterpenes and decreasing the sesquiterpenes (**Fig. 25**). Elevated temperatures can boost the emission rates of terpenoids in various plant species possessing terpene-storage structures like glandular trichomes or oil glands (Nagalingam et al., 2023). Previous studies in tomato demonstrate that moderate and severe short heat treatments enhance the emission of both mono and sesquiterpenes, a process that is consistent with the transcript upregulation for genes encoding terpene synthases involved in the biosynthesis of those compounds, β -phellandrene synthase (*TPS20*) and β -caryophyllene/ α -humulene synthase (*TPS12*), respectively (Pazouki et al., 2016;

Nagalingam et al., 2022). However, once the short stress period is finished, both the emission rate and the transcription of the *TPS* genes experience a decline, reaching lower levels than those observed under control conditions, and it is only after 24 hours that they return to the initial values (Pazouki et al., 2016; Nagalingam et al., 2022). Additionally, in an earlier report, heat or cold shock treatments were shown to trigger an increase of sesquiterpenes in tomato (Copolovici et al., 2012). The observed changes in the VOCs profiles after three weeks of daily HS could be the result of acclimatation processes to prolonged exposition to heat. A shift in monoterpene accumulation over sesquiterpenes was reproduced in the tomato accession Micro-Tom (**Fig. S4**) and in the experiments using the *jai1* mutant cv. Castlemart (**Fig. 29**), corroborating that this is not a genotype-specific response to HS.

However, unlike previous studies, the observed increase in monoterpenes was neither accompanied by an increase in gene expression of biosynthesis genes, e.g., *TPS20*, nor by genes controlling the flux through the plastidic MEP pathway like *DXS* (Wright et al., 2014). On the contrary, prolonged HS application led to a downregulation of TPS and some of the genes participating in the MEP and MVA intermediate pathways. Changes in gene expression due to heat could occur over a span of days or hours and may fluctuate depending on whether the stress is permanent or accompanied by recovery periods. The RNASeq data generated for the second objective of the present thesis was employed to analyze the expression of detected terpene synthases (TPS) in the wild type and *jai1* during the initial days following HS. Mining the transcriptome data, different annotated TPS genes were compared in HS versus CN, and their subcellular localization was recorded from literature (**Fig. 34B**). Among those expressed in type-VI GTs, *TPS20* involved in the biosynthesis of major monoterpenes: 2-carene, α -terpinene, α -phellandrene and β -phellandrene (Zhou and Pichersky, 2020), revealed an upregulation trend, especially on the second and fifth day after HS. Similarly, the highly expressed *TPS9*, known for producing germacrene in the cytosol, showed a positive trend upon heat, although the levels of δ -elemene, its detectable product in GC-MS, did not exhibit significant differences between the two conditions. In contrast, *TPS12* displayed a negative regulation from the onset of HS which could be linked to the observed drastic reduction in its sesquiterpene products after long-term HS (**Fig. 25E, 34B**).

At elevated temperatures, a predominance of monoterpenes over sesquiterpenes could indicate high enzymatic activity and fluxes of precursors towards the biosynthesis of plastid-derived terpenes, which can be retained in the storage cavities of the type-VI trichomes (Tissier et al., 2017). Most of the differences in up and down-regulation of TPS were not significant, making it difficult to correlate the changes in gene expression with a specific cell compartment, plastidic or cytosolic (**Fig. 34B**). However, considering the observed pattern, especially regarding *TPS20*, alterations in gene expression at earlier time points following heat

application, which were not captured in this RNASeq dataset, cannot be dismissed. Furthermore, these alterations do not appear to be influenced by JA, since the expression pattern is comparable between the WT and the *jai1* mutant. Thus, the downregulation of the biosynthetic and intermediate pathway genes could be a result of negative feedback regulation that occurs as part of the acclimation process to heat, but more research is required to support this hypothesis.

2.4.1.3 Metabolite profiling of trichomes under long heat stress provides insights into their changes in specialized metabolite productivity.

The overall downregulation of genes involved in the biosynthesis of isoprenoids after long HS raises the question about how these micro-organs can still accumulate SM, especially in relation to the MEP pathway. Since type-VI trichome density remained unchanged under high-temperature conditions, the increase in monoterpene content may be associated with elevated metabolic rates. To comprehend the changes occurring after prolonged HS, metabolomic profiling of polar and semipolar metabolites was performed in leaves and trichome fractions. While the leaves in HS displayed comparable profiles to the CN, the trichomes under these two conditions differ in the accumulation of certain CCM and energy metabolites (**Fig. 28B-C**). Trichomes under HS exhibited lowered levels of some intermediates of the TCA cycle. Similar results have been shown in soybean after long periods of growth in high temperatures, where the majority of the TCA intermediates are 50% reduced compared to lower temperatures (Sicher, 2013). Transcriptome and metabolome analysis of Arabidopsis plants submitted to prolonged day warm temperature (28°C, for seven days), or HS applied during seed germination, reveal a downregulation of several genes involved in the TCA cycle, as well as lowered levels of citrate, fumarate, succinate and isocitrate (Wang et al., 2020; Qian et al., 2023). Thus, the decrease in TCA cycle activity seems to be a common response to elevated temperatures, being more pronounced in the trichomes than in the leaves of tomato.

Acetyl-CoA, the initial substrate of the MVA pathway, can be produced in the plastids from pyruvate by the plastidic pyruvate dehydrogenase complex, in peroxisomes via β -oxidation of FA, in the mitochondria from pyruvate by the pyruvate dehydrogenase or in the cytosol by ATP-citrate lyase (Fatland et al., 2002). In GTs of tomato, the citrate-malate-pyruvate shuttle from the mitochondria is key to supplying acetyl-CoA in the cytosol, required for sesquiterpene biosynthesis and FAs elongation (Balcke et al., 2017). The decline in TCA intermediates could compromise the availability of acetyl-CoA in the cytosol, which, together with the downregulation of MVA pathway genes, could explain the limited amount of sesquiterpenes found in HS. However, intermediates of the MVA pathway, including HMG-CoA, mevalonate-

5-PP, and isopentenyl pyrophosphate, remained unchanged within the trichome samples (**Table S4**). The only exception was mevalonate-5-phosphate, that showed higher levels in the trichome fractions under HS ($P < 0,01$), despite the slight reduced RNA levels for the mevalonate kinase gene (**Fig. 25G, 27A**). Therefore, the changes in the expression levels of the genes participating in the MVA pathways are not aligned with the observed metabolic profiles in the trichomes. On the other hand, lowered levels of malate in trichomes at HS conditions could reflect a reduction in OAA levels. The latter is produced via the cleavage of citrate by the ATP-citrate lyase, simultaneously generating acetyl-CoA in the cytosol (Fatland et al., 2002; Balcke et al., 2017). Thus, less malate and citrate could imply lower levels of acetyl-CoA available to fuel the MVA pathway. However, the levels of acetyl-CoA were not significantly different between CN and HS samples. Since acetyl-CoA is produced in multiple cell compartments, it is not possible to determine specific changes within the mitochondria or cytosol with the method used. Thus, a potential reduction of this precursor in the cytosol could be masked or replenished by the levels in other cell organelles.

Malonyl-CoA, a building block for FAs, showed reduced levels as well ($P < 0,01$), although a negative effect was only registered in polyunsaturated FAs (**Fig. 28, Table S3**). The decrease in polyunsaturated acyl groups, including α -linolenate (18:3) and hexadecatrienoate (16:3) in the chloroplasts, constitutes a lipid metabolic response to the elevated temperatures registered in several plant species (Higashi et al., 2015; Higashi et al., 2018). The balance between saturated and unsaturated FAs has major impact in membrane stability and tolerance to heat, since the unsaturated FAs have lower melting points in comparison to their counterparts (Linder, 2000; Sharma et al., 2023). Consequently, under HS conditions, plants adjust the lipid metabolism and composition increasing the levels of saturated FAs in the membranes to preserve its fluidity properties (Sharma et al., 2023).

In contrast with the reduced TCA metabolites, intermediates of the MEP pathway accumulated at higher levels in trichomes from plants grown at 37°C, suggesting a higher flux through this pathway. Interestingly, one of these metabolites, the methyl-D-erythritol 2,4-cyclodiphosphate (MEcPP), plays a role in retrograde signaling, triggering the expression of nuclear-encoded stress-responsive genes (Xiao et al., 2012; Benn et al., 2016). MEcPP can accumulate as a response to abiotic stresses such as wounding or high light, eliciting the expression of genes such as *fatty acid hydroperoxide lyase (HPL)* (Xiao et al., 2012). Although *HPL* expression specifically in the trichomes was not measured here, it displayed slightly elevated levels in leaves, with an average \log_2FC 0,7 (**Fig. S7**), uncovering a general plant stress response.

The boost in AS secretion by type-IV trichomes (Säbel et al., 2023) and the increase in monoterpenes stored in type-VI trichomes under heat conditions, implies an increase in carbon demand. In fact, the levels of sucrose, the main carbon source (Balcke et al., 2017), were three

times higher at 37°C compared to 25°C (**Table S4**). Several metabolites involved in the nonoxidative pentose phosphate pathway, the CBB cycle and glycolysis accumulated differentially in trichomes at elevated temperature. These pathways are important to secure precursors for the MEP pathway, such as GA-3P, also enriched in trichomes under HS (**Fig 26-27**). Moreover, elevated levels of 6-phosphogluconate (6PG) hint at the potential activity of the OPP pathway, supplying necessary reducing power for the MEP pathway (Kruger and von Schaewen, 2003; Johnson et al., 2017).

Changes in SM composition within the GTs of tomato raise several questions about the potential role of these compounds in response to elevated temperatures. The transcriptome data from the days after HS application pointed out several metabolic pathways that are downregulated in heat (**Fig. S6**), including the biosynthesis of pigments that are required for light photosynthesis. In *Arabidopsis* for example, extended exposure to warm temperatures results in a significant decrease in photosynthetic efficiency, leading to a roughly 50% reduction in photosynthetic rate (Wang et al., 2020). Stress by elevated temperature can trigger structural changes in the thylakoid membranes associated with the formation of reactive oxygen species (ROS) (Pospíšil, 2016). The heightened biosynthesis of SM suggests a diversion of the flux of resources from the CCM, essentially sugars that are withdrawn from the carbon fixation on the leaves, and possibly other building blocks and cofactors transported into the GTs. Hence, it is intriguing that plants opt to synthesize these SM, despite the metabolic cost involved.

A study on the Mediterranean shrub *Halimium halimifolium* shows that heat waves increase the respiration rate by three-fold, negatively affecting the net CO₂ assimilation. Despite this negative carbon balance, the plants display an increase in the biosynthesis of VOCs upon heat treatment, by reallocating carbon most probably from the primary metabolism (Werner et al., 2020). Here it is worth mentioning, that plants were subjected to 10 days of heat treatment (38°C, day/night) and a strong increase in mono and sesquiterpene emissions was observed within the first two days. After that period, only monoterpenes displayed a daily uprise, although to a lesser extent compared to the initial values, while the sesquiterpenes gradually decreased over time (Werner et al., 2020). Another example of changes in carbon allocation occurs in seedlings of *Pinus sylvestris* submitted to drought stress. Employing ¹³CO₂ and ¹³C-pyruvate labeling it was shown that the VOC emission was maintained and, in some cases increased in drought conditions despite the drastic reduction in the net CO₂ assimilation by changing the direction of pyruvate consuming pathways (Kreuzwieser et al., 2021). This study also pointed out, that only sesquiterpene emissions were negatively affected by drought, possibly due to an inhibition of crosstalk between MEP and MVA, that potentially provides precursors from the plastids to the cytosol for the sesquiterpene biosynthesis (Kreuzwieser et al., 2021).

In summary, prolonged exposure to HS does not alter the development of type-VI GTs, but rather their productivity. Specifically, HS induces the biosynthesis of monoterpenes while reducing sesquiterpenes. After long-term HS exposure, reduced expression levels of genes involved in the intermediate pathways (MEP and MVA) as well as the terpene synthases, contrast with the observed changes in the primary metabolites and the SM produced in the GTs. Both the changes in carbon partitioning, and the increased fluxes in providing precursors, are what may determine the accumulation of the plastid-derived terpenoids. Plastidic glycolysis and the pentose phosphate pathway constitute some of the enriched pathways that could mediate the breakdown of sugars into precursors for the MEP pathway. Several plastidic isoforms from these pathways are enriched in GTs of tomato (Balcke et al., 2017). However, potential alterations in gene expression levels shortly after heat application are still unknown, as well as the possible effects in the biosynthetic pathways. Furthermore, extended exposure to heat affects the conversion of sugars into organic acids, observed here by the depletion in the TCA intermediates. Despite the impact of HS on plant physiology, the increases in AS and monoterpenes raise the question about the role of these substances in the plant response mechanisms to cope with higher temperatures. It has been shown that isoprene biosynthesis minimizes the effects of oxidative stress generated under HS conditions (Vickers et al., 2009) and can protect the photosynthesis and photosynthetic electron transport (Behnke et al., 2007). Nevertheless, their specific role in these plant appendages warrants further investigation. Concomitantly it highlights the question regarding the factors that control resource allocation of compounds that support the increase in their productivity within these cell factories in response to this abiotic stress.

2.4.2 The role of jasmonate signaling in heat stress-induced type-IV trichome initiation.

In cultivated tomato, elevated temperature prompts a transition in trichome fate, in particular replacing the non-glandular type-V trichomes with the glandular type-IV trichomes, accompanied with an exponential increase in AS (Säbel et al., 2023). By submitting the JA deficient mutant *jai1* of tomato to HS, it was found that this mutant is impaired in this developmental response (**Fig. 30**). Furthermore, it was demonstrated that HS triggers JA biosynthesis and signaling responses shortly after the increase in temperature.

How HS signals lead to JA biosynthesis, and consequently, a stress response, is not fully understood. A report in Arabidopsis and wheat (*Triticum aestivum*) suggest that heat shock factors (HSF) activate the expression of enzymes involved in JA biosynthesis such as *OPR3* (Tian et al., 2020). A more recent study showed how the *HSFA2* TF mediates the early signals

of HS through Ca^{2+} signals, and the activation of JA biosynthetic enzymes including *lipoxygenase 3 (LOX3)* and *OPR3* (Guo et al., 2024). Regarding substrates, jasmonates are synthesized from polyunsaturated FAs that are released from the plastid membranes, a process facilitated by phospholipases (Howe et al., 2018). As discussed earlier, HS promotes a turnover of FA composition, leading to a withdrawal of unsaturated FA from the plastid membranes, which could represent an increase of substrate availability for JA biosynthesis. In *Arabidopsis*, one *HEAT INDUCIBLE LIPASE1 (HIL1)* is responsible for lipid remodeling process, releasing 18:3-free fatty acids in response to HS (Higashi et al., 2018).

2.4.2.1 Evidence of a HS-induced JA-signaling response in tomato

In agreement with our results, various studies in *Arabidopsis* have reported induction of JA levels and expression of JA biosynthesis and signaling genes, including *OPR3*, *MYC2* and JAZ repressors, following short-term exposition to high temperatures. (Clarke et al., 2009; Cortijo et al., 2017; Tian et al., 2020; Agrawal et al., 2022). The JA response to heat has been associated with thermo-tolerance. For example, in wheat, the silencing of *OPR3*, one of the enzymes involved in JA biosynthesis, increases the susceptibility to HS and reduces plant biomass (Tian et al., 2020). It has been also demonstrated in *Arabidopsis*, that JA-mediated signaling pathway triggers the induction of *DREB2A* expression, promoting a heat tolerance response (Tian et al., 2020). Recently it was shown that tomato plants, when exposed to elevated temperatures for five days, exhibited higher levels of JA after wounding, in contrast to the plants grown under control conditions (Havko et al., 2020). This study suggested that heat has a priming effect to enhance the JA-dependent wound response, leading to increased phytohormone levels and expression of JA-responsive genes (Havko et al., 2020). One explanation is that higher temperatures prompt the accumulation of the *COI1* receptor, increasing the plant sensitivity to bioactive jasmonates (Havko et al., 2020). According to the transcriptome data presented here, the levels of *COI1* displayed a slight downregulation trend after the HS exposition (**Fig. S7**). This phenomenon has been reported before, when the application of MeJA in tomato triggers a downregulation of this gene (Panda et al., 2022). Thus, whether *COI1* accumulates at the protein level after prolonged HS application is something that requires further investigation.

The results of the HS experiments presented here evidenced a short- and long-term JA response to heat. Genes like *JAZ2* displayed activation within 30 minutes after onset of heat while *JAZ4* and *JAZ13* showed a later response, within six hours and with sustained increase during the days following stress application. Furthermore, our results revealed that HS application without wounding could trigger an upregulation of some of the wound induced JA-

response defense proteins including *ARGINASE2 (ARG2)*, initially identified as a wound-response gene in Chen et al. (2005); and proteinase inhibitors such as *ARPI* and *WIPI-LIKE*. At the same time, the comparisons at the transcriptome level with the *jai1* mutant revealed PIs that did not require JA perception to be induced by HS, as observed in the cases of *WIPI* and *API1*. (Fig. 32, Table S5).

2.4.2.2 The COI1 receptor is required for the HS-induced shift in trichome fate.

The lack of type-IV trichome induction under HS in the *jai1* mutant uncovers the role of JA perception in the heat-induced shift in trichome fate, and the subsequent adaptation of tomato to high temperatures. However, JA alone is insufficient to induce type-IV trichome initiation in cultivated tomato. Escobar-Bravo et al. (2016) demonstrated that MeJA application to cultivated tomato cv MoneyMaker does not induce type-IV trichome initiation. Conversely, the same treatment using a backcross line from the wild tomato *Solanum pimpinellifolium*, which produces type-IV trichomes, was able to increase type-IV trichome density, as well as the AS biosynthesis (Escobar-Bravo et al., 2016). These results suggest that there are other factors triggered by high temperature that control the switch from type-V to type-IV, in a COI1 dependent manner.

The broad spectrum of resistance associated with the AS, and therefore with type-IV trichomes, makes it an attractive trait for breeding cultivated tomato varieties. The presence of these capitate trichomes not only in wild tomato species, but also in other Solanaceae species, suggests that the capacity to develop type-IV trichomes was negatively selected during the domestication process. Recombinant inbred lines obtained from crosses between wild and cultivated tomato have been used to identify potential regulators of the type-IV GTs/AS trait by QTL mapping (Resende et al., 2002; Firdaus et al., 2013; Vosman et al., 2019). The results have allowed the identification of specific loci, but additional research is required to functionally characterize the genes within these chromosomal regions. Recently, the introgression of three alleles from the wild tomato *Solanum galapagense*, into the model tomato Micro-Tom led to an increase in type-IV trichome density in adult stages of development (Vendemiatti et al., 2022). The segregation of these chromosomal regions into lines with individual fragments reduced original achieved trichome density, indicating that the type-IV trichome trait results from epistatic interaction of several genes located within these alleles. Despite the significant increase of type-IV trichomes over the leaves (two and 15 times on adaxial and abaxial sides respectively), the levels of AS were inferior compared to the wild parent (18 to 120 times less, depending on the individual AS) (Vendemiatti et al., 2022). More recently, the dissection of one of the loci responsible for the type-IV trichome trait, along with the introgression of the gain-of-

function *Wolly* allele, resulted in a doubling of type-IV trichome density compared to the wild *S. galapagense*, with similar AS quantities (Vendemiatti et al., 2024). Overall, these findings evidence that type-IV trichome initiation and AS biosynthesis are uncoupled processes governed by distinct regulatory mechanisms. The impact of HS over cultivated tomato provides additional support for this hypothesis, since the increase in AS cannot be solely attributed to the rise in type-IV trichome density (Säbel et al., 2023).

2.4.2.3 Specialized metabolites in the JA-mediated response to elevated temperatures

Jasmonates play a significant role in regulating the biosynthesis of SM in GTs. The application of MeJA in tomato boosts the productivity of type-VI GTs, specifically of monoterpenes, as well as the AS levels, the latter exclusively in backgrounds where type-IV trichomes are constantly developed throughout the vegetative development (Escobar-Bravo et al., 2016; Escobar-Bravo et al., 2017). Like the plastid-derived terpenoids, the function of these sugar esters in the context of high temperatures is unknown. Recently it was documented that AS-deficient mutants of *Nicotiana benthamiana*, besides being more susceptible to insects, exhibit higher rates of water loss and elevated leaf temperatures when compared to the wild type (Feng et al., 2022). Therefore, these sticky substances originally described as insect immobilizers, could be acting in this case as an analogous wax protector to cope with elevated temperatures (Moghe et al., 2023; Säbel et al., 2023). The role of JA in the increased AS upon HS warrants an in-depth study.

Little is known about the regulation of JA in controlling both trichome initiation and the biosynthesis of SM in wild tomato accessions, as well as their interactions with environmental cues. The wild *S. habrochaites* displays robust adaptation to several abiotic stresses, including cold tolerance, and therefore is used in grafting techniques to improve the yield of commercial tomato varieties. A recent study showed that *S. habrochaites* has higher basal levels of JA compared to the cultivated tomato, and when this accession is used as rootstock, it induces several changes in JA biosynthesis and signaling in the cultivated scion (heterografts), triggered by cold stress (Wang et al., 2023). Hence, elevated basal levels of JA in wild tomato might contribute to enhancing their adaptive response to abiotic stresses. It is also tempting to speculate that higher JA levels could be linked to their higher GT density and productivity, as well as their ability to develop type-IV trichomes along the vegetative growth.

The number of genes involved in cholesterol and steroidal glycoalkaloids (SGAs) biosynthesis that were differentially expressed in the *jai1* versus WT under HS stands out considering the low number of DEGs obtained from the conducted comparisons. SGAs are part of the blend

of SM produced mainly in Solanaceae species, and they confer protection against pathogens and herbivores (Rangarajan et al., 2000; Friedman, 2002). In tomato, SGAs, mainly α -tomatine and dehydrotomatine are produced in foliar tissue and immature fruits (Friedman, 2002), but not in GTs. Previous studies have reported that SGAs biosynthesis is controlled by the interplay between JA and gibberellin signaling, and where TFs such as *MYC1* and *MYC2* exert a pivotal role in regulating the constitutive expression of SGAs biosynthetic genes (Panda et al., 2022; Swinnen et al., 2022). In consequence, the levels of, e.g. α -tomatine in the *jai1* are significantly lower (Panda et al., 2022). While it is already known that some of the genes display reduced expression levels in the *jai1* mutant (Panda et al., 2022), it seems that the high temperature enhances the downregulation of both cholesterol and the SGAs biosynthetic pathway genes from the onset of the HS. In contrast, in the WT, this reduction occurs sometime later, after 8 days of daily 37°C.

The expression of *MYC2* slightly increased after four hours of HS, and during the following days, both *MYC1* and *MYC2* showed rather lowered transcript levels. This could be an effect of the feedback loop inhibition after JA elicitation possibly occurring at dawn, when the plants experience a drastic change of temperature. Additionally, important positive regulators of cholesterol and SGAs such as the *APETALA2/Ethylene Response Factor (AP2/ERF; GAME9: Solyc01g090340)* and the GA repressor *DELLA (Solyc11g011260)* were downregulated in HS, with stronger effect in *jai1* (Cárdenas et al., 2016; Panda et al., 2022). Overall, these results show that the lack of JA perception could exacerbate the decline in constitutive SGAs biosynthesis under high temperatures. Havko and coauthors reported that tomato plants submitted to five days of HS become more susceptible to herbivory, with the effect being significantly greater in the *jai1* mutant. Thus, potential changes in secondary metabolic profiles resulting from heat exposure, for example in SGAs, could provide additional evidenced supporting the observations made in these herbivory bioassays (Havko et al., 2020).

2.4.2.4 Candidate genes regulating type-IV trichome development.

The number of DEGs between WT and *jai1* mutant in HS across all time points was relatively low, in comparison with the number of DEGs observed between the two temperature conditions within the genotypes (**Fig. 32**). This is particularly evident in the number of TFs included in the list that could be associated with the type-IV trichome phenotype described in HS. From the list, *MYB13* stands out as a candidate. *MYB13* exhibited contrasting expression patterns, being upregulated in the WT since the onset of the HS, while in the *jai1*, it showed rather negative regulation.

Very recently, *MYB13* was identified as a positive regulator of two gene clusters that govern the biosynthesis of phenolamides (Cao et al., 2024). Cao and coauthors showed that the accumulation of these compounds enhance tomato drought tolerance by inducing ROS scavenging and elevating the levels of the phytohormone abscisic acid. Additionally, by performing sequence analysis among different tomato accessions, they identified two haplotypes of *MYB13* correlated with the accumulation of phenolamides. The domestication process of tomato lead to negative selection of the high-producing haplotype of *MYB13*, reducing phenolamides content and in turn compromising the drought tolerance in the cultivated varieties (Cao et al., 2024).

Phenolamides are formed by phenolic moieties, mainly hydroxycinnamic acids and derivatives, that are covalently linked through amide bonds to an aromatic monoamine or an aliphatic polyamine (e.g. tyramine, agmatine, anthranilate or spermidine) (Roumani et al., 2021). These compounds are induced by wounding, and they accumulate in pollen coat, flowers, and seeds (Vogt, 2018; Roumani et al., 2021). Their presence in these tissues has been associated with plant fertility (Guo et al., 2003), but the molecular mechanisms remain unknown. The expression pattern of *MYB13* overlaps with the plant organs where the phenolamides accumulate. In Arabidopsis, the closest related gene *AtMYB13* (AT1G06180), shares only 48% and 58% of identity and similarity with the tomato amino acid sequence, respectively (**Fig. S8**). According to open databases, *AtMYB13* is associated with the GO term “regulation flower development” and it is expressed in flower organs, but also in the shoot apex (<https://bar.utoronto.ca/eplant>). In tomato, *MYB13* is expressed especially in the flower organs, including the pistil, ovules, and floral meristem, followed by lower expression in the shoot apex (**Fig S9**) (Cao et al., 2024). It is in these organs that JA plays a major role in regulating ovule development and fertility in tomato (Li et al., 2004; Schubert et al., 2019). Overall, it seems that both *AtMYB13* and *SIMYB13* display similar expression patterns and could be involved in similar biological processes, although the differences in the amino acid sequence could suggest a diversification in their biological function.

The HS experimental setup used to induce the type-IV/AS enhancement in tomato comprises a drastic daily temperature change from the night phase at 23°C, to the light phase at 37°C. The samples for the RNASeq were consistently collected during daytime, 6-7 hours after onset of HS, and therefore the events occurring shortly after the shift in temperature were not covered in the transcriptome analysis. As discussed before, phytohormone levels and JA-related genes displayed an uprise in the range of minutes after HS application. When *MYB13* transcript levels were analyzed during these early time points, this TF showed an induction, peaking at two hours after the onset of HS and subsequently a decrease, although maintaining elevated even

after six hours of HS (**Fig. 35A**). This expression pattern mirrors the observed rise of JA-Ile upon heat.

With the aim to investigate more about the function of *MYB13*, a GO enrichment analysis performed over 400 genes displaying positive correlation with *MYB13* revealed significant GO terms, including “response to wounding” and “response to external stimulus” within biological process (BP) category, linking *MYB13* with JA response (**Fig. 35B**). Interestingly, within the molecular function (MF) category, several sugar transferase activity terms stood out. The zeatin glucosyl transferase genes, *ZOG1* and *ZOX1* were found in the coexpression neighborhood of *MYB13* and fell into these MF categories, among other genes. In line with this analysis, Cao et al. (2024) could show that *MYB13* regulates the expression of *ZOG1*, which is involved in the glycosylation of feruloyl putrescine. Other possibility is that the regulation of glucosyl transferases by *MYB13* could affect the cytokinin levels by the conjugation with sugars (Mok and Mok, 2001). Cytokinin is a phytohormone tightly connected with developmental processes such as cell division and leaf expansion and cooperates with auxin in the formation and maintenance of the meristems (Hwang et al., 2012; Wybouw and De Rybel, 2019).

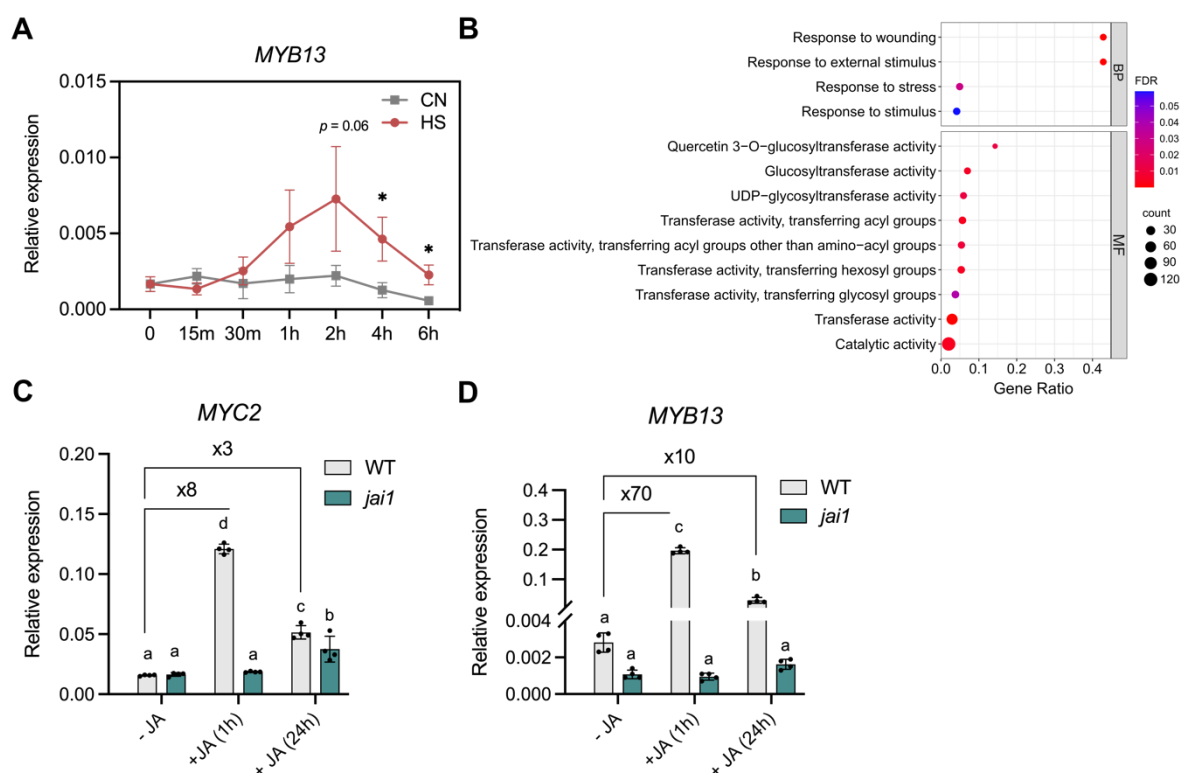


Figure 35. *MYB13* is induced by heat stress and jasmonate.

(A) Relative expression of *MYB13* after short HS exposition ($n = 3$ biological replicates). Pairwise comparisons between heat stress (HS) and control (CN) were performed using Student's *t*-test $*P < 0.05$. **(B)** GO enrichment analysis was conducted using 293 out of 400 neighboring genes of *MYB13* using Genevestigator 9.6.1 (Hruz et al., 2008) with a correlation score above 0,58. The GO enrichment

was performed using agriGO v2.0 (Tian et al., 2017). Significant enriched GO terms are displayed in the dot plot with a $DFR < 0,05$. BP, biological process; MF, molecular function. Dot plot constructed in SRPLOT (bioinformatics.com.cn/srplot). *MYB13* expression is induced by jasmonic acid. Comparison of *MYC2* (C) and *MYB13* (D) relative expression after 1 hour (h) and 24 h of JA application in the WT and *jai1* mutant ($n = 4$ biological replicates). Error bars depict standard deviation. Different letters indicate significant differences after applying two-way ANOVA with Tukey's test ($P < 0.05$).

In Arabidopsis, exposure to high temperatures leads to decreased cytokinin levels, while low temperatures result in elevated levels (Todorova et al., 2005; Prerostova et al., 2020). Evidence from Arabidopsis and from other plant species suggests associations between high cytokinin with thermotolerance, although the mechanisms remain largely unknown (Prerostova et al., 2020; Castroverde and Dina, 2021). In any case, analysis of phenolamides and cytokinin content after HS needs to be performed to elaborate on these hypotheses.

In silico analysis of the regulatory motifs within the 2 kb putative promoter region of *MYB13* revealed interesting particularities (Fig. S10). First, several conserved drought-responsive elements (DRE) were identified, two of them within the first 1 kb upstream of the transcription start site. This motif is associated with diverse abiotic responsiveness including drought, low temperature and high salt (Yamaguchi-Shinozaki and Shinozaki, 1994) and is recognized by the dehydration responsive element binding (DREB) factors, which groups several stress-responsive regulatory genes. However, *DREB* TF can also be induced by HS, as previously shown in Arabidopsis, where *DREB2A*, besides water-stress responsive, is able to activate genes involved in thermotolerance (Sakuma et al., 2006). In tomato, *SIDREB2* is induced by drought and recognizes the *cis*-DRE elements, activating the transcription of stress-resistance genes (Tao et al., 2022). Given that several *DREBs* are induced by different stresses including heat, this suggests a possible induction mechanism of *MYB13* in HS. Second, the presence of binding elements of TFs involved in the control of ovule identity (GA-5) and regulation of anther development (NST2) (Fig. S10) along with its expression pattern (Fig. S9), provides additional insights into the role of *MYB13* in flower and seed development. In fact, Cao et al. (2024) reported that the overexpression of *MYB13* negatively affect the seed number and the germination rate in the Micro-Tom background. Third, one conserved jasmonate signaling TGACG motif was found within the first 1 kb (Wang et al., 2011), which could indicate a direct JA-mediated induction of *MYB13*. To test this hypothesis, the relative expression of *MYB13* was analyzed after 1 hour and 24 hours post-JA application in the leaves of the WT and *jai1* mutant. The expression of *MYC2*, the master regulator of JA signaling pathway (Kazan and Manners, 2013), was analyzed to validate the JA treatment (Fig. 35C). The results exhibited a strong upregulation of *MYB13* after one hour, nearly 70 times more compared to the untreated control, and the induction was sustained after 24 hours, even when the levels of *MYC2* were back close to basal levels (Fig. 35D). On the other hand, *MYB13* was not induced in the *jai1*

upon JA application, confirming the results of the RNASeq data. Overall, these findings support the idea of a JA-mediated activation of *MYB13* triggered by HS.

In summary, JA signaling is necessary for the transition from type-V to type-IV trichomes induced by HS in cultivated tomato. However, JA alone is not enough to replicate the effects of HS over type-IV trichomes, as demonstrated by earlier studies (Escobar-Bravo et al., 2016). The effect of heat could regulate different factors required to initiate type-IV trichomes, that otherwise become deregulated with the progression of the vegetative growth (Vendemiatti et al., 2017). The comparative transcriptome analysis provided some insights about the JA response upon heat and uncovered a possible crosstalk with other phytohormones, particularly cytokinin.

Expression analysis and phytohormone quantification uncover the relevance of the early time points following the onset of the heat treatment, an aspect not covered in the RNASeq experiment performed in the present thesis. Results from the transcriptome analysis point out the *MYB13* TF as a potential regulator involved in the JA-mediated developmental shift to glandular trichomes upon HS in cultivated tomato. *MYB13* was recently identified as a drought response gene, involved in the regulation of the phenolamides biosynthesis genes (Cao et al., 2024). Whether these compounds are induced at elevated temperatures and if they are linked to GTs development, requires further investigation.

As observed in other plant species, changes in temperature trigger a short and long-term JA response in tomato, that potentially coordinate the defense strategies of the plant to cope with this abiotic stress. On the one hand, the uprise in AS, and to a lesser extent in monoterpenes, suggest a possible function of these compounds in HS, either to cope with potential temperature-associated changes of insect herbivory (Havko et al., 2020), or as protectants to minimize the temperature effects, water loss or oxidative stress (Vickers et al., 2009; Feng et al., 2022). On the other hand, high-temperature regimes potentially impact the constitutive biosynthesis of SGAs, an effect that is attenuated by JA, increasing the susceptibility to potential attacks of pathogens or insects. Metabolite profiling of SGAs in the leaves will be necessary to confirm this hypothesis. In tomato, wound-induced JA responses, such as those triggered by insect herbivory, interfere with the plant's ability to adapt to high temperatures, (Havko et al., 2020), which implies that there is a trade-off when plants cope simultaneously with biotic and abiotic stresses. This phenomenon may involve adjustments in the primary and specialized metabolic profiles in response to heat, potentially rendering the plants more susceptible to herbivore attacks.

3. Summary and Outlook

Glandular trichomes (GTs) are epidermal outgrowths containing dedicated glandular cells capable of synthesizing, storing, and secreting significant amounts of specialized metabolites (SM). In tomato (*Solanum lycopersicum*) and in its wild relatives, GTs produce volatiles such as mono and sesquiterpenoids, and glue-like compounds named acylsugars (AS), among others, enriching the plant's defense strategies to cope with biotic and abiotic stresses. These SM are synthesized from precursors originating from the central carbon metabolism (CCM). Despite the knowledge gained from elucidating the SM biosynthetic pathways (Schilmiller et al., 2009; Bleeker et al., 2012; Schilmiller et al., 2012; Fan et al., 2016; Leong et al., 2019; Fan et al., 2020), our understanding of how the CCM is organized to supply precursors to the specialized metabolism remains largely unexplored. Multi-omics data sets pointed to photosynthetic GTs of tomato as carbon-sink structures, equipped with distinct features in the CCM that support their high metabolic productivity (Balcke et al., 2017).

The first chapter of the present thesis addresses the role of Rubisco and PEPCK, two enzymes involved in the CCM that are enriched in GTs of tomato. A trichome-specific *Rubisco small subunit* (*RbcS-T*) was functionally characterized in both cultivated tomato and *S. habrochaites*, revealing non-significant differences in the productivity of AS. These results contrasted with the recent findings in the wild *S. pennellii*, where the *RbcS-T* orthologous gene was shown to enhance the CO₂ recycling within type-IV GTs, thereby improving the efficiency in AS biosynthesis (Ji et al., 2023). Conversely, here it was shown that when the *RbcS* nuclear-encoded mesophyll isoforms were simultaneously downregulated in type-VI GTs of cultivated tomato, the plastid-derived monoterpenes were reduced, suggesting that the potential CO₂ refixation capacity, albeit minor, is not associated with a specific small subunit isoform. Moreover, independent mutants of *PEPCK*, a C₄-photosynthesis-related enzyme, revealed a significant decrease in monoterpenes produced in type-VI GTs. Preliminary metabolomic analysis on primary metabolites within GTs of *pepck* mutant lines showed lowered levels of GA-3P and DXP, as well as NADPH levels, uncovering the role of PEPCK in the provision of precursors from the cytosol into the chloroplast to fuel the MEP pathway. The overall results illustrate how the carbon economy within GTs undergoes extensive regulation by different enzymes and mechanisms to maximize their productivity.

The second chapter focuses on the effect of heat stress (HS) on trichome productivity and development. HS can alter the trichome fate from non-glandular type-V to type-IV trichomes and boost the AS biosynthesis in cultivated tomato (Säbel et al., 2023). By examining the effect of HS over type-VI GTs, findings from this thesis indicate that elevated temperatures did not alter trichome density but the VOCs profile. Specifically, the content of plastid-derived

monoterpenes increased while cytosolic-derived sesquiterpenes were reduced. Metabolomics analysis on primary metabolites in GTs under HS revealed an increase in sucrose, and in intermediates of the pentose phosphate pathway and the CBB cycle, that all together may support the accumulation of monoterpenes and AS. Conversely, reduced organic acids could be linked to lowered levels of precursors for the MVA pathway. The contrast between the gene expression levels and the metabolic profiles uncovers more questions about the regulation of the productivity in the GTs after prolonged HS. Furthermore, by investigating the effect of HS in the *jasmonic acid-insensitive 1 (jai1)* mutant of tomato, it was discovered that the shift in trichome identity is dependent on jasmonate (JA) signaling. JA rises upon HS exposure, triggering JA signaling responses that could negatively affect other SM, particularly the steroidal glycoalkaloids (SGAs), that are produced in the leaves and whose biosynthesis is controlled by the interplay of JA and gibberellin signaling (Panda et al., 2022; Swinnen et al., 2022). After conducting a transcriptome analysis, *MYB13* TF was identified as a potential candidate for JA-mediated type-IV trichome initiation under HS conditions. Although *MYB13* was recently characterized as a master regulator of phenolamides in tomato (Cao et al., 2024), its role in determining trichome fate requires further investigation. Overall, evidence from the literature and the results presented here indicates that while JA signaling is required, HS triggers a broader range of factors that potentially regulate the shift in trichome fate in cultivated tomato.

The question of how GTs achieve high productivity remains elusive, especially concerning the interface between the primary and specialized metabolism. In photosynthetic GTs of tomato, particularly from wild relatives like *S. habrochaites*, many genes involved in the CCM occur in multiple isoforms. Some of these gene duplicates exhibit predominant expression within the secretory cells and may exert control over the metabolic fluxes (Balcke et al., 2017). Therefore, functional redundancy and coexpression of genes with essential functions in the GTs make it challenging to study their contribution to these biofactories. While tissue-specific gene targeting constitutes a valuable tool for addressing specific questions, its application for GTs requires further optimization (Decaestecker et al., 2019). Besides understanding the genetic basis of GTs productivity, identifying factors regulating this process may contribute to breeding of cultivated tomato varieties. Evidence from crossing between wild and domesticated tomato varieties demonstrates that trichome development and productivity are multigenic traits governed by distinct regulatory mechanisms (Vendemiatti et al., 2022; Kortbeek et al., 2023). Moreover, in the case of type-VI trichomes, the metabolic activity and, consequently, the accumulation of SM is the main factor that determining the volume of the storage cavity, much more than their cell wall structure (Kortbeek et al., 2023). How environmental cues can modulate GTs initiation and their metabolic activity remains largely unknown, but indeed constitutes a pertinent focus in the context of a rapidly changing climate. In addition to the

developmental shift to GTs upon HS (Säbel et al., 2023), the observed metabolic changes in GTs in response to elevated temperatures represent an interesting experimental approach to investigate molecular factors controlling the productivity within the trichomes. For example, to study the control over the flux of plastid-derived volatiles in type-VI trichomes, or to research the factors regulating the allocation of precursors and energy required to sustain the AS biosynthesis in type-IV trichomes under high temperatures. Exposing tomato plants to high light intensities recently disclosed the shifts in carbon allocation within the GTs, prompted by changes in photosynthetic activity and potential increase in energy levels (Saadat et al., 2023). Thus, it is intriguing to investigate what processes are shared or different among these abiotic factors that regulate the productivity in the glandular cells.

4. Materials and methods

4.1 Sequence analysis

Full-length protein sequence of *Nicotiana tabacum* Ribulose biphosphate carboxylase-oxygenase small chain trichome-specific (NtRbcS-T) (GenBank accession: DV157962; NCBI XP_016450162.1) was used as a query for local alignments against the tomato (*Solanum lycopersicum*) proteome using the BLASTP tool from NCBI. Candidate sequences were blasted again in Phytozome to obtain the Solyc IDs. Protein sequence alignments were performed using Clustal Omega from the EMBL-EBI (Madeira et al., 2022) and the protein pairwise sequence analyses were conducted in EMBOSS Needle, using the Needleman-Wunsch algorithm.

4.2 Vector construction

Golden gate (GG) modular cloning system was used to assemble the different constructs (Engler et al., 2008; Weber et al., 2011). All the primers used in the cloning steps are listed in **Table S6**. For the RbcS-T reporter line, a sequence comprising 2,008 base pairs upstream of the start codon of the orthologous *S. habwerehaites* RbcS-T was split into two fragments (964 bp and 1,044 bp) and amplified by PCR using the KOD hot start DNA polymerase (71086-3, Merck). Fragments were purified and cloned into the universal vector pAGM1311 and then combined into level 0 vector pAGM4023. The promoter region was then cloned in the front of enhanced green fluorescent protein (EGFP) with the OCS-terminator in level 1 vector pICH47742, and then placed in the destination vector pAGM8031 with *NptII* selection marker (pICH67131).

Gene targeting of *RbcS-T* (Solyc07g017950) and *PEPCK* (Solyc04g076880) was performed using CRISPR/Cas9 system. The expression cassette consisted of two or three single guide RNAs (sgRNAs) and the optimized *S. pyogenes* Cas9 version containing introns (Cas9i) and two nuclear localization signals (Grützner et al., 2021) driven by two times the constitutively expressed 35S promoter and the translational enhancer tobacco mosaic virus omega (TMV Ω). Each spacer was selected using the CRISPR-P v2.0 online tool (<http://crispr.hzau.edu.cn/>) and attached to the gRNA scaffold and the U6-26 terminator by PCR flip extension using customized primers (**Table S6**). Each spacer/gRNA scaffold (199 bp) was purified and cloned in front of the *S. lycopersicum* RNA polymerase III U6 promoter (SIU6p – pAGT5824) in level 1 vectors. Once the cloning of every sgRNA was confirmed by sequencing, they were incorporated in a level 2 expression vector (pAGM8031 or pAGM35831) by combining the level 1 modules: 2X35S::ZmCas9i::tOCS (pAGT5997), the sgRNAs and the *NptII* selection marker (pICH67131) for subsequent stable transformation in tomato.

For the CRISPR-tissue specific knockout system (CRISPR-TSKO), a promoter region comprising 929 bp upstream of the start codon of the putative *metallocarboxypeptidase inhibitor* (MCPI, Solyc01g067295.1.1) was cloned into level 0 vector pAGM4023. Next, the MCPI promoter (MCPIp) was placed in front of the optimized Cas9i sequence in level 1 vector pICH47811 and using the same OCS terminator sequence. To target the multiple RbcS mehophyll isoforms (*RbcS1*, *RbcS2A*, *RbcS3B*) in type-VI trichomes, one sgRNA targeting each isoform was designed as described above and cloned in level 2 expression vector pAGM35831.

The CRISPR-TSKO proof-of-concept in type-VI GTs was conducted following the strategy of (Decaestecker et al., 2019) in which Cas9 was fused to a mCherry tag using the P2A ribosomal skipping peptide in order to monitor Cas9 expression. For that purpose, the P2A sequence was amplified by primer extension and the mCherry CDS PCR product amplified from the plasmid pICSL50004. Both fragments were combined and cloned into the universal vector pAGM9121. Next, the transcriptional unit MCPIp::Cas9i-P2A-mCherry was assembled via GG and used for the level 2 expression vector. Finally, two sgRNA of the *terpene synthase 20* (*TPS20*, Solyc08g005665) were designed as described before and cloned into level 2 vector for plant stable transformation.

4.3 Transformation in *E. coli* and *A. tumefaciens*

E. coli strain DH10B chemically competent cells were used in all steps of GG vector transformation and plasmid amplification. 20 µl of GG reaction was dispensed in a 1,5 ml polypropylene tube containing 50 µl of *E. coli* competent cells and incubated for 20 min on ice. After that, the cells plus plasmid sample was placed in 42°C heat shock for 60 sec, followed by 2 min on ice. For the recovery phase, 300 µl of SOC medium was added and incubated in a thermomixer for 1 h at 37°C and 450 rpm. 80 µl of the cells were spread on LB solid media containing the appropriate antibiotics in addition to the X-Gal for blue-white selection. Plates were incubated overnight at 37°C.

A. tumefaciens strain LBA4404 (ElectroMAX™, ThermoFisher) and GV3101 containing the pMP90 Ti plasmid were transformed by electroporation. In short, 25 µl of bacterial cells in 1,5 ml polypropylene tubes were thawed on ice, and 1 µl of the desired plasmid (50-100 ng/ul) was added. The cells + plasmid mixture was transferred into cold electroporation cuvettes. Samples were electroporated in a MicroPulser Electroporator (Bio-Rad) using 1 pulse with 2,2 kV and eluted adding 1 ml of LB medium and incubated for 3 h in a thermomixer at 28°C and 450 rpm. Finally, 80 µl of the Agro culture was plated in LB solid media containing the appropriate antibiotics and incubated for 2-3 days in dark at 28°C.

4.4 Extraction of genomic DNA

Genomic DNA from plants was extracted using the protocol described by (Hosaka, 2004) with some variations. In brief, 25 to 50 mg green of leaf tissue was collected in liquid nitrogen and homogenized using metal beads. 500 μ l of extraction buffer (100 mM Tris-Cl pH 8.0, 50 mM EDTA pH 8.0, 500 mM NaCl, 1,25% SDS, and 0,2% 2-mercaptoethanol) was added to the sample and mixed on the vortex for 30 sec and centrifuge at 14,000 rpm for 30 sec. Next, 100 μ l of clear extract was transferred to a 1,5 ml tube containing 32 μ l of 5M potassium acetate and mixed up and down several times. The tube was then centrifuged at 14,000 rpm for 30 sec and 10 μ l of clear extract was diluted in 490 μ l of water. Genomic DNA was taken from the solution to perform PCR screening of the putative transgenic plants and to sequence the mutations of gene targeting created with CRISPR/Cas9.

4.5 Virus-induced gene silencing (VIGS) assay

VIGS assay was conducted utilizing tobacco rattle virus (TRV)-based vectors, whose functionality has been demonstrated in tomato (Liu et al., 2002). To downregulate *SpRbcS-T* (LOC107025405) expression, a 344-bp specific fragment was amplified from cDNA by PCR using the KOD hot start DNA polymerase (71086-3, Merck), purified and cloned either into the pTRV2 single vector and into modified *pTRV2* vector containing a fragment of the *Magnesium Chelatase Subunit H (ChlH)* as a visual marker (Szymański et al., 2020). For that purpose, both fragment and vector were digested with the enzyme BamHI. The linearized vector was isolated in a 1% agarose gel, purified, and mixed with the PCR fragments for ligation. For the downregulation of the *RbcS-M* genes, a 327-bp fragment was amplified by PCR from the gene *ribulose biphosphate carboxylase-oxigenase small chain 2B (RbcS-2B)* (LOC107010326), which contains a conserved and high similar sequence within all *RbcS* mesophyll isoforms. *RbcS-M* fragment was then cloned into *pTRV2* and *pTRV2-ChlH* as for *RbcS-T*. Primers used are listed in **Table S6**.

The vectors were transformed into the *A. tumefaciens* strain GV3101 and grown in LB liquid medium overnight with antibiotics. Bacteria was resuspended in a buffer containing 10mM MgCl₂, 10mM MES and 200 μ M acetosyringone and with an OD₆₀₀ adjusted to 0,5. Every bacterial suspension harboring *pTRV2* vectors was combined with *Agrobacterium* suspension containing the pTRV1 vector in a 1:1 ratio. The plants were inoculated by dipping toothpicks in the bacterial suspension and passing through the stem of the plants three times. Fourth to five weeks after inoculation, plant tissue was collected for qRT-PCR and metabolite analysis.

To perform the VIGS assays, wild tomato *Solanum pennellii* LA0716 plants were grown in a phytocabinet (CLF Plant Climatics, Emersacker, Germany; model AR-66L) using long day conditions (16h light, 8h darkness), 65% relative humidity and 150 to 200 μ mol*s⁻¹ m² light

intensity. The temperature was set to 25°C and 23°C during the day and night respectively. One-month-old plants were used for the VIGS assays, using 8 different biological replicates. After inoculation, the temperature of the cabinet was lowered to 20°C during day and night.

4.6 *Agrobacterium*-mediated genetic transformation of tomato

Stable transformation of cultivated (*S. lycopersicum* cv MoneyMaker) and wild (*S. habrochaites* sp. *glabratum*) tomato were performed following the protocol of Van Eck et al. (2019) with some modifications. Details of media composition can be found in **Table S7**. In short, tomato seeds were sterilized and germinated on ½ MS medium under sterile conditions. After 8 days of growth in long-day conditions (18 h light 24°C / 6 h dark 24°C), fully expanded cotyledons were cut into pieces (**Fig. S11A, G**) and placed adaxial side down on filter paper onto MS1 medium. The same day, *Agrobacterium tumefaciens* strain LBA4404 (ElectroMAX™, ThermoFisher) harboring the desired transformation vector, was grown in liquid YM medium with antibiotics. After 24 hours, cotyledons were inoculated with the bacteria resuspended in MS-L with an OD of 0,5, with occasional shaking. After 30 min, the explants were dried and placed on MS1 medium for co-culture for 48 hours in dark. Explants were then transferred to MS2 medium supplemented with 100 mg/l Kanamycin, adaxial side up. The medium was refreshed every 14 days (**Fig: S11B**). When the shoots were visible, individual explants were cut and placed in MS3 medium for an additional 14 days. When apical meristems were visible (**Fig. S11D**), shoots were cut and placed in magenta boxes containing MSR medium supplemented with 50 mg/l Kanamycin. After 30-45 days, well established and putative positive *in vitro* plants were transferred into soil (**Fig. S11E-F**). In the case of the wild tomato, explants cotyledons were placed on MS1 medium supplemented with 100 µM acetosyringone (**Fig. S11G**). The following steps in the transformation scheme were the same as for the cultivated tomato (**Fig. S11H-I**).

4.7 Trichome counting.

Type-IV trichomes were counted over the adaxial surface of leaflets of the fourth and fifth leaf of tomato plants. For that, individual leaflets were sliced into 1,5 mm wide strips perpendicular to the middle vein and flipped 90°. Pictures of the individual strips were taken using a VXH-6000 microscope coupled with a VH-Z20 T zoom lens (both Keyence, Osaka, Japan), and the counting was manually performed using the Fiji/ImageJ software. Trichome numbers were normalized to the area of the strips. For type-V and type-IV trichomes, images of the edges of the leaflets were taken for trichome counting, since the glandular cells can be precisely distinguished.

4.8 Trichome fraction and leaf material harvesting.

To isolate trichomes from the leaves, leaflets and stems of tomato plants were cut one at a time, and the tissue was brushed off with a frozen paint brush previously dipped in liquid nitrogen in close proximity to a mortar pool of liquid nitrogen, as described in Balcke et al. (2014). When a white-yellowish cloud was visible, the trichomes were sieved through a steel mesh (pore size of 150 μm) onto a clean frozen mortar and the liquid was transferred carefully to a 25 ml polypropylene tube. When liquid nitrogen was evaporated, the samples were stored in -80°C until further procedures. Leaves and trichome-free leaves were directly collected in liquid nitrogen and stored until use.

4.9 Heat stress experiments

Heat stress (HS) experiments were conducted in phytocabinets (CLF Plant Climatics, Emersacker, Germany; model AR-66L). The phytocabinet for control (CN) conditions was set to 25°C during the day and 23°C during the night, and the one for HS was set to 37°C during the day and 23°C during the night. Both phytocabinets were set to long-day conditions (16h light, 8h darkness), 65% relative humidity and 150 to 200 $\mu\text{mol}\cdot\text{s}^{-1}\text{m}^2$ light intensity. Seeds of tomato (*Solanum lycopersicum*) cv Moneymaker and the CRISPR mutants were directly germinated on soil in CN conditions. After 7-8 days when the cotyledons were fully expanded, half of the seedlings were transferred to HS and maintained for three more weeks.

In the case of the *jasmonic acid-insensitive 1 (jai1)* mutant experiments, seeds of *S. lycopersicum* cv. Castlemart were sown on soil in CN conditions. After 10 days, the plants were genotyped by PCR (**Table S6**), sorted, and individual plants were either maintained in CN or transferred to HS for a further 20 days. The HS time series was performed using WT tomato cv Moneymaker. As in previous experiments, seeds germinated in CN, and after three weeks, plants were transferred to HS at the indicated time of the day. Leaf tissue was collected following a specific time after heat application and time during the daylight phase.

4.10 JA treatment

Three-week-old tomato plants cv Castlemart grown on soil were sprayed with jasmonic acid (100 μM) and harvested after 1 hour and 24 hours of JA application. Leaflets of leaf 2 and 3 (from bottom-to-top) were combined and harvested from three plants and pooled to constitute one biological replicate.

4.11 RNA isolation, cDNA synthesis and quantitative RT-PCR

Total RNA was extracted from tomato leaves using the RNeasy[®] Plant Mini Kit (Qiagen United States, 74904) following the manufacturer's protocol. For each sample, one microgram of total

RNA was treated with DNA-free™ DNA Removal Kit (AM1906, Invitrogen) and cDNA was synthesized using the Proto-Script first strand cDNA synthesis kit (New England Biolabs). Quantitative RT-PCR was performed in a CFX Opus Real-Time PCR (Bio-Rad) employing the 5X QPCR Mix EvaGreen (Bio&SELL GmbH) with the following program. Denaturation: 95°C for 15 min; amplification: 40 cycles of 95°C for 15 sec, 58-60°C for 10 sec and 72°C for 15 sec. At the end of the cycles heating up to 95°C with a heating rate of 0.05°C sec⁻¹ was performed to generate the melting curves. Target genes were amplified from three biological replicates. The Bio-Rad CFX Maestro© software was used to calculate the Cq values and *S. lycopersicum* Elongation factor 1-alpha (*SIEF1α*) was used in all cases as the reference gene. RT-qPCR primers are listed in **Table S6**.

4.12 Quantification of VOCs by gas chromatography-mass spectrometry (GC-MS)

Volatile organic compounds, in this case terpenoids, were collected by surface extraction using leaf discs of 1 cm diameter obtained with a cork borer. Six leaf discs were placed into a 2 ml polypropylene tubes and 800 µl of *n*-hexane was added followed by 30 seconds of vortex. 20 µM Menthol was used as an internal standar (IS) when indicated. Extracts were centrifuged at 14.000 rpm for 2 min and the supernatant was transferred directly to the GC vials. Mono- and sesquiterpenes were detected using a Trace GC Ultra gas chromatograph coupled with an ATAS Optic 3 injector and an ISQ mass spectrometer (Thermo Scientific) with electron impact ionization. The chromatographic separation was performed on a ZB-5ms capillary column (30 m × 0.32 mm, Phenomenex). The flow rate of helium was 1 ml min⁻¹, and the injection temperature rose from 60 to 250 °C at 10°C sec⁻¹ during 30 sec. The GC oven temperature ramp was 50 °C for 1 min, 50–150 °C at 7°C min⁻¹ and 150–300 °C at 25 °C min⁻¹ for 2 min. Mass spectrometry was performed at 70 Ev in full scan mode with *m/z* from 50 to 450. Data analysis was done with the Xcalibur software (Thermo Scientific). Volatile abundances were estimated by dividing the peak area of each metabolite to the peak area of the IS and the leaf dry weight when indicated.

4.13 Quantification of acylsugars by liquid chromatography-mass spectrometry (LC-MS)

Acylsugars were extracted from leaf surface samples, using 1 cm diameter leaf discs obtained excised with a cork-borer. Three leaf discs were placed into 2 ml polypropylene tubes and 1 ml of 80% methanol was subsequently added. 10 µM phlorizin was used as an IS when indicated. The tubes were manually inverted for 2 min. Extracts were centrifuged at 14.000 rpm and transferred directly to the glass vials.

Acylsugars of *Solanum pennellii* were extracted following the protocol used by (Ji et al., 2023) with some modifications. Three 1 cm leaf discs from similar-size leaves were placed into 2 ml polypropylene tubes and 1 ml of extraction solvent was subsequently added. The extraction solvent consisted of acetonitrile:isopropanol:water (3:3:2, v/v/v) with 0,1% (v/v) formic acid. 10 μ M phlorizin was always used as IS.

Separation of semi-polar metabolites was performed on a Nucleoshell RP18 (2.1 x 150 mm, particle size 2.1 μ m, Macherey & Nagel, GmbH, Düren, Germany) using a Waters ACQUITY UPLC System, equipped with an ACQUITY Binary Solvent Manager and ACQUITY Sample Manager (20 μ L sample loop, partial loop injection mode, 5 μ L injection volume, Waters GmbH Eschborn, Germany). Solvents A and B were 0.3 Mm ammonium formate (adjusted to pH 3.5 with formic acid) and acetonitrile, respectively. Elution was performed for 2 min at 5% eluent B, from 2-13 min with linear gradient to 95% B, from 13-15 min at 95% B, and from 15.01-18 min at 5% B. The flow rate was set to 0,4 ml/min and the column temperature was maintained at 40°C. Mass spectrometric analysis was performed by MS1 full scan from 65-1500 Dalton and 100 ms accumulation time (ZenoToF 7600, Sciex GmbH, Darmstadt, Germany) operating in negative mode and controlled by Sciex OS software (Sciex). The source operation parameters were as follows: ion spray voltage, -4500 V / +5500 V; nebulizing gas, 60 psi; source temperature, 600 °C; drying gas, 70 psi; curtain gas, 35 psi CAD gas 7 psi. Internal mass calibration was performed every 10 samples with X500 ESI negative solution. Peak areas were determined with Multiquant 3 software (Sciex GmbH, Darmstadt, Germany). Acylsugars abundances were estimated by dividing the peak area of each metabolite by the peak area of the internal standard (IS) and the leaf dry weight when indicated.

4.14 JA-related phytohormones quantification

The levels of jasmonic acid (JA), its precursor OPDA and its conjugate JA-Ile were quantified by liquid chromatography-mass spectrometry (LC-MS) following the protocol described by (Balcke et al., 2012). 50 mg of leaf tissue was homogenized with 250 μ l of pure methanol containing deuterated standards ($[^2\text{H}_5]$ OPDA, $[^2\text{H}_6]$ JA, and $[^2\text{H}_2]$ JA-Ile). Extracts were centrifuged at full speed for 15 min and the supernatant was transferred to a new tube and diluted using 1750 μ l of water. Phytohormones were isolated using a solid phase extraction SPE on HR-XC column (Macherey Nagel Filterplates) and eluted in 900 μ l acetonitrile. Excess solvent was removed by evaporation using a speedvac for 1 hour. Separation of the phytohormones was accomplished following the procedure of the semi-polar metabolites, but using the following gradient: 2 min at 5% B, from 2-19 min linear gradient to 95% B, from 19-21 min at 95% B and from 21.01 min-24 min at 95% B. Metabolite detection was performed by scheduled multiple reaction monitoring (MRM) on a QTrap6500 (Sciex GmbH, Darmstadt, Germany) operating in negative ion mode and controlled by Analyst 1.7.1 software (Sciex

GmbH, Darmstadt, Germany). The source operation parameters were as the following: ion spray voltage, -4500 V / +5500 V; nebulizing gas, 60 psi; source temperature, 450 °C; drying gas, 70 psi; curtain gas, 35 psi.

4.15 Two-phase metabolite extraction from trichomes and leaves

Hydrophilic and semi-polar metabolites were extracted following the protocol of (Balcke et al., 2017) with some modifications. Briefly, 900 µl cold dichloromethane/ethanol (2:1) and 100 µl (for fresh weight) / 200 µl (for dry weight) of HCl pH 1,4 were added into a 2,0 ml screw cap sample tubes (Biozym, 710768) containing leaf (150 mg fresh weight) and trichome (10 mg dry weight) tissue, and additional mixture of beads (200 mg glass beads (0,75 - 1,0 mm), three small steel beads (3 mm) and one large steel bead (5 mm)). Samples and solvents were homogenized in a FastPrep bead beating (3 x 20 s, speed 5 m/s) and centrifuged for 5 min at 12,700 rpm and 4°C. The supernatant was transferred to a new polypropylene tube on ice and 50 µl of HCl pH 1,4 were added to the organic fraction. Fastprep and centrifuge were repeated, and the supernatant was combined with the first one. The combined aqueous phase was transferred to the glass vials and stored at -80°C until measurements were performed. The organic phase was collected from the bottom of the tube and transferred into a fresh 2 ml polypropylene tube. Next, 500 µl Tetrahydrofuran was added, and the Fastprep and centrifugation steps were repeated. The supernatant was then combined with the previous organic extract and the samples were dried under the nitrogen gas stream. The samples were resuspended using 180 µl of 80% methanol and 30 s vortex, followed ultrasonic water bath for 5 min. After that, samples were diluted 1:5 with 80 % methanol, centrifuged for 5 mins and dispensed into the glass vials for LC-MS.

4.16 Targeted analysis of hydrophilic metabolites of the central carbon metabolism

Separation and detection of intermediates of the central carbon metabolism was performed according to (Balcke et al., 2023). In short, injecting 5 µl of the aqueous phase into an ACQUITY UPLC (Waters Inc.) equipped with a Nucleoshell RP18 column (Macherey & Nagel, 150mm x 2 mm x 2.1µm) and using tributylammonium as ion pairing agent. Two solvents were used, Solvent A: 10mM tributylamine (pH 6,2 adjusted with glacial acetic acid), and Solvent B: acetonitrile. The gradient program was 0-2 min: 2% B, 2-18 min 2-36% B, 18-21 min 36-95% B, 21-22,5 min 95% B, 22,51-24 min 2% B. The flow rate was 0,4 ml/min and the temperature was set to 40°C. Multiple reaction monitoring (MRM-based metabolite detection was performed in negative mode electrospray ionization (ESI) on a QTrap6500 (AB-Sciex GmbH, Darmstadt, Germany: ion source gas 1: 60 psi, ion source gas 2: 70 psi, curtain gas: 35 psi, temperature: 450 °C, Ion spray voltage floating: and -4500V).

4.17 Fluorescence microscopy

Trichome and fruit fluorescent images were recorded with a Zeiss LSM780 AxioObserver confocal microscope. GFP signal depicted by the green channel was acquired with 488/522 nm excitation/emission wavelength, and chlorophyll fluorescence indicated by magenta color was acquired with 633/685 nm excitation/emission wavelength, respectively. Images were processed using the ZEN software.

4.18 Quantification of organic acids and Pi

10 mg of fresh weight isolated trichomes were ground in a bead mill using 5 mm steel beads. Metabolites were extracted by adding 200 µl of extraction solvent per sample, containing 70 % (v/v) methanol, and the internal standards (5 nmol fumaric acid, succinic acid, alpha-Ketoglutarate, malic acid, aconitic acid, citric acid, and Pi) for 20 min in a shaker. After two rounds of centrifugation (10,000 rpms for 5 min), 10 µl of the clear extract was dried in a speed vacuum. Then 20 µl of methoxyamine in pyridine (Sigma-Aldrich, St. Louis, MO, USA) was added to each tube and incubated for 1 h. After that, 35 µl of derivatization reagent was added (Silyl 991 (Macherey-Nagel, Düren, Germany) and incubated for another 45 min at 37°C. Samples were precooled and subsequently used for GC-MS/MS, Agilent 7890 GC system coupled to an Agilent 7000B triple quadrupole mass spectrometer (Agilent, Waldbronn, Germany). The GC-MS/MS measurements were conducted following the description in Chutia et al. (2021). The MassHunter Quantitative Analysis software (version B06.00, Agilent, Waldbronn, Germany) was used to integrate the peaks. Organic acids and Pi concentrations were determined using the corresponding internal standards normalized to the fresh weights.

4.19 RNA sequencing and data analysis

RNA from WT and *jai1* samples was extracted using the RNeasy© Plant Mini Kit (Qiagen United States, 74904) and DNA traces were removed using DNA-free™ DNA Removal Kit (AM1906, Invitrogen). RNA integrity (RIN > 7.0) was evaluated with BioAnalyzer using the RNA 6000 Nano kit (Agilent Technologies). RNA samples were sequenced using Illumina Sequencing PE150, Q30 ≥85% (Novogen, UK). Mapping and gene expression quantification was performed by the company. Genome assembly SL3.1 was used NCBI RefSeq assembly GCF_000188115.5, from Solanaceae Genomics Project, available at www.ncbi.nlm.nih.gov/datasets/genome/GCF_000188115.5/. Further analysis, including PCA and Gene Ontology enrichment were conducted using the IDEP.96 software (Ge et al., 2018).

4.20 Statistical and bioinformatic analyses

Pair and multiple comparisons using Student's *t*-test, one-way and two-way ANOVA, were performed in Prism 9 V 9.5.1 (528) © GraphPad Software.

Targeted metabolomics data analysis was conducted using MetaboAnalyst web-base platform (dev.metaboanalyst.ca). Signal intensities underwent log (base10) transformation and scale using pareto scaling. PCA, *t*-test, ANOVA were also performed on this platform.

GO enrichment analysis of *MYB13* neighboring genes was performed following these steps: First, the top 400 coexpressed genes were obtained from RNASeq databases deposited in Genevestigator 9.6.1 (Hruz et al., 2008) with mutual correlation > 0,58. From them, 293 genes were used to feed the agriGO v2.0 software (Tian et al., 2017). Dot plot displaying significant enriched GO terms was constructed in SRPlot (bioinformatics.com.cn/srplot).

5. References

- Agrawal AA, Conner JK, Johnson MTJ, Wallsgrove R** (2002) ECOLOGICAL GENETICS OF AN INDUCED PLANT DEFENSE AGAINST HERBIVORES: ADDITIVE GENETIC VARIANCE AND COSTS OF PHENOTYPIC PLASTICITY. *Evolution* **56**: 2206-2213
- Agrawal R, Sharma M, Dwivedi N, Maji S, Thakur P, Junaid A, Fajkus J, Laxmi A, Thakur JK** (2022) MEDIATOR SUBUNIT17 integrates jasmonate and auxin signaling pathways to regulate thermomorphogenesis. *Plant Physiology* **189**: 2259-2280
- Ahmad P, Rasool S, Gul A, Sheikh SA, Akram NA, Ashraf M, Kazi AM, Gucel S** (2016) Jasmonates: Multifunctional Roles in Stress Tolerance. **7**
- Allen DK, Ohlrogge JB, Shachar-Hill Y** (2009) The role of light in soybean seed filling metabolism. *The Plant Journal* **58**: 220-234
- Allen F, Crepaldi L, Alsinet C, Strong AJ, Kleshchevnikov V, De Angeli P, Páleníková P, Khodak A, Kiselev V, Kosicki M, Bassett AR, Harding H, Galanty Y, Muñoz-Martínez F, Metzakopian E, Jackson SP, Parts L** (2019) Predicting the mutations generated by repair of Cas9-induced double-strand breaks. *Nature Biotechnology* **37**: 64-72
- Amaral BSd, Correa KCS, Corrêa AG, Souza DHFd, Cass QB** (2019) Direct Assay to Evaluate Phosphoenolpyruvate Carboxykinase Activity. *Journal of the Brazilian Chemical Society* **30**
- Andersson I, Backlund A** (2008) Structure and function of Rubisco. *Plant Physiology and Biochemistry* **46**: 275-291
- Andrews TJ, Kane HJ** (1991) Pyruvate is a by-product of catalysis by ribulosebiphosphate carboxylase/oxygenase. *Journal of Biological Chemistry* **266**: 9447-9452
- Arya GC, Sarkar S, Manasherova E, Aharoni A, Cohen H** (2021) The Plant Cuticle: An Ancient Guardian Barrier Set Against Long-Standing Rivals. *Frontiers in Plant Science* **12**
- Bahrami AR, Chen Z-H, Walker RP, Leegood RC, Gray JE** (2001) Ripening-related occurrence of phosphoenolpyruvate carboxykinase in tomato fruit. *Plant Molecular Biology* **47**: 499-506
- Balcke GU, Bennewitz S, Bergau N, Athmer B, Henning A, Majovsky P, Jiménez-Gómez JM, Hoehenwarter W, Tissier A** (2017) Multi-Omics of Tomato Glandular Trichomes Reveals Distinct Features of Central Carbon Metabolism Supporting High Productivity of Specialized Metabolites. *The Plant Cell* **29**: 960-983
- Balcke GU, Bennewitz S, Zabel S, Tissier A** (2014) Isoprenoid and Metabolite Profiling of Plant Trichomes. In M Rodríguez-Concepción, ed, *Plant Isoprenoids: Methods and Protocols*. Springer New York, New York, NY, pp 189-202
- Balcke GU, Handrick V, Bergau N, Fichtner M, Henning A, Stellmach H, Tissier A, Hause B, Frolov A** (2012) An UPLC-MS/MS method for highly sensitive high-throughput analysis of phytohormones in plant tissues. *Plant Methods* **8**: 47
- Balcke GU, Vahabi K, Giese J, Finkemeier I, Tissier A** (2023) The Arabidopsis Concert of Metabolic Acclimation to High Light Stress. *bioRxiv*: 2023.2002.2014.528433
- Banerjee A, Sharkey TD** (2014) Methylerythritol 4-phosphate (MEP) pathway metabolic regulation. *Nat Prod Rep* **31**: 1043-1055
- Behnke K, Ehling B, Teuber M, Bauerfeind M, Louis S, Hänsch R, Polle A, Bohlmann J, Schnitzler J-P** (2007) Transgenic, non-isoprene emitting poplars don't like it hot. *The Plant Journal* **51**: 485-499
- Benn G, Bjornson M, Ke H, De Souza A, Balmont EI, Shaw JT, Dehesh K** (2016) Plastidial metabolite MEcPP induces a transcriptionally centered stress-response hub via the transcription factor CAMTA3. *Proceedings of the National Academy of Sciences* **113**: 8855-8860
- Bergau N, Bennewitz S, Syrowatka F, Hause G, Tissier A** (2015) The development of type VI glandular trichomes in the cultivated tomato *Solanum lycopersicum* and a related wild species *S. habrochaites*. *BMC Plant Biology* **15**: 289

- Bergau N, Navarette Santos A, Henning A, Balcke GU, Tissier A** (2016) Autofluorescence as a Signal to Sort Developing Glandular Trichomes by Flow Cytometry. *Frontiers in Plant Science* **7**
- Besser K, Harper A, Welsby N, Schauvinhold I, Slocombe S, Li Y, Dixon RA, Broun P** (2009) Divergent Regulation of Terpenoid Metabolism in the Trichomes of Wild and Cultivated Tomato Species *Plant Physiology* **149**: 499-514
- Bickford CP** (2016) Ecophysiology of leaf trichomes. *Functional Plant Biology* **43**: 807-814
- Bleeker PM, Diergaarde PJ, Ament K, Schütz S, Johne B, Dijkink J, Hiemstra H, de Gelder R, de Both MTJ, Sabelis MW, Haring MA, Schuurink RC** (2011) Tomato-produced 7-epizingiberene and R-curcumene act as repellents to whiteflies. *Phytochemistry* **72**: 68-73
- Bleeker PM, Mirabella R, Diergaarde PJ, VanDoorn A, Tissier A, Kant MR, Prins M, de Vos M, Haring MA, Schuurink RC** (2012) Improved herbivore resistance in cultivated tomato with the sesquiterpene biosynthetic pathway from a wild relative. *Proceedings of the National Academy of Sciences* **109**: 20124-20129
- Boughton AJ, Hoover K, Felton GW** (2005) Methyl Jasmonate Application Induces Increased Densities of Glandular Trichomes on Tomato, *Lycopersicon esculentum*. *Journal of Chemical Ecology* **31**: 2211-2216
- Bouvier J, W. , M. Emms D, Kelly S** (2023) Rubisco is evolving for improved catalytic efficiency and CO₂ assimilation in plants. *bioRxiv*: 2022.2007.2006.498985
- Bracher A, Whitney SM, Hartl FU, Hayer-Hartl M** (2017) Biogenesis and Metabolic Maintenance of Rubisco. *Annual Review of Plant Biology* **68**: 29-60
- Brand A, Tissier A** (2022) Control of resource allocation between primary and specialized metabolism in glandular trichomes. *Current Opinion in Plant Biology* **66**: 102172
- Brinkman EK, Chen T, Amendola M, van Steensel B** (2014) Easy quantitative assessment of genome editing by sequence trace decomposition. *Nucleic Acids Research* **42**: e168-e168
- Brown NJ, Palmer BG, Stanley S, Hajaji H, Janacek SH, Astley HM, Parsley K, Kajala K, Quick WP, Trenkamp S, Fernie AR, Maurino VG, Hibberd JM** (2010) C₄ acid decarboxylases required for C₄ photosynthesis are active in the mid-vein of the C₃ species *Arabidopsis thaliana*, and are important in sugar and amino acid metabolism. *The Plant Journal* **61**: 122-133
- Cao P, Yang J, Xia L, Zhang Z, Wu Z, Hao Y, Liu P, Wang C, Li C, Yang J, Lai J, Li X, Deng M, Wang S** (2024) Two gene clusters and their positive regulator SIMYB13 that have undergone domestication-associated negative selection control phenolamide accumulation and drought tolerance in tomato. *Molecular Plant* **17**: 579-597
- Cárdenas PD, Sonawane PD, Pollier J, Vanden Bossche R, Dewangan V, Weithorn E, Tal L, Meir S, Rogachev I, Malitsky S, Giri AP, Goossens A, Burdman S, Aharoni A** (2016) GAME9 regulates the biosynthesis of steroidal alkaloids and upstream isoprenoids in the plant mevalonate pathway. *Nature Communications* **7**: 10654
- Castroverde CDM, Dina D** (2021) Temperature regulation of plant hormone signaling during stress and development. *Journal of Experimental Botany* **72**: 7436-7458
- Cavanagh AP, Slattery R, Kubien DS** (2023) Temperature-induced changes in *Arabidopsis* Rubisco activity and isoform expression. *Journal of Experimental Botany* **74**: 651-663
- Chalvin C, Drevensek S, Dron M, Bendahmane A, Boualem A** (2020) Genetic Control of Glandular Trichome Development. *Trends in Plant Science* **25**: 477-487
- Chang J, Yu T, Yang Q, Li C, Xiong C, Gao S, Xie Q, Zheng F, Li H, Tian Z, Yang C, Ye Z** (2018) Hair, encoding a single C₂H₂ zinc-finger protein, regulates multicellular trichome formation in tomato. *The Plant Journal* **96**: 90-102
- Chen G, Klinkhamer PGL, Escobar-Bravo R, Leiss KA** (2018) Type VI glandular trichome density and their derived volatiles are differently induced by jasmonic acid in developing and fully developed tomato leaves: Implications for thrips resistance. *Plant Science* **276**: 87-98
- Chen H, Wilkerson CG, Kuchar JA, Phinney BS, Howe GA** (2005) Jasmonate-inducible plant enzymes degrade essential amino acids in the herbivore midgut. *Proceedings of the National Academy of Sciences* **102**: 19237-19242

- Chen Y, Su D, Li J, Ying S, Deng H, He X, Zhu Y, Li Y, Chen Y, Pirrello J, Bouzayen M, Liu Y, Liu M** (2020) Overexpression of bHLH95, a basic helix–loop–helix transcription factor family member, impacts trichome formation via regulating gibberellin biosynthesis in tomato. *Journal of Experimental Botany* **71**: 3450-3462
- Chen Z-H, Walker RP, Acheson RM, Leegood RC** (2002) Phosphoenolpyruvate Carboxykinase Assayed at Physiological Concentrations of Metal Ions Has a High Affinity for CO₂ *Plant Physiology* **128**: 160-164
- Cheng A-X, Lou Y-G, Mao Y-B, Lu S, Wang L-J, Chen X-Y** (2007) Plant Terpenoids: Biosynthesis and Ecological Functions. *Journal of Integrative Plant Biology* **49**: 179-186
- Cheng S-H, Moore Bd, Seemann JR** (1998) Effects of Short- and Long-Term Elevated CO₂ on the Expression of Ribulose-1,5-Bisphosphate Carboxylase/Oxygenase Genes and Carbohydrate Accumulation in Leaves of *Arabidopsis thaliana* (L.) Heynh.1. *Plant Physiology* **116**: 715-723
- Chini A, Fonseca S, Fernández G, Adie B, Chico JM, Lorenzo O, García-Casado G, López-Vidriero I, Lozano FM, Ponce MR, Micol JL, Solano R** (2007) The JAZ family of repressors is the missing link in jasmonate signalling. *Nature* **448**: 666-671
- Chutia R, Scharfenberg S, Neumann S, Abel S, Ziegler J** (2021) Modulation of Phosphate Deficiency-Induced Metabolic Changes by Iron Availability in *Arabidopsis thaliana*. *In International Journal of Molecular Sciences*, Vol 22
- Clarke SM, Cristescu SM, Miersch O, Harren FJM, Wasternack C, Mur LAJ** (2009) Jasmonates act with salicylic acid to confer basal thermotolerance in *Arabidopsis thaliana*. *New Phytologist* **182**: 175-187
- Conneely LJ, Mauleon R, Mieog J, Barkla BJ, Kretzschmar T** (2021) Characterization of the *Cannabis sativa* glandular trichome proteome. *PLOS ONE* **16**: e0242633
- Copolovici L, Kännaste A, Pazouki L, Niinemets Ü** (2012) Emissions of green leaf volatiles and terpenoids from *Solanum lycopersicum* are quantitatively related to the severity of cold and heat shock treatments. *Journal of Plant Physiology* **169**: 664-672
- Cordoba E, Porta H, Arroyo A, San Román C, Medina L, Rodríguez-Concepción M, León P** (2011) Functional characterization of the three genes encoding 1-deoxy-D-xylulose 5-phosphate synthase in maize. *Journal of Experimental Botany* **62**: 2023-2038
- Cortijo S, Charoensawan V, Brestovitsky A, Buning R, Ravarani C, Rhodes D, van Noort J, Jaeger KE, Wigge PA** (2017) Transcriptional Regulation of the Ambient Temperature Response by H2A.Z Nucleosomes and HSF1 Transcription Factors in *Arabidopsis*. *Molecular Plant* **10**: 1258-1273
- Dalin P, Björkman C** (2003) Adult beetle grazing induces willow trichome defence against subsequent larval feeding. *Oecologia* **134**: 112-118
- Decaestecker W, Buono RA, Pfeiffer ML, Vangheluwe N, Jourquin J, Karimi M, Van Isterdael G, Beeckman T, Nowack MK, Jacobs TB** (2019) CRISPR-TSKO: A Technique for Efficient Mutagenesis in Specific Cell Types, Tissues, or Organs in *Arabidopsis*. *The Plant Cell* **31**: 2868-2887
- Dedonder A, Rethy R, Fredericq H, Van Montagu M, Krebbers E** (1993) *Arabidopsis rbcS* Genes Are Differentially Regulated by Light. *Plant Physiology* **101**: 801-808
- Delker C, Quint M, Wigge PA** (2022) Recent advances in understanding thermomorphogenesis signaling. *Current Opinion in Plant Biology* **68**: 102231
- Devi MG** (2022) The genetics of whitefly resistance in tomato. Dissertation, Halle (Saale), Martin-Luther-Universität Halle-Wittenberg, 2022
- Donovan S, Mao Y, Orr DJ, Carmo-Silva E, McCormick AJ** (2020) CRISPR-Cas9-Mediated Mutagenesis of the Rubisco Small Subunit Family in *Nicotiana tabacum*. *Frontiers in Genome Editing* **2**
- Doubnerová Hýsková V, Miedzińska L, Dobrá J, Vankova R, Ryšlavá H** (2014) Phosphoenolpyruvate carboxylase, NADP-malic enzyme, and pyruvate, phosphate dikinase are involved in the acclimation of *Nicotiana tabacum* L. to drought stress. *Journal of Plant Physiology* **171**: 19-25
- Dudareva N, Andersson S, Orlova I, Gatto N, Reichelt M, Rhodes D, Boland W, Gershenzon J** (2005) The nonmevalonate pathway supports both monoterpene and

- sesquiterpene formation in snapdragon flowers. *Proceedings of the National Academy of Sciences* **102**: 933-938
- Dudareva N, Klempien A, Muhlemann JK, Kaplan I** (2013) Biosynthesis, function and metabolic engineering of plant volatile organic compounds. *New Phytologist* **198**: 16-32
- Dudareva N, Pichersky E, Gershenzon J** (2004) Biochemistry of Plant Volatiles. *Plant Physiology* **135**: 1893-1902
- Eastmond PJ, Astley HM, Parsley K, Aubry S, Williams BP, Menard GN, Craddock CP, Nunes-Nesi A, Fernie AR, Hibberd JM** (2015) Arabidopsis uses two gluconeogenic gateways for organic acids to fuel seedling establishment. *Nature Communications* **6**: 6659
- Engler C, Kandzia R, Marillonnet S** (2008) A One Pot, One Step, Precision Cloning Method with High Throughput Capability. *PLOS ONE* **3**: e3647
- Escobar-Bravo R, Alba JM, Pons C, Granell A, Kant MR, Moriones E, Fernández-Muñoz R** (2016) A Jasmonate-Inducible Defense Trait Transferred from Wild into Cultivated Tomato Establishes Increased Whitefly Resistance and Reduced Viral Disease Incidence. *Frontiers in Plant Science* **7**
- Escobar-Bravo R, Klinkhamer PGL, Leiss KA** (2017) Induction of Jasmonic Acid-Associated Defenses by Thrips Alters Host Suitability for Conspecifics and Correlates with Increased Trichome Densities in Tomato. *Plant and Cell Physiology* **58**: 622-634
- Evans S, Xu Y, Bergman M, Ford S, Liu Y, Sharkey T, Phillips M** (2024) Rubisco supplies pyruvate for the 2- C -methyl-D-erythritol-4-phosphate pathway. *In. bioRxiv*
- Faden F, Mielke S, Dissmeyer N** (2019) Modulating Protein Stability to Switch Toxic Protein Function On and Off in Living Cells. *Plant Physiology* **179**: 929-942
- Fahn A** (2000) Structure and function of secretory cells. *In Advances in Botanical Research*, Vol 31. Academic Press, pp 37-75
- Fan P, Leong BJ, Last RL** (2019) Tip of the trichome: evolution of acylsugar metabolic diversity in Solanaceae. *Current Opinion in Plant Biology* **49**: 8-16
- Fan P, Miller AM, Schillmiller AL, Liu X, Ofner I, Jones AD, Zamir D, Last RL** (2016) In vitro reconstruction and analysis of evolutionary variation of the tomato acylsucrose metabolic network. *Proceedings of the National Academy of Sciences* **113**: E239-E248
- Fan P, Wang P, Lou Y-R, Leong BJ, Moore BM, Schenck CA, Combs R, Cao P, Brandizzi F, Shiu S-H, Last RL** (2020) Evolution of a plant gene cluster in Solanaceae and emergence of metabolic diversity. *eLife* **9**: e56717
- Fatland BL, Ke J, Anderson MD, Mentzen WI, Cui LW, Allred CC, Johnston JL, Nikolau BJ, Wurtele ES** (2002) Molecular Characterization of a Heteromeric ATP-Citrate Lyase That Generates Cytosolic Acetyl-Coenzyme A in Arabidopsis. *Plant Physiology* **130**: 740-756
- Feng H, Acosta-Gamboa L, Kruse LH, Tracy JD, Chung SH, Nava Ferreira AR, Shakir S, Xu H, Sunter G, Gore MA, Casteel CL, Moghe GD, Jander G** (2022) Acylsugars protect *Nicotiana benthamiana* against insect herbivory and desiccation. *Plant Molecular Biology* **109**: 505-522
- Fernández-Calvo P, Chini A, Fernández-Barbero G, Chico J-M, Gimenez-Ibanez S, Geerinck J, Eeckhout D, Schweizer F, Godoy M, Franco-Zorrilla JM, Pauwels L, Witters E, Puga MI, Paz-Ares J, Goossens A, Reymond P, De Jaeger G, Solano R** (2011) The Arabidopsis bHLH Transcription Factors MYC3 and MYC4 Are Targets of JAZ Repressors and Act Additively with MYC2 in the Activation of Jasmonate Responses *The Plant Cell* **23**: 701-715
- Firdaus S, van Heusden AW, Hidayati N, Supena EDJ, Mumm R, de Vos RCH, Visser RGF, Vosman B** (2013) Identification and QTL mapping of whitefly resistance components in *Solanum galapagense*. *Theoretical and Applied Genetics* **126**: 1487-1501
- Flügge U-I, Häusler RE, Ludewig F, Gierth M** (2011) The role of transporters in supplying energy to plant plastids. *Journal of Experimental Botany* **62**: 2381-2392

- Fobes JF, Mudd JB, Marsden MPF** (1985) Epicuticular Lipid Accumulation on the Leaves of *Lycopersicon pennellii* (Corr.) D'Arcy and *Lycopersicon esculentum* Mill. *Plant Physiology* **77**: 567-570
- Fonseca S, Chini A, Hamberg M, Adie B, Porzel A, Kramell R, Miersch O, Wasternack C, Solano R** (2009) (+)-7-iso-Jasmonoyl-L-isoleucine is the endogenous bioactive jasmonate. *Nature Chemical Biology* **5**: 344-350
- Freitas JA, Maluf WR, das Graças Cardoso M, Gomes LAA, Bearzotti E** (2002) Inheritance of foliar zingiberene contents and their relationship to trichome densities and whitefly resistance in tomatoes. *Euphytica* **127**: 275-287
- Frelichowski Jr JE, Juvik JA** (2005) Inheritance of sesquiterpene carboxylic acid synthesis in crosses of *Lycopersicon hirsutum* with insect-susceptible tomatoes. *Plant Breeding* **124**: 277-281
- Friedman M** (2002) Tomato Glycoalkaloids: Role in the Plant and in the Diet. *Journal of Agricultural and Food Chemistry* **50**: 5751-5780
- Furbank RT** (2011) Evolution of the C4 photosynthetic mechanism: are there really three C4 acid decarboxylation types? *Journal of Experimental Botany* **62**: 3103-3108
- Galdon-Armero J, Fullana-Pericas M, Mulet PA, Conesa MA, Martin C, Galmes J** (2018) The ratio of trichomes to stomata is associated with water use efficiency in *Solanum lycopersicum* (tomato). *The Plant Journal* **96**: 607-619
- Gao S, Gao Y, Xiong C, Yu G, Chang J, Yang Q, Yang C, Ye Z** (2017) The tomato B-type cyclin gene, *SlCycB2*, plays key roles in reproductive organ development, trichome initiation, terpenoids biosynthesis and *Prodenia litura* defense. *Plant Science* **262**: 103-114
- García-Alcázar M, Giménez E, Pineda B, Capel C, García-Sogo B, Sánchez S, Yuste-Lisbona FJ, Angosto T, Capel J, Moreno V, Lozano R** (2017) Albino T-DNA tomato mutant reveals a key function of 1-deoxy-D-xylulose-5-phosphate synthase (*DXS1*) in plant development and survival. *Scientific Reports* **7**: 45333
- Ge SX, Son EW, Yao R** (2018) iDEP: an integrated web application for differential expression and pathway analysis of RNA-Seq data. *BMC Bioinformatics* **19**: 534
- Ghosh B, Westbrook TC, Jones AD** (2014) Comparative structural profiling of trichome specialized metabolites in tomato (*Solanum lycopersicum*) and *S. habrochaites*: acylsugar profiles revealed by UHPLC/MS and NMR. *Metabolomics* **10**: 496-507
- Glas JJ, Schimmel BCJ, Alba JM, Escobar-Bravo R, Schuurink RC, Kant MR** (2012) Plant Glandular Trichomes as Targets for Breeding or Engineering of Resistance to Herbivores. *In International Journal of Molecular Sciences*, Vol 13, pp 17077-17103
- Gong Z, Luo Y, Zhang W, Jian W, Zhang L, Gao X, Hu X, Yuan Y, Wu M, Xu X, Zheng X, Wu G, Li Z, Li Z, Deng W** (2021) A SIMYB75-centred transcriptional cascade regulates trichome formation and sesquiterpene accumulation in tomato. *Journal of Experimental Botany* **72**: 3806-3820
- Goodspeed D, Chehab EW, Min-Venditti A, Braam J, Covington MF** (2012) Arabidopsis synchronizes jasmonate-mediated defense with insect circadian behavior. *Proceedings of the National Academy of Sciences* **109**: 4674-4677
- Grützner R, Martin P, Horn C, Mortensen S, Cram EJ, Lee-Parsons CWT, Stuttmann J, Marillonnet S** (2021) High-efficiency genome editing in plants mediated by a Cas9 gene containing multiple introns. *Plant Communications* **2**: 100135
- Guo D-P, Sun Y-Z, Chen Z-J** (2003) Involvement of polyamines in cytoplasmic male sterility of stem mustard (*Brassica juncea* var. *tsatsai*). *Plant Growth Regulation* **41**: 33-40
- Guo Z, Zuo Y, Wang S, Zhang X, Wang Z, Liu Y, Shen Y** (2024) Early signaling enhance heat tolerance in Arabidopsis through modulating jasmonic acid synthesis mediated by HSF2. *International Journal of Biological Macromolecules* **267**: 131256
- Han G, Li Y, Yang Z, Wang C, Zhang Y, Wang B** (2022) Molecular Mechanisms of Plant Trichome Development. *Frontiers in Plant Science* **13**
- Havko NE, Das MR, McClain AM, Kapali G, Sharkey TD, Howe GA** (2020) Insect herbivory antagonizes leaf cooling responses to elevated temperature in tomato. *Proceedings of the National Academy of Sciences* **117**: 2211-2217

- Havko NE, Kapali G, Das MR, Howe GA** (2020) Stimulation of Insect Herbivory by Elevated Temperature Outweighs Protection by the Jasmonate Pathway. *In Plants*, Vol 9
- Hernandez JO, Park BB** (2022) The Leaf Trichome, Venation, and Mesophyll Structural Traits Play Important Roles in the Physiological Responses of Oak Seedlings to Water-Deficit Stress. *In International Journal of Molecular Sciences*, Vol 23
- Higashi Y, Okazaki Y, Myouga F, Shinozaki K, Saito K** (2015) Landscape of the lipidome and transcriptome under heat stress in *Arabidopsis thaliana*. *Scientific Reports* **5**: 10533
- Higashi Y, Okazaki Y, Takano K, Myouga F, Shinozaki K, Knoch E, Fukushima A, Saito K** (2018) HEAT INDUCIBLE LIPASE1 Remodels Chloroplastic Monogalactosyldiacylglycerol by Liberating α -Linolenic Acid in *Arabidopsis* Leaves under Heat Stress. *The Plant Cell* **30**: 1887-1905
- Hong G-J, Xue X-Y, Mao Y-B, Wang L-J, Chen X-Y** (2012) *Arabidopsis* MYC2 Interacts with DELLA Proteins in Regulating Sesquiterpene Synthase Gene Expression *The Plant Cell* **24**: 2635-2648
- Hosaka K** (2004) An easy, rapid, and inexpensive DNA extraction method, "one-minute DNA extraction," for PCR in potato. *American Journal of Potato Research* **81**: 17-19
- Howe GA, Major IT, Koo AJ** (2018) Modularity in Jasmonate Signaling for Multistress Resilience. *Annual Review of Plant Biology* **69**: 387-415
- Hruz T, Laule O, Szabo G, Wessendorp F, Bleuler S, Oertle L, Widmayer P, Gruissem W, Zimmermann P** (2008) Genevestigator V3: A Reference Expression Database for the Meta-Analysis of Transcriptomes. *Advances in Bioinformatics* **2008**: 420747
- Hu H, He X, Tu L, Zhu L, Zhu S, Ge Z, Zhang X** (2016) GhJAZ2 negatively regulates cotton fiber initiation by interacting with the R2R3-MYB transcription factor GhMYB25-like. *The Plant Journal* **88**: 921-935
- Hua B, Chang J, Wu M, Xu Z, Zhang F, Yang M, Xu H, Wang L-J, Chen X-Y, Wu S** (2021) Mediation of JA signalling in glandular trichomes by the woolly/SIMYC1 regulatory module improves pest resistance in tomato. *Plant Biotechnology Journal* **19**: 375-393
- Hua B, Chang J, Xu Z, Han X, Xu M, Yang M, Yang C, Ye Z, Wu S** (2021) HOMEODOMAIN PROTEIN8 mediates jasmonate-triggered trichome elongation in tomato. *New Phytologist* **230**: 1063-1077
- Huang X-Q, Dudareva N** (2023) Plant specialized metabolism. *Current Biology* **33**: R473-R478
- Huang Y-X, Yin Y-G, Sanuki A, Fukuda N, Ezura H, Matsukura C** (2015) Phosphoenolpyruvate carboxykinase (PEPCK) deficiency affects the germination, growth and fruit sugar content in tomato (*Solanum lycopersicum* L.). *Plant Physiology and Biochemistry* **96**: 417-425
- Huchelmann A, Boutry M, Hachez C** (2017) Plant Glandular Trichomes: Natural Cell Factories of High Biotechnological Interest. *Plant Physiology* **175**: 6-22
- Hwang I, Sheen J, Müller B** (2012) Cytokinin Signaling Networks. *Annual Review of Plant Biology* **63**: 353-380
- Ishikawa C, Hatanaka T, Misoo S, Miyake C, Fukayama H** (2011) Functional Incorporation of Sorghum Small Subunit Increases the Catalytic Turnover Rate of Rubisco in Transgenic Rice *Plant Physiology* **156**: 1603-1611
- Ji W, Mandal S, Rezenom YH, McKnight TD** (2023) Specialized metabolism by trichome-enriched Rubisco and fatty acid synthase components. *Plant Physiology* **191**: 1199-1213
- Jin J, Panicker D, Wang Q, Kim MJ, Liu J, Yin J-L, Wong L, Jang I-C, Chua N-H, Sarojam R** (2014) Next generation sequencing unravels the biosynthetic ability of Spearmint (*Mentha spicata*) peltate glandular trichomes through comparative transcriptomics. *BMC Plant Biology* **14**: 292
- Johnson SR, Lange I, Srividya N, Lange BM** (2017) Bioenergetics of Monoterpenoid Essential Oil Biosynthesis in Nonphotosynthetic Glandular Trichomes. *Plant Physiology* **175**: 681-695

- Kandoi D, Tripathy BC** (2023) Overexpression of chloroplastic *Zea mays* NADP-malic enzyme (ZmNADP-ME) confers tolerance to salt stress in *Arabidopsis thaliana*. *Photosynthesis Research*
- Kang J-H, Shi F, Jones AD, Marks MD, Howe GA** (2010) Distortion of trichome morphology by the hairless mutation of tomato affects leaf surface chemistry. *Journal of Experimental Botany* **61**: 1053-1064
- Karabourniotis G, Liakopoulos G, Nikolopoulos D, Bresta P** (2020) Protective and defensive roles of non-glandular trichomes against multiple stresses: structure–function coordination. *Journal of Forestry Research* **31**: 1-12
- Kariyat RR, Smith JD, Stephenson AG, De Moraes CM, Mescher MC** (2017) Non-glandular trichomes of *Solanum carolinense* deter feeding by *Manduca sexta* caterpillars and cause damage to the gut peritrophic matrix. *Proceedings of the Royal Society B: Biological Sciences* **284**: 20162323
- Kazan K, Manners JM** (2013) MYC2: The Master in Action. *Molecular Plant* **6**: 686-703
- Kim HJ, Seo EY, Kim JH, Cheong HJ, Kang BC, Choi DI** (2012) Research Notes : Morphological Classification of Trichomes Associated with Possible Biotic Stress Resistance in the Genus *Capsicum*. *Plant Pathol J* **28**: 107-113
- Kortbeek RWJ, Galland MD, Muras A, Therezan R, Maia S, Haring MA, Schuurink RC, Bleeker PM** (2023) Genetic and physiological requirements for high-level sesquiterpene-production in tomato glandular trichomes. *Frontiers in Plant Science* **14**
- Kortbeek RWJ, Xu J, Ramirez A, Spyropoulou E, Diergaarde P, Otten-Bruggeman I, de Both M, Nagel R, Schmidt A, Schuurink RC, Bleeker PM** (2016) Chapter Twelve - Engineering of Tomato Glandular Trichomes for the Production of Specialized Metabolites. *In* SE O'Connor, ed, *Methods in Enzymology*, Vol 576. Academic Press, pp 305-331
- Kreuzwieser J, Meischner M, Grün M, Yáñez-Serrano AM, Fasbender L, Werner C** (2021) Drought affects carbon partitioning into volatile organic compound biosynthesis in Scots pine needles. *New Phytologist* **232**: 1930-1943
- Kruger NJ, von Schaewen A** (2003) The oxidative pentose phosphate pathway: structure and organisation. *Current Opinion in Plant Biology* **6**: 236-246
- Lange BM** (2015) The Evolution of Plant Secretory Structures and Emergence of Terpenoid Chemical Diversity. *Annual Review of Plant Biology* **66**: 139-159
- Laterre R, Pottier M, Remacle C, Boutry M** (2017) Photosynthetic Trichomes Contain a Specific Rubisco with a Modified pH-Dependent Activity. *Plant Physiology* **173**: 2110-2120
- Leegood RC, Walker RP** (2003) Regulation and roles of phosphoenolpyruvate carboxykinase in plants. *Archives of Biochemistry and Biophysics* **414**: 204-210
- Leong BJ, Lybrand DB, Lou Y-R, Fan P, Schillmiller AL, Last RL** (2019) Evolution of metabolic novelty: A trichome-expressed invertase creates specialized metabolic diversity in wild tomato. *Science Advances* **5**: eaaw3754
- Li C, Wang Z, Jones AD** (2014) Chemical imaging of trichome specialized metabolites using contact printing and laser desorption/ionization mass spectrometry. *Analytical and Bioanalytical Chemistry* **406**: 171-182
- Li J, Wang X, Jiang R, Dong B, Fang S, Li Q, Lv Z, Chen W** (2021) Phytohormone-Based Regulation of Trichome Development. *Frontiers in Plant Science* **12**
- Li L, Zhao Y, McCaig BC, Wingerd BA, Wang J, Whalon ME, Pichersky E, Howe GA** (2004) The Tomato Homolog of CORONATINE-INSENSITIVE1 Is Required for the Maternal Control of Seed Maturation, Jasmonate-Signaled Defense Responses, and Glandular Trichome Development[W]. *The Plant Cell* **16**: 126-143
- Li R, Wang X, Zhang S, Liu X, Zhou Z, Liu Z, Wang K, Tian Y, Wang H, Zhang Y, Cui X** (2021) Two zinc-finger proteins control the initiation and elongation of long stalk trichomes in tomato. *Journal of Genetics and Genomics* **48**: 1057-1069
- Li Z, Sharkey TD** (2013) Metabolic profiling of the methylerythritol phosphate pathway reveals the source of post-illumination isoprene burst from leaves. *Plant, Cell & Environment* **36**: 429-437

- Lin MT, Stone WD, Chaudhari V, Hanson MR** (2020) Small subunits can determine enzyme kinetics of tobacco Rubisco expressed in *Escherichia coli*. *Nature Plants* **6**: 1289-1299
- Linder CR** (2000) Adaptive Evolution of Seed Oils in Plants: Accounting for the Biogeographic Distribution of Saturated and Unsaturated Fatty Acids in Seed Oils. *The American Naturalist* **156**: 442-458
- Liu Y, Schiff M, Dinesh-Kumar SP** (2002) Virus-induced gene silencing in tomato. *The Plant Journal* **31**: 777-786
- Lonien J, Schwender Jr** (2009) Analysis of Metabolic Flux Phenotypes for Two Arabidopsis Mutants with Severe Impairment in Seed Storage Lipid Synthesis. *Plant Physiology* **151**: 1617-1634
- Luckwill LC** (1943) *The Genus Lycopersicon: An Historical, Biological, and Taxonomic Survey of the Wild and Cultivated Tomatoes*. The University Press
- Madeira F, Pearce M, Tivey ARN, Basutkar P, Lee J, Edbali O, Madhusoodanan N, Kolesnikov A, Lopez R** (2022) Search and sequence analysis tools services from EMBL-EBI in 2022. *Nucleic acids research* **50**: W276-W279
- Maeda HA** (2019) Harnessing evolutionary diversification of primary metabolism for plant synthetic biology. *Journal of Biological Chemistry* **294**: 16549-16566
- Maleci Bini L, Giuliani C** (2006) THE GLANDULAR TRICHOMES OF THE LABIATAE. A REVIEW. *In*, Ed 723. International Society for Horticultural Science (ISHS), Leuven, Belgium, pp 85-90
- Maluf WR, Campos GA, das Graças Cardoso M** (2001) Relationships between trichome types and spider mite (*Tetranychus evansi*) repellence in tomatoes with respect to foliar zingiberene contents. *Euphytica* **121**: 73-80
- Maluf WR, de Fátima Silva V, das Graças Cardoso M, Gomes LAA, Neto ÁCG, Maciel GM, Nízio DAC** (2010) Resistance to the South American tomato pinworm *Tuta absoluta* in high acylsugar and/or high zingiberene tomato genotypes. *Euphytica* **176**: 113-123
- Martin-Avila E, Lim Y-L, Birch R, Dirk LMA, Buck S, Rhodes T, Sharwood RE, Kapralov MV, Whitney SM** (2020) Modifying Plant Photosynthesis and Growth via Simultaneous Chloroplast Transformation of Rubisco Large and Small Subunits. *The Plant Cell* **32**: 2898-2916
- Matsumura H, Shiomi K, Yamamoto A, Taketani Y, Kobayashi N, Yoshizawa T, Tanaka S-i, Yoshikawa H, Endo M, Fukayama H** (2020) Hybrid Rubisco with Complete Replacement of Rice Rubisco Small Subunits by Sorghum Counterparts Confers C4 Plant-like High Catalytic Activity. *Molecular Plant* **13**: 1570-1581
- McDowell ET, Kapteyn J, Schmidt A, Li C, Kang J-H, Descour A, Shi F, Larson M, Schillmiller A, An L, Jones AD, Pichersky E, Soderlund CA, Gang DR** (2011) Comparative Functional Genomic Analysis of *Solanum* Glandular Trichome Types. *Plant Physiology* **155**: 524-539
- Meier I, Callan KL, Fleming AJ, Gruissem W** (1995) Organ-Specific Differential Regulation of a Promoter Subfamily for the Ribulose-1,5-Bisphosphate Carboxylase/Oxygenase Small Subunit Genes in Tomato. *Plant Physiology* **107**: 1105-1118
- Mintz-Oron S, Mandel T, Rogachev I, Feldberg L, Lotan O, Yativ M, Wang Z, Jetter R, Venger I, Adato A, Aharoni A** (2008) Gene Expression and Metabolism in Tomato Fruit Surface Tissues. *Plant Physiology* **147**: 823-851
- Mirnezhad M, Romero-González RR, Leiss KA, Choi YH, Verpoorte R, Klinkhamer PGL** (2010) Metabolomic analysis of host plant resistance to thrips in wild and cultivated tomatoes. *Phytochemical Analysis* **21**: 110-117
- Moghe G, Irfan M, Sarmah B** (2023) Dangerous sugars: Structural diversity and functional significance of acylsugar-like defense compounds in flowering plants. *Current Opinion in Plant Biology* **73**: 102348
- Mok DWS, Mok MC** (2001) CYTOKININ METABOLISM AND ACTION. *Annual Review of Plant Physiology and Plant Molecular Biology* **52**: 89-118
- Morita K, Hatanaka T, Misoo S, Fukayama H** (2014) Unusual Small Subunit That Is Not Expressed in Photosynthetic Cells Alters the Catalytic Properties of Rubisco in Rice. *Plant Physiology* **164**: 69-79

- Morita K, Hatanaka T, Misoo S, Fukayama H** (2016) Identification and expression analysis of non-photosynthetic Rubisco small subunit, OsRbcS1-like genes in plants. *Plant Gene* **8**: 26-31
- Nagalingam S, Seco R, Kim S, Guenther A** (2023) Heat stress strongly induces monoterpene emissions in some plants with specialized terpenoid storage structures. *Agricultural and Forest Meteorology* **333**: 109400
- Nagalingam S, Seco R, Musaev K, Basu C, Kim S, Guenther A** (2022) Impact of heat stress on foliar biogenic volatile organic compound emission and gene expression in tomato (*Solanum lycopersicum*) seedlings. *Elementa: Science of the Anthropocene* **10**: 00096
- Nakashima T, Wada H, Morita S, Erra-Balsells R, Hiraoka K, Nonami H** (2016) Single-Cell Metabolite Profiling of Stalk and Glandular Cells of Intact Trichomes with Internal Electrode Capillary Pressure Probe Electrospray Ionization Mass Spectrometry. *Analytical Chemistry* **88**: 3049-3057
- Nautiyal AK, Gani U, Sharma P, Kundan M, Fayaz M, Lattoo SK, Misra P** (2020) Comprehensive transcriptome analysis provides insights into metabolic and gene regulatory networks in trichomes of *Nicotiana tabacum*. *Plant Molecular Biology* **102**: 625-644
- Ning J, Moghe GD, Leong B, Kim J, Ofner I, Wang Z, Adams C, Jones AD, Zamir D, Last RL** (2015) A Feedback-Insensitive Isopropylmalate Synthase Affects Acylsugar Composition in Cultivated and Wild Tomato. *Plant Physiology* **169**: 1821-1835
- Olsson ME, Olofsson LM, Lindahl A-L, Lundgren A, Brodelius M, Brodelius PE** (2009) Localization of enzymes of artemisinin biosynthesis to the apical cells of glandular secretory trichomes of *Artemisia annua* L. *Phytochemistry* **70**: 1123-1128
- Osorio S, Vallarino JG, Szecowka M, Ufaz S, Tzin V, Angelovici R, Galili G, Fernie AR** (2013) Alteration of the Interconversion of Pyruvate and Malate in the Plastid or Cytosol of Ripening Tomato Fruit Invokes Diverse Consequences on Sugar But Similar Effects on Cellular Organic Acid, Metabolism, and Transitory Starch Accumulation. *Plant Physiology* **161**: 628-643
- Panda S, Jozwiak A, Sonawane PD, Szymanski J, Kazachkova Y, Vainer A, Vasuki Kilambi H, Almekias-Siegl E, Dikaya V, Bocobza S, Shohat H, Meir S, Wizler G, Giri AP, Schuurink R, Weiss D, Yasuor H, Kamble A, Aharoni A** (2022) Steroidal alkaloids defence metabolism and plant growth are modulated by the joint action of gibberellin and jasmonate signalling. *New Phytologist* **233**: 1220-1237
- Pazouki L, Kanagendran A, Li S, Kännaste A, Rajabi Memari H, Bichele R, Niinemets Ü** (2016) Mono- and sesquiterpene release from tomato (*Solanum lycopersicum*) leaves upon mild and severe heat stress and through recovery: From gene expression to emission responses. *Environmental and Experimental Botany* **132**: 1-15
- Pospíšil P** (2016) Production of Reactive Oxygen Species by Photosystem II as a Response to Light and Temperature Stress. *Frontiers in Plant Science* **7**
- Pottier M, Gilis D, Boutry M** (2018) The Hidden Face of Rubisco. *Trends in Plant Science* **23**: 382-392
- Pottier M, Laterre R, Van Wesseem A, Ramirez AM, Herman X, Boutry M, Hachez C** (2020) Identification of two new trichome-specific promoters of *Nicotiana tabacum*. *Planta* **251**: 58
- Prerostova S, Dobrev PI, Kramna B, Gaudinova A, Knirsch V, Spichal L, Zatloukal M, Vankova R** (2020) Heat Acclimation and Inhibition of Cytokinin Degradation Positively Affect Heat Stress Tolerance of *Arabidopsis*. *Frontiers in Plant Science* **11**
- Qian W, Zhu Y, Chen Q, Wang S, Chen L, Liu T, Tang H, Yao H** (2023) Comprehensive metabolomic and lipidomic alterations in response to heat stress during seed germination and seedling growth of *Arabidopsis*. *Frontiers in Plant Science* **14**
- Quint M, Delker C, Franklin KA, Wigge PA, Halliday KJ, van Zanten M** (2016) Molecular and genetic control of plant thermomorphogenesis. *Nature Plants* **2**: 15190
- Rangarajan A, Miller AR, Veilleux RE** (2000) Leptine Glycoalkaloids Reduce Feeding by Colorado Potato Beetle in Diploid *Solanum* sp. Hybrids. *Journal of the American Society for Horticultural Science* **125**: 689-693

- Resende JTVd, Maluf WR, Cardoso MdG, Nelson DL, Faria MV** (2002) Inheritance of acylsugar contents in tomatoes derived from an interspecific cross with the wild tomato *Lycopersicon pennellii* and their effect on spider mite repellence. *Genetics and Molecular Research* **1**: 106-116
- Rodriguez AE, Tingey WM, Mutschler MA** (1993) Acylsugars of *Lycopersicon pennellii* Deter Settling and Feeding of the Green Peach Aphid (Homoptera: Aphididae). *Journal of Economic Entomology* **86**: 34-39
- Roumani M, Besseau S, Gagneul D, Robin C, Larbat R** (2021) Phenolamides in plants: an update on their function, regulation, and origin of their biosynthetic enzymes. *Journal of Experimental Botany* **72**: 2334-2355
- Saadat NP, van Aalst M, Brand A, Ebenhöf O, Tissier A, Matuszyńska AB** (2023) Shifts in carbon partitioning by photosynthetic activity increase terpenoid synthesis in glandular trichomes. *The Plant Journal* **n/a**
- Säbel R, Brand A, Bergau N, Balcke GU, Syrowatka F, Püffeld-Raorane M, Hause B, Tissier A** (2023) Heat stress induces a developmental shift from type-V to type-IV trichome dependent on jasmonate signaling in tomato. *bioRxiv*: 2023.2007.2028.551053
- Sage RF** (2002) Variation in the *k_{cat}* of Rubisco in C3 and C4 plants and some implications for photosynthetic performance at high and low temperature. *Journal of Experimental Botany* **53**: 609-620
- Sakuma Y, Maruyama K, Qin F, Osakabe Y, Shinozaki K, Yamaguchi-Shinozaki K** (2006) Dual function of an Arabidopsis transcription factor DREB2A in water-stress-responsive and heat-stress-responsive gene expression. *Proceedings of the National Academy of Sciences* **103**: 18822-18827
- Sallaud C, Rontein D, Onillon S, Jabès Fo, Duffé P, Giacalone Cc, Thoraval S, Escoffier C, Herbette Gt, Leonhardt N, Causse M, Tissier A** (2009) A Novel Pathway for Sesquiterpene Biosynthesis from Z,Z-Farnesyl Pyrophosphate in the Wild Tomato *Solanum habrochaites* *The Plant Cell* **21**: 301-317
- Schaller A, Stintzi A** (2009) Enzymes in jasmonate biosynthesis – Structure, function, regulation. *Phytochemistry* **70**: 1532-1538
- Schillmiller AL, Charbonneau AL, Last RL** (2012) Identification of a BAHD acetyltransferase that produces protective acyl sugars in tomato trichomes. *Proceedings of the National Academy of Sciences* **109**: 16377-16382
- Schillmiller AL, Miner DP, Larson M, McDowell E, Gang DR, Wilkerson C, Last RL** (2010) Studies of a Biochemical Factory: Tomato Trichome Deep Expressed Sequence Tag Sequencing and Proteomics *Plant Physiology* **153**: 1212-1223
- Schillmiller AL, Schauvinhold I, Larson M, Xu R, Charbonneau AL, Schmidt A, Wilkerson C, Last RL, Pichersky E** (2009) Monoterpenes in the glandular trichomes of tomato are synthesized from a neryl diphosphate precursor rather than geranyl diphosphate. *Proceedings of the National Academy of Sciences* **106**: 10865-10870
- Schlüter U, Weber APM** (2020) Regulation and Evolution of C4 Photosynthesis. *Annual Review of Plant Biology* **71**: 183-215
- Schubert R, Dobritsch S, Gruber C, Hause G, Athmer B, Schreiber T, Marillonnet S, Okabe Y, Ezura H, Acosta IF, Tarkowska D, Hause B** (2019) Tomato MYB21 Acts in Ovules to Mediate Jasmonate-Regulated Fertility. *The Plant Cell* **31**: 1043-1062
- Schuurink R, Tissier A** (2020) Glandular trichomes: micro-organs with model status? *New Phytologist* **225**: 2251-2266
- Schwender J, Goffman F, Ohlrogge JB, Shachar-Hill Y** (2004) Rubisco without the Calvin cycle improves the carbon efficiency of developing green seeds. *Nature* **432**: 779-782
- Serna L, Martin C** (2006) Trichomes: different regulatory networks lead to convergent structures. *Trends in Plant Science* **11**: 274-280
- Shapiro JA, Steffens JC, Mutschler MA** (1994) Acylsugars of the wild tomato *Lycopersicon pennellii* in relation to geographic distribution of the species. *Biochemical Systematics and Ecology* **22**: 545-561

- Sharma P, Lakra N, Goyal A, Ahlawat YK, Zaid A, Siddique KHM** (2023) Drought and heat stress mediated activation of lipid signaling in plants: a critical review. *Frontiers in Plant Science* **14**
- Sicher R** (2013) Combined effects of CO₂ enrichment and elevated growth temperatures on metabolites in soybean leaflets: evidence for dynamic changes of TCA cycle intermediates. *Planta* **238**: 369-380
- Simkin AJ, Faralli M, Ramamoorthy S, Lawson T** (2020) Photosynthesis in non-foliar tissues: implications for yield. *The Plant Journal* **101**: 1001-1015
- Sletvold N, Ågren J** (2012) Variation in tolerance to drought among Scandinavian populations of *Arabidopsis lyrata*. *Evolutionary Ecology* **26**: 559-577
- Smith EN, Schwarzländer M, Ratcliffe RG, Kruger NJ** (2021) Shining a light on NAD- and NADP-based metabolism in plants. *Trends in Plant Science* **26**: 1072-1086
- Sonawane PD, Pollier J, Panda S, Szymanski J, Massalha H, Yona M, Unger T, Malitsky S, Arendt P, Pauwels L, Almekias-Siegl E, Rogachev I, Meir S, Cárdenas PD, Masri A, Petrikov M, Schaller H, Schaffer AA, Kamble A, Giri AP, Goossens A, Aharoni A** (2016) Plant cholesterol biosynthetic pathway overlaps with phytosterol metabolism. *Nature Plants* **3**: 16205
- Spíchal L** (2012) Cytokinins – recent news and views of evolutionally old molecules. *Functional Plant Biology* **39**: 267-284
- Spreitzer RJ** (2003) Role of the small subunit in ribulose-1,5-bisphosphate carboxylase/oxygenase. *Archives of Biochemistry and Biophysics* **414**: 141-149
- Streatfield SJ, Weber A, Kinsman EA, Häusler RE, Li J, Post-Beittenmiller D, Kaiser WM, Pyke KA, Flügge U-I, Chory J** (1999) The Phosphoenolpyruvate/Phosphate Translocator Is Required for Phenolic Metabolism, Palisade Cell Development, and Plastid-Dependent Nuclear Gene Expression. *The Plant Cell* **11**: 1609-1621
- Sugita M, Grissem W** (1987) Developmental, organ-specific, and light-dependent expression of the tomato ribulose-1,5-bisphosphate carboxylase small subunit gene family. *Proceedings of the National Academy of Sciences* **84**: 7104-7108
- Swinnen G, De Meyer M, Pollier J, Molina-Hidalgo FJ, Ceulemans E, Venegas-Molina J, De Milde L, Fernández-Calvo P, Ron M, Pauwels L, Goossens A** (2022) The basic helix–loop–helix transcription factors MYC1 and MYC2 have a dual role in the regulation of constitutive and stress-inducible specialized metabolism in tomato. *New Phytologist* **236**: 911-928
- Szymański J, Bocobza S, Panda S, Sonawane P, Cárdenas PD, Lashbrooke J, Kamble A, Shahaf N, Meir S, Bovy A, Beekwilder J, Tikunov Y, Romero de la Fuente I, Zamir D, Rogachev I, Aharoni A** (2020) Analysis of wild tomato introgression lines elucidates the genetic basis of transcriptome and metabolome variation underlying fruit traits and pathogen response. *Nature Genetics* **52**: 1111-1121
- Takemori A, Nakashima T, Ômura H, Tanaka Y, Nakata K, Nonami H, Takemori N** (2019) Quantitative assay of targeted proteome in tomato trichome glandular cells using a large-scale selected reaction monitoring strategy. *Plant Methods* **15**: 40
- Tanney CAS, Backer R, Geitmann A, Smith DL** (2021) Cannabis Glandular Trichomes: A Cellular Metabolite Factory. *Frontiers in Plant Science* **12**
- Tao L, Yu G, Chen H, Wang B, Jiang L, Han X, Lin G, Cheng X-G** (2022) SIDREB2 gene specifically recognizing to the universal DRE elements is a transcriptional activator improving drought tolerance in tomato. *Scientia Horticulturae* **295**: 110887
- Telfer A, Bollman KM, Poethig RS** (1997) Phase change and the regulation of trichome distribution in *Arabidopsis thaliana*. *Development* **124**: 645-654
- Thines B, Katsir L, Melotto M, Niu Y, Mandaokar A, Liu G, Nomura K, He SY, Howe GA, Browse J** (2007) JAZ repressor proteins are targets of the SCFCO11 complex during jasmonate signalling. *Nature* **448**: 661-665
- Tian T, Liu Y, Yan H, You Q, Yi X, Du Z, Xu W, Su Z** (2017) agriGO v2.0: a GO analysis toolkit for the agricultural community, 2017 update. *Nucleic Acids Research* **45**: W122-W129
- Tian X, Wang F, Zhao Y, Lan T, Yu K, Zhang L, Qin Z, Hu Z, Yao Y, Ni Z, Sun Q, Rossi V, Peng H, Xin M** (2020) Heat shock transcription factor A1b regulates heat tolerance in

- wheat and Arabidopsis through OPR3 and jasmonate signalling pathway. *Plant Biotechnology Journal* **18**: 1109-1111
- Tissier A** (2012) Glandular trichomes: what comes after expressed sequence tags? *The Plant Journal* **70**: 51-68
- Tissier A** (2018) Plant secretory structures: more than just reaction bags. *Current Opinion in Biotechnology* **49**: 73-79
- Tissier A, Morgan JA, Dudareva N** (2017) Plant Volatiles: Going 'In' but not 'Out' of Trichome Cavities. *Trends in Plant Science* **22**: 930-938
- Todorova D, Genkov T, Vaseva-Gemisheva I, Alexieva V, Karanov E, Smith A, Hall M** (2005) Effect of temperature stress on the endogenous cytokinin content in *Arabidopsis thaliana* (L.) Heynh plants. *Acta Physiologiae Plantarum* **27**: 13-18
- Traw MB, Dawson TE** (2002) Differential induction of trichomes by three herbivores of black mustard. *Oecologia* **131**: 526-532
- Unver T, Budak H** (2009) Virus-Induced Gene Silencing, a Post Transcriptional Gene Silencing Method. *International Journal of Plant Genomics* **2009**: 198680
- Uzelac B, Stojičić D, Budimir S** (2021) Glandular Trichomes on the Leaves of *Nicotiana tabacum*: Morphology, Developmental Ultrastructure, and Secondary Metabolites. *In* KG Ramawat, HM Ekiert, S Goyal, eds, *Plant Cell and Tissue Differentiation and Secondary Metabolites: Fundamentals and Applications*. Springer International Publishing, Cham, pp 25-61
- Van Eck J, Keen P, Tjahjadi M** (2019) *Agrobacterium tumefaciens*-Mediated Transformation of Tomato. *In* S Kumar, P Barone, M Smith, eds, *Transgenic Plants: Methods and Protocols*. Springer New York, New York, NY, pp 225-234
- Vendemiatti E, Hernández-De Lira IO, Snijders R, Torne-Srivastava T, Therezan R, Simioni Prants G, Lopez-Ortiz C, Reddy UK, Bleeker P, Schenck CA, Peres LEP, Benedito VA** (2024) Woolly mutation with the *Get2* locus overcomes the polygenic nature of trichome-based pest resistance in tomato. *Plant Physiology*: kiae128
- Vendemiatti E, Therezan R, Vicente MH, Pinto MD, Bergau N, Yang L, Bernardi WF, Alencar SMD, Zsögön A, Tissier A, Benedito VA, Peres LEP** (2022) The Genetic Complexity of Type-IV Trichome Development Reveals the Steps towards an Insect-Resistant Tomato. *In* *Plants*, Vol 11
- Vendemiatti E, Zsögön A, Silva GFFe, de Jesus FA, Cutri L, Figueiredo CRF, Tanaka FAO, Nogueira FTS, Peres LEP** (2017) Loss of type-IV glandular trichomes is a heterochronic trait in tomato and can be reverted by promoting juvenility. *Plant Science* **259**: 35-47
- Vickers CE, Possell M, Cojocariu CI, Velikova VB, Laothawornkitkul J, Ryan A, Mullineaux PM, Nicholas Hewitt C** (2009) Isoprene synthesis protects transgenic tobacco plants from oxidative stress. *Plant, Cell & Environment* **32**: 520-531
- Vogt T** (2018) Unusual spermine-conjugated hydroxycinnamic acids on pollen: function and evolutionary advantage. *Journal of Experimental Botany* **69**: 5311-5315
- Voll L, Häusler RE, Hecker R, Weber A, Weissenböck G, Fiene G, Waffenschmidt S, Flügge U-I** (2003) The phenotype of the *Arabidopsis* *cue1* mutant is not simply caused by a general restriction of the shikimate pathway. *The Plant Journal* **36**: 301-317
- Vosman B, Kashaninia A, van't Westende W, Meijer-Dekens F, van Eekelen H, Visser RGF, de Vos RCH, Voorrips RE** (2019) QTL mapping of insect resistance components of *Solanum galapagense*. *Theoretical and Applied Genetics* **132**: 531-541
- Waadt R, Sellar CA, Hsu P-K, Takahashi Y, Munemasa S, Schroeder JI** (2022) Plant hormone regulation of abiotic stress responses. *Nature Reviews Molecular Cell Biology* **23**: 680-694
- Wagner GJ, Wang E, Shepherd RW** (2004) New Approaches for Studying and Exploiting an Old Protuberance, the Plant Trichome. *Annals of Botany* **93**: 3-11
- Walker RP, Chen Z-H, Técsi LI, Famiani F, Lea PJ, Leegood RC** (1999) Phosphoenolpyruvate carboxykinase plays a role in interactions of carbon and nitrogen metabolism during grape seed development. *Planta* **210**: 9-18
- Walters DS, Steffens JC** (1990) Branched Chain Amino Acid Metabolism in the Biosynthesis of *Lycopersicon pennellii* Glucose Esters 1. *Plant Physiology* **93**: 1544-1551

- Wang L, Ma K-B, Lu Z-G, Ren S-X, Jiang H-R, Cui J-W, Chen G, Teng N-J, Lam H-M, Jin B** (2020) Differential physiological, transcriptomic and metabolomic responses of Arabidopsis leaves under prolonged warming and heat shock. *BMC Plant Biology* **20**: 86
- Wang L, Wu B, Chen G, Chen H, Peng Y, Sohail H, Geng S, Luo G, Xu D, Ouyang B, Bie Z** (2023) The essential role of jasmonate signaling in *Solanum habrochaites* rootstock-mediated cold tolerance in tomato grafts. *Horticulture Research* **10**: uhac227
- Wang Y, Liu G-J, Yan X-F, Wei Z-G, Xu Z-R** (2011) MeJA-inducible expression of the heterologous JAZ2 promoter from Arabidopsis in *Populus trichocarpa* protoplasts. *Journal of Plant Diseases and Protection* **118**: 69-74
- Wang Y, Wen J, Liu L, Chen J, Wang C, Li Z, Wang G, Pichersky E, Xu H** (2022) Engineering of tomato type VI glandular trichomes for trans-chrysanthenic acid biosynthesis, the acid moiety of natural pyrethrin insecticides. *Metabolic Engineering* **72**: 188-199
- War AR, Paulraj MG, Ahmad T, Buhroo AA, Hussain B, Ignacimuthu S, Sharma HC** (2012) Mechanisms of plant defense against insect herbivores. *Plant Signaling & Behavior* **7**: 1306-1320
- Wasternack C, Hause B** (2013) Jasmonates: biosynthesis, perception, signal transduction and action in plant stress response, growth and development. An update to the 2007 review in *Annals of Botany*. *Annals of Botany* **111**: 1021-1058
- Weber E, Engler C, Gruetzner R, Werner S, Marillonnet S** (2011) A Modular Cloning System for Standardized Assembly of Multigene Constructs. *PLOS ONE* **6**: e16765
- Werker E** (2000) Trichome diversity and development. *In Advances in Botanical Research*, Vol 31. Academic Press, pp 1-35
- Werner C, Fasbender L, Romek KM, Yáñez-Serrano AM, Kreuzwieser J** (2020) Heat Waves Change Plant Carbon Allocation Among Primary and Secondary Metabolism Altering CO₂ Assimilation, Respiration, and VOC Emissions. *Frontiers in Plant Science* **11**
- Wright LP, Rohwer JM, Ghirardo A, Hammerbacher A, Ortiz-Alcaide M, Raguschke B, Schnitzler J-P, Gershenzon J, Phillips MA** (2014) Deoxyxylulose 5-Phosphate Synthase Controls Flux through the Methylerythritol 4-Phosphate Pathway in Arabidopsis. *Plant Physiology* **165**: 1488-1504
- Wu G, Park MY, Conway SR, Wang J-W, Weigel D, Poethig RS** (2009) The Sequential Action of miR156 and miR172 Regulates Developmental Timing in Arabidopsis. *Cell* **138**: 750-759
- Wu M, Chang J, Han X, Shen J, Yang L, Hu S, Huang B-B, Xu H, Xu M, Wu S, Li P, Hua B, Yang M, Yang Z, Wu S** (2023) A HD-ZIP transcription factor specifies fates of multicellular trichomes via dosage-dependent mechanisms in tomato. *Developmental Cell* **58**: 278-288.e275
- Wybouw B, De Rybel B** (2019) Cytokinin: A Developing Story. *Trends in Plant Science* **24**: 177-185
- Xiao Y, Savchenko T, Baidoo Edward EK, Chehab Wassim E, Hayden Daniel M, Tolstikov V, Corwin Jason A, Kliebenstein Daniel J, Keasling Jay D, Dehesh K** (2012) Retrograde Signaling by the Plastidial Metabolite MEcPP Regulates Expression of Nuclear Stress-Response Genes. *Cell* **149**: 1525-1535
- Xu J, van Herwijnen ZO, Dräger DB, Sui C, Haring MA, Schuurink RC** (2018) SIMYC1 Regulates Type VI Glandular Trichome Formation and Terpene Biosynthesis in Tomato Glandular Cells. *The Plant Cell* **30**: 2988-3005
- Xu Y, Qian Z, Zhou B, Wu G** (2019) Age-dependent heteroblastic development of leaf hairs in Arabidopsis. *New Phytologist* **224**: 741-748
- Yamaguchi-Shinozaki K, Shinozaki K** (1994) A novel cis-acting element in an Arabidopsis gene is involved in responsiveness to drought, low-temperature, or high-salt stress. *The Plant Cell* **6**: 251-264
- Yan T, Chen M, Shen Q, Li L, Fu X, Pan Q, Tang Y, Shi P, Lv Z, Jiang W, Ma Y-n, Hao X, Sun X, Tang K** (2017) HOMEODOMAIN PROTEIN 1 is required for jasmonate-

- mediated glandular trichome initiation in *Artemisia annua*. *New Phytologist* **213**: 1145-1155
- Yang C, Li H, Zhang J, Luo Z, Gong P, Zhang C, Li J, Wang T, Zhang Y, Lu Ye, Ye Z** (2011) A regulatory gene induces trichome formation and embryo lethality in tomato. *Proceedings of the National Academy of Sciences* **108**: 11836-11841
- Yang C, Li H, Zhang J, Wang T, Ye Z** (2011) Fine-mapping of the woolly gene controlling multicellular trichome formation and embryonic development in tomato. *Theoretical and Applied Genetics* **123**: 625-633
- Yang C, Marillonnet S, Tissier A** (2021) The scarecrow-like transcription factor SISCL3 regulates volatile terpene biosynthesis and glandular trichome size in tomato (*Solanum lycopersicum*). *The Plant Journal* **107**: 1102-1118
- Yang C, Ye Z** (2013) Trichomes as models for studying plant cell differentiation. *Cellular and Molecular Life Sciences* **70**: 1937-1948
- Ying S, Su M, Wu Y, Zhou L, Fu R, Li Y, Guo H, Luo J, Wang S, Zhang Y** (2020) Trichome regulator SIMIXTA-like directly manipulates primary metabolism in tomato fruit. *Plant Biotechnology Journal* **18**: 354-363
- Yoshida Y, Sano R, Wada T, Takabayashi J, Okada K** (2009) Jasmonic acid control of GLABRA3 links inducible defense and trichome patterning in *Arabidopsis*. *Development* **136**: 1039-1048
- You MK, Lee YJ, Kim JK, Baek SA, Jeon YA, Lim SH, Ha SH** (2020) The organ-specific differential roles of rice DXS and DXR, the first two enzymes of the MEP pathway, in carotenoid metabolism in *Oryza sativa* leaves and seeds. *BMC Plant Biology* **20**: 167
- Yu X, Chen G, Tang B, Zhang J, Zhou S, Hu Z** (2018) The Jasmonate ZIM-domain protein gene SIJAZ2 regulates plant morphology and accelerates flower initiation in *Solanum lycopersicum* plants. *Plant Science* **267**: 65-73
- Yuan Y, Xu X, Luo Y, Gong Z, Hu X, Wu M, Liu Y, Yan F, Zhang X, Zhang W, Tang Y, Feng B, Li Z, Jiang C-Z, Deng W** (2021) R2R3 MYB-dependent auxin signalling regulates trichome formation, and increased trichome density confers spider mite tolerance on tomato. *Plant Biotechnology Journal* **19**: 138-152
- Zhan T, Li F, Lan J, Li L, Yang Z, Xie C, Wang H, Zheng X** (2023) Functional characterization of four mono-terpene synthases (TPSs) provided insight into the biosynthesis of volatile monoterpenes in the medicinal herb *Blumea balsamifera*. *Physiology and Molecular Biology of Plants* **29**: 459-469
- Zhang F, Liu W, Xia J, Zeng J, Xiang L, Zhu S, Zheng Q, Xie H, Yang C, Chen M, Liao Z** (2018) Molecular Characterization of the 1-Deoxy-D-Xylulose 5-Phosphate Synthase Gene Family in *Artemisia annua*. *Frontiers in Plant Science* **9**
- Zhang Y, Wang D, Li H, Bai H, Sun M, Shi L** (2023) Formation mechanism of glandular trichomes involved in the synthesis and storage of terpenoids in lavender. *BMC Plant Biology* **23**: 307
- Zheng F, Cui L, Li C, Xie Q, Ai G, Wang J, Yu H, Wang T, Zhang J, Ye Z, Yang C** (2022) Hair interacts with SIZFP8-like to regulate the initiation and elongation of trichomes by modulating SIZFP6 expression in tomato. *Journal of Experimental Botany* **73**: 228-244
- Zhou F, Pichersky E** (2020) The complete functional characterisation of the terpene synthase family in tomato. *New Phytologist* **226**: 1341-1360

6. Appendix

6.1 Supplementary figures

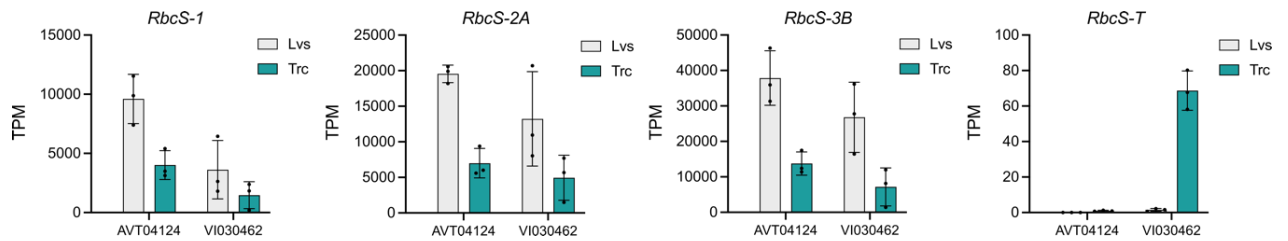


Figure S 1. Transcripts per million (TPM) reads of *RbcS* subunits in leaves and trichomes of cultivated tomato cv. AVT04124 and *S. habrochaites* sp. *glabratum*.

Abbreviations: Lvs, leaves; Trc, trichomes.

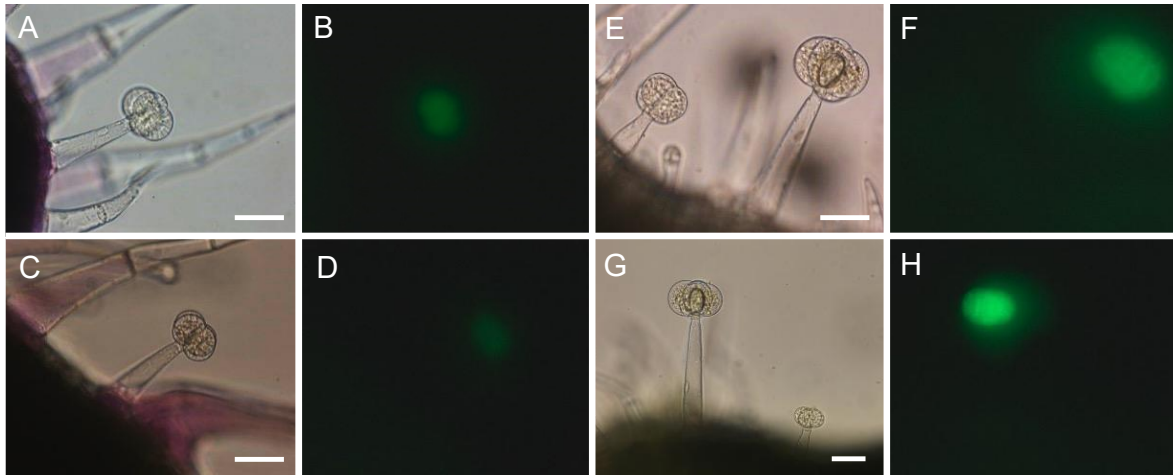


Figure S 2. pSITPS20:YFP-GUS expression in the glandular cells of type-VI trichomes.

Photos over the leaf surface (bright field **A,C**; green fluorescence **B,D**) and petiole/stems (bright field **E,G**; green fluorescence **F,H**). Images were recorded with a fluorescence microscope Axio Imager.Z2, (490-510/520-550 excitation/emission wavelength). Scale bar = 50 μm .

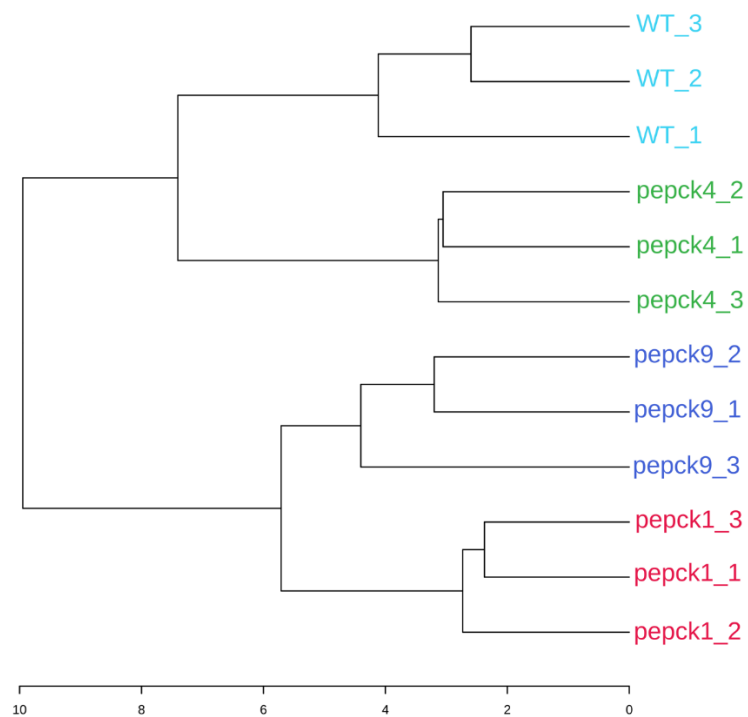


Figure S 3. Hierarchical clustering dendrogram of CCM metabolic profiles of GTs of *pepck* mutant lines.

Dendrogram performed in MetaboAnalyst software. <https://www.metaboanalyst.ca/> and displaying Euclidean distance measures with the ward clustering algorithm.

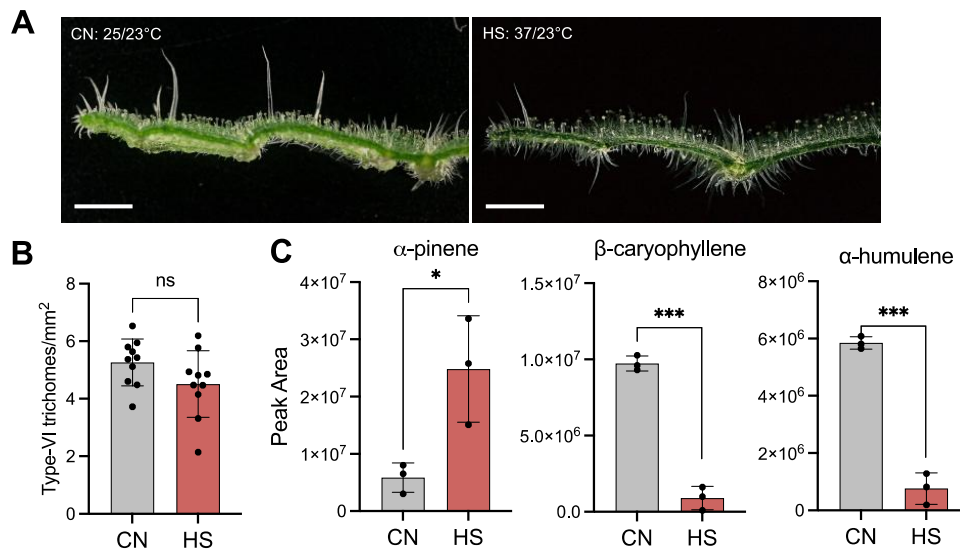


Figure S 4. Effect of heat stress on type-VI trichomes and terpenoids in Micro-Tom.

(A) 1,5 mm wide leaf strips of Micro-Tom plants growing in control (CN) and heat stress (HS) conditions for three weeks. Scale bar = 1 mm. **(B)** Type-VI trichome number ($n = 10$ biological replicates). **(C)** Estimation of mono and sesquiterpenes using gas chromatography-mass spectrometry (GC-MS) ($n = 3$ biological replicates). Error bars indicate standard deviation. * $P < 0.05$, ** $P < 0.01$, *** $P < 0.001$; using Student's t -test.

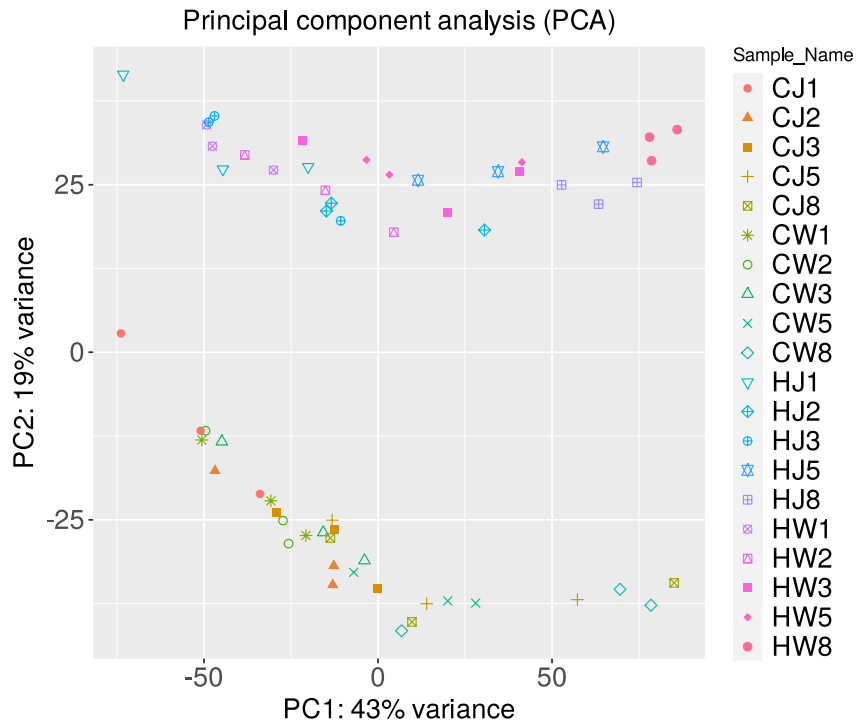


Figure S 5. Principal component analysis (PCA) of RNASeq data distribution.

A total of 60 processed samples, comprising eight time points after HS application and the corresponding control samples, the two genotypes, and three biological replicates. The data was normalized, analyzed and plotted using iDEP.96 (Ge et al., 2018). Sample abbreviation: C, control; H, heat stress; J, *jai1*; W, wild type.

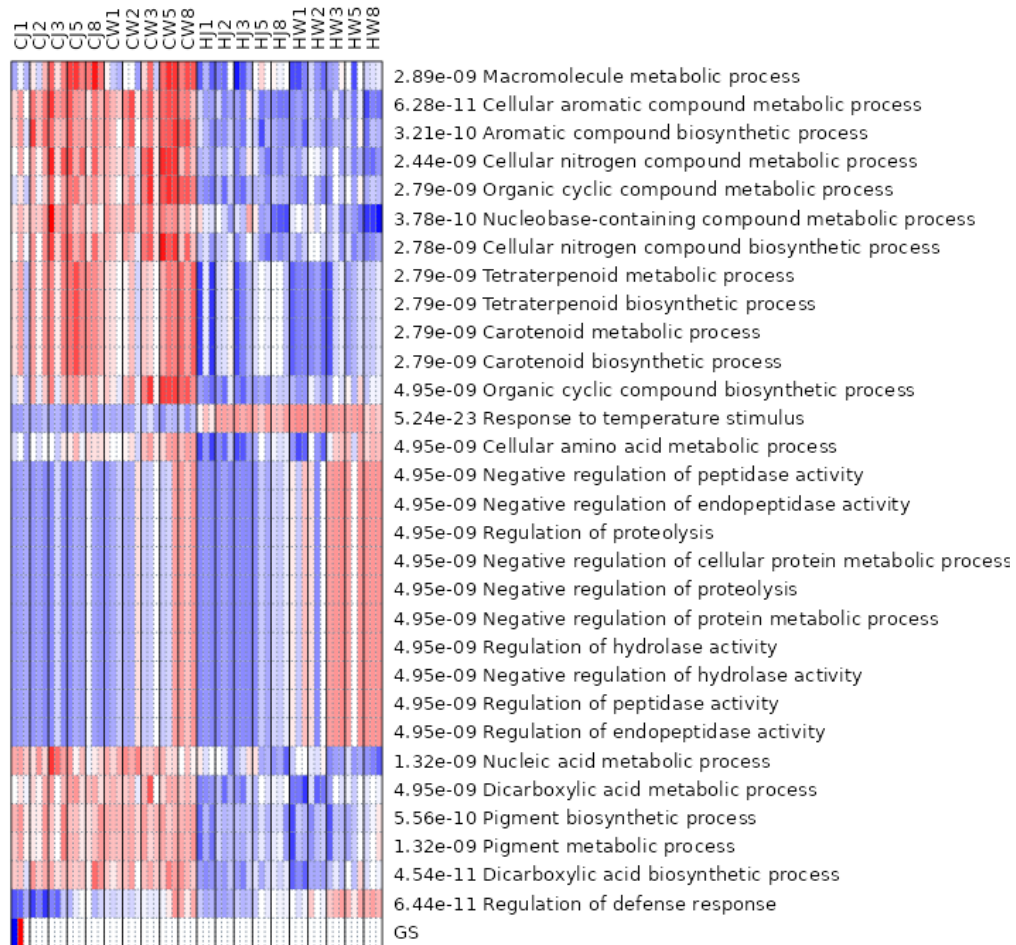


Figure S 6. Gene ontology (GO) analysis.

GO analysis depicting the top 30 GO terms of biological processes significantly enriched within the DEGs across all samples. Red scale, upregulation; blue scale, down-regulation. GO analysis performed in iDEP.96 (Ge et al., 2018) using the parametric gene set enrichment analysis (PGSEA) ($FDR < 0.05$).

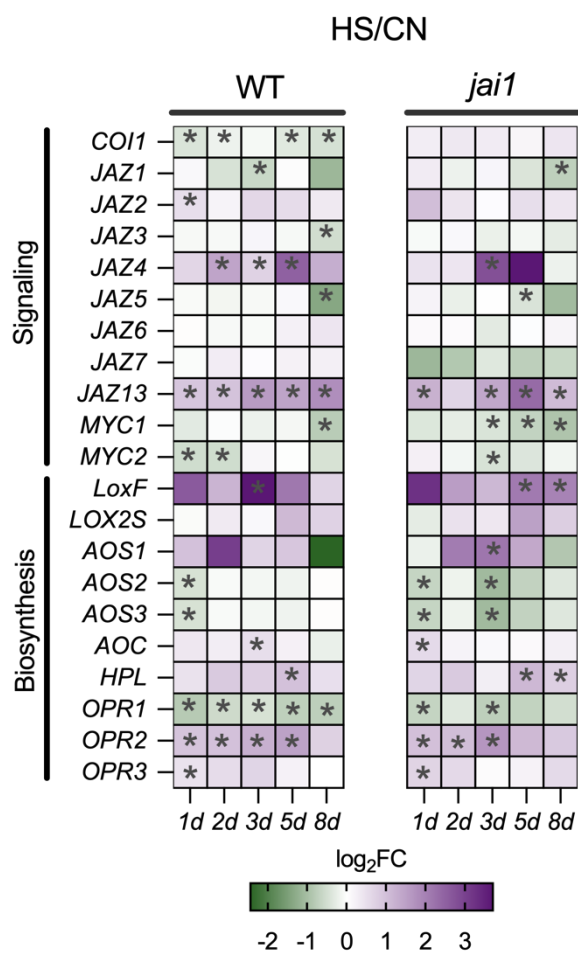


Figure S 7. Expression data (log₂FC) of heat stress (HS) vs control (CN) of genes involved in jasmonate signaling and biosynthesis.

Log₂FC of HS/CN samples at each time point in WT and *jai1* mutant. (*) indicates significant differences after pairwise comparisons using Student's *t*-test ($P < 0.05$).

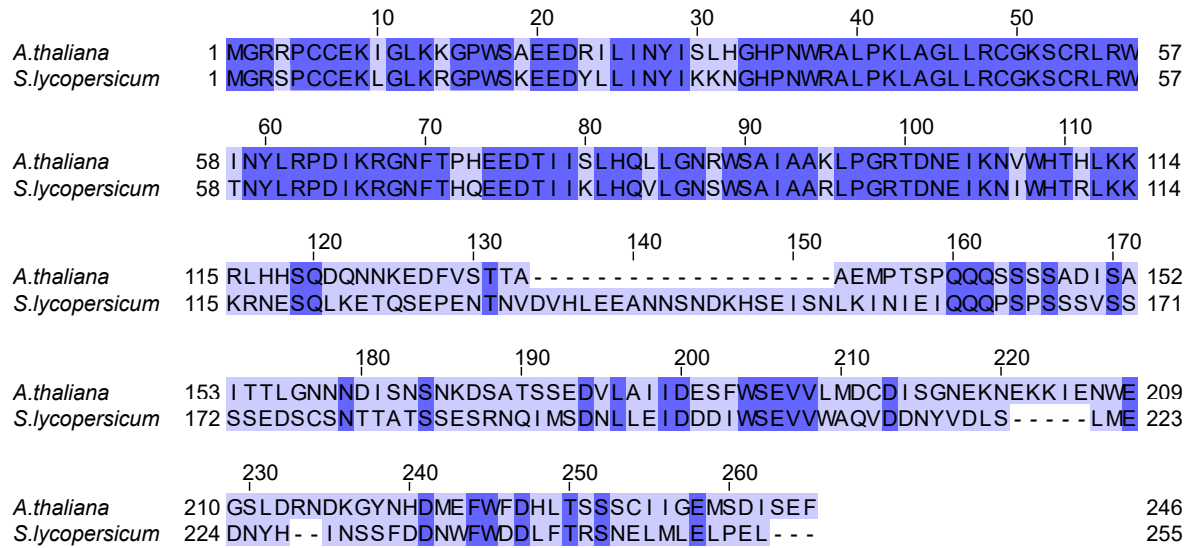


Figure S 8. Amino acid sequence alignment between *A. thaliana* MYB13 (At1g06180) and *S. lycopersicum* MYB13 (Soly06g083900).

Multiple sequence alignment performed with the Clustal Omega v1.2.4.
<https://www.ebi.ac.uk/Tools/msa/clustalo/>

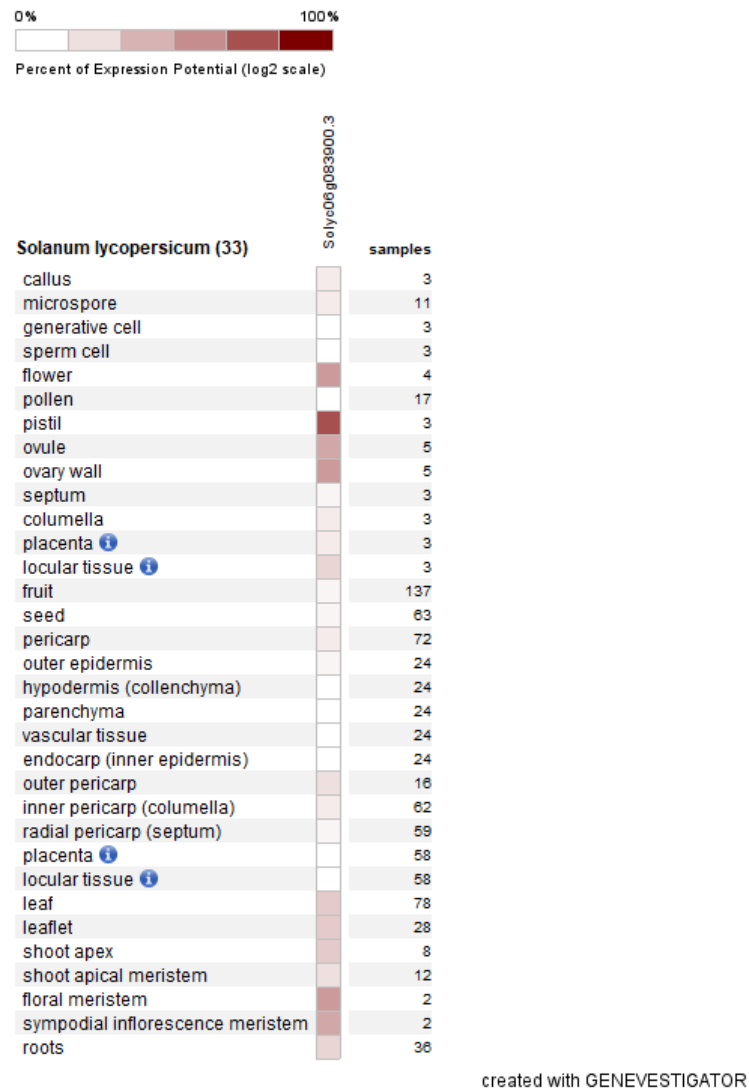
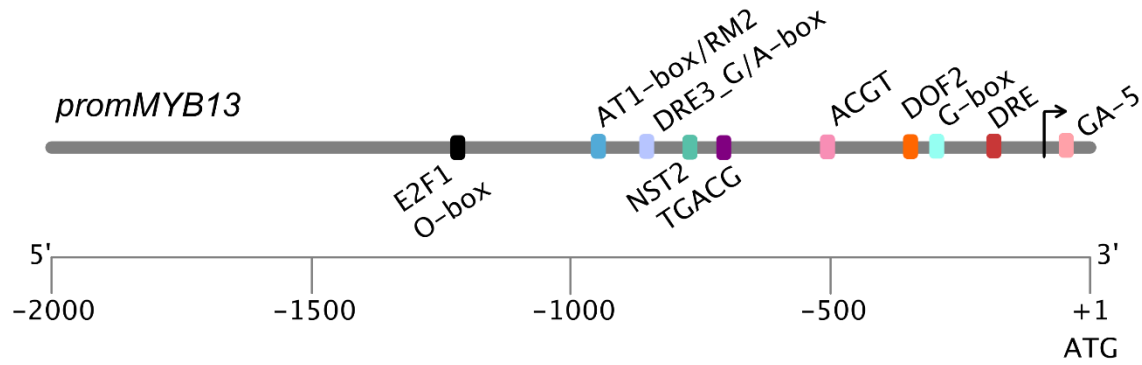


Figure S 9. Gene expression of *S. lycopersicum* MYB13 in different tissues.

Expression data from 33 anatomical parts obtained from mRNASeq data sets available in GENEVESTIGATOR database (Hruz et al., 2008).



Sequence	Strand	BE	BF	Name	Species	start	end	Associated with
AGAGAGAGA	+	GA-5	BPC1	BASIC PENTACYSSTEINE 1	<i>A. thaliana</i>	-9	-17	Ovule identity
TACCGACAT	+	DRE	DREB1A	DEHYDRATION RESPONSE	<i>A. thaliana</i>	-107	-115	Drought, temperature, salt
			DREB2A	ELEMENT BINDING PROTEIN 1A, 2A,				
			DREB2C	2C				
TACCGACAT	+	DRE	CBF1	DREB1B	<i>S. habrochaites</i>	-107	-115	Drought, temperature, salt
TACCGACAT	+	DRE	TINY	ETHYLENE RESPONSE FACTOR 40	<i>A. thaliana</i>	-107	-115	Drought, temperature, salt
TATGTGGCA	+	G-box	UNF	unknown nuclear factor	<i>O. sativa</i>	-345	-353	Light response
ATGaAAAGGAG	+	DOF2	DOF2	Amidase family protein	<i>A. thaliana</i>	-381	-391	
CACACGTC	+	ACGT	UNF	unknown nuclear factor	<i>P. vulgaris</i>	-580	-587	
TGACG	+	TGACG-motif	UNF	unknown nuclear factor	<i>H. vulgare</i>	-771	-776	MeJA
gTcACGTCCG	+	ACGT3/DRE3	UNF	unknown nuclear factor	<i>A. thaliana</i>	-855	-864	ABA, temperature
TGTCACGTcGGa	+	G/A-box	HY5	ELONGATED HYPOCOTYL 5	<i>A. thaliana</i>	-854	-865	Light response
TAATTATTCTTA	+	AT1-box	UNF	unknown nuclear factor	<i>P. sativum</i>	-976	-988	
TAATTATTTCTAAT	+	Regulatory motif2	USENF	unknown seed embryo nuclear factor	<i>G. max</i>	-974	-988	
TGCGTTCCG	-	NST2	NST2	NAC SECONDARY WALL THICKENING PROMOTING FACTOR2	<i>A. thaliana</i>	-848	-857	Anther development
TTCCGGCCA	-	E2F1	E2F1	E2F TRANSCRIPTION FACTOR 1	<i>Z. mays</i>	-1331	-1339	Cell cycle
gTTCCGgCCAAT	-	O-box (AB11)	ORA47	DREB subfamily A-5 of ERF/AP2 transcription factor family.	<i>A. thaliana</i>	-1330	-1341	

Figure S 10. Transcription factor binding sites found within the 2kb upstream sequence of *MYB13*.

Binding elements (BE) and associated binding factors (BF) predicted by Nsite v6.2014, Softberry Inc (softberry.com) and PlantCARE (bioinformatics.psb.ugent.be). Mismatches with the conserved sequence motif are depicted in lowercase letters.

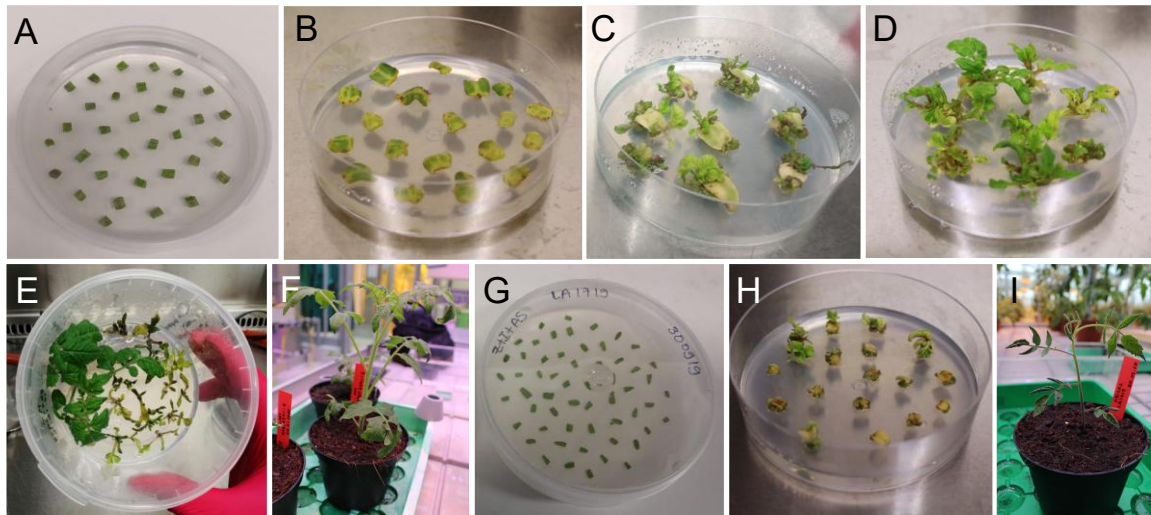


Figure S 11. *Agrobacterium*-mediated genetic transformation of tomato.

(A) Cotyledon pieces of cultivated tomato used for *Agrobacterium* inoculation. (B) Cotyledons on MS1 selection medium, 14 days after transformation. (C) Explants with emerging shoots at the sliced side of the cotyledons. (D) Shoots on MS2 medium. (E) Regenerated plants grown in MSR medium for 30 to 45 days. (F) Plants after two weeks transferred into soil. (G) Cotyledon pieces of wild tomato *S. habrochaites*. (H) Shoots of *S. habrochaites* emerging from cultured cotyledons on MS2 medium. (I) Wild tomato plants after two weeks transferred into soil.

6.2 Supplementary tables

Table S 1. Acylsugars of from the three *Solanum* species detected by liquid chromatography-mass spectrometry (LC-MS/MS).

Letters S for sucrose and G for glucose indicate the type of sugar core. Numbers before colon indicates the number of acyl chains, and after colon the total carbon number. The numbers in parenthesis depict the carbon composition of each acyl chain. Reference of AS of *S. pennellii* was obtained from Ji et al. (2023). Fragments in bold are the most abundant according to Ji et al. (2023).

Annotation	[M + HCOO] ⁻ -RT (min)	Main Fragments (m/z)	Species	Program	
Phlorizin	435.129	6.6	167.03, 273.07	IS	24min
S3:15(5,5,5)	639.2856	10.66	101.06, 341.10, 407.15, 425.16, 509.22, 593.28	lycopersicum	24min
S3:22(5,5,12)	737.3921	16.38	101.06, 199.16, 323.09, 425.16, 509.22, 607.33, 691.38	lycopersicum	24min
S4:16(2,4,5,5)	667.2814	11.04	101.06, 411.14, 495.20	lycopersicum	24min
S4:17(2,5,5,5)	681.2959	11.70	101.06, 425.16, 509.22	lycopersicum	24min
S4:24(2,5,5,12)	779.4051	17.42	199.16, 323.09, 425.16, 607.33	lycopersicum	24min
S3:15(5,5,5)	639.287	8.42	101.06, 341.10, 425.16, 509.22	habrochaites	18min
S4:20(5,5,5,5)	723.344	10.50	101.06, 341.10, 425.16, 509.22, 593.28	habrochaites	18min
S3:22(5,5,12)	737.397	12.36	199.17, 341.10, 425.16, 509.22, 607.33	habrochaites	18min
G3:12(4,4,4)	435.1874	6.4	87.04 , 125.02, 143.0, 213.07 , 301.13, 347.13, 389.18	pennellii	24min
G3:12(4,4,4)	435.1874	7.4	87.04 , 125.02, 143.0, 213.07 , 301.13, 347.13, 389.18	pennellii	24min
G3:14(4,5,5)	463.2189	12.2	87.04, 101.06 , 227.09 , 315.14, 329.16, 375.17, 417.21	pennellii	24min
G3:14(4,5,5)	463.2189	12.9	87.04, 101.06 , 125.02, 143.03, 227.10 , 315.14, 329.16, 375.16, 417.21	pennellii	24min
S3:18(4,5,9)	681.3328	15.4	87.04, 101.06, 157.12, 393.14, 407.15, 411.15, 425.17, 495.21 , 551.27, 635.32	pennellii	24min
S3:18(4,4,10)	681.3328	15.9	87.04, 171.14, 393.14, 411.15, 481.19 , 565.29, 635.33	pennellii	24min
S2:18(4,4,10)	681.3328	16.4	87.04, 171.14, 393.14, 411.15, 481.19 , 565.29, 635.33	pennellii	24min
S3:19(4,5,10)	695.3485	17.3	87.04, 101.06, 171.14, 393.14, 407.16, 411.15, 495.21 , 565.29, 649.34	pennellii	24min
S3:19(4,5,10)	695.3485	17.7	87.04, 101.06, 171.14, 393.14, 407.16, 411.15, 495.21 , 565.29, 649.34	pennellii	24min
S3:20(5,5,10)	709.3641	18.5	101.06, 171.14, 407.15, 425.17, 509.22 , 579.30, 663.36	pennellii	24min
S3:20(5,5,10)	709.3641	18.7	101.06, 171.14, 407.15, 425.17, 509.22 , 579.30, 663.36	pennellii	24min
S3:20(5,5,10)	709.3641	19.0	101.06, 171.14, 407.15, 425.17, 509.22 , 579.30, 663.36	pennellii	24min
S3:20(5,5,10)	709.3641	19.2	87.04, 101.06, 171.14, 185.15, 407.15, 425.16, 495.21 , 509.22, 579.30, 663.35	pennellii	24min
S3:20(4,4,11)	709.3641	19.7	87.04, 199.17, 393.1402, 481.19 , 495.2091, 593.32, 663.36	pennellii	24min
S3:20(4,4,11)	709.3641	20.1	87.04, 199.17, 393.1402, 481.19 , 495.2091, 593.32, 663.36	pennellii	24min
G3:18(4,5,9)/(4,4,10)	519.2800	20.4	87.04, 101.06, 125.02, 157.12, 171.14, 213.08 , 227.09, 301.13, 315.13, 347.13, 361.15, 473.27	pennellii	24min
G3:18(4,4,10)	519.2800	20.8	87.04, 125.02, 143.03, 171.14, 213.08 , 259.19, 301.13, 347.13, 473.27	pennellii	24min
G3:18(4,4,10)	519.2800	21.2	87.04, 125.02, 143.03, 171.14, 213.08 , 259.19, 301.13, 347.13, 473.27	pennellii	24min
S3:21(5,6,10)	723.3798	20.0	101.06, 115.07, 171.14, 407.15, 425.16, 439.18, 523.24 , 579.30, 593.32, 677.37	pennellii	24min
S3:21(5,5,11)	723.3798	20.4	101.06, 185.15, 407.15, 425.17, 509.22 , 593.32, 677.37	pennellii	24min
S3:21(5,6,10)	723.3798	20.4	101.06, 115.07, 171.14, 407.15, 425.17, 523.24 , 579.30, 593.32, 677.37	pennellii	24min
S3:21(5,5,11)	723.3798	20.5	101.06, 115.07, 171.14, 185.15, 407.15, 425.17, 509.22 , 523.24, 579.30, 593.32, 677.37	pennellii	24min
S3:21(4,5,12)	723.3798	20.9	87.04, 101.06, 199.17, 393.14, 407.15, 411.15, 425.17, 495.21 , 593.32, 677.37	pennellii	24min
S3:21(4,5,12)	723.3798	21.4	87.04, 101.06, 199.17, 393.14, 407.15, 411.15, 425.17, 495.21 , 593.32, 677.37	pennellii	24min
G3:19(4,5,10)	533.2956	21.4	87.04 , 101.06, 125.02, 147.06, 171.14, 213.08, 227.09, 315.14, 361.15, 487.29	pennellii	24min
G3:19(4,5,10)	533.2956	21.7	87.04, 101.06, 125.02, 133.05, 171.14, 213.08, 227.09 , 315.14, 361.15, 487.29	pennellii	24min
G3:19(4,5,10)	533.2956	22.1	87.04, 101.06, 125.02, 133.05, 143.03, 171.14, 213.08, 227.09 , 315.14, 361.15, 487.29	pennellii	24min
G3:19(4,5,10)	533.2956	22.5	87.04, 101.06, 125.02, 133.05, 143.03, 171.14, 213.08, 227.09 , 315.14, 361.15, 487.29	pennellii	24min
G3:20(5,5,10)/(4,6,10)	547.3113	22.9	87.04, 101.06, 125.02, 143.03, 147.06, 171.14, 213.08, 227.09 , 329.16, 375.17, 501.31	pennellii	24min
G3:20(5,5,10)/(4,6,10)	547.3113	23.3	101.06, 125.02, 143.03, 171.14, 227.09 , 329.16, 375.17, 501.31	pennellii	24min
G3:20(5,5,10)/(4,5,11)	547.3113	23.6	101.06, 125.02, 143.03, 171.14, 227.09 , 329.16, 375.17, 501.31	pennellii	24min
G3:20(4,5,11)/(4,4,12)	547.3113	24.1	87.04, 125.02, 133.05, 143.03, 185.15, 199.17, 213.08 , 301.13, 347.13, 501.31	pennellii	24min
G3:20(4,4,12)	547.3113	24.4	87.04, 125.02, 133.05, 143.03, 199.17, 213.08 , 301.13, 347.13, 501.31	pennellii	24min
G3:21(5,5,11) (5,6,10)	561.3269	24.3	101.06, 115.07, 171.14, 185.15, 227.09 , 241.11, 343.18, 389.18, 515.32	pennellii	24min
G3:21(5,6,10)/(4,5,12)	561.3269	24.7	87.04, 101.06, 171.14, 185.15, 227.09 , 329.16, 375.16, 515.32	pennellii	24min
G3:21(4,5,12)	561.3269	25.1	87.04, 101.06, 125.02, 143.03, 199.17, 227.09 , 245.17, 315.14, 361.15, 515.32	pennellii	24min
G3:21(4,5,12)	561.3269	25.5	87.04, 101.06, 125.02, 133.06, 199.17 , 227.09 , 245.17, 315.14, 361.15, 515.32	pennellii	24min

Table S 2. Top 30 polar metabolites sorted by FDR values after one-way ANOVA analysis, from WT and *pepck* mutant lines.

Statistical analysis was performed in MetaboAnalyst software. <https://www.metaboanalyst.ca/>.

	Abbreviation	Metabolite	p.value	FDR
1	chloride	chloride	4.32E-05	0.00371
2	IP5_sum	D-myo-inositol pentakisphosphates	7.07E-05	0.00371
3	Glucose/Fructose	monosaccharides	0.000483	0.01289
4	ALT	allantoin	0.000491	0.01289
5	RIB1,5 BP	D-ribulose 1,5-bisphosphate	0.000624	0.0131
6	S7P	sedoheptulose 7-phosphate	0.001051	0.01573
7	CoA	coenzyme A	0.001237	0.01573
8	Malo-CoA	malonyl-CoA	0.001301	0.01573
9	sulfate	sulfate	0.001365	0.01573
10	NADPH	NADPH	0.00154	0.01573
11	UDP-NAcGA	Uridine-diphosphate-N-acetylglucosamine	0.001648	0.01573
12	GLA	glutamic acid	0.001818	0.01591
13	PRPP	alpha-phosphoribosylpyrophosphoric acid	0.002153	0.01664
14	AKG	2-ketoglutaric acid	0.00236	0.01664
15	NiAc	nicotinic acid	0.002435	0.01664
16	GAP	glyceraldehyde 3-phosphate	0.002536	0.01664
17	DXP	1-deoxy-D-xylulose 5-phosphate	0.003278	0.02024
18	ADPR	ADP-D-ribose	0.006414	0.0373
19	ASC	ascorbic acid	0.00675	0.0373
20	Sucrose	disaccharides	0.00745	0.03824
21	CarbamoylAla	3-ureidopropionic acid	0.007647	0.03824
22	HMG-CoA	3-hydroxy-3-methylglutaryl-CoA	0.008317	0.03954
23	ARG	arginine	0.00866	0.03954
24	THR	threonine	0.009153	0.04004
25	phosphate	phosphate	0.010932	0.0442
26	SHIK	shikimic acid	0.010952	0.0442
27	FAD	flavin adenine dinucleotide	0.011366	0.0442
28	FUM	fumaric acid	0.012313	0.04617
29	PEP	phosphoenolpyruvate	0.01297	0.04696
30	dTTP	thymidine-5'-triphosphate	0.014169	0.04811

Table S 3. Polar metabolites significantly different between trichomes under control (CN) vs heat stress (HS) treatment.

Pair comparisons using T-test ($FDR < 0,05$). Data was analyzed using MetaboAnalyst software.
<https://www.metaboanalyst.ca/>.

	Abbreviation	Metabolite	p.value	FDR
1	GA1P	glucosamine 6-Phosphate	1.23E-05	0.00144
2	GLUCURON	D-Glucuronic Acid	4.67E-05	0.00273
3	3-OH-PYR	3-Hydroxypyruvic acid	0.00021	0.00771
4	MEVA5P	mevalonate-P	0.000322	0.00771
5	GAP	glyceraldehyde 3-phosphate	0.000385	0.00771
6	CA	ureidosuccinic acid	0.000528	0.00771
7	S1,7BP	sedoheptulose 1,7-bisphosphate	0.000602	0.00771
8	TRP	tryptophan	0.000723	0.00771
9	sucrose	disccharides	0.000725	0.00771
10	ADP-glucose	ADP-glucose	0.000772	0.00771
11	MEP	2-C-methyl-D-erythritol 4-phosphate	0.000792	0.00771
12	MEcPP	2-C-methyl-D-erythritol 2,4-cyclodiphosphate	0.000827	0.00771
13	G1P	glucose-1-phosphate	0.000857	0.00771
14	RA	D-ribonic acid	0.001658	0.01386
15	FBP	fructose 1,6-bisphosphate	0.002473	0.01929
16	chloride	chloride	0.003074	0.02248
17	3,5-cAMP	cyclic AMP	0.003571	0.02458
18	MAL	D-malic acid	0.004217	0.02741
19	pentanoates	pentanoates	0.004546	0.02785
20	FUM	fumaric Acid	0.004761	0.02785
21	CITRUL	citrulline	0.005866	0.03163
22	sulfate	sulfate	0.005948	0.03163
23	Cytidine	cytidine	0.007081	0.03456
24	phosphate	phosphate	0.007089	0.03456
25	Malo-CoA	malonyl-CoA	0.007557	0.03514
26	ORO	orotic acid	0.007987	0.03514
27	G6P	alpha-D-glucose 6-phosphate	0.008279	0.03514
28	SER	serine	0.008409	0.03514
29	GLA	glutamic Acid	0.01003	0.03878
30	UDP-glc	UDP-glucose	0.010122	0.03878
31	RIBU5P+XU5P	ribulose 5-phosphate + D-xylulose 5-phosphate	0.010275	0.03878
32	PHE	phenylalanine	0.011435	0.04181
33	3DeHy-SHIK	3-dehydroshikimate	0.011842	0.04199
34	E4P	erythrose 4-phosphate	0.014156	0.04872

Table S 4. Peak area of hydrophilic metabolites detected in trichome fractions.

Abbreviations: TC: trichomes control, TH: trichomes under heat stress.

Metabolite	Peak area						Log(2) FC		
	Sample	TC_1	TC_2	TC_3	TH_1	TH_2	TH_3	HS vs CN	p-value
1 1-deoxy-D-xylulose 5-phosphate		274314	238503	288302	323960	390989	546404	0.65	0.0856
2 2,3-cAMP		28956	28257	23918	23671	379	37658	-0.39	0.5873
3 2-Deoxyribose 5-phosphate		198178	176993	231220	236835	284464	398416	0.60	0.1073
4 2-ketoglutaric acid		1504528	1830309	1672994	2086430	1822614	2477473	0.35	0.0963
5 2'-Phospho-ADP-ribose		26978	20679	22271	459587	1005266	397726	7.29	0.3230
6 3,5-cAMP		22458	22053	21179	43382	74686	62011	1.45	0.0138
7 3-dehydroshikimate		106491	105904	82683	46457	66307	51607	-0.84	0.0114
8 3-Hydroxypyruvic acid		593778	643708	595243	311023	258716	274572	-1.12	0.0001
9 3-Methylcrotonyl CoA		2577	3369	2295	2754	3111	3235	0.14	0.4611
10 3-phosphoglycerate		1130039	1074010	1075490	1115058	1219448	1465958	0.21	0.1756
11 5'-Guanylic acid		20527	21267	21420	21696	25680	28239	0.26	0.0981
12 6-phosphogluconic acid		30152	48549	45003	58688	73537	101812	0.92	0.0566
13 AcCoA		190029	215163	188831	176961	198010	217401	0.00	0.9715
14 acetoacetyl-CoA		3307	3097	2695	2934	4297	3941	0.30	0.1960
15 acetyl-CoA		2633392	2705072	2326259	2624780	2938087	3202279	0.19	0.1456
16 Adenosine 5'-diphosphate		247948	282631	247984	230217	314185	384847	0.26	0.3377
17 Adenosine 5'-diphosphoribose		11578	8783	29164	124701	3438815	141063	6.22	0.3309
18 adenosine 5'-monophosphate		96612	79226	83776	90079	123335	132417	0.41	0.1072
19 ADP-glucose		10953	5323	7827	53097	52783	62027	2.80	0.0002
20 allantoin		105856	117776	134656	96811	104333	113810	-0.19	0.2105
21 alpha-D-glucose-6-phosphate		6835015	5865699	6321254	9027624	10859090	12774714	0.78	0.0152
22 Arginine		138752	118337	129806	92869	130661	120377	-0.17	0.3234
23 Aspartic acid		6883446	6515806	4580782	3406727	4749889	4569896	-0.50	0.1022
24 ATP		5771478	5847611	5657685	5940840	7752414	8918664	0.39	0.1099
25 CarbamoylAla		10917	9316	9774	10346	11953	12879	0.23	0.1217
26 CDP-ME		5045	4012	5503	3955	4432	5168	-0.10	0.5847
27 CDP-MEP		3574	5104	4549	6193	7380	11230	0.91	0.0716
28 Citric acid		69317697	56562024	51271487	39429740	42957412	45337619	-0.47	0.0428
29 Citrulline		460926	442579	448021	227600	300080	300247	-0.71	0.0021
30 CMP		28990	32635	28926	30502	41804	45320	0.38	0.1234
31 Coenzyme A		1081	722	2842	1793	779	2756	0.20	0.8064
32 Cytidine		3551	5335	5378	9058	11441	12414	1.21	0.0059
33 Cytidine 5'-diphosphate		22050	21503	26167	18742	26530	32774	0.16	0.5553
34 Cytidine triphosphate		1060322	1063646	1077255	901500	1167712	1187495	0.02	0.8511
35 dATP		39388	33548	29619	22446	32317	35181	-0.19	0.4296
36 Deoxyguanylic acid		69339	57954	59822	61120	81418	96450	0.35	0.1855
37 D-Glucuronic Acid		405117	407770	331828	64100	66439	77894	-2.46	0.0002
38 Digalacturonic acid		69728	73691	68179	54224	73441	81122	-0.02	0.9142
39 Dihydroxyacetone phosphate		784590	558759	633698	932255	1024092	1147099	0.65	0.0145
40 Dimethylallyl pyrophosphate		58976	65151	50765	48536	58525	70218	0.02	0.9209
41 D-pantothenic acid		891193	934181	815439	777791	960247	732253	-0.10	0.5057
42 D-ribulose 1,5-bisphosphate		138560	65740	89231	111987	109488	69757	-0.01	0.9774
43 Erythrose 4-phosphate		284695	226158	239877	350626	399793	490713	0.73	0.0216
44 Flavin adenine dinucleotide		23144	28846	26784	27097	32026	32436	0.22	0.1494
45 Fructose-1,6-diphosphate		461916	319028	384365	887742	891896	1148080	1.33	0.0035
46 Fumaric acid		6774905	6554111	5576120	3879644	4334080	4370520	-0.59	0.0063
47 Galactonic acid		18518284	15627347	16482525	14894448	15976338	16184424	-0.11	0.2765
48 Gluconic acid		18394031	15785205	16260162	14585899	16449433	16237635	-0.09	0.3487
49 Glucosamine 6-phosphate		16235	15316	15648	58171	68611	66524	2.03	0.0001
50 Glucose/Fructose		324462	210891	192593	109645	123528	155599	-0.90	0.0599
51 Glucose-1-phosphate		1324128	1294934	1150886	2763205	3422311	3888717	1.42	0.0031
52 Glutathione		4563568	427838	14999045	12476022	11597560	16923416	1.04	0.2056
53 Glyceraldehyde 3-phosphate		3747	3651	3054	9999	10884	13356	1.71	0.0015
54 glycerate 2-phosphate		582842	578907	552884	600321	635455	745651	0.21	0.1180
55 Glycerophosphoric acid		1057686	1064671	1037278	1125209	1434280	1470730	0.35	0.0576
56 Glycine		69599	57264	83792	75928	85696	83406	0.22	0.2354
57 GTP		631622	681068	633660	636866	913117	999889	0.39	0.1432
58 Guanosine		193236	183755	184095	210105	274195	314006	0.51	0.0601
59 Guanosine diphosphate		36237	39144	40136	32087	45814	56883	0.22	0.4267
60 HMBPP		7186	12682	14863	9886	12359	10761	-0.07	0.8221
61 HMG-CoA		39304	39973	36903	33115	37131	39774	-0.08	0.3934
62 Isocitric acid		2708260	2132371	1759083	1619520	1753588	1794446	-0.35	0.1647
63 Isopentenyl pyrophosphate		7192	5803	5788	7723	5432	6585	0.07	0.7136
64 Isovaleryl-coenzyme A		1761	2095	1648	2516	3576	4095	0.89	0.0320
65 L-glutamic acid		11662018	11227762	10315650	12974501	14323713	14372387	0.33	0.0096

Metabolite	Peak area						Log(2) FC		
	Sample	TC_1	TC_2	TC_3	TH_1	TH_2	TH_3	HS vs CN	p-value
66 L-glutamine		940820	975377	1200546	676499	1226590	878720	-0.16	0.5689
67 L-lysine		45802	48262	43056	31816	46625	40770	-0.20	0.2607
68 L-proline		3615	1903	2445	1681	3073	3515	0.05	0.8977
69 L-serine		194046	169503	206926	250039	259849	280661	0.47	0.0067
70 L-threonine		137957	132250	142555	127387	211441	150515	0.25	0.3691
71 L-tryptophan		113560	94631	90715	220213	280718	263786	1.36	0.0013
72 L-tyrosine		57696	56689	56916	50347	69424	73299	0.17	0.3645
73 Malic acid		260925574	259927699	224806101	160486098	180264855	178455088	-0.52	0.0050
74 Malonyl-CoA		77107	56835	59694	33208	37669	40254	-0.80	0.0145
75 MEcPP		172895	253472	234936	666345	783797	863649	1.81	0.0009
76 Methyl-D-erythritol Phosphate		625197	663521	548899	1690293	2537929	2396267	1.85	0.0038
77 Methylmalonyl-coenzyme A		13877	13201	10936	7696	8025	10568	-0.53	0.0371
78 Mevalonate-P		16044	14845	15272	44764	64672	53900	1.82	0.0025
79 Mevalonate-PP		4072	3982	5296	5047	4744	4382	0.09	0.5870
80 NAD+		491452	452277	422211	377799	4713	557573	-0.54	0.4357
81 NADH		468	621	2497	2293	2705	4201	1.36	0.0987
82 NADP+		69063	90507	54756	66539	466	86656	-0.48	0.5105
83 NADPH		2348	1000	33502	25319	5439	21891	0.51	0.6897
84 Nicotinic acid		16491	34148	12997	8553	9429	5334	-1.45	0.1139
85 Orotic acid		186073	174395	133303	71933	95310	64469	-1.09	0.0092
86 Orotidylic acid		29924	29128	30994	22998	29998	35210	-0.03	0.8723
87 Oxaloacetic acid_1		23602	27083	20033	17425	14980	13908	-0.61	0.0236
88 Oxoglutatione		1210482	803798	1295966	1251158	2652648	1988909	0.83	0.1173
89 Phenylalanine		160666	191017	146847	261297	431829	387480	1.12	0.0212
90 Phosphoenolpyruvate		448217	474713	382831	502496	529073	662366	0.38	0.0838
91 Phytic acid		6275	9978	7706	5339	10144	9065	1.04	0.9188
92 PRPP		99374	117191	91770	139473	231934	251000	0.01	0.0412
93 Quinic acid		10225588	10828886	8923435	7846815	9464199	8402551	-0.22	0.1255
94 Ribonic acid		1000044	947994	823234	421196	516565	504489	-0.94	0.0018
95 Ribulose 5-phosphate+Xylulose 5-phosphate		296550	318175	283001	413332	473936	584153	0.71	0.0200
96 Sedoheptulose 1,7-bisphosphate		17890	13741	17327	54170	62377	79906	2.00	0.0031
97 Sedoheptulose 7-phosphate		272920	301108	219691	297782	430264	465093	0.59	0.0772
98 Shikimic acid		590733	649841	584370	655418	796724	926311	0.38	0.0849
99 Succinic acid		842648	901036	880210	806461	747805	741500	-0.19	0.0151
100 Succinyl-coenzyme A		3575	5012	3961	3889	3899	3454	-0.16	0.3916
101 Sucrose		59335	63472	62389	181207	200737	281260	1.84	0.0065
102 Thymidine triphosphate		81105	76187	61239	37144	56525	46678	-0.64	0.0334
103 Trigalacturonic acid		18045	24095	25835	28912	53547	47516	0.94	0.0566
104 UDP-glucose		32890801	35154825	34598646	43159825	48979225	56266229	0.53	0.0167
105 UDP-NAcGA		1979837	2063024	2126536	1724344	2139277	2355177	0.01	0.9351
106 Ureidosuccinic acid		25511	22715	23680	9780	8866	7068	-1.48	0.0002
107 Uric acid		55768370	51604783	53496969	51626249	63481551	63839194	0.15	0.2237
108 Uridine		27004	27513	39063	34673	55788	56132	0.65	0.0950
109 Uridine 5'-diphosphate		112206	113742	126348	55703	80097	97222	-0.60	0.0365
110 Uridine 5'-monophosphate		136290	140625	123039	138581	202813	233375	0.52	0.1097
111 uridine 5'-triphosphate		7397570	7090967	6660264	3649125	5090926	4993302	-0.62	0.0085
112 Valeric acid		1402378	1329345	1328490	1209912	1140634	1147378	-0.22	0.0047
113 Xanthosine monophosphate		10372	7143	15281	20920	13978	28666	0.95	0.1023

Table S 5. Differentially expressed genes (DEGs) in heat stress (HS) compared to control (CN) conditions in the WT, *jai1* or both genotypes(-1.5 < log₂FC < 1.5; P < 0.05).

Comparison	Abbreviation	Gene ID	LOC ID	Annotation	
HS (<i>jai1</i> vs WT)	<i>MYB13</i>	Solyc06g083900	101260654	Transcription factor MYB13-like	
	<i>ARPI</i>	Solyc11g021060	543962	Potato type II proteinase inhibitor family	
	<i>WIPI</i>	Solyc09g083440	101246961	Wound-induced proteinase inhibitor 1	
	<i>WIPI-like</i>	Solyc09g084490	101248423	Wound-induced proteinase inhibitor 1-like	
	<i>API1</i>	Solyc03g098780	101262903	Aspartic protease inhibitor 1	
	<i>HBP2</i>	Solyc07g061800	101255514	Heme-binding protein 2-like	
	<i>ASAH2</i>	Solyc05g051670	101255998	Acylsugar acylhydrolase	
	<i>ARG2</i>	Solyc01g091170	544271	Arginase 2	
	<i>JAZ3</i>	Solyc01g005440	100191114	Jasmonate ZIM-domain protein 3	
	<i>NRT1-like</i>	Solyc05g005940	101261026	NRT1/ PTR FAMILY 1.2-like (nitrate transporter/peptide transporter)	
	<i>MYC2-like</i>	Solyc01g096370	101264068	Transcription factor MYC2-like	
	<i>SMO3</i>	Solyc01g091320	104649012	Methylsterol monooxygenase 1	
	<i>CYP</i>	Solyc02g090350	101252644	Geraniol 8-hydroxylase:Cytochrome P450	
	<i>ZOX1</i>	Solyc07g043480	101254402	Zeatin O-xylosyltransferase (GAME17)	
	<i>GAD2</i>	Solyc07g043420	544002	2-oxoglutarate-dependent dioxygenase 2 (GAME11)	
	<i>C5-SD2</i>	Solyc02g086180	101264777	Delta(7)-sterol-C5(6)-desaturase	
	<i>NRT1</i>	Solyc05g005980	107196795	NRT1/ PTR FAMILY 1.2 (nitrate transporter/peptide transporter)	
	<i>CSLG2</i>	Solyc07g043390	101255510	Cellulose synthase-like protein G2	
	<i>GAME6</i>	Solyc07g043460	101255011	Cytochrome P450 CYP72A219	
	<i>ZOG1</i>	Solyc11g066670	101268254	Zeatin O-glucosyltransferase	
	<i>SMO4</i>	Solyc06g005750	101258266	Methylsterol monooxygenase	
	<i>7-DR2</i>	Solyc06g074090	101256596	7-dehydrocholesterol reductase	
	<i>ZOX1-LIKE</i>	Solyc05g053120	101248301	Zeatin O-xylosyltransferase-like	
	<i>SSR2</i>	Solyc02g069490	101244831	Delta(24)-sterol reductase-like 2C	
	Both (<i>jai1</i> vs WT)	<i>PII3</i>	Solyc11g022590	544001	Trypsin and protease inhibitor I3
		<i>NAOD</i>	Solyc08g076970	101268129	N2-acetylornithine deacetylase
		<i>ER</i>	Solyc12g096780	101247598	Enoyl-[acyl-carrier-protein] reductase2C mitochondrial-like
		<i>RIDA</i>	Solyc07g064600	101248695	Inducible plastid-lipid associated protein-Endoribonuclease L-PSP family
		<i>DIVARICATA</i>	Solyc05g052610	101257376	transcription factor DIVARICATA:Myb-like DNA-binding domain
		<i>PD30</i>	Solyc12g019320	101266307	protein DETOXIFICATION 30-like
<i>JAZ7</i>		Solyc11g011030	543601	Pto-responsive gene 1 protein Divergent CCT motif PF06200:tify domain	
<i>RING</i>		Solyc10g008410	101262459	E3 ubiquitin-protein ligase :Zinc finger, C3HC4 type (RING finger)	
<i>COI1</i>		Solyc05g052620	543911	Coronatine-insensitive 1	
<i>TIC32</i>		Solyc03g025390	101257739	Short-chain dehydrogenase TIC 32	
<i>MHPC</i>		Solyc03g123390	101251165	2-hydroxy-6-oxononatrienedioate hydrolase	
CN (<i>jai1</i> vs WT)		<i>R1A-3</i>	Solyc05g054010	101251780	Putative late blight resistance protein homolog R1A-3
		<i>UNPR</i>	Solyc05g052210	101266516	Uncharacterized protein
		<i>OSS2</i>	Solyc10g009150	101245207	organ-specific protein S2
		<i>UNPR</i>	Solyc05g002344	101253592	Uncharacterized protein

Table S 6. Primers used in the present dissertation.

Primer Name	Gene ID	Used in	Primer Sequence (5' --> 3')
Rbc-Aprom-Fw	Solyc07g017950	Promoter	TTGGTCTCTACATGGAGATTGTTTACCAG TAAAAAATTCTCATGTTTAGAAGATG
Rbc-Aprom-Rv		Promoter	AAGGTCTCAACAATAGCTTTGGTAAAAGT TTCATTTAAGAATTTATTTTTATATAATAC
Rbc-Bprom-Fw		Promoter	TTGGTCTCTACATGCTATGAGATATGTTA ATTTATTAATAATGGATATATTGG
Rbc-Bprom-Rv		Promoter	AAGGTCTCAACAACATTGTTTGCTCTTAA CTATCAACTACTTTAGTTATG
SIRbcS-T-sgRNA1	Solyc07g017950	CRISPR	TTGGTCTCTATTGGTAATTGTATCCTTAA CAGCGTTTAAGAGCTATGCTGGAAACAG CATAG
SIRbcS-T-sgRNA2		CRISPR	TTGGTCTCTATTGGTAATCAACCTCCTTT GCAAGTTTAAGAGCTATGCTGGAAACAG CATAG
SIRbcS-T-sgRNA3		CRISPR	TTGGTCTCTATTGATGTAGAGACGATATT TACGGTTTAAGAGCTATGCTGGAAACAG
ShRbcS-T-sgRNA1		CRISPR	TTGGTCTCTATTGGTAATCAACCTCCTTT GCAAGTTTAAGAGCTATGCTGGAAACAG C
ShRbcS-T-sgRNA2		CRISPR	TTGGTCTCTATTGGTAATTGTATCCTTAG CAGCGTTTAAGAGCTATGCTGGAAACAG C
SIPEPCK-sgRNA1	Solyc04g076880	CRISPR	TTGGTCTCTATTGGGATCATTATCACGT CAAGTTTAAGAGCTATGCTGGAAACAG C
SIPEPCK-sgRNA2		CRISPR	TTGGTCTCTATTGCGTCATTGACACGAGA GACGGTTTAAGAGCTATGCTGGAAACAG
RbcS-3B-sgRNA	Solyc02g085950	CRISPR	TTGGTCTCTATTGTCAGCTGCTGTTGCCA CCCGTTTAAGAGCTATGCTGGAAACAG C
RbcS-2A-sgRNA	Solyc03g034220	CRISPR	TTGGTCTCTATTGGCTCGTCAGACAAATC AGGAGTTTAAGAGCTATGCTGGAAACAG C
RbcS-1-sgRNA	Solyc02g063150	CRISPR	TTGGTCTCTATTGAGTTCCCCTGGATACT ACGAGTTTAAGAGCTATGCTGGAAACAG C
TPS20-sgRNA1	Solyc08g005665	CRISPR	TTGGTCTCTATTGTTCTTCTATGACACA GCATGTTTAAGAGCTATGCTGGAAACAG C
TPS20-sgRNA2		CRISPR	TTGGTCTCTATTGGTTTGCTTGCACTAAC CAAAGTTTAAGAGCTATGCTGGAAACAG C
SpV/RbcST-Fw	Sopen07g006810	VIGS	AAAAAGGATCCCTCCATCCTCGTAGAT ATCGTCTCTAC
SpV/RbcST-Rv		VIGS	AAAAAGGATCCTGTCAATAGGATTCCAA GTCTTCATGCAG
SpV/RbcSM-Fw	Sopen02g030630	VIGS	AAAAAGGATCCGCATGCAGGTGTGCCA CCAATTAAC
SpV/RbcSM-Rv		VIGS	AAAAAGGATCCGACGAACATTGTGCAAT CCGATGATACG
MCPIprom-Fw	Solyc01g067295	CRISPR- TSKO	TTGAAGACTAGGAGCTAACTTATCCTGA GCTAGAAGTTATGAC
MCPIprom-Rv		CRISPR- TSKO	AAGAAGACTACATTATGTGATGCTACTTT GATTGGAAAATGG

P2A-ABR-Fw		CRISPR-TSKO	TTGAAGACATCTCATTTCGGGTGCTACCA ACTTCAGCCTTCTTAAGCAGGCCGGTGA TGTGG
P2A_R/TS		CRISPR-TSKO	AAGAAGACTACATTGGACCAGGATTTTCT TCCACATCACCGGCCTGCTTAAG
mCherry-Fw		CRISPR-TSKO	TTGAAGACATAATGGTGAGCAAGGGCGA GG
mCherry-Rv		CRISPR-TSKO	AAGAAGACTACTCGAAGCTCACTTGTAC AGCTCGTCCATG
WT_COI1_Rv jai1_Fw WT/jai1_Fw	Solyc05g052620	Genotyping	CCATGGAGTCCATCACCTAACAGT GTGGTCAGATCAGAGCCCTCTATT GTGGAGACGATATGTTGAGACTAA
Rbc-Seq-T1-Fw Rbc-Seq-T1-Rv Rbc-Seq-T2-Fw Rbc-Seq-T2-Rv Rbc-Seq-T3-Fw Rbc-Seq-T3-Rv	Solyc07g017950	Genotyping	CCACTTCCACAACAAAAACACAC TGCAAAAGTTCTTTCATGCTG ACACACACGTACACTATCTTCTCC GGGAAGAGTCATTGCAGCCA TTGAGGAGGGGATGTGTGTG TGCATGTACCTTAGATTCAAACACTACA
PEPCK-Seq-T1-Fw PEPCK-Seq-T1-Rv PEPCK-Seq-T2-Fw PEPCK-Seq-T2-Rv	Solyc04g076880	Genotyping	TAGGCTTCAACACGAATATGAGAC AATGGAGGGTGGGTAAGCAC GCTAGCTGGGAGTTCATGGG GTGTGGATTGTGAACAGGTGC
TPS20-Ex3-Seq/Fw TPS20-Ex3-Seq/Rv	Solyc08g005665	Genotyping	ATCAGCCTCCCTGTTTCA CGAGGGAGTACTGGTTGTCAC
EF1 α -Fw EF1 α -Rv	Solyc06g005060	qRT-PCR	GGAACCTTGAGAAGGAGCCTAAG CAACACCGACAGCAACAGTCT
SIRbcST-Fw SIRbcST-Rv	Solyc07g017950	qRT-PCR	ACTGCATGAAGTCTTGAATCCT GTCAAATTC AAGGCAAGGAACCC
SIRbcS1-Fw SIRbcS1-Rv	Solyc02g063150	qRT-PCR	CAATTGTCTCATCGGCAGCC TAACGCGTCCACCATTGCTA
SIRbcS2A-Fw SIRbcS2A-Rv	Solyc03g034220	qRT-PCR	GCAATATGGCTTCTCTGTCA TTGTAACAGGGAAAGTGGCTGA
SIRbcS3B-Fw SIRbcS3B-Rv	Solyc02g085940	qRT-PCR	CTCAGGCATGGGTCCGTATC GGAGGATTCAAACAAGCTTCCC
SpRbcST-Fw SpRbcST-Rv	Sopen07g006810	qRT-PCR	CAACTGAGCTCTAGCCTTAAGAG GCTATTACCACTTACTGCCTTG
SpRbcS1-Fw SpRbcS1-Rv	Sopen02g014220	qRT-PCR	TGCCTACAAGCCAGAAGGATAC TCTCATAACTTGGTCGGAATCG
SpRbcS2A-Fw SpRbcS2A-Rv	Sopen03g007000	qRT-PCR	CCTCTGTTATTTCTCTGCAGC TTGTAACAGGGAAAGTGGCTGA
SpRbcS2B-Fw SpRbcS2B-Rv	Sopen02g030630	qRT-PCR	TGTCAACAATGGCTTCTCT AAACAGGGAAAGAAGCAGTGGA
SpRbcS2C.1-Fw SpRbcS2C.1-Rv	Sopen02g030610	qRT-PCR	TCGGATTTCGACAATGTTCTGCA AGCAAACGGAAAATGCGAACAG
PEPCK-Fw2 PEPCK-Rv2	Solyc04g076880	qRT-PCR	ATTCTGGACCCCGTGAACAC TGCCAGGATCTCCTCAGTCA
MCPI-Fw MCPI-Rv	Solyc01g067295	qRT-PCR	GGGTGCACGCGATATGTCAG CCTTGATCAAATGCATCATTTGC
ELIP1-Fw ELIP1-Rv	Solyc09g082690	qRT-PCR	GTATGGCTGAGGAGGGTGAG CAAATCCAATCATGGCTAGCCTAC

TPS9-Fw TPS9-Rv	Solyc06g059885	qRT-PCR	GCAATTCACCAACCAAGATGGG GACTCGAGATGAGTGGTGG
TPS12-Fw TPS12-Rv	Solyc06g059930	qRT-PCR	CGTTACTGGTTGAGTCTGTCC CTTGATTATTTGAAATATTCCGGAGG
TPS20-Fw TPS20-Rv	Solyc08g005665	qRT-PCR	GAATTATGCCAAGCTCAACACC TCGGATAATTCAGGCTCGGGGATAAC
NDPS1-Fw NDPS1-Rv	Solyc08g005673	qRT-PCR	GCTCGTGGACTCAACAAGATTTT CCCTTATCCTTTGCCCATCTCC
AACT-Fw AACT-Rv	Solyc07g045350	qRT-PCR	GAGGTGCCTGGAGGAAGAGG TGAGCAGCATCCGCGTAGCC
HMGS-Fw HMGS-Rv	Solyc08g007790	qRT-PCR	GAGGCTCATGATGGAGCAAGC ACAGGCATTAGTTGAGTCAACTCC
HMGR1-Fw HMGR1-Rv	Solyc02g082260	qRT-PCR	ATGCCAGCAACATCGTCTCTGC CCTGGTGCATCTCTATTTGCACC
MK-Fw MK-Rv	Solyc01g098840	qRT-PCR	CTGGTATTGACAACACAGTGAGC CGCAAGGTCCTCTCAGAGACG
FPS1-Fw FPS1-Rv	Solyc12g015860	qRT-PCR	TCATCGCCGGATTGTCCAGT CCCAGCACCTCTGGGTCAGC
DXS1-Fw DXS1-Rv	Solyc01g067890	qRT-PCR	GGCTTATGACCAGGTAGTGCATG TGGCGGCAGCAGTTGCTACC
DXS2-Fw DXS2-Rv	Solyc11g010850	qRT-PCR	GGCATAACCAATTGAGGTCCGT GATCCTTCTTCGACAGTGATCAAG
DXR-Fw DXR-Rv	Solyc03g114340	qRT-PCR	CATGACTGGAGTTCTAAGTGCAGC CTGGCTGCGTAGTCTCGAGC
CMK-Fw CMK-Rv	Solyc01g009010	qRT-PCR	GTAATTGCTGCTGGCCGAGGAC ATACCACTCGTTGGCTGGTCCG
HSP70-Fw HSP70-Rv	Solyc11g002068	qRT-PCR	TAGGCAAGTTTGAGCTCTCTGG GACCCTTGTCGTTGGTGATAGT
COI1-Fw COI1-Rv	Solyc05g052620	qRT-PCR	CGAATCGTCGTGGAAGAGTTC GTTTATGTGCCATTCTCCATC
JAZ2-Fw JAZ2-Rv	Solyc12g009220	qRT-PCR	AGTGATTCATCGTCGTCATCGT TGTGCCTTCTCTGGTTGATCAG
JAZ4-Fw JAZ4-Rv	Solyc12g049400	qRT-PCR	CCCACCACCACTCAGACTAATG TTATGCATTTGGTATGGCGCTC
JAZ10-Fw JAZ10-Rv	Solyc08g036620	qRT-PCR	CCTAGCAACTTGTGATGGAGG TGATGAAGGCTCAGACAGCTT
MYC2-Fw MYC2-Rv	Solyc08g076930	qRT-PCR	CGGAATTCGTTTTGATGGAAG AACAAAGTTCACATTGGCACTGG
SIMYB13-Fw SIMYB13-Rv	Solyc06g083900	qRT-PCR	CAACTGCAACGAGTTCAGAGTC ATCGACTTGTGCCATACTACC

Table S 7. Composition of media used for stable genetic transformation of tomato.

Media name	Composition
½ MS	Murashige & Skoog (MS) salts including Vitamins (2,2 g/l), Sucrose (1,5%), plant Agar (0,8%).
MS-L	Murashige & Skoog (MS) salts including Vitamins (4,4 g/l), Sucrose (3%).
MS1	Murashige & Skoog (MS) salts including Vitamins (4,4 g/l), Sucrose (3%), TC Gel (5,2 g/l), trans-Zeatin (2 mg/l), IAA (0,1 mg/l).
MS2	Murashige & Skoog (MS) salts including Vitamins (4,4 g/l), Sucrose (3%), TC Gel (5,2 g/l), trans-Zeatin (2 mg/l), IAA (0,1 mg/l), Ticarcillin (300 mg/l), Kanamycin (100 mg/l).
MS3	Murashige & Skoog (MS) salts including Vitamins (4,4 g/l), Sucrose (3%), TC Gel (5,2 g/l), trans-Zeatin (1 mg/l), IAA (0,1 mg/l), Ticarcillin (300 mg/l), Kanamycin (100 mg/l).
MSR	Murashige & Skoog (MS) salts including Vitamins (4,4 g/l), Sucrose (3%), TC Gel (5,2 g/l), Ticarcillin (100 mg/l), Kanamycin (50 mg/l).

Acknowledgement

I would like to start by expressing my sincere gratitude to Prof. Dr. Alain Tissier, for opening the door for me at the IPB and giving me the opportunity to pursue my PhD in the iPHACTORY project, funded by the Deutsche Forschungsgemeinschaft (DFG). I am grateful for his guidance, constant supervision, and valuable feedback during these four years.

In the same manner, I would like to say thank you to many people who contributed to the completion of this work by sharing their knowledge and expertise. To Dr. Tom Schreiber for introducing me to the golden gate cloning system and guiding me in the construct design. To Dr. Ulschan Bathe for training me in the use of the GC-MS. To Dr. Gerd Balcke and Dr. Yaming Liu, for their assistance with metabolomics and data analysis. To Dr. Ramona Schubert, for her pieces of advice on genetic transformation of tomato. To Dr. Khabat Vahabi, for his kind support during the sample preparation of the RNASeq experiment, and to Esther Harding, for her input in the transcriptome data analysis. To Hagen Stellmach and Prof. Dr. Bettina Hause, for their introduction to confocal laser microscopy. To Dr. Sayantan Panda, for sharing his experience with the VIGS technique and jasmonate signaling. To Dr. Jörg Ziegler and Dr. Samuel Ngure Kariithi, for their help in the quantification of organic acids from trichomes. To my PhD colleague, friend, and trichome buddy Robert Säbel, with whom I formed a great team and jointly contributed to the research field of glandular trichomes. I am also thankful to everyone in the SZB department for their support and for providing a good work environment. My gratitude also goes to thesis committee for evaluating the present dissertation.

This time of learning and professional growth at IPB was equally marked by amazing people I met, and to whom I extend my deepest gratitude. I would like to say thank Ramona Schubert, Tina Petrić, Heena Yadav and Khansa Mekkaoui for extending their sincere friendship and supporting me in the challenging transition of living far away from my country. All now in different places, but still in touch, thank you for being there. To Micha Devi and Kathleen Helmstedt, thank you for warmly welcoming me into the AG Tissier group and for your help in all matters related to the trichomes. To Dario Esposto and Fiona Smith, for cheering me up and always encouraging me to keep on going -you are my favorite team-. My heartfelt gratitude goes to Esther for her sincere friendship and the dedicated time she spent reviewing and correcting the writing of the present work. I appreciate it a lot. I want to thank my Sunday church group, especially Prof. Imming, for sharing his knowledge, his messages, and thoughts.

I would like to take this opportunity to acknowledge my former professors and mentors Dr. Mauricio Quimbaya and Dr. Lorena López, for their invaluable support in preparing the PhD applications. Similarly, I extend my gratitude to my former supervisor, Dr. Paul Chavarriaga

and the Trafo team at CIAT. They provided the foundational scientific training and confidence necessary for me to continue my graduate studies.

Quiero darle las gracias infinitas a mi familia en Colombia, que desde el otro lado del Atlántico, a veces a -6 o -7 horas de diferencia, siempre estuvieron pendientes de mí. A mi familia en Holanda, que me recibió muchas veces y me hizo sentir como si estuviera en casa. A mi abuela, gracias por tu inmenso apoyo y amor durante tus últimos años de vida, que desde el cielo, sigo sintiendo que estas siempre a mi lado. A mi hermana, por su apoyo y cariño. Y a mi mamá, mi motor, mi fuerza, y mi fortaleza. Gracias por tu amor infinito y tus oraciones. Sin ti, llegar hasta aquí, no hubiese sido posible.

Finalmente, le agradezco a Dios, por cuidarme y bendecirme cada día.

To all, Gracias, Thank you, Danke schön.

Curriculum Vitae

Alejandro Brand Durán

Education and working experience

- 2019-2024 **PhD student / Doktorarbeit**
 Department of Cell and Metabolic Biology
 Leibniz Institute of Plant Biochemistry, Halle (Saale)
 Supervisor: Prof. Dr. Alain Tissier
 “Tomato glandular trichomes: insights into productivity and development”
- 2014-2019 **Research assistant.** Advanced Breeding Platform
 Alliance Bioversity International - CIAT, CGIAR, Cali-Colombia
<https://alliancebioiversityciat.org/>
 Development of transformation protocols for cassava (*Manihot esculenta*, Crantz) and rice (*Oryza sativa*) elite cultivars.
- 2009-2014 **Diplom in Biology (Biotechnology and conservation biology)**
 Pontificia Javeriana University Cali-Colombia
<http://www.javerianacali.edu.co/>
 Thesis: Expression analysis of *Arabidopsis LEC1* and *LEC2* orthologous genes in somatic embryo development of cassava (*Manihot esculenta* Crantz).
 Supervisor(s): Dr Paul Chavarriaga-Aguirre, Prof. Dr. Mauricio Quimbaya

Conferences

Oral Presentations

Brand, A., Tissier A., Elucidating the role of Rubisco and PEPCK in the photosynthetic glandular trichomes of tomato. In: **XVII SOLANACEAE2022 International Conference** on the Plant Family of Solanaceae”, Thessaloniki, Greece, November 1-5, 2022. <https://sol2022.web.auth.gr/>

Brand, A., Quimbaya, M., and Chavarriaga., P. *Arabidopsis LEC1* and *LEC2* orthologs genes are key regulators of somatic embryogenesis in cassava. In: IX **REDBIO** Conference. Lima, Perú. Jun 27th-July 1th, 2016. <http://www.redbioperu.com.pe/>

Brand, A., Quimbaya, M., and Chavarriaga., P. Identification and characterization of *Arabidopsis LEC1* and *LEC2* orthologous genes in cassava somatic embryo development (*Manihot esculenta*, Crantz) In: **World Congress on Root and Tuber Crops** gathering the Third Conference of the Global Cassava Partnership for the 21st Century and the 17th Symposium of the International Society for Tropical Root Crops. Nanning, Guangxi, China. Jan 18-23, 2016. <http://www.gcp21.org/wcrtc/>

Courses and workshops

Genome Editing Symposium, Changing Agricultural Research in Latin America. DuPont Plant Sciences Symposia series. International Center for Tropical Agriculture-CIAT. October 17-18th 2017. Cali, Colombia. (Organizer and attendee).

https://ciat.cgiar.org/event/symposium_genome_editing/

Plant Genome Editing Workshop, Fort Collins, Colorado State University, July 9-11th 2017. Colorado, EEUU. (Attendee) <https://qtl2017.wordpress.com>

Publications

Säbel, R., **Brand, A.**, Bergau, N., Balcke, G.U., Syrowatka, F., Püffeld-Raorane, M., Hause, B., Tissier, A. (2023) Heat stress induces a developmental shift from type-V to type-IV trichome dependent on jasmonate signaling in tomato. bioRxiv: 2023.2007.2028.551053.

Saadat, N. P., van Aalst, M., **Brand, A.**, Ebenhöf, O., Tissier, A., & Matuszyńska, A. B. (2023). Shifts in carbon partitioning by photosynthetic activity increase terpenoid synthesis in glandular trichomes. *The Plant Journal*. <https://doi.org/10.1111/tpj.16352>

Brand, A., & Tissier, A. (2022). Control of resource allocation between primary and specialized metabolism in glandular trichomes. *Current Opinion in Plant Biology*, 66, 102172.

Sánchez, F. J., Arciniegas, J. P., **Brand, A.**, Vacca, O., Mosquera, A. J., Medina, A., & Chavarriaga, P. (2022). Metabolic engineering of cassava to improve carotenoids. In *Methods in Enzymology* (Vol. 671, pp. 31-62). Academic Press.

Brand, A., Quimbaya, M., Tohme, J., & Chavarriaga-Aguirre, P. (2019). Arabidopsis LEC1 and LEC2 orthologous genes are key regulators of somatic embryogenesis in cassava. *Frontiers in Plant Science*, 10, 673.

Chavarriaga-Aguirre, P., **Brand, A.**, Medina, A., Prías, M., Escobar, R., Martínez, J., ... & Tohme, J. (2016). The potential of using biotechnology to improve cassava: a review. *In Vitro Cellular & Developmental Biology-Plant*, 52, 461-478.

Eidesstattliche Erklärung

Hiermit erkläre ich, dass ich die vorliegende wissenschaftliche Arbeit selbständig und ohne fremde Hilfe angefertigt habe. Ich erkläre, dass ich keine anderen als die von mir angegebenen Quellen und Hilfsmittel benutzt habe und die den Werken wörtlich und inhaltlich entnommenen Stellen als solche kenntlich gemacht habe. Ich versichere weiterhin, dass ich mich erstmals mit dieser Arbeit um die Erlangung des Doktorgrades bewerbe. Diese Arbeit wurde an keiner anderen Fakultät oder Universität zur Begutachtung eingereicht.

Alejandro Brand Durán

Halle (Saale), den 27.05.2024